



UNIL | Université de Lausanne

Unicentre

CH-1015 Lausanne

<http://serval.unil.ch>

Year : 2019

YEAST-TO-HYPHA TRANSITION IN FISSION YEAST

Kinnaer Cassandre

Kinnaer Cassandre, 2019, YEAST-TO-HYPHA TRANSITION IN FISSION YEAST

Originally published at : Thesis, University of Lausanne

Posted at the University of Lausanne Open Archive <http://serval.unil.ch>

Document URN : urn:nbn:ch:serval-BIB_9FC4214B7F2B9

Droits d'auteur

L'Université de Lausanne attire expressément l'attention des utilisateurs sur le fait que tous les documents publiés dans l'Archive SERVAL sont protégés par le droit d'auteur, conformément à la loi fédérale sur le droit d'auteur et les droits voisins (LDA). A ce titre, il est indispensable d'obtenir le consentement préalable de l'auteur et/ou de l'éditeur avant toute utilisation d'une oeuvre ou d'une partie d'une oeuvre ne relevant pas d'une utilisation à des fins personnelles au sens de la LDA (art. 19, al. 1 lettre a). A défaut, tout contrevenant s'expose aux sanctions prévues par cette loi. Nous déclinons toute responsabilité en la matière.

Copyright

The University of Lausanne expressly draws the attention of users to the fact that all documents published in the SERVAL Archive are protected by copyright in accordance with federal law on copyright and similar rights (LDA). Accordingly it is indispensable to obtain prior consent from the author and/or publisher before any use of a work or part of a work for purposes other than personal use within the meaning of LDA (art. 19, para. 1 letter a). Failure to do so will expose offenders to the sanctions laid down by this law. We accept no liability in this respect.



Département de Microbiologie Fondamentale

YEAST-TO-HYPHA TRANSITION IN FISSION YEAST

Thèse de doctorat ès Sciences de la Vie (PhD)

présentée à la

Faculté de Biologie et de Médecine
de l'Université de Lausanne

par

Cassandra KINNAER

Master diplômée de l'Université Paul Sabatier, Toulouse, France

Jury

Prof. Michel Chapuisat, Président
Prof. Sophie Martin, Directrice de Thèse
Dr Snezhana Oliferenko, Expert
Prof. Dominique Sanglard, Expert

Lausanne, 2019



Département de Microbiologie Fondamentale

YEAST-TO-HYPHA TRANSITION IN FISSION YEAST

Thèse de doctorat ès Sciences de la Vie (PhD)

présentée à la

Faculté de Biologie et de Médecine
de l'Université de Lausanne

par

Cassandra KINNAER

Master diplômée de l'Université Paul Sabatier, Toulouse, France

Jury

Prof. Michel Chapuisat, Président
Prof. Sophie Martin, Directrice de Thèse
Dr Snezhana Oliferenko, Expert
Prof. Dominique Sanglard, Expert

Lausanne, 2019



UNIL | Université de Lausanne

Faculté de biologie
et de médecine

Ecole Doctorale

Doctorat ès sciences de la vie

Imprimatur

Vu le rapport présenté par le jury d'examen, composé de

Président·e	Monsieur	Prof. Michel Chapuisat
Directeur·rice de thèse	Madame	Prof. Sophie Martin
Experts·es	Madame	Dre Snezhana Oliferenko
	Monsieur	Prof. Dominique Sanglard

le Conseil de Faculté autorise l'impression de la thèse de

Madame Cassandre Kinnaer

Master en Sciences, Technologies, Santé Université Paul Sabatier / Toulouse III,
France

intitulée

Yeast-to-hypha transition in fission yeast

Lausanne, le 8 mars 2019

pour le Doyen
de la Faculté de biologie et de médecine

Prof. Michel Chapuisat

AKNOWLEDGMENTS

First and foremost, I would like to thank **Sophie** for giving me this extremely cool and challenging project. I also thank you for the general trust you entitled me with. A big thank you for the opportunity and for giving me this great life in Lausanne. I also thank you for hiring this awesome lab I call family.

I want to thank the entire team for the atmosphere not only prolific in terms of science but also for all the friendships and laughs over the years. I cherished every lame jokes and inappropriate comments I will miss you more than I can say. Un merci tout spécial à **Vincent** sans qui je me demanderais encore comment lancer une PCR et à côté de qui j'ai littéralement passé 5 années de ma vie. Qu'est-ce-qu'on aura refait le monde et rigolé. A big thank you to **Laura** for the support, technical and emotional. Every day I learn from you and I look up to you a lot. A big meow to my cat ladies **Magda** and **Veneta**, I found friends for life. I thank you for the support as well, for cheering me up when I was down, for the ladies night and for all the cat pictures. Special thanks to **Omaya** for starting this whole thing and for making me feel like I belonged since day one. Thank you to **Aleks** for being the mignonest. I thank **Serge Pelet and his lab** (past and current!) for the support over the years.

Thanks to **all the people of the DMF**, being at work was always a pleasure.

I want to thank my second lab family, the **Fungibrainers**. We had the most fun. They told us we had to network, I think we did that and more. Thank you to **Valeria** for always accepting to be my lovely roommate, **Paola** for not killing us in Aubergine and **Pat** for the wisdom of purification. Thank you to **Pavlos** for making me laugh always, thank you to Future of Science's™ **Gigi** for generally being on the receiving end of our lame jokes. I don't remember, is it something like this, but not this? Thank you to guapito **Hugo** for the story of adopting a hedgehog for the night, I'm still laughing. Thank you to **the rest of the gang** for the many memories.

Un grand merci à mes amis. **Marjorie** merci pour tout, mais surtout merci de t'être offensée que je mange seule chez moi un jour d'automne 2009. Merci de m'avoir donné un parfait petit lion à gâter et chérir. Merci à **Garance #braintwins** for life, et **Bola** pour m'accompagner encore et toujours plus loin dans divers concerts de Coldplay et autres obsessions. Merci à **Thaïs**, cat lady extraordinaire, merci pour les rires, tes dessins fabuleux et tout ce qui nous unis. Merci à **Dan** et **Claudia** pour toutes ces fondues de la bonne humeur.

Big thank you to Niantic for making sure I walk at least 50kms per week. It truly kept me sane. Thank you to **all the friends I made along the way** at ADAS, at ballet and with PoGo Lausanne.

Un grand merci à mes frères, **Robin** et **Mathias** pour me supporter dans mes lubies. Vous êtes mon cœur. Un grand merci à ma cousine **Alexandra**, mon oncle **Jean Marc** et ma tante **Patricia** pour le soutien et l'amour que vous nous apportez. Alex, on peut partir à Disney pour trois semaines maintenant. Merci à **Antonella** et **Jacques** pour leur soutien et pour m'avoir nourrie tous les dimanches soir depuis 5 ans. J'aimerais aussi remercier **Jean-Phi** pour ses ronrons incessants.

Merci à **Thomas**. Merci pour ton soutien sans failles, ton amour, les nombreuses aventures, les babiches, les chansons d'animal, les gratouilles, les pâtes aux brocolis et tout le reste.

Enfin, je remercie ma **maman** qui a toujours rêvé de faire des études mais qui n'a jamais pu. Merci pour l'effort surhumain que tu as mis dans mon éducation. Tu nous manques.

YEAST-TO-HYPHA TRANSITION IN FISSION YEAST

Cassandra Kinnaer, Département de Microbiologie Fondamentale

Scientific summary

Most cells are polarized and they adopt a wide variety of morphologies. Cell polarization relies on the deposition of polarity factors at a restricted part of the cell, allowing growth and shaping of the cell form at a very constrained spatiotemporal location. Cell functionality is fundamentally tied to cell function and we know that several diseases originate from an improper cell shape. For example, sickle cell disease arises when red blood cells are defective for cell membrane elasticity and develop an abnormal cell shape impairing their ability to move freely in the blood vessels causing severe anemia.

Some fungi have been described to inherently switch between two cell morphologies; they are called dimorphic species. Typically, these species will alternate between yeast growth and filamentous growth, characterized by a tremendously elongated and polarized cell shape called hypha. During my thesis, I studied the transition in morphology displayed by poorly studied fission yeast; *Schizosaccharomyces japonicus*. This species has been previously described to transition to filamentous growth to escape a harmful environment. In **chapter 1** of my thesis, I describe the discovery of an inducer for filamentation independent of stress, the fruit extracts. I then detail the morphological transition from cytological observation and evidence the diverging roles of the cytoskeleton in the transition. The filamentous form of *S. japonicus* is particularly interesting because it seems to diverge a lot from other filamentous species indicating a different filamentation form. For example, I showed that it did not assemble a Spitzenkörper, a vesicular structure formed by most filamentous species. During the dimorphic switch there is translation of symmetrical mode of growth embodied by the yeast morphology towards an asymmetrical system represented by the hyphal form. This transition allows for fascinating questions like, how does an asymmetrical system position nucleus or division plane? In **chapter 2**, I continued my description of this unstudied species by looking at the localization of actin based motors called Myosin V. By doing so, I uncovered an overlapping between cytoskeletal tracks and a potential alternate mechanism to move cargoes in the cell in fission yeast. Finally in **chapter 3**, I did a transcriptomic analysis of the transition from yeast to hypha to elucidate potential genes involved in the morphological switch. This work evidenced a complete rewiring of gene expression after the transition.

LA TRANSITION DE LEVURE A HYPHE CHEZ LA LEVURE FISSIPARE

Cassandra Kinnaer, Département de Microbiologie Fondamentale

Résumé scientifique

Dans le règne du vivant, les cellules adoptent une multitude de morphologies diverses et variées. Ce processus de polarisation cellulaire dépend de la déposition de facteurs de polarité à un endroit très précisément défini de la cellule afin de limiter la croissance cellulaire dans le temps et l'espace. Le bon fonctionnement d'une cellule est directement dépendant de sa forme et plusieurs pathologies humaines qui découlent d'une morphologie cellulaire anormale sont connues. Par exemple, la drépanocytose est due à une baisse d'élasticité de la paroi cellulaire, ce qui entraîne une morphologie altérée de la cellule, une mauvaise circulation des globules rouges dans le système sanguin et une anémie très sévère.

Certains champignons sont capables d'alterner entre deux types de morphologie cellulaire dans leur cycle de vie, on parle alors d'espèces dimorphiques. Typiquement, ces espèces vont alterner entre une morphologie de type levure et de type filamenteuse, c'est-à-dire une cellule très allongée et polarisée aussi appelée hyphe. Pendant ma thèse, j'ai étudié la transition dimorphique observée chez une levure fissipare très peu étudiée, *Schizosaccharomyces japonicus*. Cette espèce a tendance à former des hyphes pour s'échapper d'un environnement peu favorable. Dans le **chapitre 1** ma thèse, je décris la découverte d'un inducteur sans stress de la transition dimorphique, les extraits de fruits. Je décris ensuite en détails la transition cytologique observée en présence de cet inducteur et je mets en évidence les rôles divergents du cytosquelette. La forme filamenteuse de *S. japonicus* est particulièrement intéressante parce qu'elle apparaît très différente de ce qui est observé dans d'autres espèces, indiquant qu'un mode de filamentation alternatif est possible. Par exemple, j'ai montré que cette espèce n'assemble pas une structure vésiculaire formée par la plupart des espèces filamenteuses : le Spitzenkörper. La transition morphologique chez *S. japonicus* s'accompagne aussi du passage d'un système de croissance symétrique à asymétrique, ce qui m'a permis d'aborder des questions d'ordre très fondamental concernant le positionnement du site de division ou du noyau cellulaire. Dans le **chapitre 2**, j'ai poursuivi ma description du cytosquelette en analysant la localisation de moteurs d'actine, les myosines de type V, et ai mis en évidence l'existence d'une potentielle coopération entre les câbles du cytosquelette dans les levures de fission afin de bouger des vésicules de transport dans la cellule. Enfin, dans le **chapitre 3**, afin de mieux comprendre les bases génétiques de cette transition, j'ai aussi effectué une étude transcriptomique lors du changement de forme cellulaire. Ce travail a notamment mis en évidence un réarrangement total de l'expression génique lors de la transition.

LA TRANSITION DE LEVURE A HYPHE CHEZ LA LEVURE FISSIPARE

Cassandra Kinnaer, Département de Microbiologie Fondamentale

Résumé Grand Public

L'unité de base du vivant connu est la cellule. Dans le règne du vivant, les cellules adoptent une multitude de formes diverses et variées, qui correspondent à leur fonction cellulaire. Le bon fonctionnement d'une cellule est directement dépendant de sa morphologie et plusieurs pathologies humaines qui découlent d'une morphologie anormale de cellules sont connues. Par exemple, la drépanocytose est due à une morphologie cellulaire altérée qui entraîne une mauvaise circulation des globules rouges dans le système sanguin et cause une anémie très sévère.

Certaines espèces de champignons sont capables de changer de morphologie cellulaire dans certaines circonstances. Pendant ma thèse, j'ai étudié l'une de ces espèces, une levure fissipare, ou levure de fission, appelée *Schizosaccharomyces japonicus*. Elle alterne entre une morphologie de levure de fission, c'est-à-dire une morphologie de petits cylindres microscopiques et une morphologie d'hyphe qui correspond à une forme cylindrique beaucoup plus allongée qui peut atteindre le millimètre. Mon travail de thèse visait à décrire le plus précisément possible cette transition de forme cellulaire. Nous avons d'abord découvert une nouvelle méthode d'induction de cette transition, en effet *S. japonicus* forme des hyphe en grandissant en présence de jus de raisin. J'ai décrit le changement de localisation du cytosquelette et de diverses autres protéines. La transition morphologique chez *S. japonicus* s'accompagne aussi du passage d'un système de croissance symétrique à asymétrique, ce qui m'a permis d'aborder des questions d'ordre très fondamental concernant le positionnement du site de division ou du noyau cellulaire. Afin de mieux comprendre les bases génétiques de cette transition qui est mal connue dans cet organisme, j'ai aussi effectué une étude transcriptomique lors du changement de forme cellulaire. Ce travail a notamment mis en évidence un réarrangement total de l'expression génique lors de la transition.

En résumé mon travail de thèse offre une description d'un processus important de la vie cellulaire dans une espèce très largement méconnue.

Table of Contents

Introduction.....	3
Chapter 1: Yeast-to-hypha transition in <i>Schizosaccharomyces japonicus</i> in response to environmental stimuli.....	20
1.1. Introduction.....	22
1.2. Results	23
1.2.1. Fruit extracts induce filamentation in <i>Schizosaccharomyces japonicus</i>	23
1.2.2. The yeast-to-hypha transition involves extreme vacuolization and dramatic increase in cell size.....	25
1.2.3. <i>S. japonicus</i> does not assemble a classical Spitzenkörper	27
1.2.4. Actin based trafficking is increased in the hyphal form and is essential for the transition	28
1.2.5. Microtubules are dispensable for polarized growth of <i>S. japonicus</i>	30
1.2.6. <i>S. japonicus</i> hyphae display complete cell divisions and altered growth controls	32
1.2.7. Highly asymmetric cell division of a fission yeast in <i>S. japonicus</i>	34
1.3. Discussion	37
1.3.1. A mycelium formed of single cells.....	37
1.3.2. Asymmetrical division in fission yeasts	39
1.3.3. Size control	40
1.4. Materials and Methods	42
Chapter 2: Myosin V localization in <i>S. japonicus</i>	57
2.1 Introduction.....	58
2.2 Results	59
2.2.1 Myosin-V in <i>S. japonicus</i>	59
2.2.2 Colocalisation study in fission yeast.....	61
2.3 Discussion & perspectives	64
2.3.1. A cooperation between actin and microtubules?	64
2.3.2. Is Myo52 essential in <i>S. japonicus</i> ?	65
2.4 Material and Methods.....	66
Chapter 3: Transcriptome analysis of the yeast-to-hypha transition in <i>Schizosaccharomyces japonicus</i>	67
3.1. Introduction.....	68
3.2. Results	71
3.2.1. Solid-to-solid induction of hyphal growth.....	71
3.2.2. A protocol for robust RNA extraction from cells embedded in agar.....	72

3.2.3. mRNA sequencing and sequencing data analysis	74
3.2.4. Statistical analyses.....	74
3.2.5. Early timepoints analysis	76
3.2.6. Late timepoint analysis.....	80
3.2.7. Deletions of genes of interest and phenotype assessment	81
3.2.8. RGE does not trigger an oxidative stress response	87
3.3. Discussion and perspectives.....	89
3.4. Material and Methods.....	91
General conclusions and perspectives	93
References.....	95
Annexes	104

Introduction

From star shaped neurons to simpler rod shaped yeast, cells come in a wide variety of morphologies. Polarization at the cellular level is defined as the asymmetry in distribution of functions or components within the cell. Cell polarization is an essential process of life governing a wide range of functions such as cell motility, cell differentiation and cell transport. Cell morphology is directly correlated to an asymmetry in distribution of polarity factors within the cell to target and restrict cell growth to a specific location.

Such processes can be quite intricate to study in animals both due to the scale of their multicellularity and the harrowing complexity of their diverse cell shapes. The field of cell polarity relies on certain fungi as models. Fungi represent one of the most diverse branch of the tree of life with an estimated 2 to 4 million species with only 120 000 currently described (Choi and Kim, 2017; Hawksworth and Lucking, 2017). They diverged from the metazoan branch about 1.5 billion years ago (Wang et al., 1999) (**Fig. 1.1**).

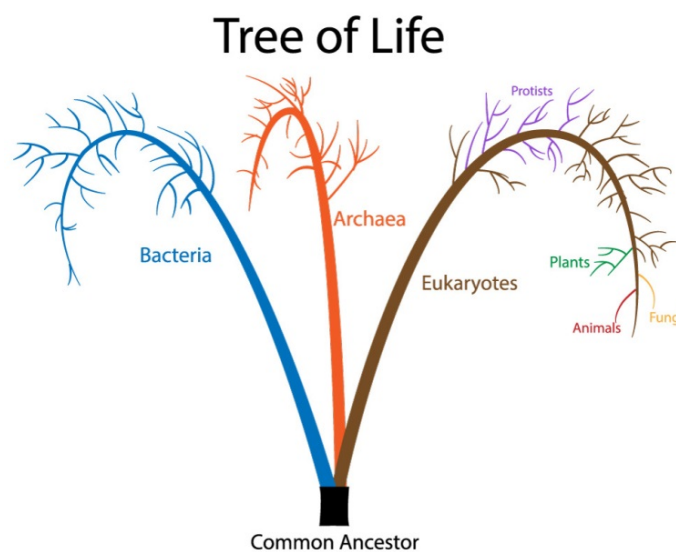


Figure 1.1. Tree representing the three branches of life.

Source: <https://mrrittner.weebly.com/unit-3-the-cell.html>

The last common ancestor between fungi and animals is commonly thought to have been an aquatic unicellular flagellated eukaryote that was roaming the ocean in the Proterozoic earth (King, 2004). Interestingly, fungi seem to be genetically closer to animals than to the plants they were once classified with. Fungi are generally described as heterotroph eukaryotes that contain chitin in their cell wall, and which are unable to photosynthesize due to the absence of chloroplasts. Fungi can reproduce both sexually and asexually and can display very intricate and complex lifecycles. Most species grow predominantly as hypha, a very polarized and elongated tubular cell that can branch and fuse with other hyphae creating an incredibly complex multicellular network called a mycelium.

However, some species can be morphologically very distinct and grow as unicellular yeast. Other species can exhibit the two lifestyles and these are called dimorphic organisms. Filamentous species can display a wide variety of morphological features, for example some can produce septate or aseptate (or coenocytic) hyphae, controlling the level of interconnectedness displayed by the mycellium. Fungi in their mycelial form are multicellular. Interestingly, multicellularity evolved several times in eukaroytes (Parfrey and Lahr, 2013). Fungi evolved it in parallel of the animal branch, in a convergent evolutionary process probably triggererd by similar environemental pressure. The extreme apical growth displayed by filamentous fungi is tremendously useful to study polarisation processes. Moreover, dimorphic species are of particular interest; their alternance in growth types provides a particularly useful set up for comparison purposes.

Phylogeny of fungi

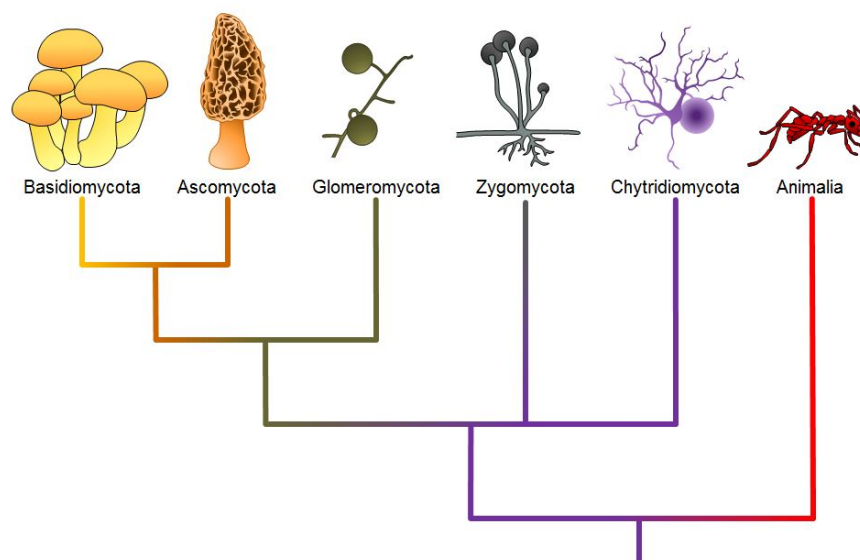


Figure 1.2. Tree representing the five main phyla of fungi and the animal branch. Separation between animal and fungi date back 1.5 billion years ago. **Source:** OpenStax Biology 2nd Edition.

Establishing phylogeny for fungi is tricky due to the lack of fossil record and absence of clear common phenotypical traits. One way to classify them is to combine a sequence homology approach and biological observations made about the reproduction mode of the concerned species. In doing so, five main phyla distinguish themselves; the Chytridiomycetes, Zygomycetes, Glomeromycetes, Basidiomycetes and Ascomycetes (**Fig. 1.2**).

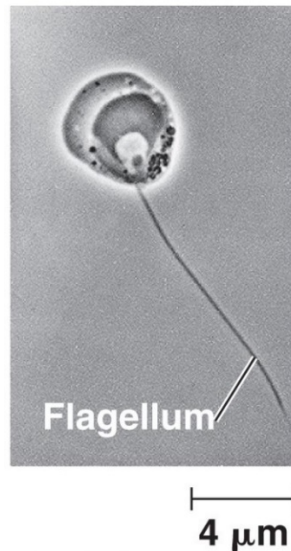


Figure 1.3. Microscopy image of a sexual flagellated spore from the Chytrid family.

The Chytrids are an early-diverging lineage that presumably branched out over 500 million years ago and they are the only fungi to have retained flagellar motility from the last eukaryotic common ancestor (**Fig. 1.3**). Chytrids are mostly unicellular but some can be multicellular and form a coenocytic mycelium. They can be pathogenic, a famous example being *Batrachochytrium dendrobatidis* which contributed greatly to the worldwide amphibian population decline observed since the 1980s (Lips et al., 2006).

The Zygomycetes are a small family whose most famous member is *Rhizopus stolonifer* or the bread mold, is known for being the most often culprit for kitchen and fridge contaminations. They reproduce sexually and asexually and form a sporangium (**Fig. 1.3**). They produce a vast coenocytic mycelium.



Figure 1.4. Microscopy image of sexual sporangia filled produced by *Rhizopus stolonifer*.

Source: Eric McKenzie, PaDIL.

The Glomeromycetes are a poorly studied branch of fungi. It contains 230 species, most of which form symbiosis with the root of plants forming arbuscular mycorrhizae. The coenocytic hyphae of

these species penetrate the cortical cells of roots in a highly developed mutualistic symbiosis. Members of this family reproduce asexually by forming glomerospores at the hyphal tips but recent studies showed that some species contained the necessary genes for meiosis underlying the fact that they probably have a cryptic sexual cycle as well (Halary et al., 2011).

The Basidiomycetes, or club fungi, is the branch containing most the mushrooms. They are easily recognizable thanks to their club-shaped fruiting body, the basidium. They can have both a sexual and an asexual cycle, with the sexual cycle being apparently predominant in their life cycle. In their sexual cycle, they form septate hyphae which will meet and fuse with the opposite mating type to form a “dikaryon” mycelium which will contain the haploid nuclei of both mating, unfused until the emergence of a terminal structure called the basidium. After meiosis, the spores will be released from the fruiting body.

The Basidiomycetes also contain species that grow as unicellular yeasts (ex. *Cryptococcus neoformans*) or dimorphic fungus (ex. *Ustilago maydis*, see **Fig. 1.5**).

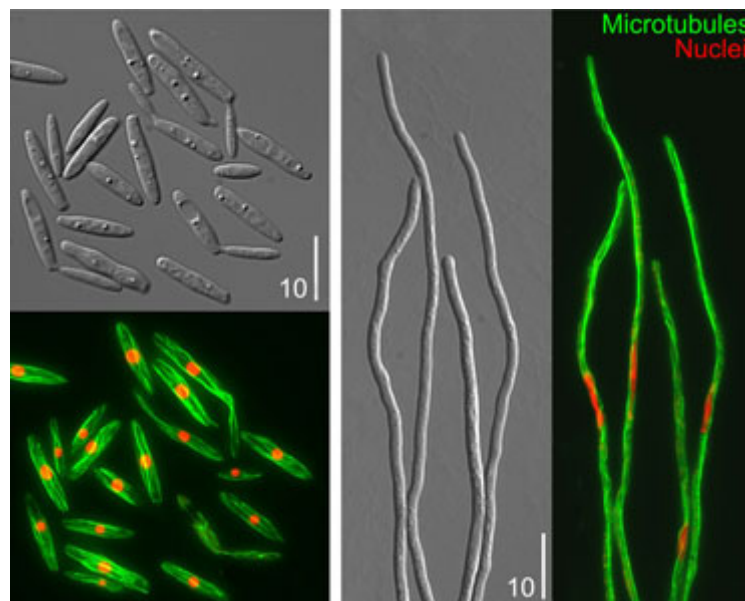


Figure 1.5. *Ustilago maydis* grows as yeasts (left) or hyphae (right) (taken from: (Steinberg and Perez-Martin, 2008)).

The Ascomycetes is a sister phylum to the Basidiomycetes and both branches are referred to as Dikarya due to the state of two unfused haploid nuclei found in some of their species sexual cycles. Ascomycetes contain most of the known fungal species (over 64 000) and they can be filamentous, unicellular or dimorphic. Filamentous species tend to produce septate hyphae. Ascomycetes are sometimes referred to as the sac fungi due to the appearance of the terminal structure containing the newly formed spores after the sexual cycle; the ascus. Ascomycetes asexual cycle is predominant

and very diverse, yeasts can divide by medial fission (Schizosaccharomycetes) or budding (Saccharomycetes) and filamentous species produce spores from conidiophores, specific asexual structures generally formed at hyphal tips. The sexual cycle of Ascomycetes is also very varied and complex but the meiotic products (typically four to eight spores) are always present in a terminal structure called the ascus. Sexual reproduction can occur between homothallic and/or heterothallic partners depending on the species. We have not identified a sexual cycle for all species and one example is *Aspergillus niger* who seem to only reproduce asexually.

It is interesting to note that yeasts appear in both the Saccharomycetes and the Schizosaccharomycetes families but their last common ancestor is thought to have been filamentous underlying the convergent evolution that occurred in parallel in both branches to regain unicellularity and it is probably due to similar environmental pressure and adaptation to a partial or total aquatic lifestyle (Berbee and Taylor, 1993).

Fission yeasts

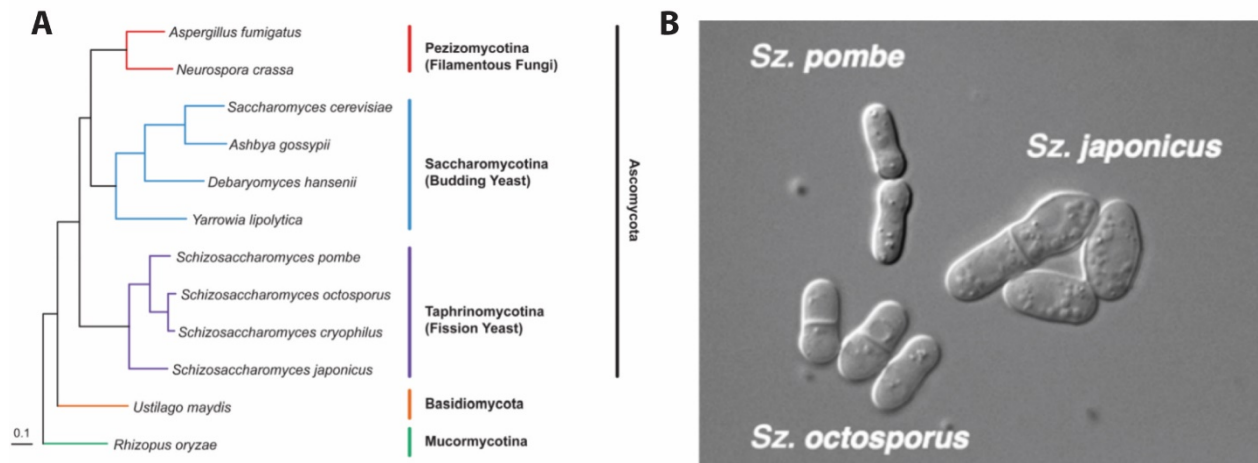


Figure 1.7. (left) Phylogenetic analysis of 12 species across the fungal tree. (right) Microscopy image of a fission yeast co-culture (*S. pombe*, *S. japonicus* and *S. octosporus*).

Source: (Rhind et al., 2011)(left) and Broad Institute (right) but taken from: (Niki, 2014).

Schizosaccharomycetes are also known as fission yeasts, because they grow as rod-shaped yeasts and they belong to the Ascomycetes phylum. During vegetative growth, they grow from the cell poles, divide in the cell middle to give rise to two daughter cells of equal sizes. There are four known members in the family; *Schizosaccharomyces pombe*, *Schizosaccharomyces japonicus*, *Schizosaccharomyces octosporus* and *Schizosaccharomyces cryophilus* (**Fig. 1.7A; B**). *S. pombe* is by far the most studied organism of the family and is a well-established model organism in the cell cycle (Nobel Prize of Medicine, 2001) and cell polarity fields. *S. cryophilus* was isolated recently as being a contaminant from a *S. octosporus* culture, they are closely related to each other and probably diverged last (Helston et al., 2010; Rhind et al., 2011). In the phylogenetic tree, the most distant cousin of the family is *S. japonicus* who diverged from the fission yeast common ancestor 220Mya (Rhind et al., 2011) possibly retaining some features from ancestral fission yeasts. Fission yeast sexual cycle gives rise to asci containing 4 or 8 spores depending on the species. *S. pombe* produces a 4-spores ascus while the other three species produce 8 spores per meiotic round. These asci are easily isolated and readily dissectible providing great terrain for genetic investigations.

Cell polarization in *S. pombe*

Fission yeast *S. pombe* has been used for decades in the field of cell polarity because of its simpler cell shape and ease of handling (reviewed here (Martin and Arkowitz, 2014)). Polarized secretions of vesicles targeted for exocytosis at the cell poles ensures growth through the long axis and a constant diameter throughout the life cycle. Cytoskeletal tracks and their associated motors move cargo in the cells providing membrane influx as well as enzymes to remodel the cell wall and permit growth. During mitosis *S. pombe* stops growth, and after medial fission, cells will resume growth but at first, only at the old cell pole. Only after a process named New End Take Off, or NETO, can they start growing in a bipolar fashion (Martin, 2009; Martin and Chang, 2005; Mitchison and Nurse, 1985) (**Fig. 1.8**).

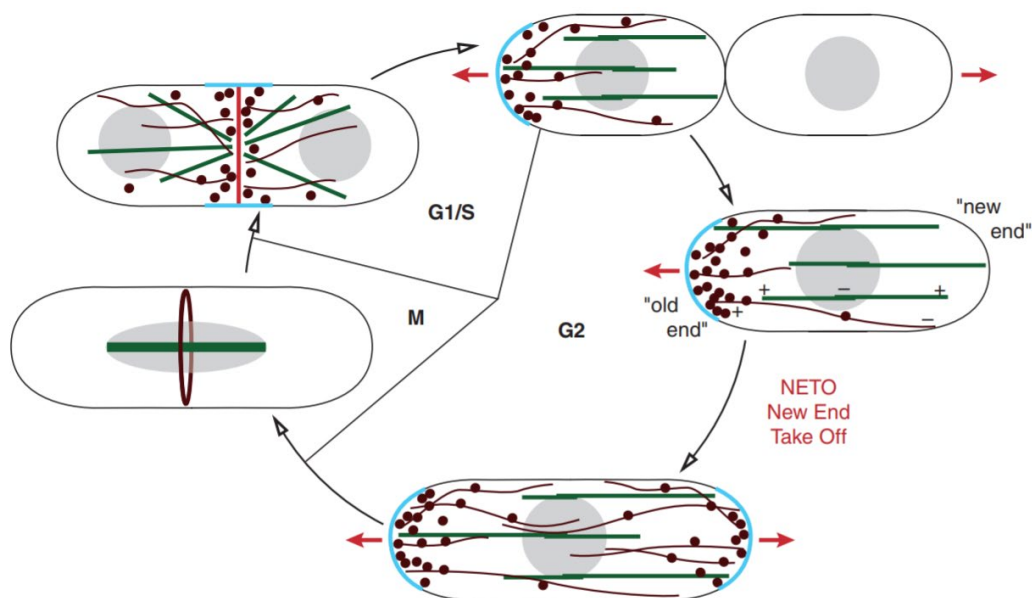


Figure 1.8. Asexual cell cycle of *S. pombe* showing growth patterns. After mitosis and medial fission, growth (blue) resumes at the old cell pole. In G2 phase, cytoskeletal reorganization will permit growth at the newly formed cell end, in a process called NETO. The actin patches (dots) and cables are noted in brown and microtubules tracks are in green. (taken from (Chang and Martin, 2009))

Microtubules are present in bundles in the cytoplasm across the long axis of the cell. They are highly dynamic on their plus end tip, oriented towards the cell poles and stable on their minus end tip, on the nuclear membrane (Hagan, 1998). They deposit the cell end markers Tea1 and Tea4 to label the cell pole as a growth site. Tea4 will recruit formin For3, which will in turn nucleate actin cables activating polarized exocytosis and effectively start cell growth at the new end (Martin and Chang, 2005) (**Fig. 1.9**). For3 is a nucleator of actin cables that is implicated in polarized processes (Feierbach and Chang, 2001; Nakano et al., 2002)

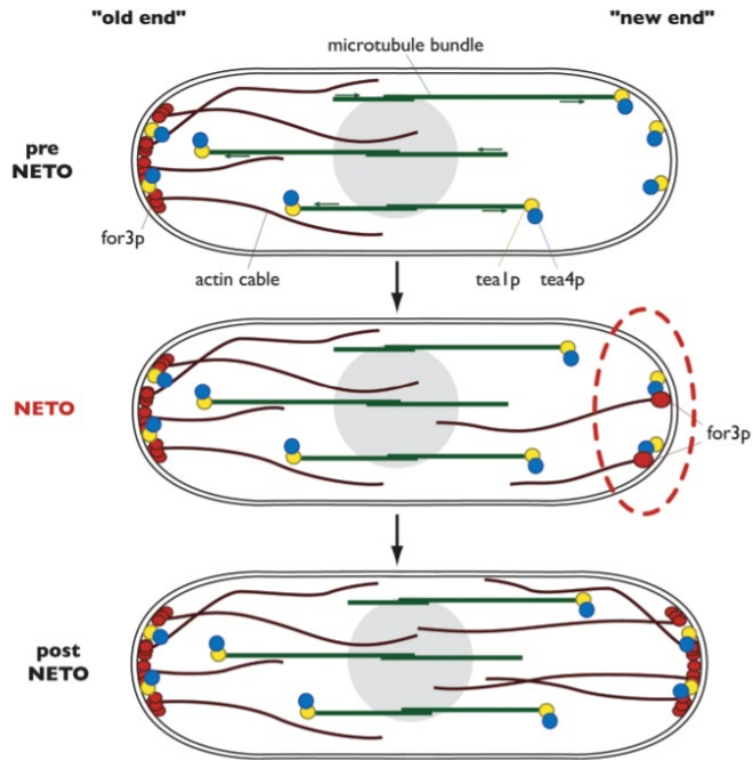


Figure 1.9. Deposition of polarity proteins Tea1/Tea4 by the microtubules will recruit Formin For3 and initiate actin cable polymerization. (taken from (Martin and Chang, 2005))

Actin is necessary for cell polarization and is present in several structures in the cells; actin patches which are necessary for endocytosis, actin cables which provide tracks to move cargo in the cell and actin rings at the division plane for cytokinesis (Kovar et al., 2011) (**Fig. 1.10**). Myosins are motors that operate on actin tracks and several classes with different functions exist (Woolner and Bement, 2009). Two type-V myosins have been identified in *S. pombe*. Myosin 51 does not actively participate in growth but is involved in cytokinetic ring formation (Wang et al., 2014) while Myosin 52 mediates polarized secretion of exocytic vesicles (Lo Presti and Martin, 2011; Motegi et al., 2001; Win et al., 2001). Deletion of Myo52 in *S. pombe* yields dramatic growth defects (Motegi et al., 2001; Win et al., 2001).

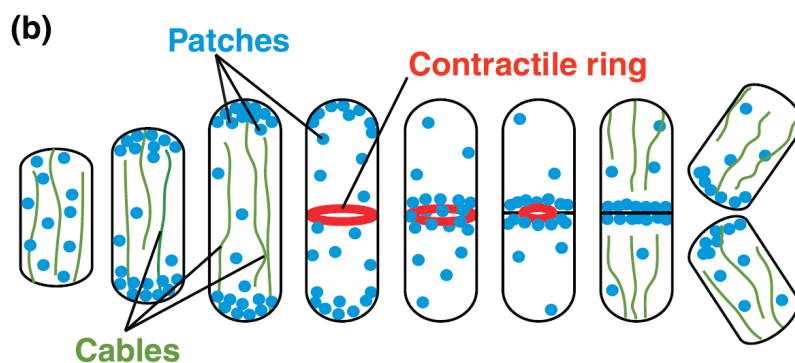


Figure 1.10. Actin organization in *S. pombe* (taken from: (Kovar et al., 2011)).

Signaling of polarization in *S. pombe* is dictated at the upstream level by a conserved Rho GTPase called Cdc42. Rho GTPases are at the core of polarity processes in most eukaryotes (Bi and Park, 2012; Etienne-Manneville, 2004; Park and Bi, 2007). They can fluctuate between an activated, GTP-bound state and an inactivated GDP-bound state. Inhibitors of Rho GTPases are called GAPs (GTPase-activating proteins) and three have been identified in *S. pombe* Rga3, Rga4 and Rga6 (Gallo Castro and Martin, 2018; Revilla-Guarinos et al., 2016; Tatebe et al., 2008). On the other hand activators of Rho GTPases are called GEFs (Guanine nucleotide exchange factors) and two were described in *S. pombe* namely Gef1 and Scd1. (Coll et al., 2003; Hirota et al., 2003). Cdc42 is essential and the use of conditional allele revealed severe polarity phenotypes with isotropic growth (Miller and Johnson, 1994). Studies have shown that the active form of Cdc42 oscillates in localization between the two growing poles during bipolar growth indicating a very dynamic process and the existence of positive and negative feedbacks dictating active Cdc42 localization (Das et al., 2012) (**Fig. 1.11**).

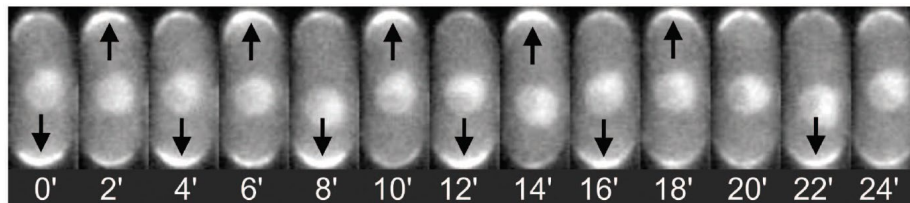


Figure 1.11. Oscillations of the localization of active Cdc42 (CRIB-GFP probe) during cell growth (taken from: (Das et al., 2012)).

Interestingly, *S. pombe* possesses a parallel morphogenesis pathway with polarized secretions in an actin-independent manner through the exocyst system. Both systems are controlled upstream by Cdc42. (Bendezu and Martin, 2011; Martin et al., 2007).

While microtubules contribute to cell polarization by delivering cell end markers at the cell poles they are not directly involved in polarized growth in *S. pombe* (**Fig. 1.8; 1.9**) (Martin, 2009). Although interestingly, re-routing of actin based transport on to microtubules is sufficient to target polarity proteins at the cell tips and maintain cell polarity (Lo Presti and Martin, 2011). Microtubules however play a major role in nuclear positioning. Fission yeasts place their nuclei in the cell middle and this is achieved through pushing forces exerted by the microtubules on the cell poles and the nucleus itself, effectively centering it (Daga et al., 2006). Nuclear positioning will in turn dictate the placement of the medial division plane (Tolic-Norrelykke et al., 2005) through the positive signaling of an anillin-like protein called Mid1 (Sohrmann et al., 1996), which shuttles in and out of the nucleus and positions cortical nodes at the future location of the septum. Association of Mid1 to the plasma membrane depends in part on kinase Cdr2 (Almonacid et al., 2009). DYRK kinase Pom1 forms gradient at the cell tips and inhibits septation at the cell poles (Huang et al., 2007; Padte et al., 2006; Rincon et al., 2014) (**Fig. 1.12**).

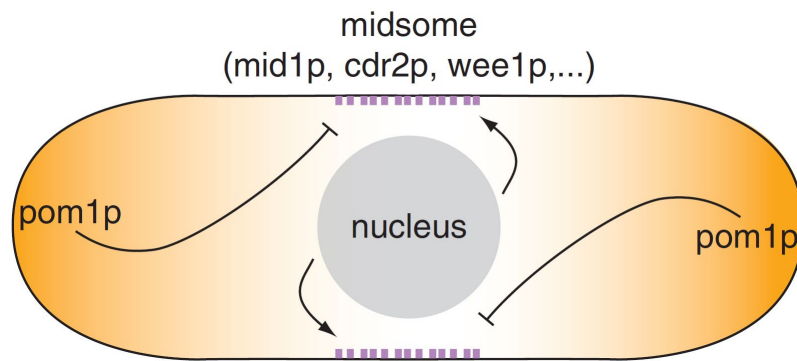


Figure 1.12. Players involved in septum positioning in *S. pombe* (taken from (Chang and Martin, 2009)).

Microtubule shrinking and growing is controlled by two main stabilizers called Tip1 (CLIP170 homolog) and Mal3 (EB1 homolog) (Brunner and Nurse, 2000; Busch and Brunner, 2004). Deletion of either promotes microtubule catastrophe and cells harbor shorter microtubules bundles.

Another aspect of growth of yeast cells must take into account the tremendous turgor pressure they are subjected to and how that may be involved in growth mechanisms (Minc et al., 2014).

Polarization processes in filamentous fungi

The most striking even of growth as hyphae is the dramatic elongation of the cell size. Filamentous fungi grow through fast cell tip expansion; the process is continuous and uncoupled with cell cycle, unlike what we have described in the previous paragraph for fission yeast (Riquelme et al., 2003). To accommodate with filamentous growth, cells must bring lipids and cell wall synthases to sustain cell growth and remodel the cell wall. Efficient polarized secretion of vesicles is essential. Actin localizes as rings, cable and patches in the cell. At the hyphal tips, there is an accumulation of actin patches and cables (Berepiki et al., 2011) (**Fig. 1.13**).

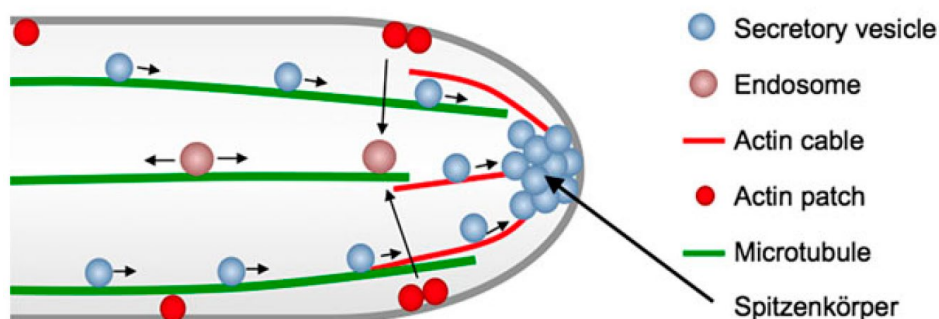


Figure 1.13. Hyphal tip organization of *Aspergillus nidulans* (taken from: (Takeshita, 2016)).

Interestingly, filamentous fungi like *Aspergillus nidulans* only produces a single formin (Gladfelder, 2006; Harris et al., 1997), and actin cables are generally difficult to observe. However, actin cables

are essential for polarized growth (Berepiki et al., 2011; Harris et al., 1997; Torralba et al., 1998). Studies of the deletion of actin based motors MyoV in *A. nidulans* and *U. maydis* (Taheri-Talesh et al., 2012; Weber et al., 2003) yielded polarity phenotypes with respectively issues in hyphal morphology and improper dimorphic switch.

Cdc42 is involved in the polarization processes of the following species, *Candida albicans* (Bassilana et al., 2003), *Penicillium marneffei* (Boyce et al., 2003), *Ustilago maydis* (Mahlert et al., 2006), *Aspergillus nidulans* (Virag et al., 2007) and *Aspergillus niger* (Kwon et al., 2011).

Evidences of oscillatory mechanisms controlling growth have been evidenced in *A. nidulans* and *N. crassa* with Ca^{2+} pulses at the growing tip possibly synchronizing vesicle exocytosis (Silverman-Gavrila and Lew, 2003; Takeshita et al., 2017) reminiscent of the oscillatory behavior of Cdc42 activation in fission yeast (**Fig. 1.11**).

Interestingly, the core mechanisms of cell end marking and growth site selection appear to be maintained in *A. nidulans* (**Fig 1.14**), and homologs of the Tea complex have been identified (reviewed here: (Fischer et al., 2008)). Perturbations of the Tea complex leads to hyphal morphology defects like highly curved hyphae and “zigzag” hyphae (Fischer et al., 2008; Konzack et al., 2005; Takeshita et al., 2008).

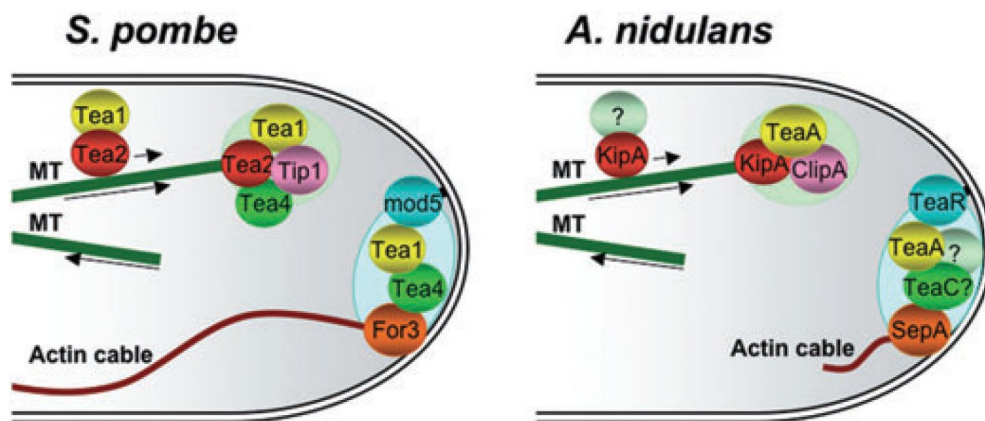


Figure 1.14. Cell end marking for growth initiation in species *S. pombe* and *A. nidulans*. Homologs of Tea1/Tea2/Tea4 and the formin For3 have been identified (taken from: (Fischer et al., 2008)).

Microtubules localize along the long axis of the cell (**Fig. 1.15**). The role of microtubules in polarization processes is a little more controversial with conflicting reports on their role in hyphal tips extension in the dimorphic yeast *Candida albicans* (Akashi et al., 1994; Yokoyama et al., 1990). Some filamentous fungi seem to compensate their less developed actin cytoskeleton by relying on the microtubules for transport. In *A. nidulans*, disruption of the microtubule cytoskeleton with drug

treatment caused a reduction of 10 times of the hyphal growth rate (Horio and Oakley, 2005). Moreover, deletion of microtubule based motor kinesin-1 in several species caused defects in hyphal growth rate (Requena et al., 2001; Schuchardt et al., 2005; Seiler et al., 1997). These findings evidence the potential role of microtubules as tracks for long range transport of polarity components.

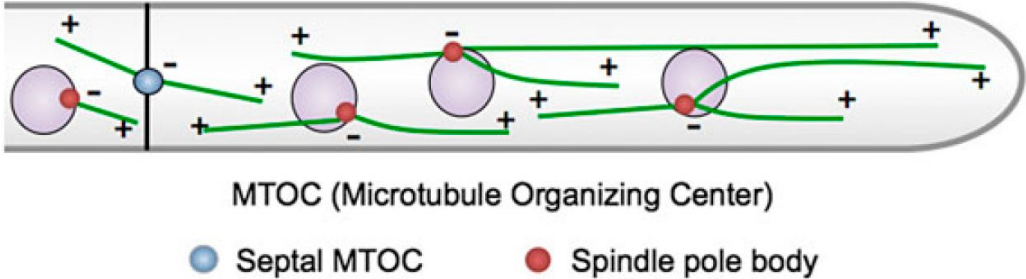


Figure 1.15. Microtubule organization in *A. nidulans* (taken from: (Takeshita, 2016)).

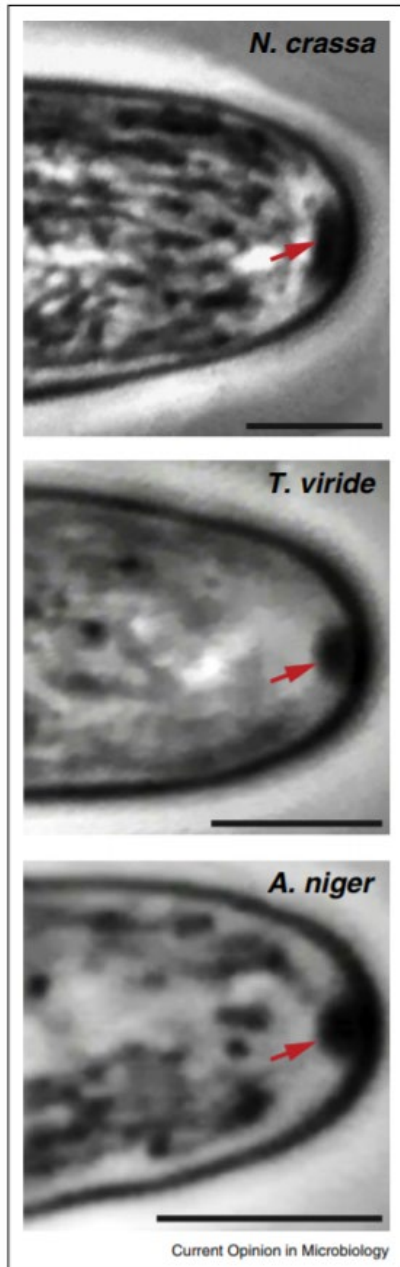


Figure 1.16. Hyphal tips of several filamentous fungi looked under phase contrast microscopy. The phase dark accumulation is the Spitzenkörper (taken from: (Riquelme and Sanchez-Leon, 2014))

Microtubules are also involved in the proper positioning of the Spitzenkörper, literally translating as “apical body”. This structure was identified in 1957 at the hyphal tips of the filamentous species *Polystictus versicolor* (Girbardt, 1957). This fungal specific organelle is composed of an accumulation of vesicles in a spherical structure positioned at the growing tip (Fig. 1.13). It dictates hyphal growth speed and directionality potentially by controlling in time and space the exocytic events at the cortex (Harris et al., 2005; Riquelme et al., 2018; Riquelme et al., 1998; Riquelme and Sanchez-Leon, 2014; Virag and Harris, 2006). It is observable under phase contrast microscopy conditions as a phase-dark object (Fig. 1.16) (Riquelme and Sanchez-Leon, 2014) and by fluorescent labelling using either endocytic dyes like FM4-64 (Fischer-Parton et al., 2000) or tagging the vesicles directly (Sanchez-Leon et al., 2015). The Spitzenkörper is present in most filamentous fungi of the Ascomycetes and Basidiomycetes and generally absent from earlier lineages of fungi (Grove and Bracker, 1970). However, studies showed that Zygomycetes specie *Conidiobolus coronatus* (Fisher et al., 2018) and Chytrid *Allomyces macrogynus* (Vargas et al., 1993) also assembled a Spitzenkörper. Studies have reported that the presence of a

Spitzenkörper is correlated with an increased in growth rate (Fisher et al., 2018; Kohli et al., 2008). Spitzenkörper was absent or unstable in kinesin-1 deletions in several species indicating a vital role of the microtubule tracks for Spitzenkörper formation and maintenance (Lehmler et al., 1997; Seiler et al., 1997).

Work initiated in *N. crassa* suggests the Spitzenkörper possibly interplays with other polarity systems namely the polarisome and the exocyst at the hyphal tips (Araujo-Palomares et al., 2009; Fischer et al., 2008; Riquelme et al., 1998; Riquelme and Sanchez-Leon, 2014). The details of how the different systems might communicate which each other are still under investigation. (Fig. 1.17)

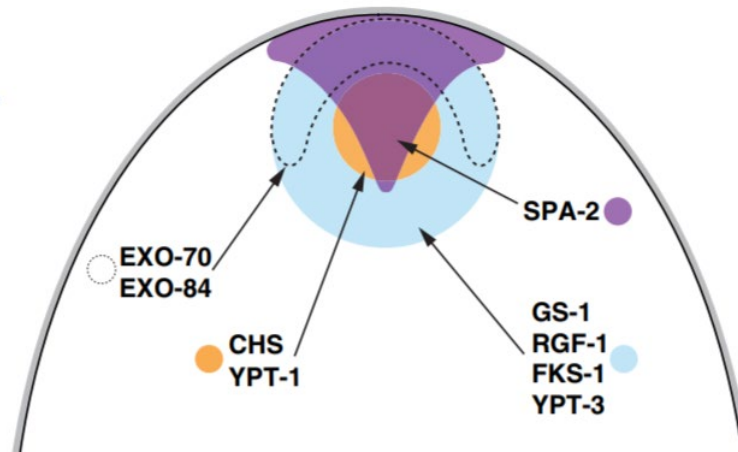


Figure 1.17. Polarity components located at the hyphal tips in *N. crassa*. Polarisome is in purple, SPK in orange and blue and the exocyst is circled with a dotted line (taken from: (Riquelme and Sanchez-Leon, 2014)).

Microtubules are involved in nuclear division but also nuclear positioning in filamentous fungi. Dimorphic or filamentous species are generally multinuclear and they must space out their nuclei evenly in the mycelium. In both *A. nidulans* and *N. crassa*, mutants with abnormal nuclear positioning have been identified and the genes affected are generally coding either for microtubule based dynein or its regulator, dynactin (Minke et al., 1999; Xiang et al., 1994; Xiang and Fischer, 2004). This indicates nuclei might migrate on the microtubule tracks to catch up with the incessant and continuous tip growth (Fig. 1.18).

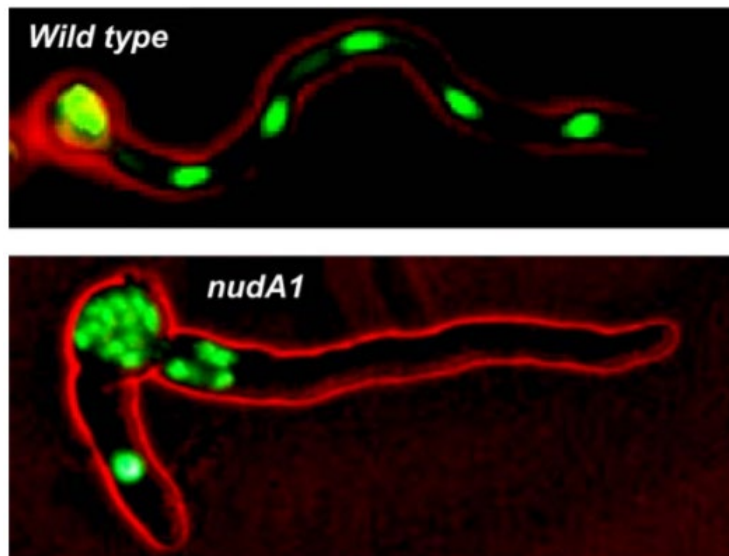


Figure 1.18. NudA1, carrying a mutation in the heavy chain of dynein shows abnormal distribution of nuclei (in green) in the cytoplasm, when compared to wild type cells (taken from: (Xiang and Fischer, 2004)).

Hyphal growth is also correlated with the apparition of vacuolated compartments in filamentous species (Gow and Gooday, 1982b; Weber, 2002). It is believed they contribute to growth through turgor pressure, and the impairment of vacuolar biogenesis provokes issues in hyphal growth and substrate invasion (Johnston et al., 2009; Johnston et al., 2013).

Dimorphism triggers and control

Dimorphism is triggered by a wide variety of conditions like change in pH or temperature, nitrogen or nutrient starvation, and the presence of serum or cAMP in the growth media to name a few (Cao et al., 2007; Cullen and Sprague, 2012; Martin et al., 2013a; Sanchez-Martinez and Perez-Martin, 2001).

Transduction of dimorphism and filamentation signals is dependent on conserved cascades, one of which is the Mitogen Activated Protein Kinase (MAPK) pathway. *Saccharomyces cerevisiae* can trigger pseudohyphal growth in different conditions and the MAPK has been extensively studied in this organism (reviewed here: (Cullen and Sprague, 2012)). A well described downstream event in the activation of the different cascades is the regulation of Flo11, a protein involved in flocculation that is essential to pseudohyphal growth and media invasion in this species (Lo and Dranginis, 1998).

***S. japonicus* as a model to study dimorphic transition**

S. japonicus is the earliest diverging species of the fission yeast clade (Rhind et al., 2011). It was initially isolated from strawberries by a Japanese team in the 1920's (Yukawa and Maki, 1931). A decade later, an American team isolated a variant named *versatilis* from home canned grape juice (Klar, 2013; Wickerham and Duprat, 1945). Fruit extracts therefore potentially represent a natural habitat for this yeast. This species was immediately characterized as dimorphic (Wickerham and Duprat, 1945; Yukawa and Maki, 1931) and alternating between fission yeast and vegetative filamentous growth. While this species is not extensively studied, a few triggers for the dimorphic switch have already been identified. Initial reports described nutrient and nitrogen starvation as inducers of the filamentation process (Sipiczki et al., 1998b). Recently, DNA damage through the action of Camptothecin (CPT) was also reported to trigger hyphal growth (Furuya and Niki, 2010; Furuya and Niki, 2012). These three methods of induction are stressful conditions, yeasts are immobile and triggering filamentation might represent a way to flee from harmful environment. *S. japonicus* transition to invasive growth is more readily achieved on solid substrate, but one recent study states serum (Fetal Bovine Serum) can induce filamentation in liquid (Papp et al., 2014). On the other hand, hyphae can also revert back to yeast growth. It was shown that both light and temperature can synchronize successive mitotic rounds and effectively break down the hyphal form into yeasts (Okamoto et al., 2013; Sipiczki et al., 1998b). Interestingly, *S. japonicus* possesses two white-collar receptors sensitive to blue light ranging from 470nm to 520nm (Okamoto et al., 2013). This is a fascinating finding as other filamentous fungi like *N. crassa* and *A. nidulans* present orthologs of those genes and can also react to light (Fuller et al., 2015). Caffeine and cAMP are also negative regulators of filamentation (Sipiczki et al., 1998a), the latter contrasting with dimorphic yeast *C. albicans* in which filamentation is promoted by cAMP (Bahn and Sundstrom, 2001). The dimorphic switch of *S. japonicus* in nutrient starvation conditions involves monopolar elongation of the cells, branching and vacuolization at the non-growing part of the cell (Sipiczki et al., 1998a). Recent work implicated the dependence on Cdc42 and regulator Ras1 for filamentation in this species (Nozaki et al., 2018). Random mutagenesis studies isolated mutants incapable of hyphal growth, they typically showed defects in polarization and vacuolization (Bozsik et al., 2002; Enczi et al., 2007).

Dimorphism is usually linked with pathogenicity (Nemecek et al., 2006), but *S. japonicus* is nonpathogenic (Sipiczki et al., 1998b). Recent sequencing of the genome (Rhind et al., 2011), development of efficient transformation protocol (Aoki et al., 2010; Aoki and Niki, 2017) and other genetic tools (Aoki et al., 2017; Furuya and Niki, 2011; Klar, 2013; Niki, 2014) place this species as an attractive model to study dimorphism in this distant ascomycete clade. It has already proven to be a powerful organism to use in comparative and evolutionary biology, recent advances on divergence in

mitotic strategies showed that while *S. pombe* goes through a closed mitosis, *S. japonicus* undertakes an open mitotic process (Gu et al., 2012; Yam et al., 2011). Another difference between the two species occurs in division plane placement and it was shown that in its yeast form *S. japonicus* is unaffected by the deletion of Mid1, protein carrying the positive signal for division plane positioning in *S. pombe* (Gu and Oliferenko, 2015; Gu et al., 2015).

In my thesis I provided an extensive description of the filamentation observed in *S. japonicus*. After the initial discovery of the fruit extracts as novel inducers of filamentation by Dr Omayya Dudin, I studied their inducing capabilities and the morphological change observed in *S. japonicus* in their presence. I analyzed the localization and the role of the cytoskeleton in diverse polarized processes in the cell. I described an asymmetrical organization of the hyphal cells and studied how this impacted nuclear and division site positioning. I analyzed the localization and the role of type-V myosins in polarity. Finally, wanting to understand the genetic bases of the dimorphic switch, I performed RNA sequencing to study transcriptomic changes during the transition from yeast-to-hyphae.

Chapter 1: Yeast-to-hypha transition in *Schizosaccharomyces japonicus* in response to environmental stimuli

This work was submitted to Molecular Biology of the Cell (MBoC).

Summary:

In this chapter, I describe the filamentation observed in fission yeast *Schizosaccharomyces japonicus* in presence of natural stimuli. A previous lab member, Dr Omaya Dudin identified fruit extracts as natural inducers of filamentation in this poorly understood dimorphic species and I conducted the rest of the project. The following work is mainly descriptive and aims to propose a simple way to induce dimorphism in a genetically tractable organism. Highlights of this work include the discovery of successive morphological forms transitioning from yeast to hypha, diverging roles for cytoskeleton in regards to polarity processes and the description of a switch between a symmetric and asymmetric growth system in fission yeast.

Yeast-to-hypha transition of *Schizosaccharomyces japonicus* in response to environmental stimuli

Cassandre Kinnaer, Omayra Dudin¹ and Sophie G Martin*

Department of fundamental microbiology, Faculty of Biology and Medicine, University of Lausanne, Biophore building, CH-1015 Lausanne, Switzerland

*Author for correspondence: Sophie.Martin@unil.ch

¹ Current address: Institut de Biologia Evolutiva (Consejo Superior de Investigaciones Científicas – Universitat Pompeu Fabra), Barcelona, Spain.

Abstract

Many fungal species are dimorphic, exhibiting both unicellular yeast-like and filamentous forms. *Schizosaccharomyces japonicus*, a member of the fission yeast clade, is one such dimorphic fungus. Here, we first identify fruit extracts as natural, stress-free, starvation-independent inducers of filamentation, which we use to describe the properties of the dimorphic switch. During the yeast-to-hypha transition, the cell evolves from a bipolar to a unipolar system with 10-fold accelerated polarized growth but constant width, vacuoles segregated to the non-growing half of the cell, and hyper-lengthening of the cell. We demonstrate unusual features of *S. japonicus* hyphae: these cells lack a Spitzenkörper, a vesicle distribution center at the hyphal tip, but display more rapid cytoskeleton-based transport than the yeast form, with actin cables being essential for the transition. *S. japonicus* hyphae also remain mononuclear and undergo complete cell divisions, which are highly asymmetric: one daughter cell inherits the vacuole, the other the growing tip. We show these elongated cells scale their nuclear size, spindle length and elongation rates but display altered division size controls. This establishes *S. japonicus* as a unique system that switches between symmetric and asymmetric modes of growth and division.

1.1. Introduction

Cellular morphologies are extremely varied. However, the overall mechanisms generating polarity are thought to be conserved across the species (Nelson, 2003). In fungi, whose shapes are defined by an external rigid cell wall, the location of polarity factors on specific cortical regions locally drives cell growth through cell wall expansion and remodeling, to generate specific cell morphologies. Many fungal species are dimorphic, exhibiting distinct morphologies depending on growth conditions. In this study, we used the fission yeast *Schizosaccharomyces japonicus* (*S. japonicus*), a dimorphic species from the early diverging ascomycete fission yeast clade, to describe the changes occurring during the dimorphic switch.

S. japonicus is estimated to have diverged 220Mya from its well-studied cousin *Schizosaccharomyces pombe* (*S. pombe*), with which it displays at least 85% orthologous genes (Rhind et al., 2011). It can grow either in the yeast form, of dimensions slightly larger than *S. pombe*, or in a filamentous form (Niki, 2014). While fungal dimorphism is usually associated with pathogenicity (Nemecek et al., 2006), *S. japonicus* is non-pathogenic to humans making it a convenient model to study the transition in growth mode. It was initially isolated on strawberries from a field in Japan in 1928 (Yukawa and Maki, 1931) and a variant was discovered over a decade later in grape extracts by an American team (Wickerham and Duprat, 1945). The *S. japonicus* yeast form resembles *S. pombe*: cells are rod-shaped, divide medially, grow in a bipolar manner (Sipiczki et al., 1998a) and use the small GTPase Cdc42 for cell morphology (Nozaki et al., 2018). In *S. pombe*, Cdc42 controls cell shape by activating the formin For3 and the exocyst complex for polarized exocytosis of secretory vesicles (Martin and Arkowitz, 2014). However, it also displays important differences, notably in having a semi-open mitosis (Yam et al., 2011) and in division site positioning. In *S. pombe*, septum positioning relies on positive signals from the nucleus, itself placed medially by associated microtubules pushing against both cell poles, and on negative signals preventing septum assembly at cell poles. The anillin-related protein Mid1 conveys the positive signal, whereas the DYRK-family kinase Pom1 serves to inhibit septation at cell poles (Celton-Morizur et al., 2006; Chang et al., 1997; Huang et al., 2007; Padte et al., 2006; Sohrmann et al., 1996). In *S. japonicus*, Pom1 kinase similarly controls medial division, but Mid1 is not required for division site placement (Gu et al., 2015).

S. japonicus filamentous form is triggered in response to environmental stresses (Sipiczki et al., 1998b), such as nutritional or nitrogen starvation, and DNA damage stresses (Furuya and Niki, 2010), suggesting that the switch from a small cell to a fast growing hypha serves as an escape mechanism from harsh environmental conditions. Filamentous growth is also light-repressed, as blue light perception by two *white-collar* light receptors present in *S. japonicus* and not in *S. pombe* induces hyphal cell division (Okamoto et al., 2013). Filamentous growth in *S. japonicus* is poorly

characterized, though it is thought to share some traits common to other filamentous fungi, such as the presence of a large vacuole at the back of the cell (Sipiczki et al., 1998a).

Filamentous fungi, whether dimorphic (such as *Candida albicans* or *Ustilago maydis*) or not (like *Neurospora crassa* or *Aspergillus nidulans*) grow through rapid apical extension mediated by a vesicle flux towards the growing tip (Riquelme, 2013). Polarized trafficking of vesicles provides the necessary membrane and wall-remodeling material to accommodate the rapid growth, from half to several μm per minute, of the filamentous form. Vesicles targeted for tip fusion typically accumulate in a spherical organelle, called the Spitzenkörper, which is located close to the growing tip and controls hyphal growth rate and orientation (Riquelme and Sanchez-Leon, 2014). Lower fungi, such as Zygomycetes, and non-fungal Oomycetes do not require a Spitzenkörper to grow but most other filamentous fungi assemble one and it is generally described as a landmark of true filamentous growth (Grove and Bracker, 1970; Read et al., 2010). The hyphal form of most filamentous fungi and dimorphic yeasts is multinuclear and its cytoplasm can be compartmentalized by septa that may be incomplete, maintaining cytosolic connection (reviewed in (Steinberg et al., 2017)). This contrasts with the yeast form, which is generally mononuclear and undergoes complete septal division, underlying a need for proper spatial coordination between mitosis and cytokinesis.

In this work, we describe the *S. japonicus* switch from yeast to hypha. We first identify fruit extracts as new inducers of hyphal formation that are independent of nutrient starvation. The *S. japonicus* hyphal form grows much faster and longer than the yeast form, but displays unique features amongst filamentous fungi. Indeed, it lacks a Spitzenkörper, undergoes complete cell divisions and remains mononuclear. We find that cytoskeleton-based transport is more rapid in the hyphal than yeast form, with actin cables necessary for polarized growth, while microtubules contribute to nuclear positioning. *S. japonicus* hyphae divide asymmetrically: the front cell inherits a larger portion of the cytoplasm and no vacuole, and exhibit altered size, growth and division controls. Thus, the *S. japonicus* yeast-to-hypha transition involves the conversion of a symmetric to an asymmetric cell.

1.2. Results

1.2.1. Fruit extracts induce filamentation in *Schizosaccharomyces japonicus*

Since *S. japonicus* was originally isolated from strawberries and grapes (Wickerham and Duprat, 1945; Yukawa and Maki, 1931), which may represent a natural habitat, we investigated whether these fruits alter the fungus growth behavior. Previous work established that induction of *S.*

japonicus filamentation occurs upon stress by nutrient depletion and/or DNA damage (Aoki et al., 2017).

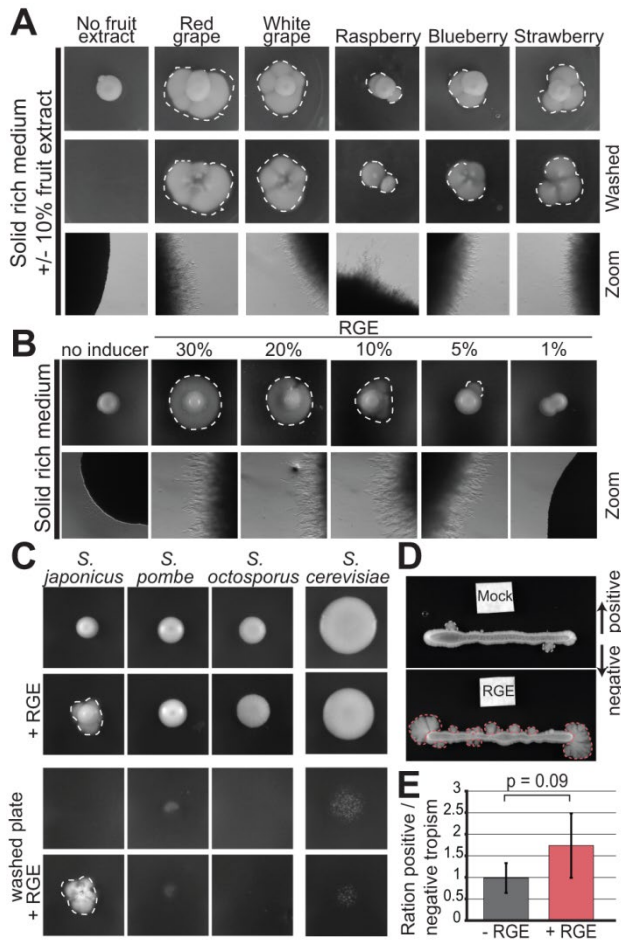


Figure 2.1. Fruit extracts induce invasive filamentation in *S. japonicus*. **A.** *S. japonicus* growing in agar plates on solid rich media (YE), supplemented or not with 10% fruit extracts before (up) and after (middle) washing of the plate, as well as the same plates imaged under a stereomicroscope (down). **B.** *S. japonicus* growing on solid rich media supplemented or not with a range of concentration of red grape extract (RGE) and the same plate under the stereomicroscope. **C.** *S. japonicus*, *S. pombe*, *S. octosporus* and *S. cerevisiae* growing on solid rich media (YE or YPD) and supplemented or not with RGE before (up) and after (down) washing of the plate. **D.** Tropism experiment to assess the directionality of *S. japonicus* hyphal growth. White filter squares were soaked with YE (up) or RGE (down). **E.** Ratio of positive vs. negative growth tropism in experiments such as in (D). Positive tropism denotes growth towards and negative tropism away from the filter; $P = 0.09$, t. test. Error bars show standard deviations. Dotted lines highlight penetrative filamentous growth.

On solid rich media in absence of stress, *S. japonicus* primarily grows in the yeast form (Fig. 2.1A). By contrast, within 3 days of growth on rich media plates supplemented with fruit extracts, *S. japonicus* colonies extended filaments at their periphery, appearing as a white halo around the yeast colony. The filamentation observed at colony edges was invasive as it persisted after plate washing, indicating that the elongated cells have penetrated the solid media (Fig. 2.1A). Invasive growth was observed with grape (red or white) and strawberry extracts, but also with other berry extracts. Filamentation was increased in presence of higher concentration of red grape extract (RGE) and decreased with lower concentrations (Fig. 2.1B). Note that in low-concentration RGE, filamentation was often observed only on parts of the colony's periphery, suggesting that the transition to the hyphal mode is a sporadic event in these conditions. In this work we used 10% RGE to induce filamentation. RGE did not induce filamentation in other fission yeast species, nor in *Saccharomyces cerevisiae*, which can form pseudohyphae in certain conditions (Gimeno et al., 1992) (Fig. 2.1C). We note that the ability of RGE to induce filamentation on rich media suggests this is independent of

nutrient stress, contrasting with previous reports associating filamentation with escape from stress (Furuya and Niki, 2010; Sipiczki et al., 1998b). This underlies the existence of different triggers and/or mechanisms by which *S. japonicus* transitions in growth forms. A tropism assay showed that *S. japonicus* filaments formed at least as much towards the red grape extract as away from it (**Fig. 2.1D-E**). Thus, although we cannot fully exclude oxidative stress as the trigger for the fruit extract-induced switch, this indicates it is not a repellent. Initial characterization of the molecular properties of the RGE inducer showed that it is unlikely to be a nucleic acid, a protein or a lipid and that it is heat-resistant. Phase separation with chloroform/methanol further defined that the inducer is water-soluble. However, the molecular identity of the inducer remains to be identified, as limited screening through candidate molecules present in fruit extracts, including glucose or fructose supplementation, was so far unsuccessful (**Table 2.1**). In summary, fruit extracts represent new, likely stress-free, inducers for the switch to hyphal growth in *S. japonicus*.

1.2.2. The yeast-to-hypha transition involves extreme vacuolization and dramatic increase in cell size

Microscopy of hyphal cells growing on solid media proved to be challenging due to the invasiveness of hyphae. Therefore, we performed imaging experiments in microfluidic chambers. In this set up, the cells are trapped between a flexible top layer made out of polydimethylsiloxane and a bottom glass layer, neither of which they can penetrate. Because blue light is inhibitory to filamentation (Okamoto et al., 2013), long-term microscopy was performed either with cells carrying a deletion of the white-collar light receptors *Wcs1* and *Wcs2* or in the presence of a blue-light filter. In these growth conditions, we observed a progressive transition over 24h to the filamentous form at the edges of micro-colonies (**Fig. 2.2A**) (**Movie S1**). Three successive stages in the transition from yeast to hypha can be described. The first landmark of filamentation is the appearance of multiple vacuoles all over the cytoplasm (Sipiczki et al., 1998a), forming a vacuolated yeast form. The vacuoles then polarized to one cell end in what we will refer as the transition form. Finally, once the vacuoles fused together into one or several large vacuoles we refer to them as the hyphal form (**Fig. 2.2B**). We confirmed that the organelles identified as vacuoles by DIC are indeed vacuoles, as these accumulate the water-soluble dye Lucifer Yellow (**Fig. S1**). We also note that Lucifer Yellow accumulates in smaller vacuoles present in the front of the hypha, which are difficult to detect by DIC. While the yeast and vacuolated yeast forms mainly grow in a bipolar manner, the transition and hyphal forms are always monopolar underlying a change in mode of growth (**Fig. 2.2C**). In time course experiments, the earliest sign of vacuolization was observed 12h after RGE induction, vacuole

polarization at one end of the cell occurred after 18h and hyphae were observed 24 hours after induction (Fig. 2.2D).

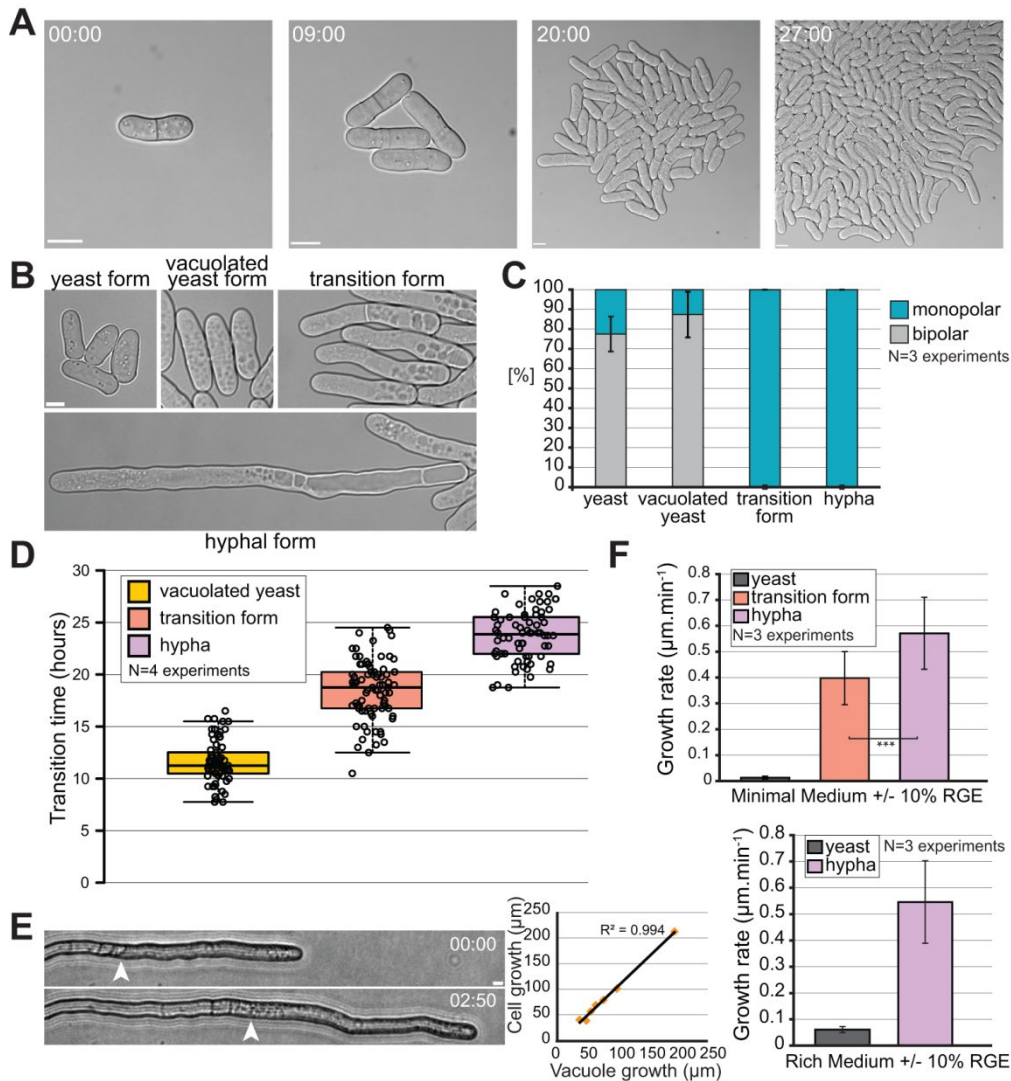


Figure 2.2. Kinetics of the morphological yeast-to-hypha transition. **A.** DIC microscopy images of mini-colony formation in a microfluidics chamber. **B.** DIC microscopy images of the four identified morphological states of *S. japonicus* during the yeast-to-hypha transition in a microfluidic chamber. **C.** Quantification of monopolar and bipolar cells in the four morphological state of *S. japonicus* (n=51 hyphae and >100 cells for the other states). Yeast cells were quantified without RGE, the other forms 8-30h after RGE addition. **D.** Quantification showing time at which each morphological state first appeared after induction with RGE in microfluidic chambers (n>70 cells per state). Box plot shows first and third quartile and median, whiskers extend 1.5 times the interquartile range from the first and third quartile. **E.** Brightfield microscopy images showing a growing hypha on solid media (edge of vacuole shown with arrowhead) and quantification showing a correlation between the growth of the vacuole over time and the growth of an entire hypha over the same amount of time. N=7 hyphae over 5 separate experiments. $R^2 = 0.994$, linear regression. **F.** Quantification of the growth rate of different morphological forms on minimum and rich media (in minimal medium, n=60 yeasts and >30 cells for the other states; in rich medium, n=60 yeasts and 17 hyphae). Error bars show standard deviations. Time in h:min. Scale bars: 5µm.

In the hyphal form, recognizable by its partitioning of the cytosol to the growing end of the cell and the vacuole to the back end, cell extension was strongly correlated with vacuole growth, (**Fig. 2.2E**). This suggests that the turgor pressure, which is an important driving force for growth, is supported by vacuole growth. Hyphae also grow about ten times faster than the yeast form (**Fig. 2.2F**). Indeed, hyphae extend at an average rate of 0.58 $\mu\text{m}/\text{min}$, whether RGE is added to rich or minimum medium, a rate comparable to that observed in other filamentous fungi, such as *Candida albicans* and *Aspergillus nidulans* which respectively grow at an average rate of 0.76 $\mu\text{m}/\text{min}$ and 0.5 $\mu\text{m}/\text{min}$ (Gow and Gooday, 1982a; Horio and Oakley, 2005). The monopolar transition form also displayed rapid growth rates, though slightly slower than hyphae (**Fig. 2.2F**).

1.2.3. *S. japonicus* does not assemble a classical Spitzenkörper

In an effort to compare *S. japonicus* hyphae to other filamentous fungi and dimorphic yeasts we looked for the presence of a Spitzenkörper at the hyphal tip. The accumulation of vesicles at the Spitzenkörper can be visualized in phase contrast microscopy as a dense spherical organelle (Riquelme and Sanchez-Leon, 2014) or fluorescently labeled with amphiphilic dyes like FM4-64 (Fischer-Parton et al., 2000) or with tagged Rab11 GTPase (Ypt3 in fission yeast), which decorates the vesicles (Cheng et al., 2002). It can also be seen by the accumulation of type V myosin (Crampin et al., 2005). In *S. japonicus*, neither phase contrast imaging, nor FM4-64 showed a spherical signal at hyphal tips. Similarly, GFP-Ypt3 and Myo52-GFP did not reveal a spherical fluorescent signal, though they accumulated at the cortex of hyphal tips, consistent with local vesicle delivery at the site of growth (**Fig. 2.3A**). We further tagged other components of the polarization machinery: the exocyst component Exo70 and polarity proteins Bud6 and Spa2, thought to associate with formins, decorated the hyphal tip cortex; the microtubule-delivered Tea1 protein also assumed a localization similar to that described in the cousin species *S. pombe* (**Fig. 2.3B**; movie S2) (Riquelme and Martinez-Nunez, 2016; Takeshita et al., 2008). None of these markers exhibited a Spitzenkörper-like localization. We conclude that *S. japonicus* does not assemble a classical Spitzenkörper like other filamentous fungi. Moreover, the localization of these polarity factors was similar in the hyphal and the yeast form, with the exception of Bud6, which decorated a notably wider region around the hyphal tip, and comparable to that of their homologues in *S. pombe* (**Fig. 2.3C**). This suggests that the transition from yeast to hyphal form occurs without major re-organization of the polarity and trafficking machineries.

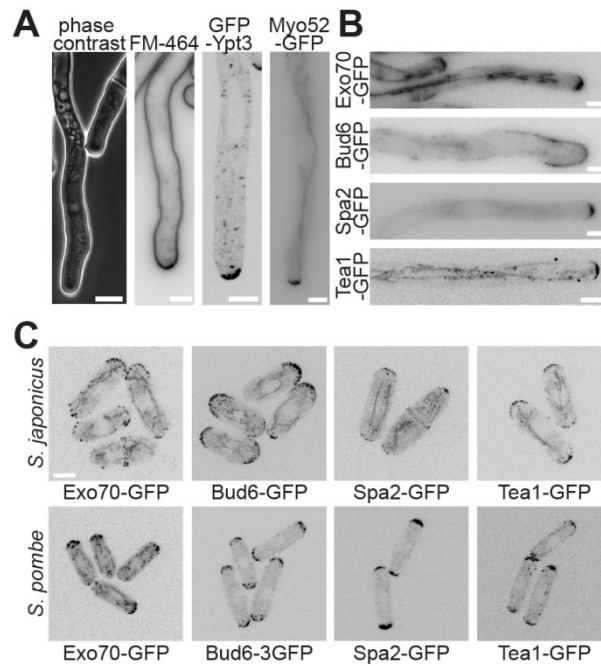


Figure 2.3. Localization of polarity factors in fission yeasts. **A.** Hyphal tips of *S. japonicus* visualized with a phase contrast objective, stained with the amphiphilic dye FM4-64, marked with GFP-tagged Rab11 GTPase Ypt3 and expressing Myo52-GFP. Note that there is a slightly darker area at the tip of the hypha in the phase contrast image, but this is also present in the yeast form next to it, suggesting it does not represent a Spitzenkörper. **B.** Fluorescence images of GFP-tagged polarity proteins Exo70, Bud6, Spa2 and Tea1 at *S. japonicus* hyphal tips. **C.** Fluorescence images of the same polarity proteins in *S. pombe* and *S. japonicus* yeast form. Scale bars: 5µm.

1.2.4. Actin based trafficking is increased in the hyphal form and is essential for the transition

Although *S. japonicus* does not assemble a Spitzenkörper, live imaging of vesicles tagged with GFP-Ypt3 revealed an important change during the transition from yeast to hypha. Ypt3 vesicles accumulate at the growing tips in both the yeast and the hyphal form of *S. japonicus* and their movement can also be tracked in the cytosol (Fig. 2.4A; Movie S3-4). Ypt3 fluorescence intensity was significantly increased at hyphal tips compared to yeast cell tips (Fig 2.4B), suggesting a stronger accumulation of vesicles. This is likely to reflect an increase in membrane traffic to sustain the increase in cell growth. Interestingly, we found that the speed of individual vesicles was also on average significantly faster in hyphae than in yeast (Fig. 2.4C). Similar fast vesicle speeds and accumulation at cell tip were also observed in the transition form, suggesting that the change in the rate of trafficking happens at the beginning of the transition.

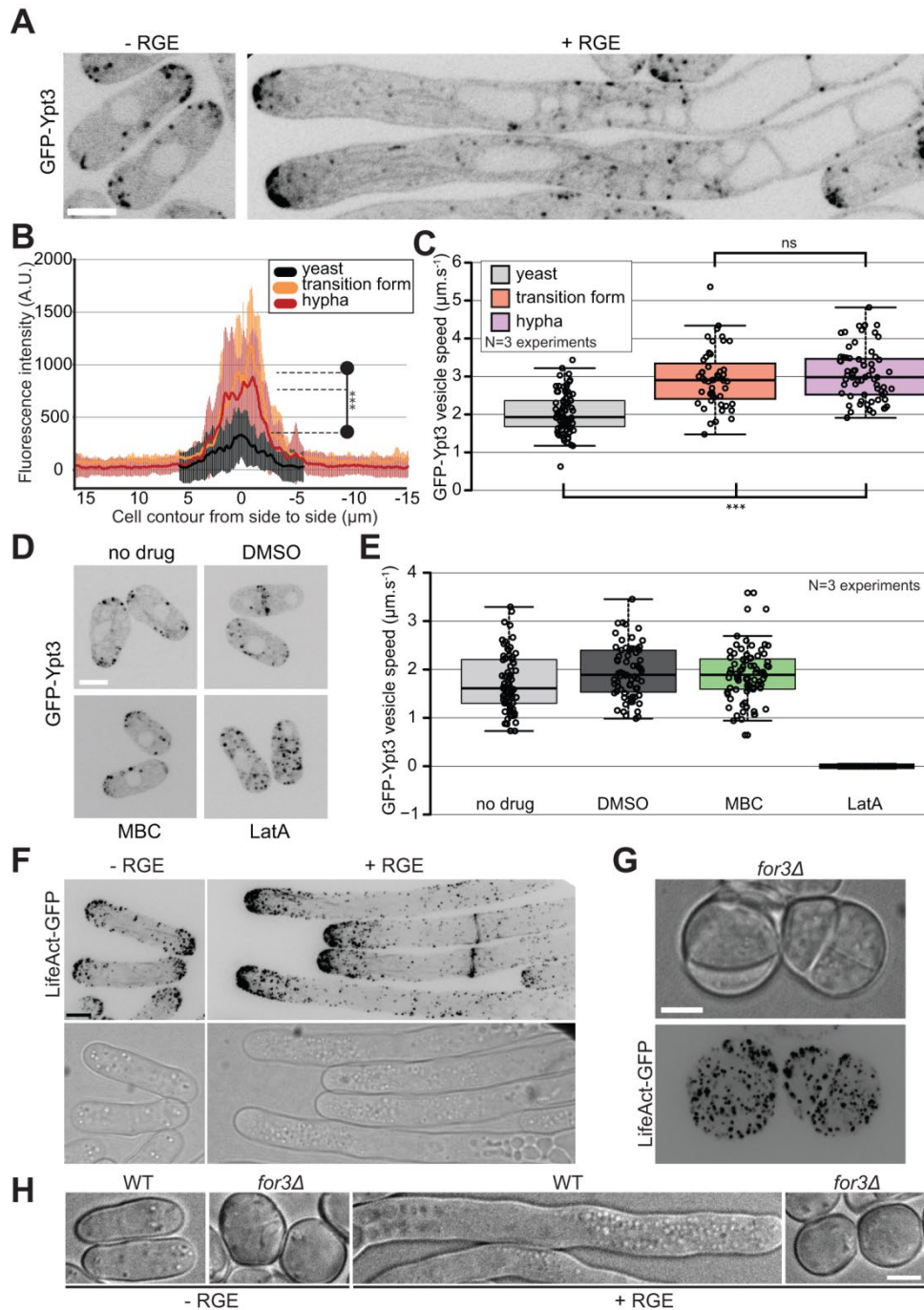


Figure 2.4. Actin based trafficking is increased in the induced forms. **A.** Middle plane fluorescence images of *S. japonicus* cells expressing GFP-Ypt3 in both non-inducing and inducing conditions. **B.** Quantification of GFP-Ypt3 fluorescence intensity at the tips of yeasts ($n=32$), transition forms ($n=13$) and hyphae ($n=18$). Shaded areas correspond to standard deviations. *** indicates $P < 1.2 \times 10^{-5}$; t. test. **C.** Quantification of vesicle trafficking speed in yeasts, transition form and hyphae. *** indicates $P < 4.82 \times 10^{-10}$; ns indicates $P=0.44$, t. test. **D.** Middle plane fluorescence images of GFP-Ypt3 in cells treated or not with solvent dimethyl sulfoxide (DMSO), microtubule-depolymerizing MBC or actin-depolymerizing LatA. **E.** Quantification of vesicle trafficking speed in cells treated as in (D). **F.** F-actin localization in *S. japonicus* observed with marker LifeAct-GFP in both yeast and hyphal forms. Images are maximum intensity projections of 16 z-stacks ($0.5 \mu\text{m}$). **G.** Fluorescence images of LifeAct-GFP in *for3Δ* mutants showing absence of actin cables and disorganized patches. **H.** DIC images of wild type and *for3Δ* mutants under non-inducing and inducing conditions. Box plots show first and third quartile and median, whiskers extend 1.5 times the interquartile range from the first and third quartile. Scale bars: $5 \mu\text{m}$.

Ypt3 trafficking occurred on F-actin, as actin depolymerization with LatA abolished all vesicle trafficking and cell tip localization (Cheng et al., 2002) (**Fig. 2.4D-E; Fig. S2A**). By contrast, microtubule depolymerization with MBC had no effect on Ypt3 trafficking. F-actin labeled with LifeAct-GFP was organized in actin patches, cables and rings in *S. japonicus* (Alfa and Hyams, 1990). We noticed an accumulation of actin structures at the tips of growing hyphae coinciding with the increased growth rate for the hyphae (**Fig. 2.4F**, see **Fig. 2.2F**). Deletion of For3, the formin responsible for actin cable assembly in *S. pombe* (Feierbach and Chang, 2001), led to loss of actin cables in *S. japonicus*, as in *S. pombe*. However, the resulting mutant cells were sicker than their *S. pombe* counterparts (Bendezu and Martin, 2011; Feierbach and Chang, 2001), with impairment in growth and high cell mortality (**Fig. 2.4G, Fig. S2B**). *for3Δ* mutant cells did not polarize growth, even in presence of the inducer (**Fig. 2.4H**). *S. pombe* relies on two morphogenesis pathways; actin cables nucleated by For3 and the exocyt. A complete loss of polarity and isotropic growth is achieved by deleting both components (Bendezu and Martin, 2011). We therefore investigated if the exocyst complex had any role in morphogenesis in *S. japonicus*. Cells lacking Exo70 could grow as rod-shaped yeasts and transitioned to hyphal growth in the microfluidics chambers in presence of RGE (**Fig. S6A**). However, further analysis revealed that the dimorphic switch was inhibited on solid substrate (**Fig. S6B-C**). Microscopic observations of cells growing at the colony periphery on solid media in presence of the inducer showed they were all yeast (data not shown). This excludes that the phenotype observed could be uniquely due to a defect in solid invasion. Thus, *S. japonicus* yeast and hyphal growth rely on transport of vesicles on actin cables for polarized growth, with increased rates of vesicular transport in the hyphal form.

1.2.5. Microtubules are dispensable for polarized growth of *S. japonicus*

We used GFP-Atb2 (alpha-tubulin) to examine the microtubule cytoskeleton. Microtubules form bundles aligned along the length of the cell of both yeast and hyphal forms (Alfa and Hyams, 1990; Sipiczki et al., 1998a). In the yeast form, microtubule organization resembled that described in *S. pombe*, growing from cell middle towards cell ends, sliding along cell sides and shrinking upon touching the cell tip (**Fig 2.5A; Movie S5**). In the hyphal form, microtubule bundles were significantly longer, extending over the length of the cytoplasmic segment and were often observed to bend (**Fig. 2.5A; Movie S6**). The bundles extended to the hyphal growing tip where they occasionally touched the membrane to deposit polarity factors (see **Movie S2**). Microtubules also extended through the vacuole-occupying cell segment, though rarely reached the other cell end (**Fig 2.5B; see Fig. 2.7E**). However, short-term microtubule depolymerization with MBC did not impair polarized growth in either yeast (data not shown) or hyphal form (**Fig. 2.5C**).

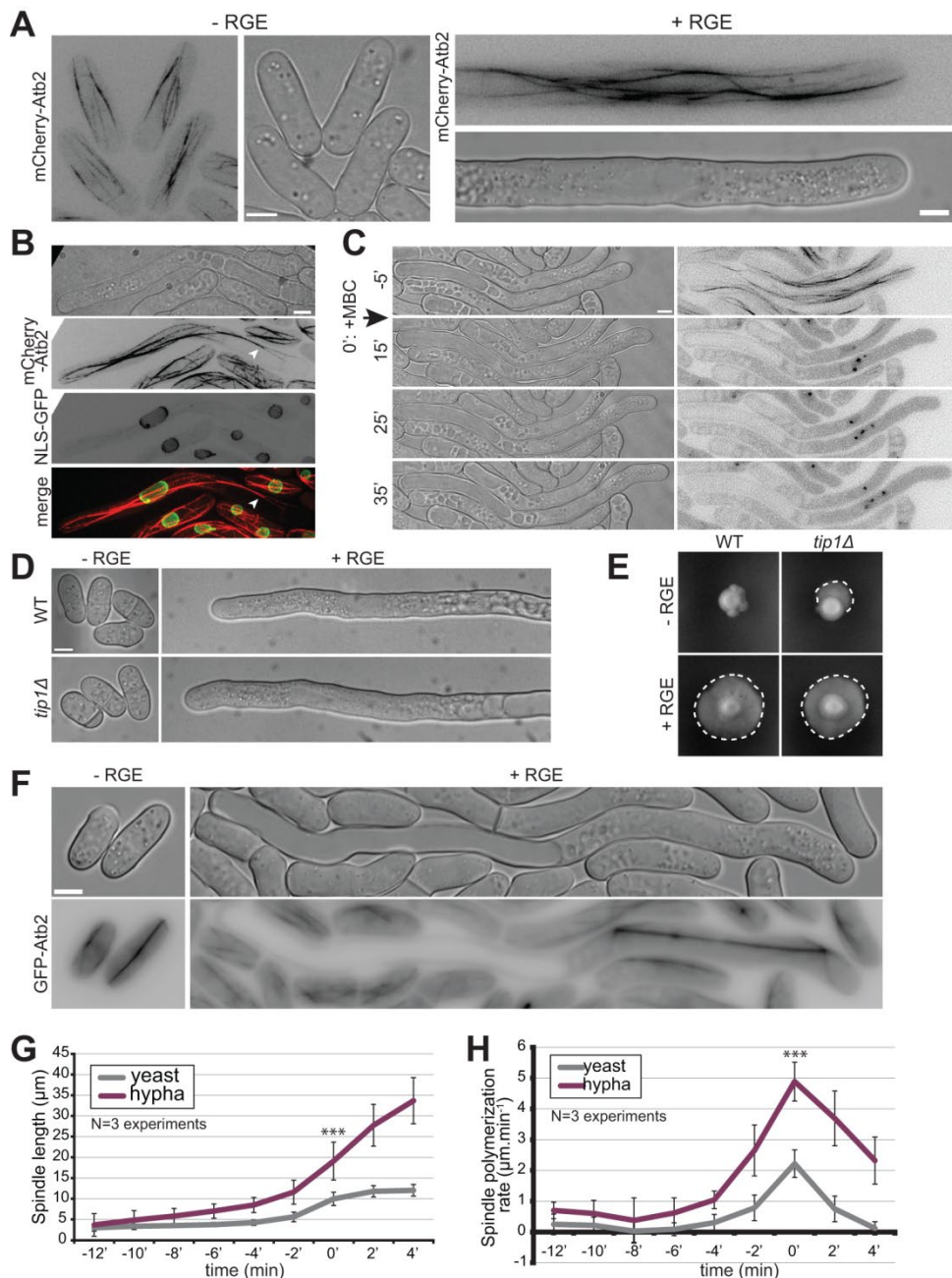


Figure 2.5. Microtubules are not involved in hyphal growth. **A.** Microtubule organization in *S. japonicus* yeast and hyphal forms expressing mCherry-Atb2. Images are maximum intensity projections of 8-14 z-stacks. **B.** Images of an induced strain tagged with mCherry-Atb2 and NLS-GFP showing microtubules can penetrate the space between the plasma membrane and the vacuole (arrowhead). **C.** Microtubule depolymerization does not perturb hyphal growth. MBC was added at time 0 in a microfluidic chamber. **D.** Wildtype and *tip1Δ* cells grown in microfluidic chambers in inducing and non-inducing conditions. **E.** Wildtype and *tip1Δ* strains grown on solid media in non-inducing and inducing conditions. Dotted lines highlight penetrative filamentous growth. **F.** Mitotic spindles labeled with GFP-Atb2 in yeast and hypha. **G.** Quantification of spindle length over time, aligned on the steepest slope and averaged (n=30 cells per cell type). **H.** Quantification of spindle elongation rates over time. Individual profiles were aligned on the highest rate and averaged (n=30 cells per cell type). *** indicates $P < 1.59 \times 10^{-10}$; t. test. Error bars show standard deviations. Scale bars: 5μm.

Because long-term MBC treatment during the yeast-to-hypha transition gave inconclusive results, likely due to effects on cell proliferation through disruption of the mitotic spindle, we assessed the role of microtubules during the transition by deleting the microtubule plus-tip-associated CLIP-170 homologue Tip1. Though *tip1Δ* cells had some defects, notably in septum positioning, they retained the ability to polarize in the yeast form and to form hyphae within the same timeframe as wild-type (**Fig. 2.5D-E**). Hyphae could also still penetrate the agar on solid medium (data not shown). We conclude that microtubules and microtubule plus-tip factors are not important for yeast-to-hypha transition or for hyphal growth.

Microtubules labeling also allowed us to visualize mitotic spindles, which elongated to significantly longer sizes in hyphae than yeast cells: they reach over 30μm in length, almost covering the entire cytosolic hyphal segment (**Fig. 2.5F-G**). Interestingly, the rate of spindle elongation was also significantly increased (about 2.5-fold) (**Fig. 2.5H**), such that the total duration of mitosis tended to be even shorter in hyphae. We observed also less spindle buckling in hyphae (Yam et al., 2011). This suggests that the rates of microtubule-dependent motors and thus dependent forces, like those of actin-dependent motors driving vesicle movements, are increased in hyphae.

1.2.6. *S. japonicus* hyphae display complete cell divisions and altered growth controls

We were surprised to observe that mitotic divisions were always followed by formation of septa that fully constricted, giving rise to two daughter cells throughout the yeast-to-hypha transition (**Fig. 2.6A; Fig. S3A**). This was the case in cells lacking blue-light receptors as well as wild-type cells grown in the dark. Indeed, most filamentous fungi are multinucleated, with some forming septa that do not constrict but help compartmentalize an increasingly complex filamentous network (Mourino-Perez and Riquelme, 2013). Consistent with the completion of cytokinesis, *S. japonicus* remained mononuclear even in the filamentous form (Sipiczki et al., 1998a) (**Fig. 2.6B-C**). The nuclei were elongated in the hyphal form with nuclear length correlating well with cytoplasm length, respecting the rule of constant nuclear to cytoplasm ratio (Neumann and Nurse, 2007) (**Fig. 2.6D**). This observation, together with the absence of Spitzenkörper described above, sets *S. japonicus* hyphae apart from other filamentous fungi, casting them as more similar to the yeast form than expected.

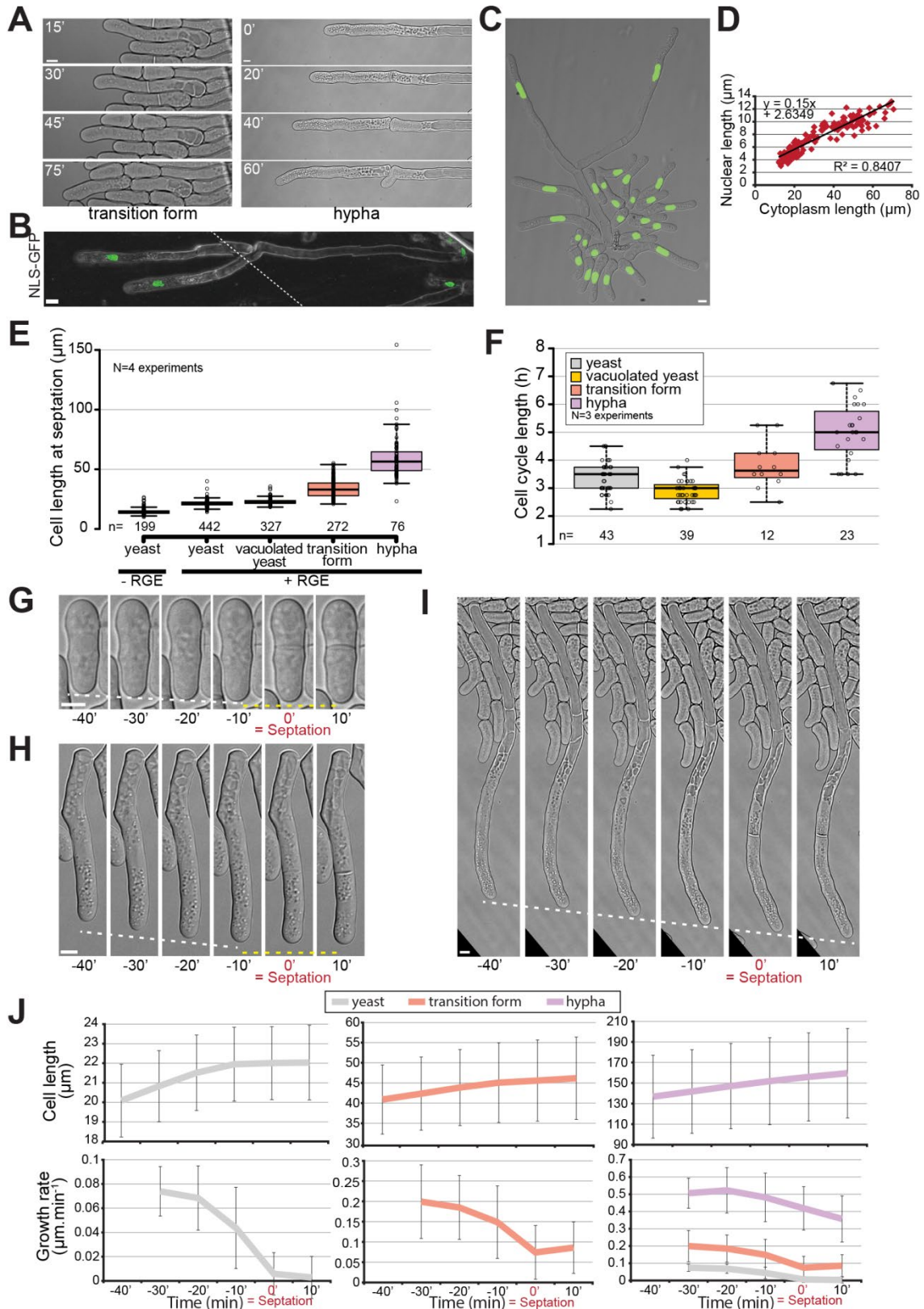


Figure 2.6. *S. japonicus* produces mononuclear hypha. **A.** DIC images of transition and hyphal forms showing completion of septation. **B.** Tiled confocal microscopy image of hyphae expressing NLS-GFP growing on gelatin plates. Dotted line shows the location of the tiling. **C.** Strain expressing NLS-GFP growing in inducing conditions in a microfluidics plate. **D.** Correlation between nuclear length and cytoplasm length (n=178 cells). **E.** Quantification of cell length at septation in the different morphological forms of *S. japonicus*. **F.** Quantification of cell cycle length in the different morphological forms of *S. japonicus*. **G-I.** DIC images of cell growth in

microfluidic plates up to the septation event. White dotted lines show tip growth. Yellow dotted lines show absence of, or reduced, growth. **J.** Analysis of cell length and growth rate over time aligned on septation time for yeast (grey), transition (orange) and hyphal (purple) forms (n> 18 cells per cell type). Box plots show first and third quartile and median, whiskers extend 1.5 times the interquartile range from the first and third quartile. In (J), error bars show standard deviations. Scale bars: 5µm.

Interestingly, in comparison to the yeast form, *S. japonicus* hyphae appeared to show distinct growth control. First, measurement of cell size at division showed an increase throughout the yeast-to-hypha transition whereas cell width remained roughly constant, suggesting an alteration in cell size regulation during the transition (**Fig. 2.6E**; **Fig. S3B**). This increase in size was not only due to the fast growth of the transition and hyphal forms as the length of the cell cycle also increased (**Fig. 2.6F**). Second, while *S. japonicus* yeast form and *S. pombe* stop growing during septation (Mitchison and Nurse, 1985), we found that the transition and hyphal forms continued to grow (**Fig. 2.6G-I**), similar to what is observed in other filamentous fungi (Riquelme et al., 2003). However, in these forms the growth rate decreased during septation, interestingly by a similar absolute value as in yeasts (**Fig. 2.6J**). We envisage competition for polarity factors between the growing end and the septation site as a reason for this decrease.

1.2.7. Highly asymmetric cell division of a fission yeast in *S. japonicus*

One fascinating aspect of hyphal division is that this cell division is inherently highly asymmetric (Sipiczki et al., 1998a). Indeed, hyphae (and transition forms) have polarized vacuoles to the back end of the cell and grow in a monopolar manner. Septation always occurred within the cytoplasm-containing cell segment. During cell division, one daughter cell retained the previously built vacuole and little cytosol and paused before growing a branch from the septation point. The other cell inherited most of the cytosol and the hyphal tip, which kept growing as described above. This cell rapidly rebuilt its vacuole close to the septation point (**Fig. 2.7A**; **Movies S7-S8**). Similar behaviors were observed in the transition form (**Fig. S4**). This raises the question of how hyphae position their division site.

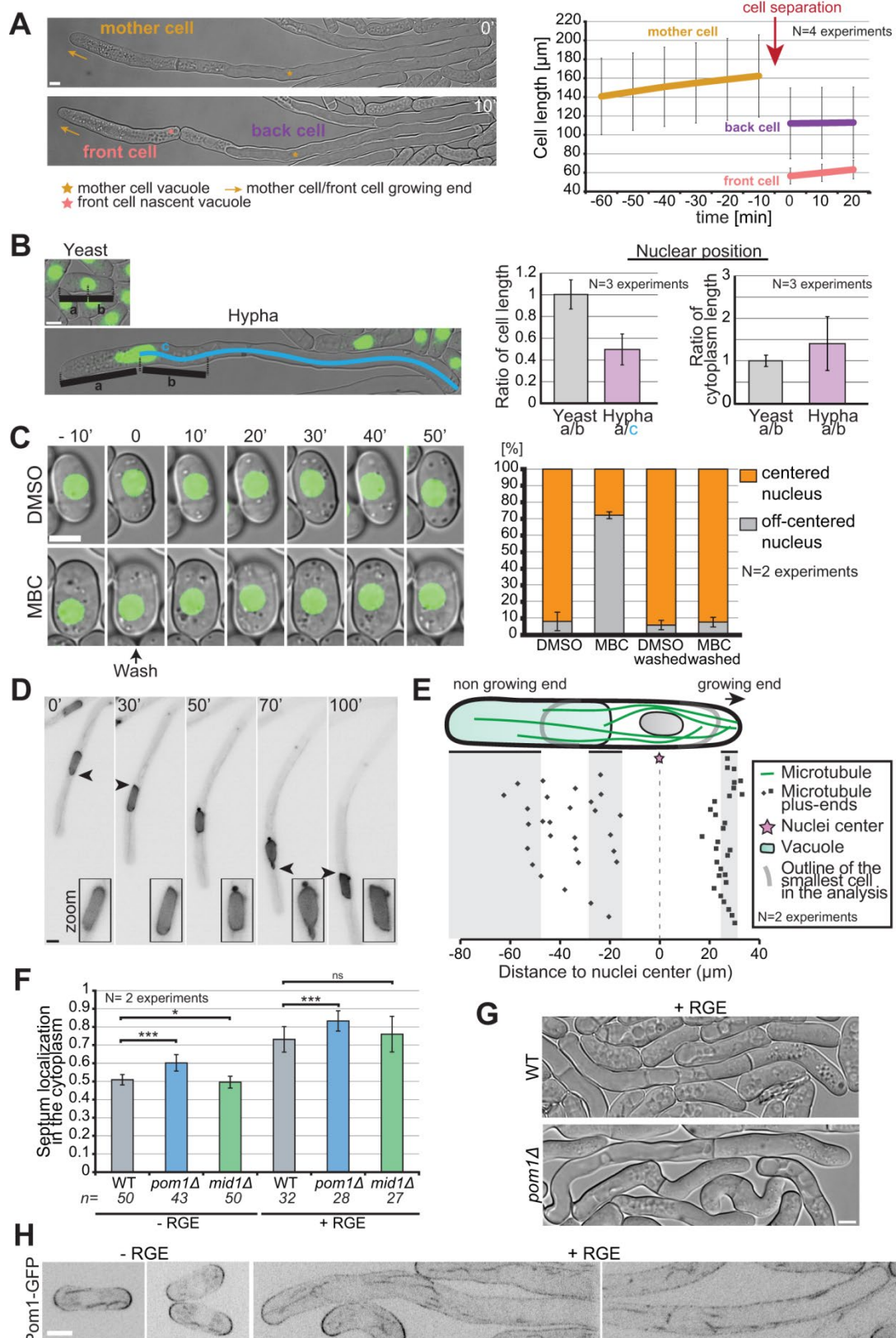


Figure 2.7. Asymmetric cell division in *S. japonicus*. **A.** Hyphae divide asymmetrically, giving rise to a front cell that retains the growing end but has to rebuild a vacuole, and a back cell that retains the vacuole but has to rebuild a growing end (left). Hyphal cell length recording over time aligned on cell separation (right) ($n=20$ hyphae). **B.** Quantification of nuclear positioning in the cell and in the cytoplasm. Positioning was calculated through ratios as explained in the left panel ($n>50$ cells per cell type). **C.** Microtubules contribute to nuclear positioning. Cells were grown in microfluidics chambers for three hours with DMSO or MBC and then washed

for 50 minutes with EMM-ALU. Nuclear position was quantified before and after the wash in >65 cells per condition. Note that most nuclei re-centered rapidly after wash-out but we quantified after 50min to include a few delayed cells. **D.** Fluorescence images of a hypha expressing NLS-GFP showing an example of nuclear shape alteration over time. Arrowheads point to nuclear envelope protrusion indicative of exerted forces. Insets show zoom on the nucleus. **E.** Schematic of the localization of microtubule plus-ends in the hyphal form. Each dot represents a microtubule plus end position. The nuclear position was used as reference point in all measurements. Shaded areas show the range of positions of the cell front, vacuole front and cell back (n=50 microtubule tips in 10 hyphae). **F.** Quantification of septum position in the cytoplasm of yeast and hyphae, in WT, *pom1Δ* and *mid1Δ* strains. ns: P=0.22; *: P=0.03; ***: P<9.08x10⁻⁰⁸; t. test. **G.** DIC images of septated WT and *pom1Δ* hyphae. Septation plane positioning in *pom1Δ* hyphae is biased towards the vacuole. **H.** Middle plane fluorescence images of Pom1-GFP in inducing and non-inducing conditions. In the hyphal form we show both the front and the back of cells. Scale bars: 5μm.

We first investigated the mode of nuclear positioning. In *S. pombe*, the nucleus is positioned at mid-cell due to microtubules anchored at the nuclear envelope exerting pushing forces against both cell poles (Daga et al., 2006; Tran et al., 2001). In *S. japonicus* yeast cells, nuclei were at mid-cell, as in *S. pombe*. By contrast, in hyphae, nuclei were not at mid-cell, but were displaced towards the cell front because the vacuole occupies the back of the cell. However, they were also not centered within the cytosolic segment, but displaced towards the vacuole (**Fig. 2.7B**). To examine the role of microtubules in nuclear positioning, we performed depolymerization experiments. In the yeast form, after over three hours of depolymerization with MBC about 70% of the cells showed a misplaced nucleus. After washout, most cells rapidly re-centered their nucleus to the cell middle, indicating microtubules control nuclear positioning (**Fig. 2.7C**). Similar experiment in the hyphal form proved to be challenging, but examination of nuclear morphology during hyphal growth showed frequent nuclear shape deformation indicative of forces exerted on the nuclear membrane (**Fig. 2.7D**). Nuclear envelope deformations were seen on both sides of the nucleus, suggesting that microtubules exert forces from both sides. We noted above that microtubules penetrate the vacuole-occupied cell segment (see **Fig. 2.5B**). The quantification of microtubule plus-end positioning within the cell showed a strong accumulation close to the hyphal tip, where accordingly to data in *S. pombe* they are expected to exert pushing forces. On the vacuole side, most microtubules were able to penetrate the space between the vacuole and the plasma membrane, though the majority ended within the first half of the vacuole length, suggesting that the pushing force may be partly dissipated (**Fig. 2.7E**). Thus, we hypothesize that the force exerted on the nuclei by microtubules growing towards the vacuole is weaker than that produced by microtubules growing towards the hyphal tip, leading to the observed bias in nuclear positioning towards the vacuole.

Similar to nuclei, hyphal septa were always positioned within the cytosolic cell segment, though they were off-centered towards the vacuole (**Fig. 2.7F**). This position was unaltered in *mid1Δ* hyphae,

indicating that, as in the yeast form (Gu et al., 2015), Mid1 is not involved in septum positioning in *S. japonicus*. However, the pre-divisional nuclear position did not predict the septum position, which was better, though not perfectly predicted by the middle of the anaphase spindle (**Fig. S5**). We note that, as in the yeast form, hyphal mitosis is semi-open (**Fig. S5**) (Yam et al., 2011). These observations suggest that positive signals for septum assembly may be conferred by the spindle.

Pom1 kinase constrains septum placement to mid-cell in *S. japonicus* yeast form, as it does in *S. pombe* (Gu et al., 2015). Similarly, we found that *pom1Δ* hyphae showed septum mispositioning, where the septum was excessively displaced towards the vacuolar segment (**Fig. 2.7F**). In *S. pombe*, this has been attributed to Pom1 gradients from cell poles exerting negative control to prevent septation at cell tips. Similar distribution is apparent in *S. japonicus* yeast cells (**Fig. 2.7G**). Curiously, in hyphae, though Pom1-GFP accumulated at cell poles, it was also very distinctly present along cell sides, and did not form an obvious long-range concentration gradient (**Fig. 2.7G**). This raises the question of how Pom1 conveys positional information for septum placement.

1.3. Discussion

1.3.1. A mycelium formed of single cells

It is believed that all Ascomycetes descend from a common filamentous ancestor (Berbee and Taylor, 1993). The fission yeasts form an early-diverging ascomycete clade, amongst which *S. japonicus* is the most divergent, suggesting that *S. japonicus* has retained an ancestral ability to filament present in the last common fission yeast ancestor (Sipiczki, 2000). In the fungal kingdom, filamentation leads to the formation of a mycelium, a complex multicellular network that underlies fungal spread and can reach several meters across (Islam et al., 2017; Smith et al., 1992). Mycelia are typically formed of a single, large common cytosol, which completely lacks septa in lower fungi, or is compartmentalized by incomplete, pore-containing septa in higher fungi (Steinberg et al., 2017). As a result, mycelia can typically be considered as a multinucleated syncytia. Hyphal fusion, or anastomosis, further increases the level of interconnectedness in fungi (Heaton et al., 2012; Read et al., 2010; Read et al., 2009), and this plays an important role in nutrient exchange within the fungus (Simonin et al., 2012). Although having a single cytoplasm extended over such lengths can appear risky, septate hyphae can easily seal off their septa, an absolutely vital process to prevent loss of cytoplasm in case of damage on the mycelium (Riquelme et al., 2018), in case of unfavorable environment (van Peer et al., 2010), or during aging (Bleichrodt et al., 2015). In this work we offer a description of a different kind of mycelium in *S. japonicus*.

The dimorphism observed in *S. japonicus* leads to the formation of extremely polarized and elongated single cells that are highly invasive of solid substrate similar to what is displayed by other filamentous organisms. In this work, we describe fruit extracts as novel inducers for the yeast-to-hypha transition in *S. japonicus*. Previously, nutrient starvation and DNA damage had been described as methods of induction of dimorphism in this fungus. Our method of induction appears to be specific for *S. japonicus*, as it did not trigger morphological transition in other fission yeasts or in *S. cerevisiae*, which forms penetrative pseudohyphae in response to nitrogen starvation (Gimeno et al., 1992). We note that filamentous forms have been reported for *S. pombe* (Amoah-Buahin et al., 2005), though RGE did not promote their formation. Cues triggering dimorphism are very varied in fungi; for example *Candida albicans* undergoes hyphal formation through a multitude of signals including serum and pH (reviewed in (Sudbery, 2011)), and *Ustilago maydis* filamentation can be triggered by sexual pheromones and the resulting dikaryotic hyphae will infect maize plants (Nadal et al., 2008). Interestingly, *S. japonicus* was isolated from both strawberries and grape extracts (Wickerham and Duprat, 1945; Yukawa and Maki, 1931), both of which we have shown to promote hyphal growth. This raises the question of its natural habitat and which morphological form it adopts in the wild. The hyphae produced by *S. japonicus* grow in average at $0.58\mu\text{m}\cdot\text{min}^{-1}$, a rate similar to what is observed in true filamentous fungi *Aspergillus nidulans* ($0.5\mu\text{m}\cdot\text{min}^{-1}$, (Horio and Oakley, 2005)) and fellow dimorphic yeast *C. albicans* ($0.75\mu\text{m}\cdot\text{min}^{-1}$ (Gow and Gooday, 1982a)). Thus, in appearance, the transition of *S. japonicus* leads to the formation of a macroscopic mycelium.

However, in contrast to other mycelia, our study reveals that the *S. japonicus* mycelium is fragmented. Indeed, *S. japonicus* hyphae not only place septa, similar to what is observed in septate hyphae of higher fungi, but also fully divide after mitosis. As a result, all hyphae are mononuclear, an unusual feature for a filamentous organism. After hyphal division, both front and back cells resume growth, with the back one resuming growth at an angle behind the recently formed septum, which superficially resembles a branch point. However, we never observed true branching. The lack of a Spitzenkörper in *S. japonicus* hyphae is another point of divergence from other filamentous Ascomycetes. Indeed, the Spitzenkörper, a vesicle supply center that promotes and orients hyphal growth, is largely associated with Ascomycetes and Basidiomycetes septate hyphae, but is usually absent from early-diverging fungal lineages. Instead, we find that *S. japonicus* hyphae accumulate secretory vesicles at the growing tip in a less clustered pattern, similar to what was observed in yeast growth and filamentous Zygomycetes species (Grove and Bracker, 1970; McClure et al., 1968; Roberson et al., 2010). Finally, the strict dependence of hyphae on actin-based transport and independent from microtubules also cast it apart from many other filamentous fungi, which use microtubules for long-range transport (Egan et al., 2012). These characteristics raise the question of

whether the *S. japonicus* filamentous form should be considered true hyphae or pseudohyphae. Its complete septation and mononuclearity and its lack of Spitzenkörper are pseudohyphae characteristics. However, the very large vacuoles in *S. japonicus* filaments are a feature of hyphae. In many ways, except for the apparent absence of a Spitzenkörper, *S. japonicus* hyphae appears quite similar to those of *C. albicans*, which also form mononucleate compartments and rely on actin-based transport (Sudbery, 2011). Thus, the filamentation process of *S. japonicus* described here represents an intermediate form of filamentation and participates to the wide variety of filamentous forms in fungi.

1.3.2. Asymmetrical division in fission yeasts

An interesting aspect of the yeast-to-hypha transition in *S. japonicus* is the conversion of a symmetrical to an asymmetrical system. In the yeast form, the cell grows at both poles and divides in the middle, generating two apparently equivalent daughters, similar to the case of *S. pombe*. By contrast, *S. japonicus* hyphae are morphologically and functionally very asymmetrical. Division yields a front cell that contains most of the cytoplasm and the unique growing tip, and is shorter than the back cell, which is largely filled with an ever-growing vacuole and has to re-initiate growth with a delay. This asymmetrical conversion is already apparent early in the transition when cells switch to a monopolar mode of growth, which coincides with the accumulation of initially fragmented vacuoles to the back of the cell. Because *S. japonicus* can be easily induced to switch from a symmetrical to an asymmetrical division, the signals and mechanism of this conversion are rich grounds for future investigations.

One aspect we explored in a little more detail is the question of nuclear and septum positioning. While nucleus and septum are placed at mid-cell in the yeast form, in wild type hyphae we have shown that both are displaced away from the middle. The positioning mechanism for the nucleus can be inferred from work in *S. pombe*, which showed that microtubules anchored at the nuclear membrane exert pushing forces against cell poles, such that force balance is achieved when the nucleus is centered in the cell (Daga et al., 2006; Tran et al., 2001). Microtubules also exert forces for nuclear positioning in *S. japonicus*, as illustrated by the observations that decentered nuclei are re-centered upon microtubule regrowth in yeast and the nuclear envelope is deformed by microtubules in hyphae. However, the nucleus is positioned neither in the middle of the hypha nor in the middle of the cytoplasmic region, but closer to the vacuole. We suggest that microtubule-dependent pushing forces position the nucleus, as in *S. pombe*, but that forces only become balanced at a non-medial

position due to force dispersion when microtubules encounter the less rigid vacuole at the back of the cell compared to the rigid cell wall at the front.

The positioning of the septum is more mysterious. In *S. pombe*, septum positioning at mid-cell is widely thought to rely on two complementary signals – a positive nuclear signal transmitted through the anillin-like protein Mid1, and a negative cell pole signal dependent on Pom1 kinase (Celton-Morizur et al., 2006; Chang et al., 1997; Huang et al., 2007; Padte et al., 2006; Sohrmann et al., 1996). In *S. japonicus* yeast cells, recent work showed that Mid1 plays no significant role in septum positioning (Gu et al., 2015). We confirm this in hyphae, as septum position is not altered in *mid1Δ* cells. Consistently, we find that the septum position is poorly predicted by the pre-divisional nucleus, indicating that septum position is defined at later time than in *S. pombe*. The septum was closer to but not perfectly predicted by the center of the anaphase spindle, suggesting positioning signals may be more similar to those used in metazoan cells, where the spindle is the key determinant (Oliferenko et al., 2009). By contrast, Pom1 kinase regulates division site positioning in both yeast and hyphae ((Gu et al., 2015) and this work). For this function, Pom1 was proposed to form an inhibitory concentration gradient from the cell poles that counteracts the localization of medial cytokinetic node precursors, which in consequence preferentially form at mid-cell (Bhatia et al., 2014; Celton-Morizur et al., 2006; Padte et al., 2006; Rincon et al., 2014). The long distance between the growing pole and the septum (over 50μm on average) calls this view into question, at least in hyphae. Indeed, although Pom1-GFP distribution in yeast cells was very similar to that described for *S. pombe* (Hachet et al., 2011), in hyphae it was only mildly enriched at tips and decorated most of the plasma membrane without forming an obvious long-range concentration gradient from the tip to the site of division. The cortex at the back of the cell, occupied by the vacuole, was also strongly decorated by Pom1, without enrichment at the back cell pole. This raises the question of how Pom1 conveys positional information for division in hyphae.

1.3.3. Size control

The *S. japonicus* yeast-to-hypha transition also provides an excellent system to study principles of size control. As the cell dramatically lengthens during the transition, several aspects of growth and division control are notably altered. *S. pombe* is arguably one of the best-studied systems for size control, due in part to its highly reproducible length at division. Measurements of cell size homeostasis concur in proposing that the system functions as a sizer (Wood and Nurse, 2015), with recent work suggesting that the key dimension informing on division timing is the surface area (Pan et al., 2014). Whether this holds true for *S. japonicus* yeast form is currently not known, but the

much longer cell length at division of transition and hyphal cells indicates a profound change or relaxation in the mode of size control. Because cell cycle length is also increased during the transition, a simple timer model, where increased cell size would be acquired due to faster growth during a set time, is also unsatisfactory. However, we note that the often observed correlation between cell and nuclear size (Jorgensen et al., 2007; Neumann and Nurse, 2007; Webster et al., 2009) is also present in *S. japonicus*. This correlation is spectacular, covering over 7-fold variations in size. The observed correlation occurs when nuclear size is compared with the cytoplasmic hyphal compartment rather than the whole cell, whose length varies according to the size of the vacuole. This is in agreement with data in *S. pombe* that support the idea that cytoplasmic volume determines nuclear size (Neumann and Nurse, 2007). These observations suggest that any size control in hyphae may monitor cytosolic and/or nuclear volume excluding vacuoles rather than length or surface area.

Many aspects of cell physiology are faster in the hyphae. First, polarized growth is over ten-fold faster, despite cell width remaining roughly constant. This indicates the surface of the cell tip is not the limiting factor for polarized growth and that growth material must be supplied at an increased rate. Second, we find that secretory vesicles indeed display faster linear movements in hyphae. This increase in transport rate may contribute, but is unlikely to fully explain the increase in growth rate, because it is considerably milder (about 1.5-fold). However, it indicates that myosin (likely myosin V) motors inherently move faster, or are less impeded in their progression in the hypha. Third, it is intriguing that spindle elongation rates are similarly increased (about 2.5-fold). As spindle elongation primarily relies on the action of kinesin motors, this suggests that kinesin motor speed is increased by a similar factor as myosin. As the duration of anaphase (as measured by the spindle elongation phase) is similar in yeast in hyphae, this produces much longer spindles in hyphae. Finally, we found that, in contrast to the yeast form, polar growth does not cease during hyphal division. In *S. pombe*, antagonism between two signaling pathways, the SIN and MOR pathways, is thought to control the alternation between cytokinesis and polarized growth (Ray et al., 2010). This suggests that crosstalk between these two signaling pathways, and more generally between growth and division, is altered upon hyphal transition.

In summary, our detailed description of the yeast-to-hypha transition in *S. japonicus* provides the founding work for addressing important fundamental cell biological questions. The identification of fruit extracts as inducer permits a simple stress-free induction to study an important morphological transition. In particular, the conversion of the cell from a symmetrical to an asymmetrical division system and the massive changes in size in a single cell promise to reveal novel principles in division, growth and size control.

1.4. Materials and Methods

Strains and media. The original wild-type auxotrophic *S. japonicus* strains were kindly provided by H. Niki (Furuya and Niki, 2009). The *S. japonicus* open reading frames (ORF) used in this study are the following: Atb2 (SJAG_02509), For3 (SJAG_04703), Spa2 (SJAG_03625.5), Bud6 (SJAG_04624.5), Tea1 (SJAG_01738), Exo70 (SJAG_04960), Ypt3 (SJAG_03915), Tip1 (SJAG_002695), Pom1 (SJAG_02392), Myo52 (SJAG_03011), Mid1 (SJAG_01143), Wcs1 (SJAG_02860) and Wcs2 (SJAG_05242). Cells were typically cultured in rich media (YE: yeast extract, 5g; glucose, 30g/liter) for agar plate based experiments and in Edinburgh minimal medium (EMM) supplemented with the appropriate amino acids (EMM-ALU) for microfluidic-based experiments. For plate experiments, 2 μ l of a standardized cell concentration from a liquid pre-culture were deposited to form the initial colony. The fast growth of *S. japonicus* yeast cells in YE would entirely fill the microfluidic plates before transitioning to hyphae in presence of the inducer, which is why we chose to work with minimum media in this case. Red grape extract was obtained from blending 500g of red grapes; the current batch of inducer was made from Crimson seedless grapes from Brazil. The blended grapes were placed in 50ml Falcon tubes and centrifuged at 10000rpm for 25min at room temperature (Eppendorf A-4-62). After recovery of the liquid supernatant by pipetting, the extract was placed in clean 50ml tubes and centrifuged a second time (10000rpm, 15min). Depending on the batch of grapes this step was sometimes repeated. The grape extract was then filtered through a 0.22 μ m filter (Millipore), aliquoted and kept at -20°C for a maximum of 2 years before degradation of the inducing capabilities. Hyphal formation was induced by adding 10% of red grape extract (RGE) to liquid or solid media, unless otherwise stated. Crosses were done on SPAS media as previously described (Furuya and Niki, 2009) and strains were selected by random spore analysis.

S. pombe and *S. octosporus* cells were grown either on YE plates or, for imaging, in EMM-ALU. *S. cerevisiae* was grown on YPAD plates.

Strains construction in *S. japonicus*. The genome has been sequenced (Rhind et al., 2011) and is available at: <http://fungidb.org/fungidb/>

We used homologous recombination to introduce GFP or mCherry fluorescent markers, or to delete a gene. Most of the plasmids constructed in this study were derived of pJK-210 backbone containing the *ura4+* cassette from *S. japonicus*. This plasmid was constructed and kindly provided by Dr. S. Oliferenko (Crick Institute, London).

To create a gene deletion, the 5' untranslated region (UTR) was linked with an inverted 3' UTR fragment (1Kb each at least), separated by a unique restriction site, by PCR stitching and cloned in a *ura4+*-containing pJK210 plasmid. Homologous recombination in *S. japonicus* is only efficient when homology between the fragment to be integrated and the genomic locus extend to the very end of the fragment. We thus chose 3' and 5' UTR fragments in such a way that stitching reconstitutes a blunt restriction enzyme site. Typically, we reconstructed a *Sma*I restriction site (CCCGGG) by choosing a 5'UTR region to amplify that started with GGG and a 3'UTR region that ended with CCC. Linearization of the plasmid and transformation led to gene replacement by the plasmid through homologous recombination.

To create Ypt3 fluorescently tagged N-terminally with GFP the same procedure was used and the linked 3' and 5' UTR regions were inserted before the GFP coding sequence containing no stop codon. The ORF, with a stop codon, was inserted after the GFP and the plasmids were linearized with *Sma*I reconstructed between the stitched 3' UTR and 5' UTR regions.

To create a N-terminally tagged protein mCherry-Atb2, we generated a plasmid containing the putative promoter of Atb2 (we amplified 1.4Kb upstream of the Atb2 ORF) followed by the mCherry coding region without the stop codon and the ORF of Atb2. This plasmid was linearized with *Afe*I located in the *ura4* coding sequence on the plasmid and was transformed in a strain with a mutated *ura* locus where it reconstructed a functional *ura* gene.

To create a protein tagged with a fluorescent marker at the C-terminus, we amplified at least 1kB of the end of the ORF containing a restriction site and no stop codon, and inserted it in the plasmid containing GFP or mCherry coding sequences. After linearization, the plasmid was transformed and inserted in the native loci of the genes of interest.

To mark the nuclei, we expressed GFP tagged with two nuclear localization signals using the promoter for Atb2 to drive the expression from the *ura* locus.

Transformation was done as previously described (Aoki et al., 2010). Briefly, the cells were grown to exponential phase and then washed in ice-cold water and 1M sorbitol. After incubation with 1M DTT, the cells were put in contact with at least 300ng of linearized plasmid. Transformation of the cells was achieved through electroporation in 0.2cm cuvettes, with those exact settings: 2.3KV, 200 Ω , 25 μ F (Gene Pulser II, Biorad). Cells were left in liquid YE medium overnight to recover and plated the next day on selective media (EMM-AL, lacking uracil).

In the case of the construction of Pom1-GFP strain, we linked together a fragment of the 3' UTR region with a fragment of the end of the ORF without the stop codon and we cloned the stitched fragment in

a pFA6a-GFP-kanMX plasmid in front of the fluorescent marker. After linearization the plasmid was transformed in a wildtype prototroph strain following the same transformation protocol and selected on YE-G418 plates. All strains were checked for correct insertion of the plasmid with diagnostic PCR and in the case of deletions we also used primers inside the coding region and confirmed the ORF was properly deleted.

Microscopy imaging. Wide-field microscopy was performed on a DeltaVision platform (Applied Precision) composed of a customized inverted microscope (IX-71; Olympus), a 60x/1.42 NA oil objective, a camera (CoolSNAP HQ2; Photometrics or PrimeBSI CMOS; Photometrics), and a color combined unit illuminator (Insight SSI 7; Social Science Insights). Figures were acquired using softWoRx v4.1.2 software (Applied Precision). Spinning-disk microscopy was performed using an inverted microscope (DMI4000B; Leica) equipped with an HCX Plan Apochromat 100x/1.46 NA oil objective and an UltraVIEW system (PerkinElmer; including a real-time confocal scanning head [CSU22; Yokagawa Electric Corporation], solid-state laser lines, and an electron-multiplying charge-coupled device camera [C9100; Hamamatsu Photonics]). Stacks of z-series confocal sections were acquired at 0.5-to-1 μ m intervals using Volocity software (PerkinElmer). Confocal microscopy tile scan images were acquired with a Zeiss laser scanning microscope (LSM 710) mounted with an EC Plan-Neofluar 40X/1.30NA oil objective. Images of growing yeast colonies on agar plates were imaged with a Leica MZ16 FA stereomicroscope (magnification 80-100 times). Images of growing hyphae on agar pads were imaged with a Leica brightfield microscope mounted with a 20X air objective. Phase contrast imaging was acquired on Nikon Eclipse Ti microscope, mounted with a 100X phase contrast objective.

Hyphal transition experiments. Cellasic ONIX microfluidics system was routinely used to image the transition (CellAsic system, Millipore, USA, (Lee et al., 2008)). To image the yeast form, cells were grown overnight in 3ml of liquid EMM-ALU to OD₆₀₀ = 0.4 and then loaded in the plate 2 hours prior to imaging to give them time to settle. To image the hyphal form, the cells were grown in liquid EMM-ALU overnight up to an OD₆₀₀ of 0.1-0.2, loaded in the microfluidics plate and grown in EMM-ALU-10%RG for 12 to 15hours before imaging at 3 psi (20.7 kPa) in complete darkness (plate surrounded with aluminum foil) to induce hyphal formation. To observe the transition on solid agar plates (agar bacteriological, Oxoid, LP0011), we typically cultured *S. japonicus* overnight in 3ml EMM-ALU and let the cells grow to exponential phase. Cells were then spun down and concentrated before being plated on solid agar plates containing 10% of red grape extract. Hyphal growth was assessed 4 to 12 days later, as indicated. To assess growth rate in rich media, cells were grown on YE-2%agar

microscopy pads supplemented or not with RGE for 12 hours before imaging. For the confocal microscopy imaging, *S. japonicus* hyphae were grown on EMM-ALU 12% gelatin (Sigma-Aldrich, #48723) plates supplemented with 10% RGE for 8 days before a piece of gelatin containing hyphae was cut out and mounted on a slide for imaging.

Drug treatments and stainings. To depolymerize actin, we used a 20mM stock of Latrunculin A (LatA) dissolved in dimethyl sulfoxide (DMSO) to exponentially growing cells to a final concentration of 200 μ M. Methyl benzimidazole carbamate (MBC, Sigma) was used for the depolymerization of microtubules. A stock solution at 2.5mg/ml in DMSO or ethanol was made freshly on the day of the experiment and exponentially growing cells were treated at a final concentration of 25 μ g/ml for 10min at 30°C. To depolymerize microtubules in the microfluidics chambers we flowed in EMM-ALU containing 25 μ g/ml at 3psi, which led to total depolymerization within 10-15 min, similar to the timing observed in liquid cultures. To wash the drug away, we flowed in EMM-ALU at 3 psi and recovery of the cytoskeleton was observed within a few minutes. FM4-64 stainings on growing hyphae were performed in microfluidics chambers as previously described (Fischer-Parton et al., 2000). To label vacuoles with Lucifer Yellow, cells were pre-grown in EMM-ALU+10%RGE for 24h at 25°C in the microfluidics device, incubated for 1h with 4mg/ml Lucifer Yellow in H₂O and further washed for 1h with EMM-ALU+RGE before imaging.

Treatment of RGE. To identify the molecule in the red grape extract responsible for the morphological transition, we submitted the RGE to a variety of physical and enzymatic treatments. RGE was treated with 16u of proteinase K (NEB, 800u/ml), 20u and 100u of DNase I (NEB, 2000u/ml) and 1000u of RNase If (NEB, 50000u/ml). RGE was boiled to 95°C for 20min. RGE was subjected to chloroform/methanol mix (1:1) and left to phase separate overnight at -20°C. Both resulting aqueous and organic phase were dried with a nitrogen stream and subsequently suspended in PBS 1X. All treated RGE were then included in solid agar plates and tested for hyphal inducing capabilities (see Table 1).

Supplementation of YE media. To identify the molecule in the red grape extract responsible for the morphological transition, we also tried supplementing rich media with several likely molecular components of RGE and assess for hyphal formation. Liquid YE media was individually supplemented with an additional 40g.L⁻¹ glucose, with 100g.L⁻¹ fructose, with concentrations ranging from 2mg.L⁻¹ to

40mg.L⁻¹ resveratrol (Enzo Lifesciences) or with 270mg.L⁻¹ ascorbic acid. All supplemented YE media were then included in solid agar plates and tested for hyphal inducing capabilities (see Table 1).

Tropism assay. Cells were grown to exponential phase in YE and concentrated 10 times. On large petri dishes (120mmx120mm) containing YE-2%agar, we drew a 6 cm line in the middle of the plate on which 50µl of cells were deposited. 2 cm away from the center of the line, we dropped a small piece of chromatography paper (Whatman, 0.34mm, #3030-917) on which we pipeted 50µl of RGE or YE (control). Plates were covered with aluminum foil and left at 30°C for 12 days before quantification of the area of hyphal growth. A ratio of positive tropism (growth towards the filter) on negative tropism (growth away from the filter) was calculated for both the experiment and the control plates for each plate and averaged over two experiments.

Identification of the different morphological forms. In all our experiments we determined the stage of the morphological transition by looking at the polarity stage (monopolar/bipolar), the general localization of the vacuoles (all around the cytoplasm or already polarized at one pole) and the number of vacuoles.

Yeast: bipolar growth, no apparent vacuoles

Vacuolated yeast: bipolar growth, vacuoles all around the cytoplasm

Transition form: monopolar growth, many small vacuoles polarized at the non-growing end

Hypha: monopolar growth, one or two larger vacuole(s) at the non-growing end

Bipolar/monopolar quantification. On DIC (differential interference contrast) movies we recorded how many cells had one or two poles growing in the different forms of the morphological transition.

Growth rate calculations. On DIC movies we calculated the growth rate by measuring the change in cell or vacuole length over time. Cell growth rates on minimum media were calculated from cells growing in microfluidics plates in inducing and non-inducing conditions and were averaged over three experiments. Cell growth rates on rich media were calculated from cells growing on agar pads in inducing and non-inducing conditions and were averaged over three experiments. The correlation of

cell growth and vacuole growth was calculated from cells growing on agar pads in inducing conditions, each point in the graph representing a distinct hypha for which we calculated the extension length of the cell and the vacuole over the total time of the movies. We note that movies were of different length but it clearly demonstrates the correlation between both extension lengths.

Fluorescence levels. On spinning disk medial focal planes of GFP-Ypt3 tagged cells (150 ms exposure, 100% laser power) we calculated the fluorescence intensity at the tips of yeasts and transitioning cells by drawing a segmented line of 15 pixels in width around the cell periphery. We subtracted background noise averaged from two different fields of view per experiment. Fluorescence profiles were aligned to the geometric cell tip and averaged by cell type and over three experiments.

Quantification of vesicle speed. On spinning disk movies we manually measured the total trajectory of individual Ypt3 dots and derived the rate by dividing by the total time. Data was averaged over three experiments and averaged by cell type. Box plots were generated with <http://shiny.chemgrid.org/boxplotr/>

Quantification of lengths. Spindle length was measured at each timepoint from apparition to complete elongation on epifluorescence movies of cells tagged with GFP-Atb2. Cell length was measured by drawing a line across the cell length from cell pole to cell pole on transmitted light images on septating cells. Box plots were generated with <http://shiny.chemgrid.org/boxplotr/>. Nuclear length was calculated by drawing a line across the nuclei tagged with NLS-GFP construct on epifluorescence images.

Cell cycle quantification. Cell cycle duration was quantified from septation to septation event. On transmitted light movies containing the entire transition from yeast to hypha we started our quantification by recording at what time the hypha septated at the end of the movie and then “went back in time” to the beginning of the movie following the lineage of the selected hypha and recording the time of each septation events in the lineage from final hypha to initial yeast. Results were averaged by cell type and over three experiments. Box plots were generated with <http://shiny.chemgrid.org/boxplotr/>

Nuclear and septum positioning. To assess nuclear positioning in the cells we measured the lengths from each cell tip to the middle of the nucleus on cells expressing NLS-GFP and plotted both lengths as a ratio. For the induced forms we plotted growing end length over non-growing end length. Cells were averaged by cell type and over three experiments. To assess nuclear positioning in the cytoplasm in yeast we used the same data as for nuclear positioning in the cell as the entire cell length is filled with cytoplasm. To assess nuclear positioning in the cytoplasm in hyphae we calculated the lengths from the growing cell tip to the middle of the nucleus and from the middle of the vacuolization zone to the middle of the nuclei. The vacuolization zone is the region in front of the large vacuole where small vacuoles are continuously delivered to the large one. We plotted the growing end length over non-growing end length. Results were averaged over three experiments. To assess septum positioning we plotted a ratio of the length from the growing cell tips to the septum over the length of the cytoplasm from transmitted light images. We averaged by cell type and over two experiments.

Quantification of microtubules plus-end localization. To measure microtubule plus end positions in hyphae, we used the center of the nucleus as reference point and measured the distance to each microtubule plus end. 10 hyphae, with a total of 50 microtubules were quantified. Microtubules pointing towards the growing tip have a positive distance value; those growing into the vacuolar compartment have a negative value. These distances were plotted on a graph, shown in Figure 7E. The accompanying schematic drawing indicates interval distances for the position of the vacuole and the two cell ends.

Microtubule depolymerizing drug washing. In microfluidic chambers we flowed cells with EMM-ALU supplemented with MBC (25 μ g/ml final concentration) for three hours before washing with EMM-ALU only. We assessed nuclear positioning in a strain expressing NLS-GFP before and after the wash. Even though microtubule re-polymerization occurred in the first 10 minutes (data not shown), we quantified the nuclear centering 50 minutes after wash because some cells were slower to reposition their nuclei than others.

<i>RGE treated with:</i>	<i>yeast-to-hypha transition?</i>	<i>Conclusion</i>
Boiled	yes	Inducer is not labile
RNase	yes	Inducer is not RNA
DNase	yes	Inducer is not DNA
Proteinase K	yes	Inducer is not a protein
Chloroform	no	Inducer is not a lipid
MetOH	yes (in soluble phase)	Inducer is a soluble component

<i>agar plates +</i>	<i>yeast-to-hypha transition?</i>	<i>Conclusion</i>
Red grape extract	+++	Inducer is in RGE
White grape extract	+++	Inducer is in WGE
Blueberry extract	+++	Inducer is in BE
Strawberry extract	+++	Inducer is in SE
Raspberry extract	+++	Inducer is in RE
Glucose	-	Inducer is not extra glucose
Fructose	-	Inducer is not fructose
Resveratrol	-	Inducer is not resveratrol
Ascorbic acid	-	Inducer is not ascorbic acid
Volatile chambers	-	Inducer is not a volatile
Ethanol	+	Small induction
Apple pectin	-	Inducer is not apple pectin
Aspartic acid	+	Small induction
Cellulose phosphate	+	
Gelatin	++	

Table 2.1: Hyphal inducing properties of fruit extracts and candidate molecules

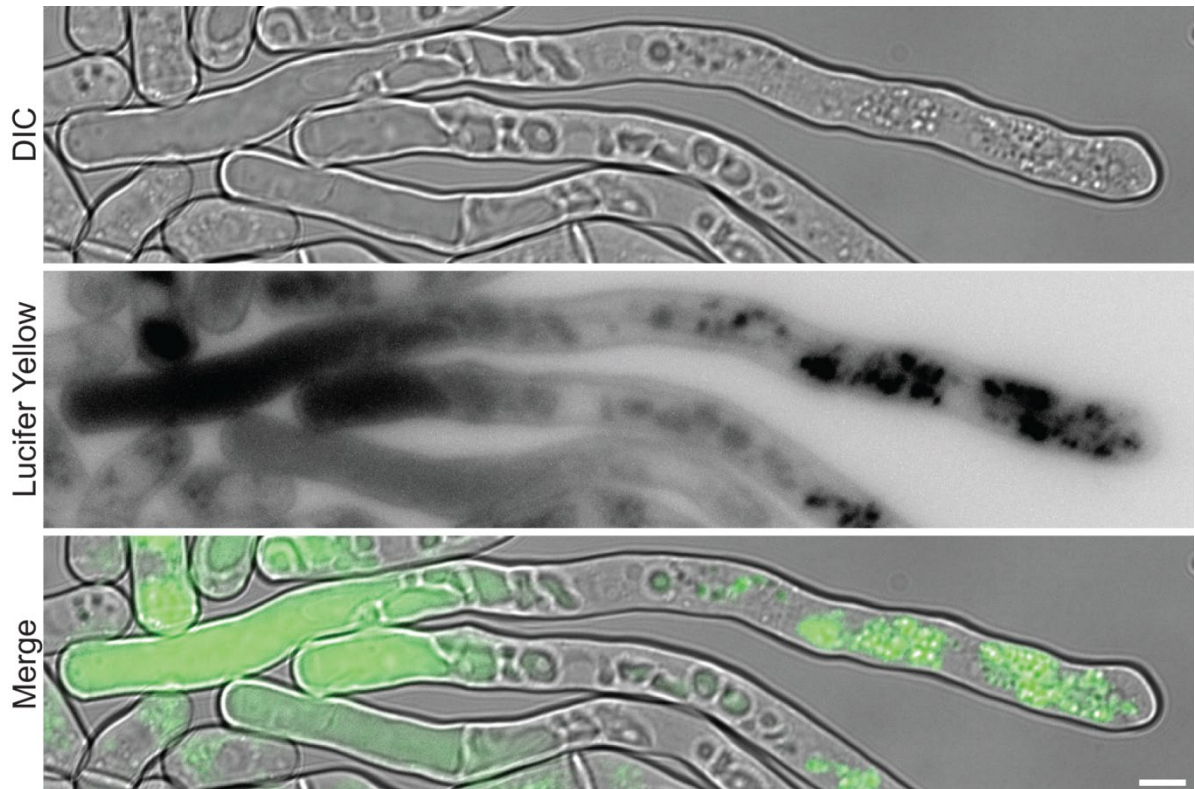


Figure S1. Vacuole staining with Lucifer Yellow. Microscopy images showing several hyphae stained with Lucifer Yellow, which accumulates both in the large vacuoles at the back of the cell and in much smaller organelles in the front half. Scale bar 5 μ m.

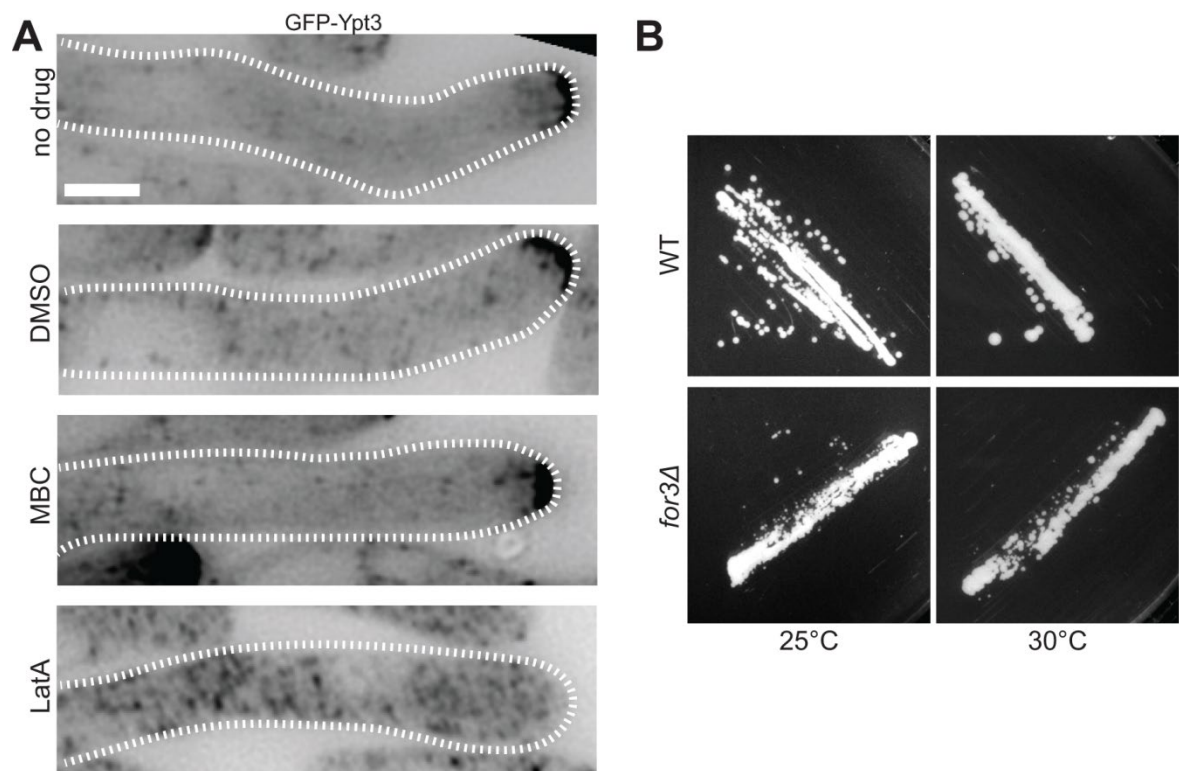


Figure S2. Importance of formin For3 and F-actin in polarized growth. A. Middle plane images of GFP-Ypt3 in

hyphae grown in a microfluidics chamber in presence or not of DMSO, MBC or LatA. **B.** *S. japonicus* WT and *for3Δ* strains growing on solid rich media for three days at 25°C or 30°C. Scale bar: 5µm.

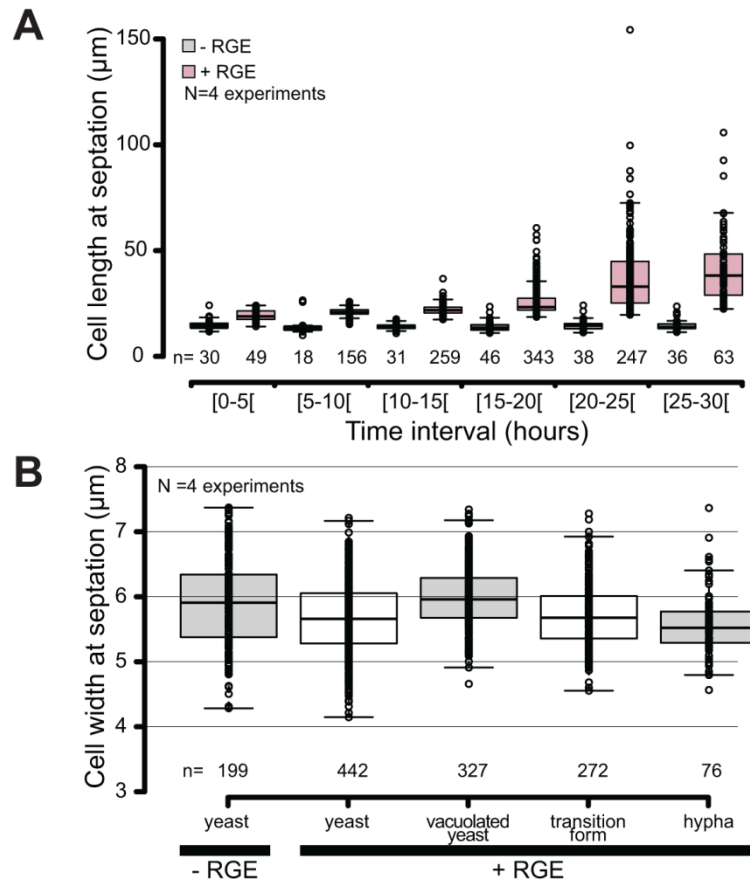


Figure S3. Measurement of cell width and length at septation. **A.** Box plot of septation length of cell populations over 30 hours in microfluidic chambers. Box plots show first and third quartile and median, whiskers extend 1.5 times the interquartile range from the first and third quartile. **B.** Box plot of cell width at septation in the different morphological forms of *S. japonicus*.

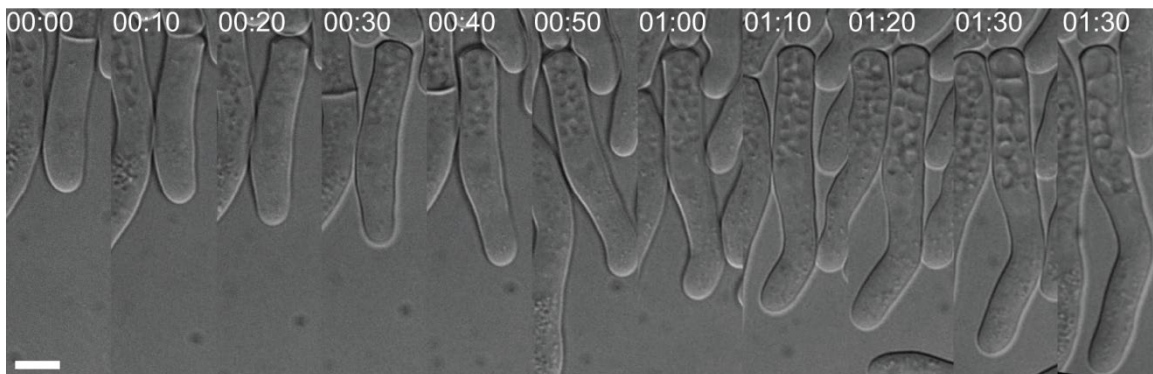


Figure S4. Asymmetric formation and partitioning of vacuoles in the transition form. DIC microscopy image showing division of a cell growing in RGE highlighting vacuole formation at the back of the front daughter cell. Time in h:min. Scale bar: 5µm.

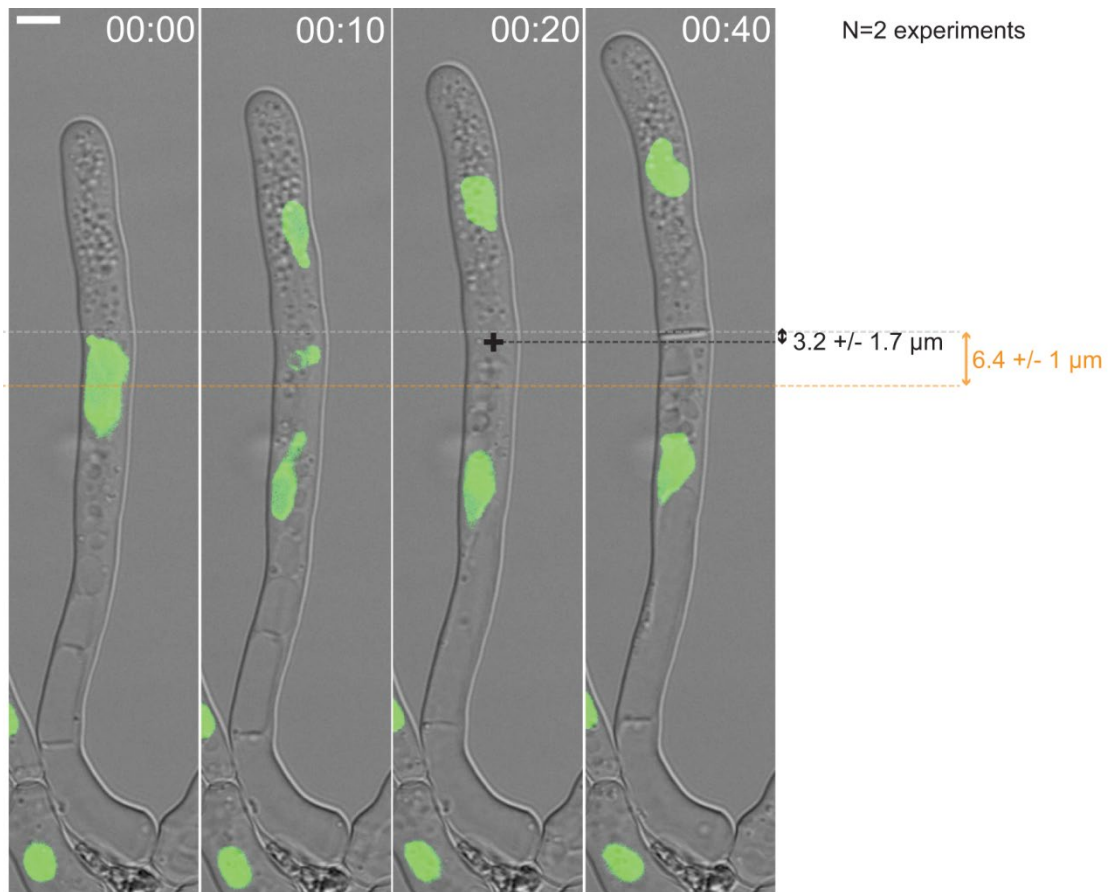


Figure S5. Septum position is better predicted by the middle of the anaphase spindle than the position of the pre-divisional nucleus. Timelapse imaging of a hypha where the positions of the pre-divisional nucleus (orange dotted line), the inferred middle of the anaphase spindle (black cross) and the septum (grey dotted line) are marked. The arrows show the distance between the position of the septum and that of either the pre-divisional nucleus or the middle of the anaphase spindle with their respective average and standard deviations over 20 cells. Time in h:min. Scale bar: 5 μm .

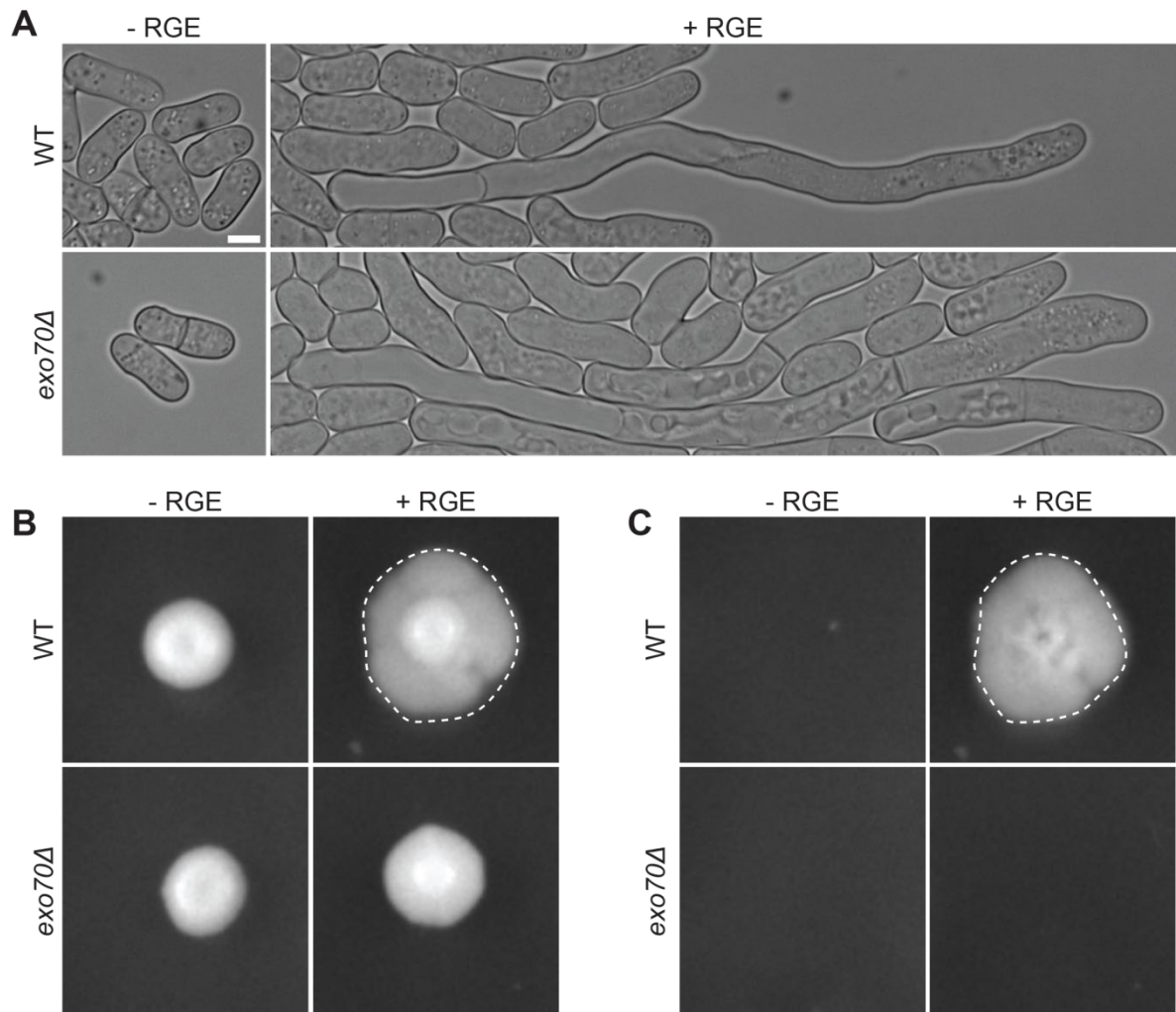


Figure S6. Hyphal growth in *exo70Δ* cells. **A.** WT and *exo70Δ* cells growing in a microfluidic chambers supplemented or not with RGE. **B.** WT and *exo70Δ* cells growing on solid media supplemented or not with RGE. **C.** Same plate as in (B) but washed. Experiment was duplicated. Dotted line highlight hyphal formation. Scale bar: 5 μ m.

Supplemental videos are available by scanning the following QR codes:



Movie S1. Yeast-to-hypha transition of *S. japonicus*. DIC movie of a growing *S. japonicus* mini colony in a microfluidic chamber in presence of the inducer RGE. Time is in h:min. Scale bar: 5 μ m.



Movie S2. Tea1 deposition at hyphal tips. Spinning disk movie of the hyphal form tagged with Tea1-GFP. Images are maximum intensity projections of 11 z-stacks (0.5 μ m step size). Time is in min:sec. Scale bar: 5 μ m.



Movie S3. Vesicle trafficking in the yeast form. Spinning disk movie showing middle plane section of the yeast form tagged with GFP-Ypt3. Time is in min:sec. Scale bar: 5 μ m.



Movie S4. Vesicle trafficking in the hyphal form. Spinning disk movie showing middle plane section of the hyphal form tagged with GFP-Ypt3. Time is in min:sec. Scale bar: 5 μ m.



Movie S5. Microtubule organization in the yeast form. Spinning disk movie of the yeast form tagged with GFP-Atb2. Images are maximum intensity projections of 10 z-stacks (0.5 μ m step size). Time is in min:sec. Scale bar: 5 μ m.



Movie S6. Microtubule organization in the hyphal form. Spinning disk movie of the hyphal form tagged with mCherry-Atb2. Images are maximum intensity projections of 9 z-stacks (0.5 μ m step size). Time is in min:sec. Scale bar: 5 μ m.



Movie S7. Asymmetrical division in the hyphal form. DIC movie showing hyphal growth and division. The front daughter cell rebuilds a vacuole after division. Time is in h:min. Scale bar: 5 μ m.



Movie S8. Vacuole fusion. DIC movie showing fusion of smaller vacuoles into an increasingly larger one. Time is in h:min. Scale bar: 5 μ m.

Figure	Name	Genotype	Species	Source
1A-D, 2A-E, 3A, 6. AE-J, 7A, S1, S3, S4A-B, MS1, MS7-8	JSM020	<i>h+ mat-2017 wcs1::natMX6 wcs2::kanMX6</i>	<i>S. japonicus</i>	(Okamoto et al., 2013)
4H, 5D-E, 7F, S2B	JSM023	<i>h+ ade6sj-domE ura4sj-D3</i>	<i>S. japonicus</i>	(Furuya and Niki, 2009)
3A, 4A-E, S2A, MS3-4	JCK060	<i>h+ GFP-ypt3-ura4+ ade6sj-domE</i>	<i>S. japonicus</i>	This study
6B-D, 7B-D, S5	JCK090	<i>h+ p^{Atb2}-NLS-GFP-NLS-ura4+ wcs1::natMX6 wcs2::kanMX6</i>	<i>S. japonicus</i>	This study
5B-C, 7E	JCK093	<i>h- p^{Atb2}-mCherry-Atb2-ura4+ p^{Atb2}-GFP-NLS-GFP-ura4+</i>	<i>S. japonicus</i>	This study
5F-H, MS5	JSM003	<i>h- p^{Atb2}-GFP-Atb2::ura4+ ade6sj-domE</i>	<i>S. japonicus</i>	(Yam et al., 2011)
4F, 5A, MS6	JCK027	<i>h- p^{Act1}-Lifeact-GFP-ura4+ p^{Atb2}-mCherry-Atb2-ura4+</i>	<i>S. japonicus</i>	This study
3A	JCK005	<i>h+ myo52-GFP-ura4+ ade6sj-domE ura4sj-D3</i>	<i>S. japonicus</i>	This study
3B-C	JCK024	<i>h+ spa2-GFP-ura4+ ade6sj-domE</i>	<i>S. japonicus</i>	This study
3B-C	JCK0026	<i>h+ bud6-GFP-ura4+ ade6sj-domE</i>	<i>S. japonicus</i>	This study
3B-C, MS2	JCK033	<i>h+ tea1-GFP-ura4+ ade6sj-domE</i>	<i>S. japonicus</i>	This study
3B-C	JCK056	<i>h+ exo70-GFP-ura4+ ade6sj-domE</i>	<i>S. japonicus</i>	This study
4G	JCK049	<i>h+ for3::ura4+ Lifeact-GFP-ura4+ ade6sj-domE</i>	<i>S. japonicus</i>	This study
4H, S2B	JCK031	<i>h+ for3::ura4+ ade6sj-domE</i>	<i>S. japonicus</i>	This study
5D-E	JCK061	<i>h+ tip1::ura4+ ade6sj-domE</i>	<i>S. japonicus</i>	This study
7F	JSM046	<i>h+ mid1::ura4 ade6sj-domE urasj-D3</i>	<i>S. japonicus</i>	(Gu et al., 2015)
7F	JCK003	<i>h+ pom1::ura4+ ade6sj-domE</i>	<i>S. japonicus</i>	This study
7G	JSM018	<i>h- pom1-GFP::kanMX6</i>	<i>S. japonicus</i>	This study
3C	YSM735	<i>h+ bud6-3GFP-kanMX ade6-M216 leu1-32 ura4-D18</i>	<i>S. pombe</i>	(Martin and Chang, 2006)
3C	YSM1023	<i>h- spa2-GFP ade6- leu1- ura4-</i>	<i>S. pombe</i>	Lab strain
3C	YSM1253	<i>h+ tea1-GFP-kanMX ade6- leu1- ura4-</i>	<i>S. pombe</i>	(Martin et al., 2005)
3C	YSM2075	<i>h- exo70-GFP-kanMX ade6-M210 leu1-32 ura4-D18</i>	<i>S. pombe</i>	(Bendezu et al., 2012)
1C	YSM1371	<i>h+ WT (975) ade6+ leu1+ ura4+ his7+</i>	<i>S. pombe</i>	Lab strain
1C	YSM2336	<i>h90 WT</i>	<i>S. octosporus</i>	(Rhind et al., 2011)
1C	W303	<i>α leu2-3 trp1-1 can1-100 ura3-1 ade2-1 his3-11</i>	<i>S. cerevisiae</i>	(Ralser et al., 2012)
S6	JCK114	<i>h+ exo70::ura4 ade6sj-domE</i>	<i>S. japonicus</i>	This study

Table S1. List of the strains used in this study.

Acknowledgements

We thank Snezhana Oliferenka (Crick Institute, London) for critical technical help at the start of the project. We thank her and Hironori Niki (National Institute of Genetics, Japan) for strains and reagents. This work was supported by an ITN funding (FungiBrain) and SNF grant (310030B_176396) to SGM. We are thankful to Serge Pelet and his group, as well as the Martin group for critical reading of the manuscript.

Author contributions

Conceptualization: CK and SGM. Investigation: OD discovered the inducing action of fruit extracts and constructed the Pom1-GFP strain; CK performed all experiments. Writing: CK wrote the original draft; SGM and CK edited it. Funding acquisition: SGM.

Chapter 2: Myosin V localization in *S. japonicus*

Summary:

In this chapter I investigated the localization of type V myosins in *S. japonicus* and evidenced a colocalization between an actin-based motor, Myo51, and microtubules. This led me to uncover a colocalization between actin and microtubules in fission yeast underlying a putative alternate mechanism to move cargoes in the cytoplasm.

2.1 Introduction

In **chapter 1**, I described actin cables as essential for polarized processes in *S. japonicus*. To continue this investigation further I studied type-V myosins (MyoV) a family of actin-based motors.

Myosins belong to a family of motor proteins involved in diverse motility processes in eukaryotes. Myosins are very diverse with 18 known classes with widely different functions. MyoV are processive motors walking on actin tracks and move cargoes (organelles, vesicles, proteins, etc...) within the cell. They are highly conserved in eukaryotes and deletion of one of the myoV in humans is associated with the onset of a rare recessive autosomal disease; Griscelli syndrome (Menasche et al., 2003).

In fission yeast there is two different myoV; respectively Myo51 and Myo52 (Motegi et al., 2001; Win et al., 2001). These proteins contain a N-terminal motor domain that interacts with F-actin and ATP, an arm containing several IQ repeats, a coil-coil domain for dimerization of the motors and a globular tail that binds the cargo (Trybus, 2008). In *S. pombe* both MyoV are involved in actin cable organization (Lo Presti et al., 2012). Single deletion of *myo51* has no obvious effects on cell morphology but deletion of *myo52* had dramatic effects on polarity (Motegi et al., 2001; Win et al., 2001). Myo51 is involved in cytokinetic ring assembly (Wang et al., 2014) and does not appear to actively move cargo on actin cable but rather just decorate actin structures.

MyoV has also been implicated in polarized processes in filamentous fungi. Indeed, deletion of *myoE*, the only type V myosin identified in *Aspergillus nidulans* causes defects in hyphal tip growth and subsequent hyphal colony establishment (Taheri-Talesh et al., 2012). Defects in polarization and growth rate were also reported in cells lacking *myo5* in the dimorphic yeast *Ustilago maydis* (Weber et al., 2003).

In this chapter, I studied the localization of the cytoskeleton and associated motors in comparison to each other in the yeast form and the hyphal form of *S. japonicus* but also in *S. pombe* in order to elucidate their role in the polarity processes in this species. Through colocalization studies I uncovered an overlap between the localization of cytoskeletal components underlying a putative cooperation between tracks in fission yeast.

2.2 Results

2.2.1 Myosin-V in *S. japonicus*

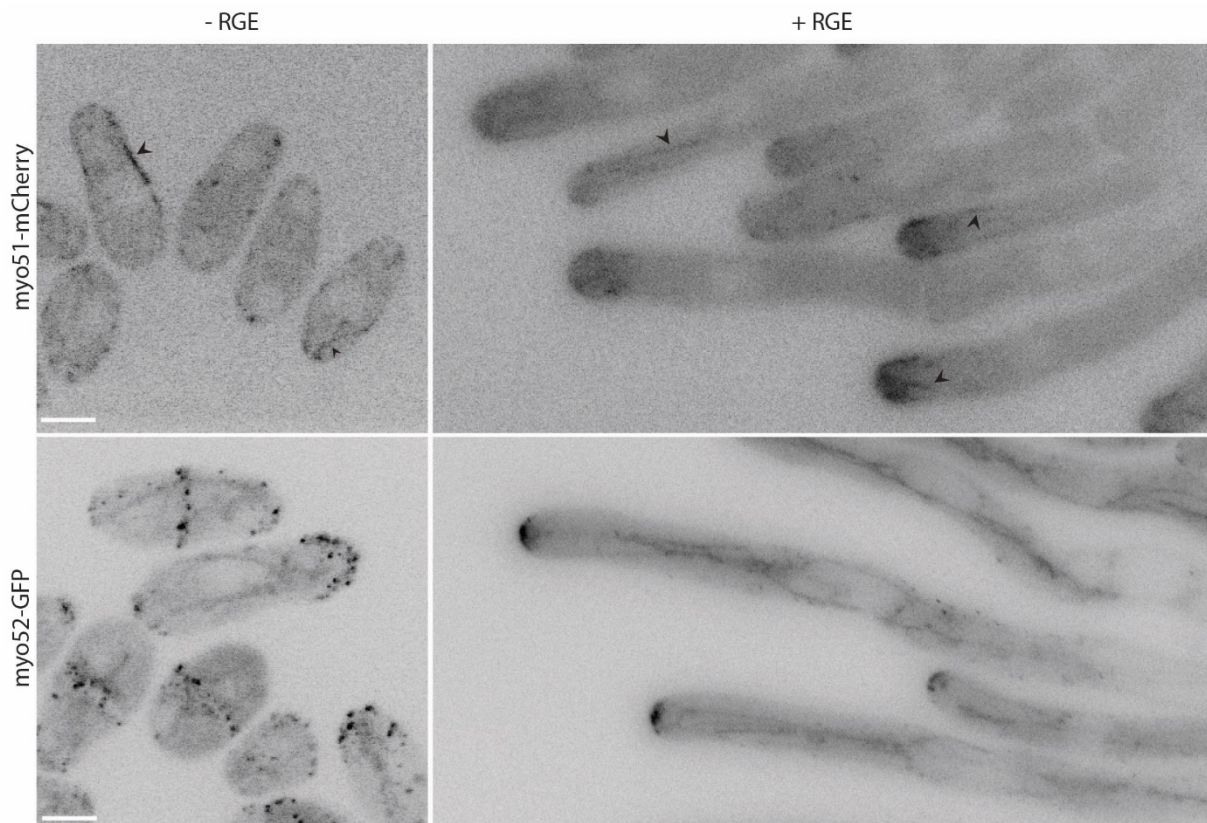


Figure 3.1. *MyoV* localization in *S. japonicus*. These images are maximum intensities projections of 5-6 z-stacks (0.5 μ m step). Myo51 forms cables in the cytoplasm (arrows). In the hyphal form we also observe an accumulation at the growing tip. Myo52 forms dots that localize at the tips and at the division site. Note: there is a lot of auto fluorescence in the GFP channel, the filamentous-like structure in the cytoplasm is probably mitochondria. In the hyphal form, Myo52 forms a dynamic cap at the growing end. Scale bars: 5 μ m.

Initial investigation focused on studying the localization of Myo51 and Myo52 in *S. japonicus*. The localization of Myo51 was tricky to assess due to its very faint signal but I observed Myo51-mCherry formed cable-like structures in the cytoplasm (**Fig. 3.1** upper panel) and was also located at the septum of dividing cells (data not shown), similar to its localization in *S. pombe* (Lo Presti et al., 2012). Myo52-GFP formed dots accumulated at the growing tips of the cells (**Fig. 3.1** lower panel), and I could observe some of those dots travelling to the tips (data not shown) again reminiscent of its localization in *S. pombe*. In the hyphal form Myo51 cables can also be seen in the cytoplasm and both MyoV accumulate at the growing tip of hyphae. The localization of Myo51 at the hyphal tips was very reminiscent of the localization of actin filaments as described in **Chapter 1**. By contrast, Myo52-mCherry localized as a very dynamic cap at the hyphal tips. Both localization patterns suggest a potential role in polarized growth.

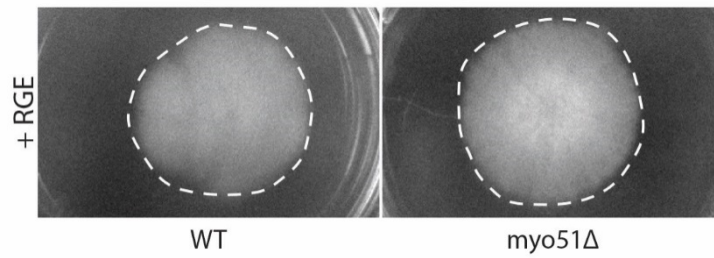


Figure 3.2 WT and Myo51 Δ cells growing on solid media supplemented with RGE. Pictures are taken from below the plate. Dotted line highlights hyphal formation after 4 days of growth.

I set out to analyze the impact of the deletion of MyoV in *S. japonicus* more particularly in the context of filamentation. I successfully deleted *myo51* and the mutant cells showed no phenotype of length or width in the yeast form (data not shown) similar to what is observed in *S. pombe*. Mutant cells were also still able to transition to hyphal growth on solid media with no apparent colony establishment issues (**Fig. 3.2**). I attempted to delete *myo52* several times but it was always unsuccessful leading me to believe this gene could be essential in *S. japonicus*.

2.2.2 Colocalisation study in fission yeast

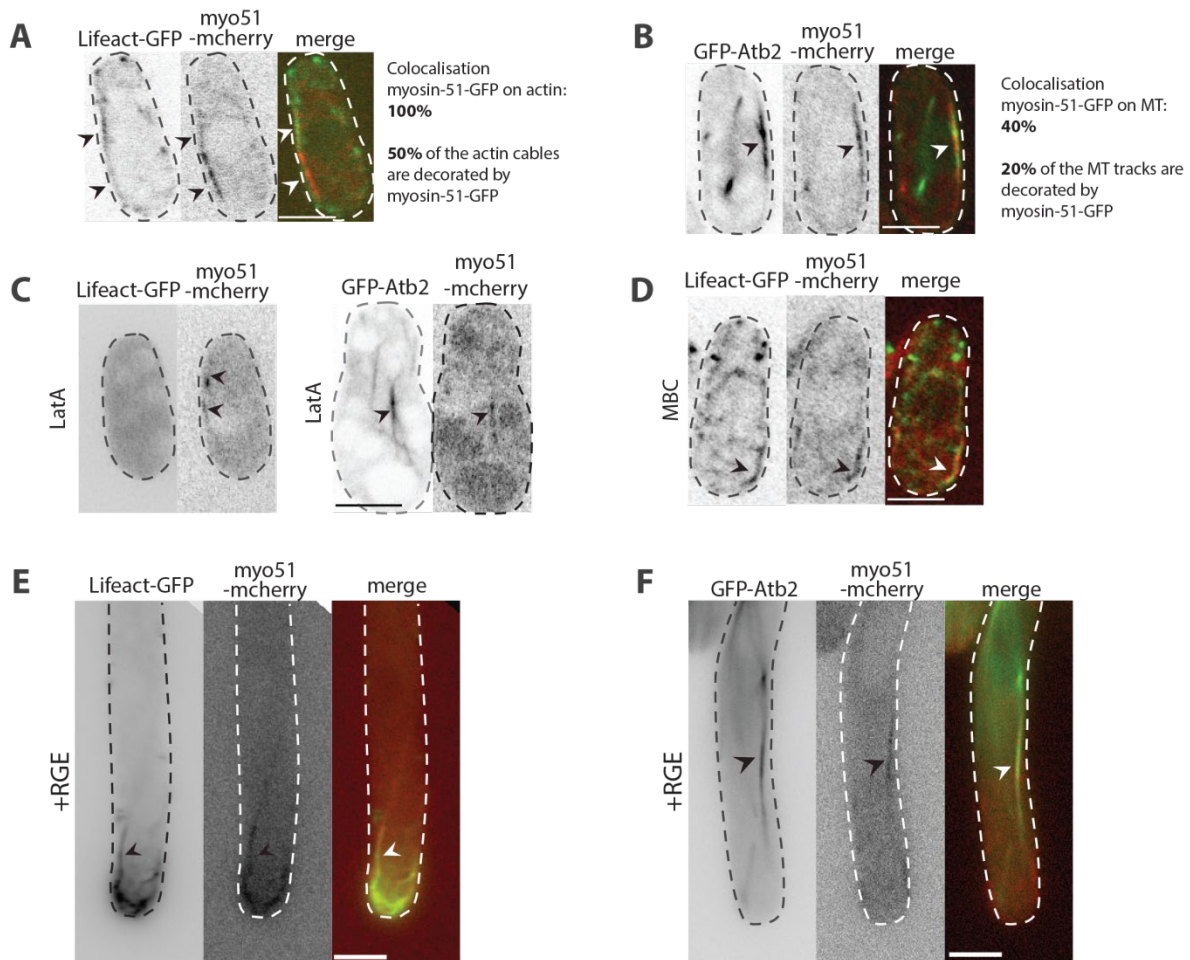


Figure 3.3. Colocalizations of cytoskeletal components. **A.** Myo51-mCherry colocalizes with actin tracks marked with Lifact-GFP. **B.** Myo51-mCherry colocalizes with microtubule tracks marked with GFP-Atb2. **C.** Actin depolymerization with LatA, Myo51 cables can still be observed and they colocalize with the microtubule tracks. **D.** Microtubule depolymerization with MBC shows that Myo51 still binds actin cables. **E. F.** Colocalization between Myo51 and the cytoskeleton tracks is also observable in the hyphal form. Images are middle plane sections acquired on a spinning disk microscope. Scale bars: 5µm.

The localization of Myo51 as cables scattered in the cytoplasm led me to investigate its localization in comparison to the cytoskeleton. It is known that Myo51 decorates actin cables in *S. pombe* (Lo Presti et al., 2012). I found that in *S. japonicus* as well, Myo51 filaments colocalized with actin cables in both the yeast form and the hyphal form (**Fig. 3.3A**, **Fig. 3.3E**). Surprisingly, actin depolymerization using LatA did not eliminate all cable-like organization of Myo51, in fact some cables remained and colocalized with microtubules (**Fig. 3.3C**). Upon microtubule depolymerization with MBC, the Myo51 cables still colocalized with actin tracks (**Fig. 3.3D**). I quantified this colocalization by counting the number of Myo51 cables in the yeast form and looked at the frequency of colocalization with microtubules or actin. I found that in 100% of the instances in which I observed Myo51 cables they colocalized on the actin (n=12 cells) but in 40% of the cases those cables also colocalized with the microtubules (n=7 cells) (**Fig. 3.3A**; **Fig. 3.3B**). At the cytoskeletal level, 20% of the microtubules (n=7

cells) and 50% of the actin tracks are colocalizing with Myo51 cables (n=12 cells) (**Fig. 2.3A**; **Fig. 2.3B**). In experiments in which I depolymerized both cytoskeletal tracks, I could not observe any Myo51 cables in the cytoplasm anymore (data not shown). These experiments indicate that Myo51 associates with both actin cables and microtubules.

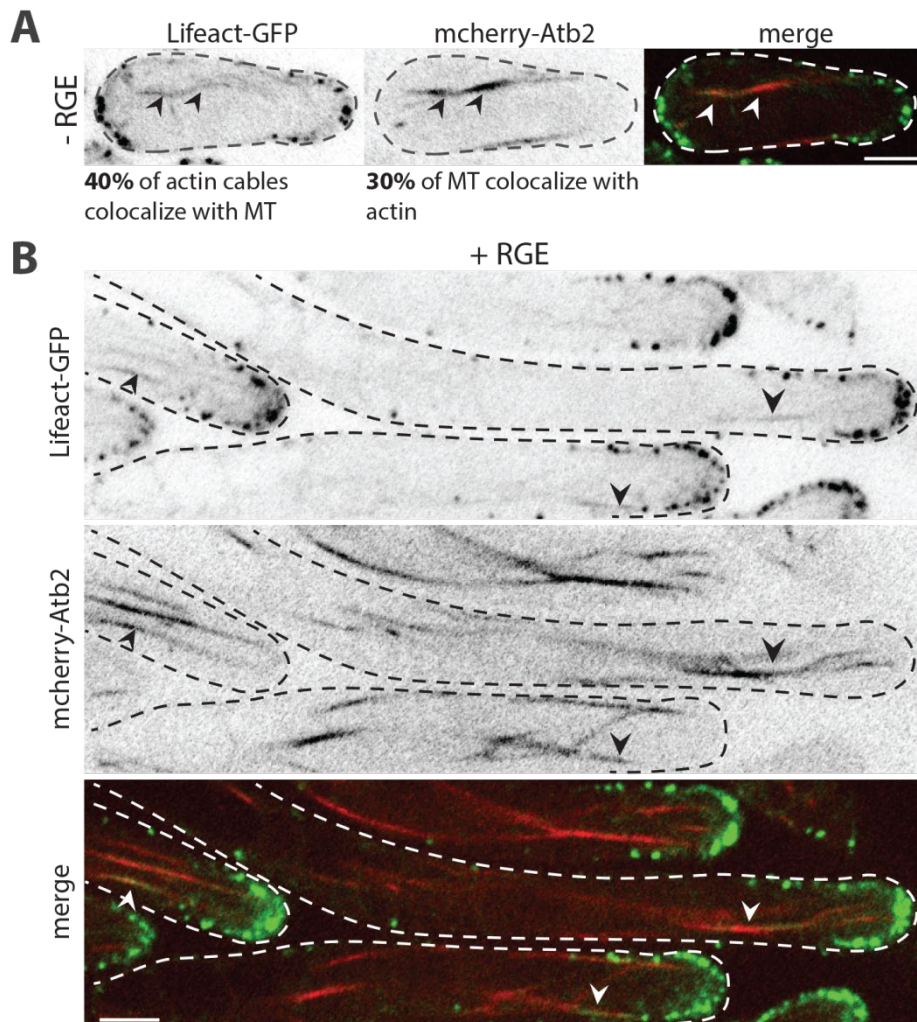


Figure 3.4. Middle plane sections of spinning disk images showing a strain tagged with Lifact-GFP and mCherry-Atb2 showing that actin cables and microtubule tracks colocalize partially in both the yeast form (**A**) and the hyphal form (**B**). Scale bars: 5µm.

These experiments led me to investigate the localization of both cytoskeletons in regards to each other so I engineered a strain that was tagged for both microtubules (mCherry-Atb2) and actin (Lifact-GFP). I found that actin and microtubule cables partially colocalized in both the yeast form (**Fig. 3.4A**) and the hyphal form (**Fig. 3.4B**). I quantified the colocalization in the yeast form and found that an average of 40% of all actin cables colocalized with microtubule array and 30% of the microtubules colocalized with actin (n=21 cells). Because Myo51 was colocalizing with both actin and microtubules I investigated whether it could possibly be the link between the two cytoskeletons. I

found that *myo51Δ* cells still showed partial overlap of actin and microtubules (**Fig. 3.5**) indicating that the partial colocalization of the cytoskeleton is independent of Myo51.

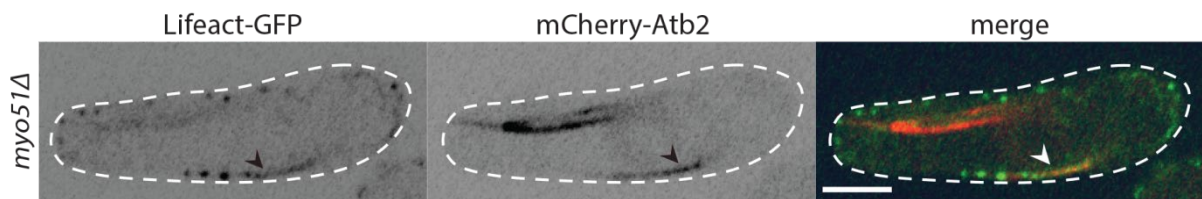


Figure 2.5. The colocalisation of actin cables and microtubule tracks is independent of Myo51. These images are spinning disk middle plane sections. Scale bar: 5µm.

Finally, I looked at the colocalization of actin and microtubule cables in *S. pombe* and evidenced a cytoskeleton overlapping in this species as well (**Fig 3.6**). This result shows that a putative cooperation between the cytoskeleton could be conserved in fission yeast.

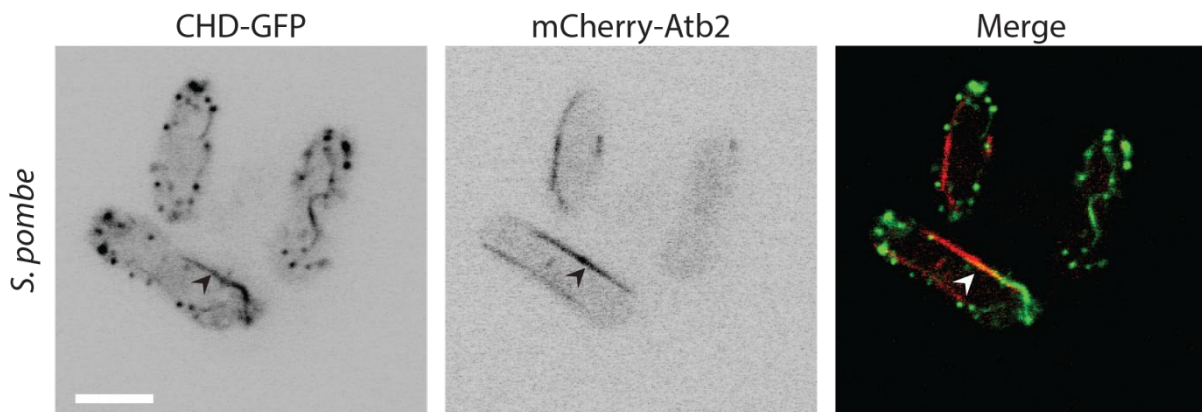


Figure 3.6. Spinning disk images of *S. pombe* tagged with actin marker CHD-GFP and microtubule marker mCherry-Atb2 showing colocalization between the two types of cytoskeleton (arrows). Scale bar: 5µm.

2.3 Discussion & perspectives

2.3.1. A cooperation between actin and microtubules?

Even though actin filaments and microtubule cables are two different components of the cytoskeleton, with distinct roles, evidence through the years suggests a functional cooperation between the two across several species for a wide variety of functions (Goode et al., 2000). Actin regulates microtubule organization in motile cells (Rodriguez et al., 2003). There has been evidence of interaction between the cytoskeleton in transport of organelles in several organisms (Brown, 1999; Goode et al., 2000). In fission yeast, cell end markers Tea1/Tea4 are deposited at the poles by the microtubules and associated kinesin-like Tea2. Tea4 will recruit For3 that will in turn nucleate actin cables initiating cell growth (Martin et al., 2005). In the budding yeast *Saccharomyces cerevisiae* there is cooperation between actin filaments and microtubule cables for the proper spindle positioning during mitosis. A protein called Kar9 serves as a link between actin and microtubules by binding both the tail of Myo2p (type-V myosin) a motor on the actin and a regulator of the microtubule plus-end binding protein (Fischer et al., 2008; Liakopoulos et al., 2003). A similar cooperation has been recently found in the filamentous fungus *Aspergillus nidulans* in which they identified a Kar9 homolog named MigA. Like Kar9, MigA can also indirectly link actin and microtubules and is involved in microtubule capture at the hyphal tips (Manck et al., 2015). There is also evidence of cooperation between Myosin-V and kinesins in the filamentous fungus *Ustilago maydis* for correct polarization of the cells and subsequent hyphal growth (Schuchardt et al., 2005). Interestingly, as described in this chapter, I observed an overlap of Myo51 with the cables of actin and microtubules as well as a colocalization between the cytoskeletal filaments even in absence of Myo51. This suggests a potential synergy between the cytoskeleton and I am wondering if this could be beneficial for cell growth, for example facilitating the delivery of cargo to the tips. In itself a cooperation of the cytoskeleton cannot explain how *S. japonicus* undergoes hyphal growth because I have observed the same cytoskeleton colocalization in the yeast form of *S. japonicus* and in *S. pombe*. However, cooperation through overlapping between cytoskeletal tracks has never been evidenced in fission yeast and is a fascinating perspective. Future efforts could be concentrated on studying the localization of kinesins and myosins in respect to each other. Moreover, generating Myo51 truncations to understand which part of the protein is necessary for the colocalization to microtubules and understand if it is a direct or indirect relationship could be useful (see material and methods).

2.3.2. Is Myo52 essential in *S. japonicus*?

In *S. pombe*, Myo52 transport exocytic vesicles along the actin cables and towards the cells poles (Lo Presti and Martin, 2011) and the mutant for *myo52* shows a severe polarity phenotype and growth defects (Motegi et al., 2001; Win et al., 2001). I have tried for over two years to generate a *myo52* mutant in *S. japonicus*. I have tried several times to replace the entire ORF with a selection marker and tried to generate genes truncations in the N-terminal part. All methods were unsuccessful, with only unusual recombinant growing on selective plate. They always retained the full ORF and somehow still acquired the selection cassette, making me believe *myo52* might be essential in this species. Because *S. japonicus* can achieve such a dramatic polarization it could be that the role of Myo52 in growth and polarization is even more important than in *S. pombe*. This finding, along with the much sicker phenotype observed in *for3Δ* cells (see **Chapter 1**) suggests that the extreme polarized processes in *S. japonicus* possibly relies much more on actin tracks than *S. pombe*. Future efforts could be placed on confirming the essentiality of Myo52 in *S. japonicus* by transforming the deletion construct in a stable diploid (Furuya and Niki, 2011) and dissecting the octads after sporulation. If the gene is indeed essential, a 4:4 segregation of dead and alive offspring is expected. A second step could be to work on generating a thermosensitive allele of *myo52* to study its polarity phenotype alone and doubled with the deletion of *myo51*.

2.4 Material and Methods

Strains and media. Strains and plasmids were generated using the same techniques as explained in **Chapter 1**. Strains were grown according to what is described in **Chapter 1**.

Figure	Strain	Genotype	Source
3.2	JCK001	h+ myo51::ura4 ade6sj-domE ura4sj-D3	This study
3.1	JCK005	h+ myo52-GFP::ura4+ ade6sj-domE ura4sj-D3	This study
3.1	JCK007	h+ myo51-mCherry::ura4+ ade6sj-domE ura4sj-D3	This study
3.3A, C, D, E	JCK019	h- Lifeact-GFP-ura4 myo51-mCherry-ura4 ade6sj-domE ura4sj-D3	This study
3.3A, C, F	JCK020	h- GFP-Atb2-ura4 myo51-mCherry-ura4 ade6sj-domE ura4sj-D3	This study
3.4A, B	JCK027	h- Lifeact-GFP-ura4+ mCherry-Atb2-ura4+ ade6sj-domE	This study
3.5	JCK039	h? myo51::ura4 Lifeact-GFP-ura4 mCherry-Atb2-ura4 ade6sj-domE	This study
3.2	JSM23	h+ ade6sj-domE ura4sj-D3 ura4-	(Furuya and Niki, 2009)
3.6	YLL369	h+ nmt41-CHD_GFP-leu+; aur-mCherry-atb2 leu1- ura4-	Lab stock

Table 3.1. Table of strains used in this chapter.

Depolymerization experiments. Depolymerization experiments were performed as described in **Chapter 1**.

Truncations of Myo51.

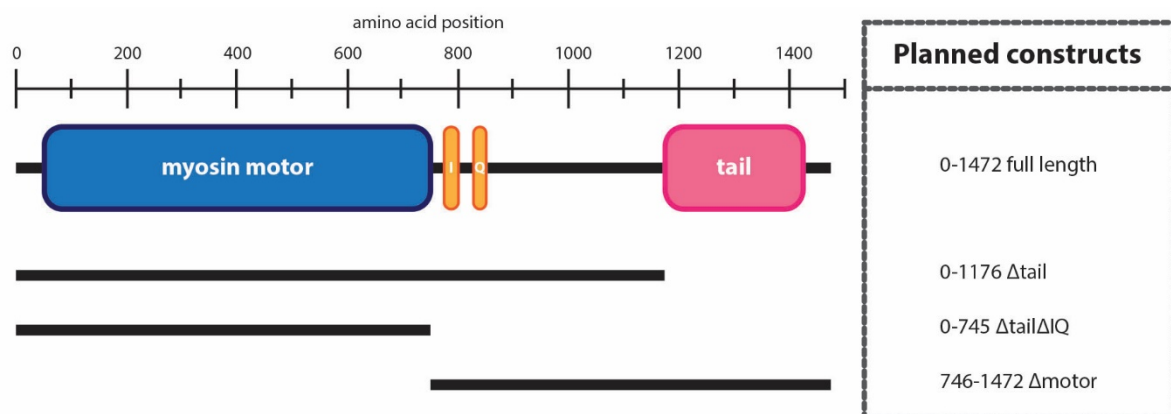


Figure 3.7. Schematic representing the different truncations of protein Myo51 planned for this experiment.

With the help of a technician trainee (Roman Bernard, Ecole ESSanté), I planned to dissect the different domains of Myo51 and elucidate which part of the protein is responsible for the colocalization with with microtubules. The idea was to generate truncated alleles of Myo51 (**Fig. 3.7**) fused with mCherry and look at their localization in respect to actin and microtubule cables. The project was initiated and we managed to construct two of the plasmids planned, namely myo51- Δ motor-mCherry (pCK085) and myo51- Δ tail Δ IQ-mCherry (pCK084). I transformed these plasmids several times but few colonies grew and they were all incorrect. If obtained, these strains should later be crossed to strains carrying either LifeAct-GFP (JSM37) or GFP-Atb2 (JSM3) to see if the colocalization between actin or microtubules with the truncated versions of Myo51 is maintained.

Chapter 3: Transcriptome analysis of the yeast-to-hypha transition in *Schizosaccharomyces japonicus*

Summary:

In this chapter, I studied the transcriptome changes occurring during the yeast-to-hypha transition in *S. japonicus*. The goal of these experiments was to obtain first genetic clues as to how this species can undergo such dramatic morphological transition. I first designed an RNA extraction protocol for hyphal cells growing invasively in agar, and continued with RNA sequencing and data analysis. I identified a list of putative interesting genes and deleted some of the candidates to assess their hyphal capabilities in microfluidics and solid environments. More than half of the genome was differentially expressed in the hyphal form underlying a rich and complex phenomenon and a complete re-routing of gene expression after the transition. This study provides rich ground for future work.

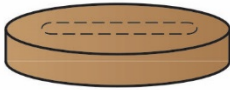
3.1. Introduction

The yeast and hyphal cells are two morphologically very distinct types of cells and little information has been gathered to understand which genes could be involved in this transition (Bozsik et al., 2002; Enczi et al., 2007). Inference from what we know from polarity mechanisms in *S. pombe* is likely not sufficient to explain entirely hyphal formation because the species diverged 220Mya (Rhind et al., 2011) and *S. pombe* is incapable of dimorphic switch, at least not in the scale and relative eagerness observed in *S. japonicus* (Amoah-Buahin et al., 2005). I hypothesized that the genetic basis of the morphological difference between yeast and hypha could be assessed through RNA sequencing and transcriptome analysis performed during the dimorphic transition. Cells undergoing morphological change must trigger whole new genomic expression responses and studying the transcriptome would help uncover genes responsible for the dimorphic switch as well as information on how fast the new transcription program occurs after contact with the inducer. Such studies have been carried out in dimorphic species like *Histoplasma capsulatum* (Edwards et al., 2013), *Candida tropicalis* (Wu et al., 2016) and *Ophiostoma novo-ulmi* (Nigg and Bernier, 2016) and specific dimorphism and filamentation related genes have been isolated (Martin et al., 2013b). In this experiment I aimed to compare the transcriptome of non-induced yeast and cells induced for the morphological change at different timepoints encompassing both early responsive genes (1h to 12h) and late responsive genes at 3 days of growth.

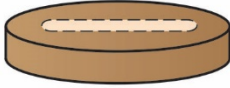
While establishing this protocol I faced several challenges. The first one concerns the fact that *S. japonicus* does not filament in liquid media and the transition on solid media immediately implicates that the hyphal cells are completely embedded in agar. While RNA extraction from liquid culture is relatively straightforward, it is not the case from cells growing within the agar, I therefore had to design a protocol that would retrieve the cells of interest from inside the agar without compromising RNA integrity. The second issue relates to the solid media induction as well; I usually grow the cells in liquid media before deposition on solid media containing RGE the next day (liquid-to-solid induction of dimorphism) but I realized that by doing so I would probably upregulate genes involved in adaptation to solid media which could mask the transcriptome of actual genes of interest. I therefore designed a purely solid-to-solid method of induction of dimorphism. Another issue arose from the fact that *S. japonicus* cannot be synchronized to produce hyphae-only population, I therefore included in the protocol a step in which I attempt to exclude most of the non-induced cells from the induced experiment. Finally, an issue we could not bypass as it is intrinsic to our induction method; RGE contain a lot more glucose than standard media and I expect upregulation of glucose metabolism and catabolism in the induced cells. But as seen in **chapter 1**, we already know glucose is not the inducer, so all genes related to glucose pathways will be ignored from the analysis. In

summary, in this chapter I will describe the protocol I designed which involves a solid to solid induction of dimorphic switch and RNA extraction from embedded sample preservation in liquid nitrogen. The goal of this study is to obtain a list of genes of interest and delete them to assess hyphal formation phenotype in the hope of shedding light of the genetic basis of hyphal formation in *S. japonicus*.

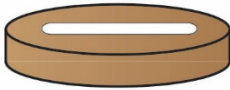
Day 1



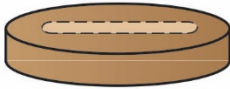
Precut the agar to delimit where to deposit the cells



Add a line of 50 μ L of cells (OD0.4-0.6) in the previously delimited part. Leave to dry for 5min at the flame.

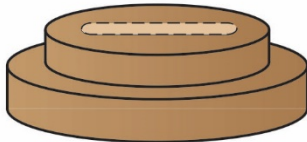


Add a piece of Whatman paper (cut out so that it is roughly the size of the delimited part) on top of the cells.

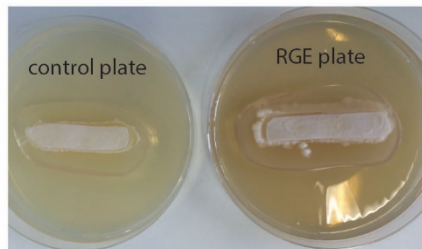
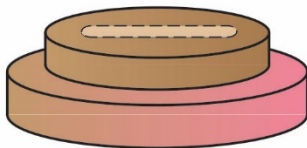


Add a line of 100 μ L of concentrated cells (50-100 times concentrated) on the paper.

Day 2

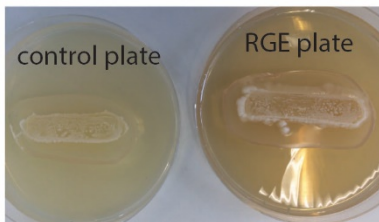


Cut out a big piece of agar containing cells and paper. Mount on fresh agar plates containing either YE-agar (control) or YE-agar supplemented with RGE.



example plates

After 0H, 1H, 3H, 6H, 12H, 73H:



Discard the filter and top cells.



Cut a piece of agar containing cells and freeze down the sample IMMEDIATELY in liquid nitrogen.

Crush the frozen piece of agar with mortar until powder is obtained.

Fill eppendorf with the powder and add buffer RA1 from NucleoSpin[®] RNA extraction kit (Macherey-Nagel)

Heat at 50 $^{\circ}$ C for 5-10min to melt the agar.

Figure 4.1. Protocol for solid-to-solid induction of filamentation in *S. japonicus* and cell disruption prior to RNA extraction.

3.2. Results

3.2.1. Solid-to-solid induction of hyphal growth

As mentioned before, to avoid upregulation of different genes related to adaptation to solid media, I designed a solid-to-solid method of induction for filamentation in *S. japonicus* (**Fig 4.1**). On rich media (YE) agar plates I outlined with a blade a zone which will serve as guide for the rest of the protocol. In the outlined zone I deposited a line of exponentially growing cells from a liquid culture. After 5 minutes of drying by the flame, I deposited on top of the cells a piece of whatman paper cut so that it is the size of the delimited part. On top of the paper, I added a concentrated line of cells from the same liquid culture (50-100 times concentrated). Typical transitioning colonies growing on solid media contain the yeast colony on top and the transitioning cells below, invading the media. The aim is to trap the bottom cells (which are the cells of interest, the one that will transition/penetrate the agar) between agar and paper. By constructing this trap I hope to restrict the transcriptomic analysis to cells undergoing the morphological transition and exclude the large number of yeast cells on top of the transitioning cells. These cells are left to grow on agar for one night for adaptation to solid environment. On day two, I cut a piece of agar from the plate containing the cells and whatman paper and “transplanted” it on fresh YE plates containing or not the inducer RGE – this is the solid to solid induction method. The inducer diffuses through the agar to trigger hyphal formation in our cells of interest. Visible hyphal formation on the transplanted plate occurred in a couple of days, similar to what I described for the liquid-to-solid induction of filamentation (data not shown).

Since there is little information about the genetic changes for *S. japonicus* dimorphism in presence of RGE, we did not know when the expected change in transcriptomics might occur. I therefore spanned the experiment over three days. I extracted RNA at time 0 for control purposes then 1h, 3h, 6h, 12h after plate transplantation on induced media or not, these timepoints are referred to as the early timepoints by contrast to extraction at 73h which is the late timepoint. Each timepoint is duplicated; in the end I will analyze data from 24 samples (**Fig. 4.2**).

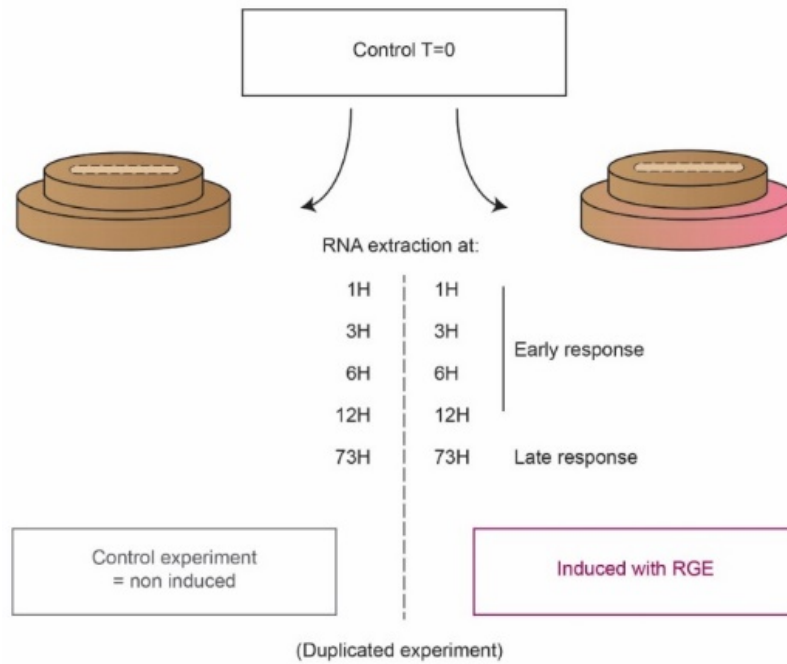


Figure 4.2. Experimental design of this transcriptomic analysis.

3.2.2. A protocol for robust RNA extraction from cells embedded in agar

After induction for the period of time needed for the experiment, the filter along with the cells on top (all of which we assume are yeasts in both control and RGE conditions) are discarded, leaving only the cells that were trapped between paper and agar. I then quickly cut out a piece of agar containing the cells and freeze it down immediately in liquid nitrogen. With a mortar I crushed the cell-agar mixture until obtaining powder that I transferred in an Eppendorf tube. Total RNA extraction was performed using the NucleoSpin® RNA extraction kit from Macherey-Nagel respecting the given protocol but adding a step at the start: the frozen cell mix was resuspended in the RA1 buffer and the mix is heated at 50°C for 10min to dissolve the agar before carrying on with the extraction. The aim was to filter out the agar from the broken cells after the first passage on columns from the kit. I checked with the manufacturer beforehand that heating up RA1 was not detrimental to it (**Fig. 4.3**).

RNA isolation

Protocol at a glance (Rev. 17)











Mini		
NucleoSpin® RNA		
1 Homogenize sample		30 mg
2 Lyse cells		350 µL RA1 50°C 3.5 µL β-mercaptoethanol Mix
3 Filtrate lysate		11,000 x g, 1 min
4 Adjust RNA binding conditions		350 µL 70% ethanol Mix
5 Bind RNA		Load sample 11,000 x g, 30 s
6 Desalt silica membrane		350 µL MDB 11,000 x g, 1 min
7 Digest DNA		95 µL DNase reaction mixture RT, 15 min
8 Wash and dry silica membrane		1 st wash 200 µL RAW2 2 nd wash 600 µL RA3 3 rd wash 250 µL RA3
		1 st and 2 nd 11,000 x g, 30 s
		3 rd 11,000 x g, 2 min
9 Elute highly pure RNA		60 µL RNase-free H ₂ O 11,000 x g, 1 min

Figure 4.3. Total RNA extraction using the the NucleoSpin® RNA extraction (Macherey-Nagel) with the added melting step at 50°C to dissolve agar. Cells are then filtered out of the agar after the first passage on column (step 3 in the protocol).

Purity and integrity of total RNA extraction was assessed by the Fragment Analyzer (Agilent) at the Genomic Technologies Facility (GTF, Génopode building, UNIL). The machine calculates the RNA Quality Number (RQN) which is an integrity scale ranging from 1 to 10, computing the 18S and 28S ribosomal RNA peaks and the resolution between peaks. It indicates the degradation status of the sample, with 1 being a completely degraded sample and 10 a sample of excellent purity. All 24 samples were pure (RQN ranging from 8.9 to 10, and with concentrations ranging from 6ng.µl⁻¹ to 164ng.µl⁻¹ (example of sample 1 separation in **Fig 4.4**, and see **Annexe 1** for the purity analyses of the 24 samples).

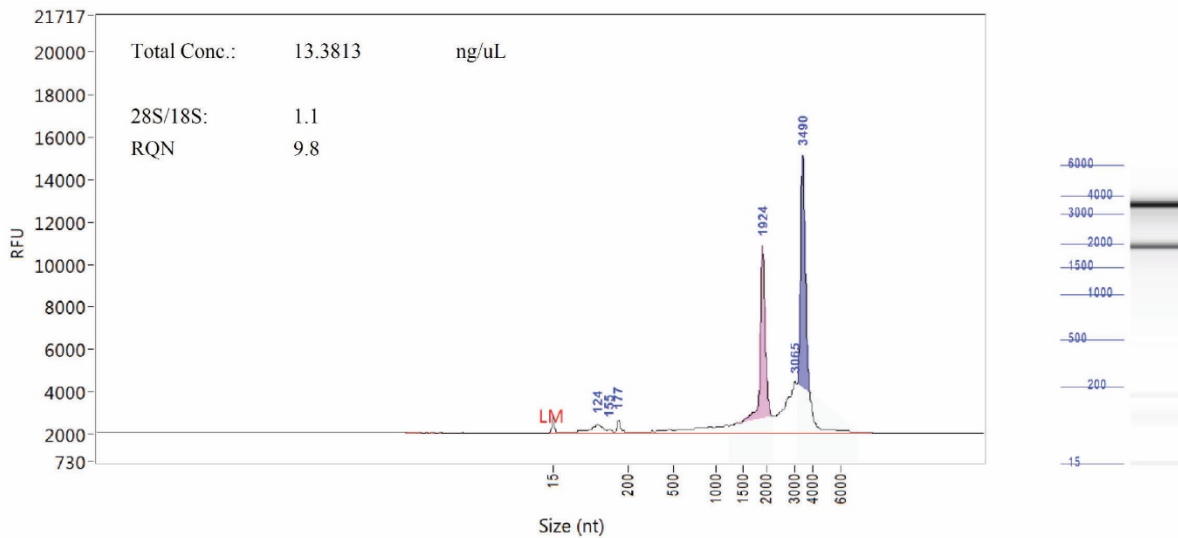


Figure 4.4. Example of the separation of total RNA extracted from sample 1 ran on the Fragment Analyzer (Agilent). LM is the marker peak. The blue and pink peaks are the large and small ribosomal RNA peaks. Also indicated are the total concentration of the RNA sample, the ratio 28S/18S ribosomal peaks and the RQN.

3.2.3. mRNA sequencing and sequencing data analysis

RT-PCR and Illumina sequencing were performed by Johann Weber and Richter Hannes at the GTF as described in the material and methods.

Data processing was performed by Sandra Calderon at the GTF as described in the material and methods.

3.2.4. Statistical analyses

Statistical controls and analysis were performed by Sandra Calderon at the GTF using R (version 3.2.3). 4875 genes, covering 98% of the genome, showed one count per million in at least one sample, the determined cut off rate to include or not a gene in the analysis. She then performed statistical controls to assess the quality of the data, mainly correlation between the samples and duplicates, and a principal component analysis (PCA).

Data extracted from duplicates closely clustered together indicating a robust data set. However, data from the late timepoint highly diverged from the data of the early timepoints. This is explained by the fact that at 73 hours most cells will have transitioned to hyphal growth, a stark difference to the earlier timepoints which will show data from a cell mix of different stages of the morphological transition and probably some non-induced cells (**Table 4.1; Fig. 4.5**).

One thing I noticed is that early and late timepoints clustered separately regardless of their induction with RGE. This indicates that the growth in presence of the inducer is not the only event sparking a variation in the data set but the growth on plate for a longer period of time also alters gene expression.

SampleID	Description	Condition	TimePoint
01	control T=0	control	0
02	control T=0_2	control	0
03	control T=0_3	control	0
04	control T=0_4	control	0
05	control non induced T=1h	control	1
06	control non induced T=1h_2	control	1
07	induced T=1h	induced	1
08	induced T=1h_2	induced	1
09	control non induced T=3h	control	3
10	control non induced T=3h_2	control	3
11	induced T=3h	induced	3
12	induced T=3h_2	induced	3
13	control non induced T=6h	control	6
14	control non induced T=6h_2	control	6
15	induced T=6h	induced	6
16	induced T=6h_2	induced	6
17	control non induced T=12h	control	12
18	control non induced T=12h_2	control	12
19	induced T=12h	induced	12
20	induced T=12h_2	induced	12
21	control non induced T=73h	control	73
22	control non induced T=73h_2	control	73
23	induced T=73h	induced	73
24	induced T=73h_2	induced	73

Table 4.1. List of the 24 samples of the analysis: 6 timepoints for both control and induced with RGE experiments, the whole duplicated.

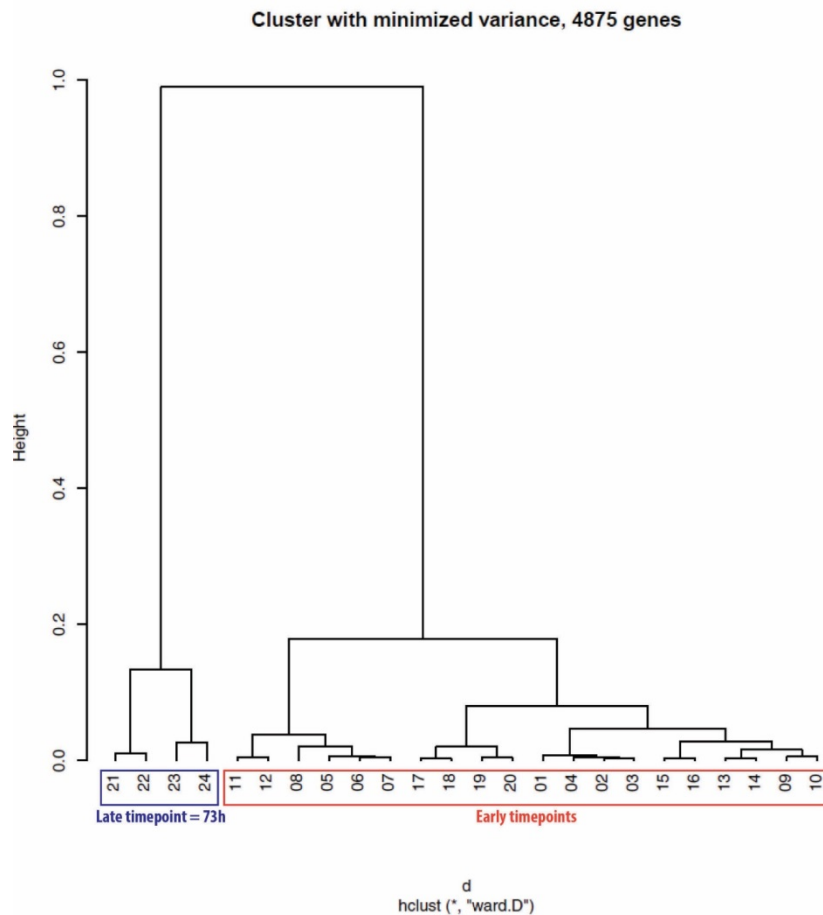


Figure 4.5. Variance clustering analysis showing a good correlation between duplicates and a great variance between the late and early timepoints. Refer to **Table 4.1** for the correspondence between number and sample description.

I requested for two different statistical analyses to reveal potential genes of interest. The first one is a statistical analysis comparing differential gene expression between induced and non-induced conditions at each timepoint and the second one is a statistical test looking at variation of gene expression over the course of the experiment. For the latter test, S. Calderon advised to exclude the 73h timepoint because it was too divergent from the earlier timepoints and could perturb the data, the second analysis was therefore performed on the early timepoints only.

3.2.5. Early timepoints analysis

For timepoints 1h to 12h I asked for an analysis overtime to identify genes whose expression varied at least once significantly during the experiment (F test). After setting up a cut off rate of 5% of false discovery rate (FDR), 122 genes were sorted. The complete list of those genes is located in **Annexe 3**.

In this list, 81 genes found an ortholog in *S. pombe*. From the remaining 41 genes, 23 were annotated as coding for hypothetical proteins (**Fig. 4.6**). Since *S. pombe* cannot undergo dimorphism with the

same ease as *S. japonicus* (Amoah-Buahin et al., 2005), potential gene of interests might reside in the hypothetical category.

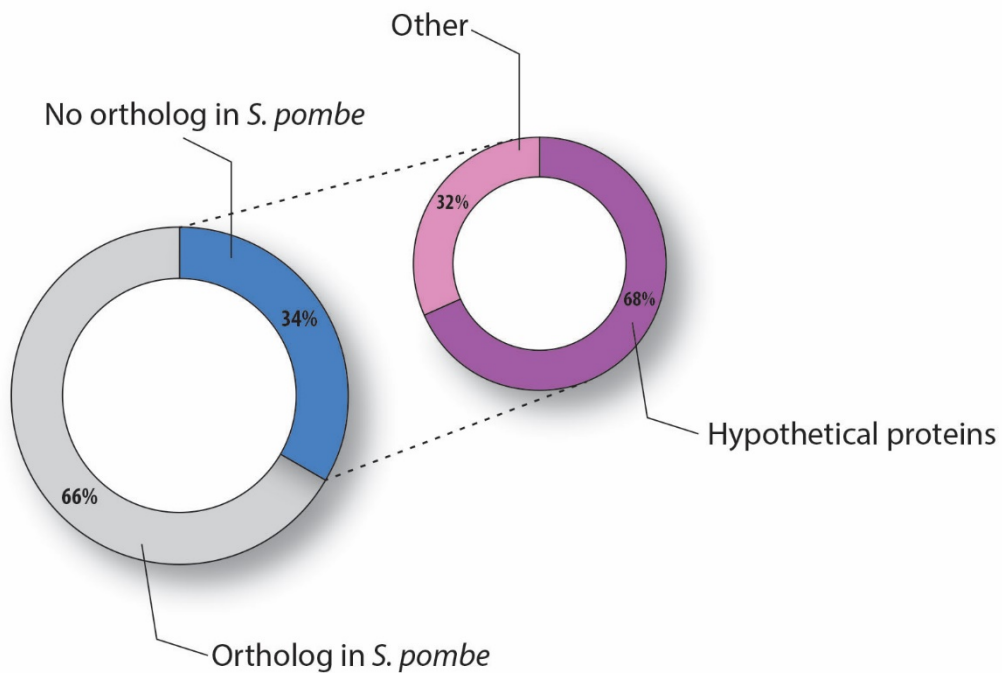


Figure 4.6. Pie chart displaying the proportion of genes having orthologs in *S. pombe* in the early timepoint analysis. Out of the genes having no orthologs in *S. pombe* a good portion code for hypothetical proteins of undefined functions.

I also decided to do a cluster analysis on the 122 genes to identify behavior patterns in gene expression (represented as a heatmap in **Fig. 4.7**).

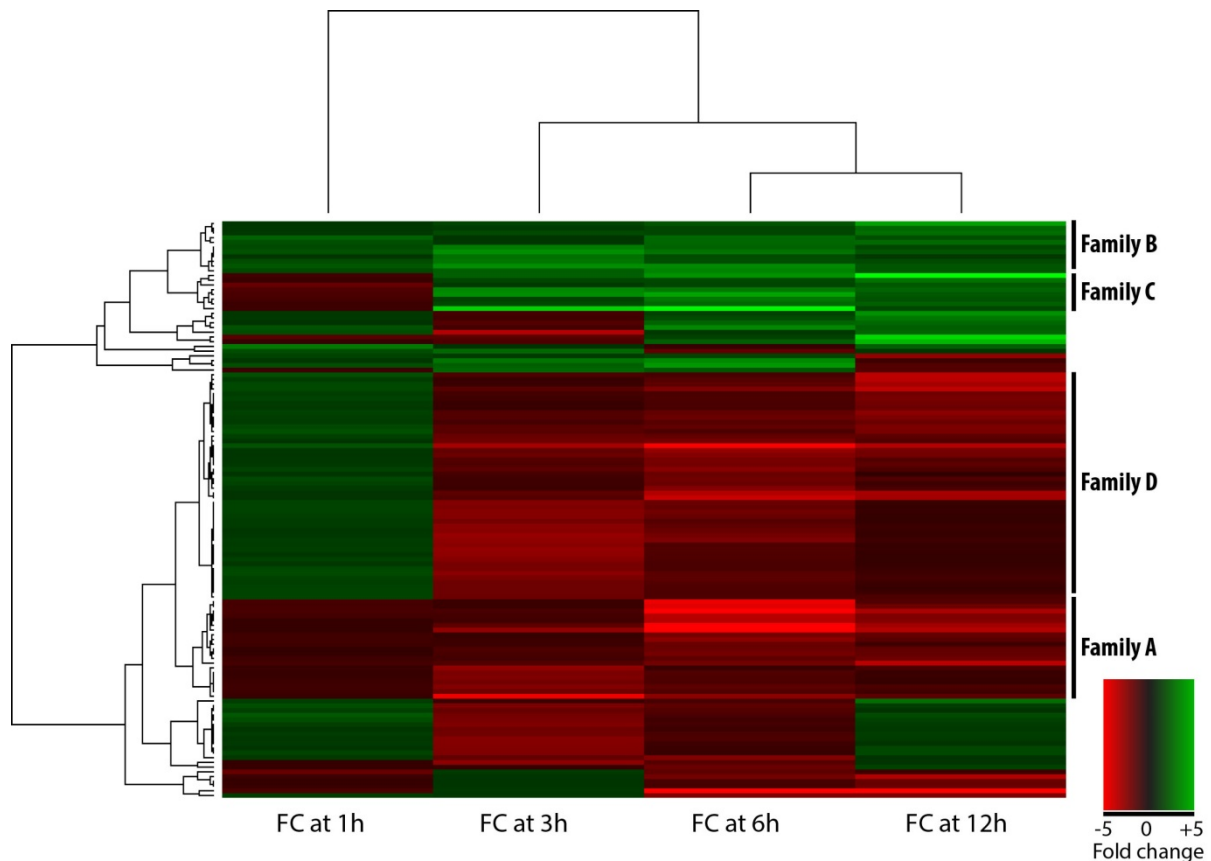


Figure 4.7. Heatmap generated after clustering of the data pertaining to the early timepoint analysis. Each line is one gene, and the 4 columns are the fold change of each gene at each of timepoints of the early timepoint analysis. In red is the downregulation and in green the upregulation represented as a fold change (FC).

The generated heatmap shows trends; indeed, the minimum requirement to be included in the analysis is the existence of significant fold change in expression in at least one of the timepoints. Therefore, it is important to note that not all change in fold change represented in the heatmap is significant but at least one per gene is. Noticeable patterns were immediately visible and I decided to do perform a gene ontology analysis on some of the clusters.

The first category that caught my attention is the cluster that was composed of 16 genes that were downregulated in the presence of RGE from the beginning of the experiment (**Fig. 4.7** family A). When applicable, I compared with the gene ontology of the corresponding *S. pombe* orthologs and found that a majority acted in transport and transmembrane transport processes. Interestingly, I observed a downregulation of two genes putatively involved in response to stress (SJAG_01084 and SJAG_01095) (**Fig 4.8**).

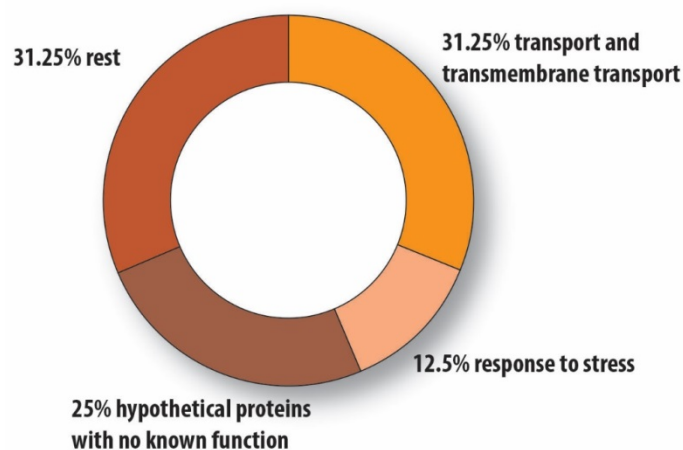


Figure 4.8. Pie chart showing the different gene functions associated with the 16 genes that are downregulated during the early timepoints of this experiment.

Another interesting trend in gene expression was the gene family always upregulated in presence of RGE (**Fig. 4.7** family B). As predicted, I found an upregulation of metabolic pathways and particularly the glucose metabolism pathway. This is explained by the fact that the RGE brings a lot of glucose that the cells clearly consume. Interestingly, I found an upregulation of the gene coding for alpha-amylase Mde5, a protein implicated in the cell wall organization and biogenesis (**Fig 4.9**). With the change in cell size during the transition (see **Chapter 1**), a consequent remodeling of the cell wall in the hyphal form is expected.

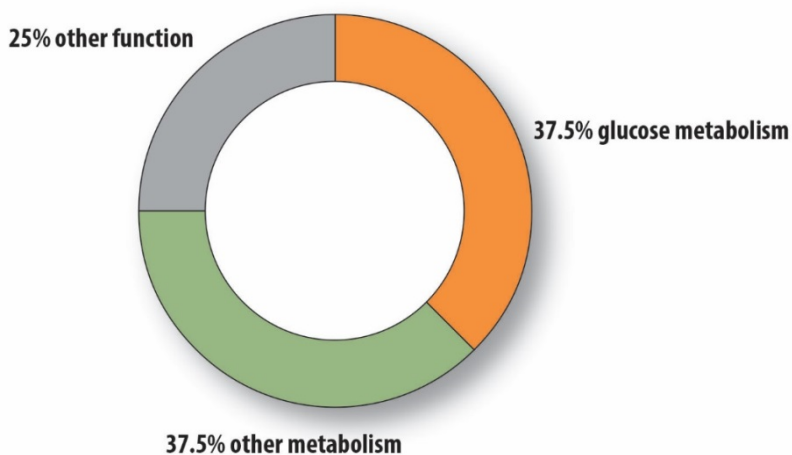


Figure 4.9. Pie chart showing the different functions associated with the 8 genes that are upregulated during the early timepoints of this experiment.

The third family I want to discuss is the cluster of genes seemingly upregulated from 3h after induction (**Fig. 4.7** family C). Again, I noticed that a good portion of them were hypothetical proteins so I systematically performed a blast analysis of their protein sequence and analyzed putative protein domains to narrow down their function (**Fig. 4.10**, and paragraph **3.2.7** for deletion of some of these genes of interest).

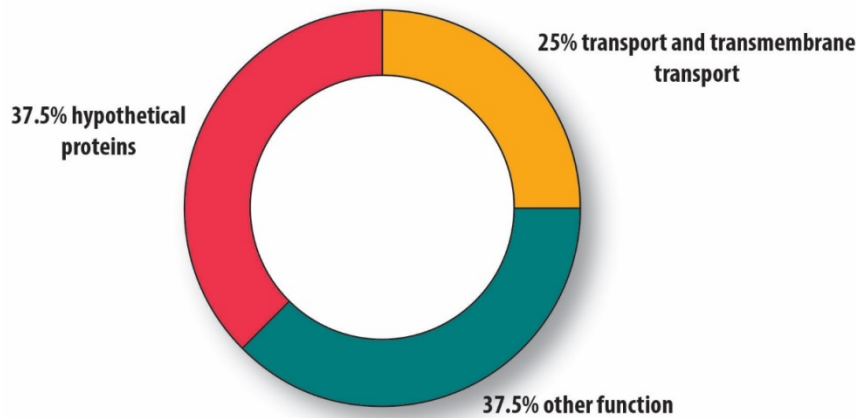


Figure 4.10. Pie chart showing the different functions associated with the 8 genes that are upregulated starting from 3H after induction from RGE in the early timepoint analysis.

I note also that the largest cluster contains 46 genes that are downregulated after timepoint 3h but gene ontology analysis was inconclusive (data not shown) (**Fig. 4.7** family D).

Surprisingly, few genes pertaining to polarity processes showed any change in gene expression and many genes with unknown function showed a significant fold change during the experiment. I will focus on some of those genes later on in this chapter.

3.2.6. Late timepoint analysis

	ALL	UP	DOWN	ALL.FC2	UP.FC2	DOWN.FC2
induced.vs.control_73h	2580	1311	1269	858	683	175

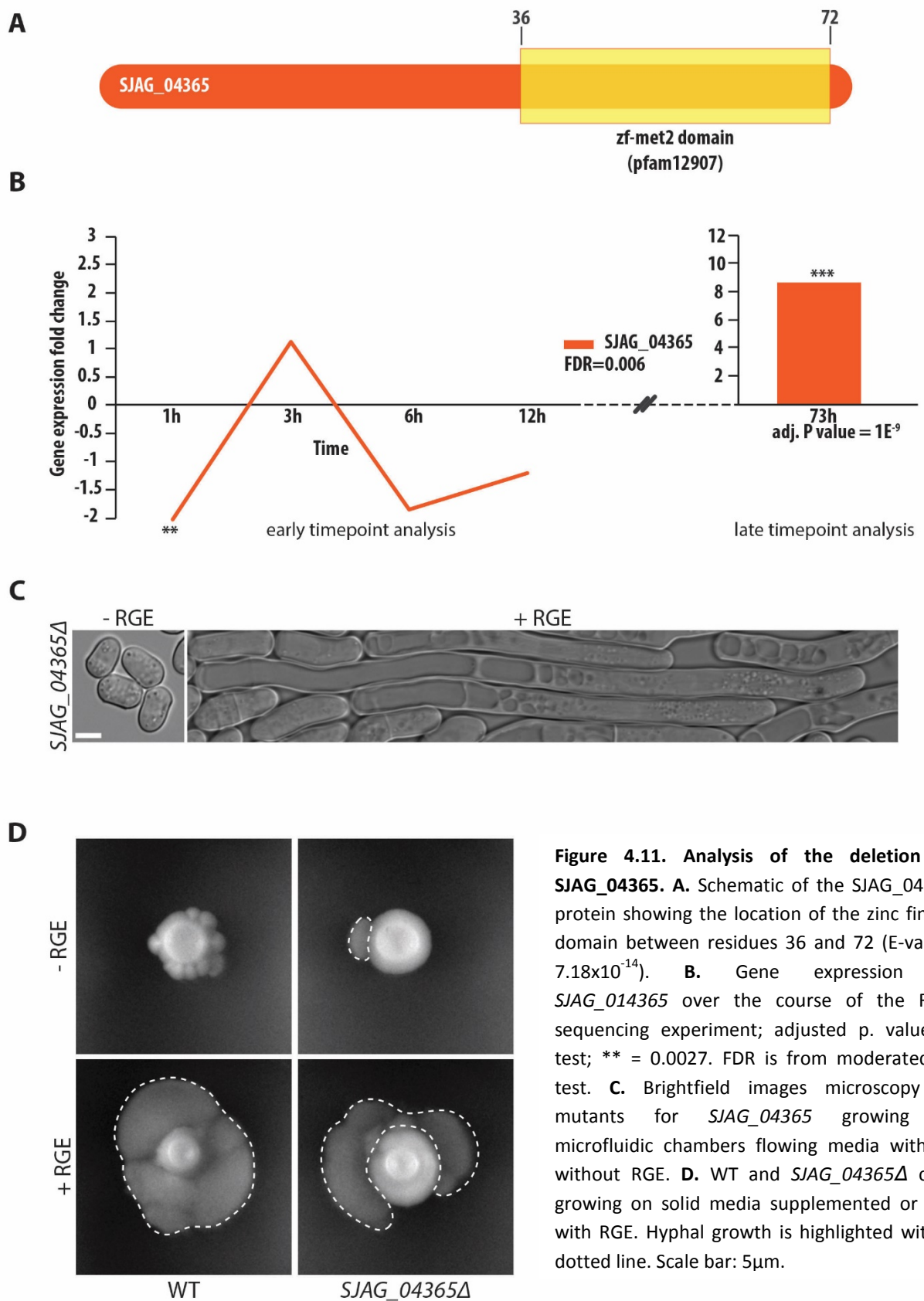
Table 4.2. Number of genes found with significant differential expression with False Discovery Rate (FDR) cut-off = 0.05. UP: upregulated; DOWN: downregulation. FC2: fold change of 2.

For the late response to the inducer, the timepoint at 73 hours, we compared with a moderated T test the expression levels between induced and non-induced conditions. Interestingly, over half the genome of *S. japonicus* was significantly altered in expression (**Table 4.2**). Even with a more stringent cut off (FDR 5%, FC 2), 858 genes showed significant fold change expression at 73h after induction with RGE. This result suggests that the transcriptome is deeply altered after the transition from yeast-to-hypha. I noticed that most of these genes were upregulations (683/858) contrasting with the early timepoint analysis which showed a bias towards downregulation (**Fig. 4.7**). The complete list of the gene of this analysis is available in **Annexe 4**.

3.2.7. Deletions of genes of interest and phenotype assessment

I deleted genes of interest and assessed if the single deletions yielded any phenotype in hyphal formation in microfluidic chambers or on solid media. Genes of interest were selected according to their expression behavior and putative protein domains.

SJAG_04365 – Hypothetical protein. Protein domain analysis revealed a zinc binding domain in C-terminus indicating a putative transcription factor (**Fig. 4.11 A**). Protein blast showed the presence of orthologs of unknown function in the filamentous Aspergilli family. This gene is significantly downregulated at 1h and up regulated at 73 h (**Fig. 4.11 B**). This behavior indicates this gene could be essential for proper hyphal growth and otherwise downregulated in the yeast form. Deletion of the gene yielded no obvious polarity phenotype, the mutant cells could transition and grow as hyphae on solid and microfluidic environments (**Fig. 4.11 C-D**).



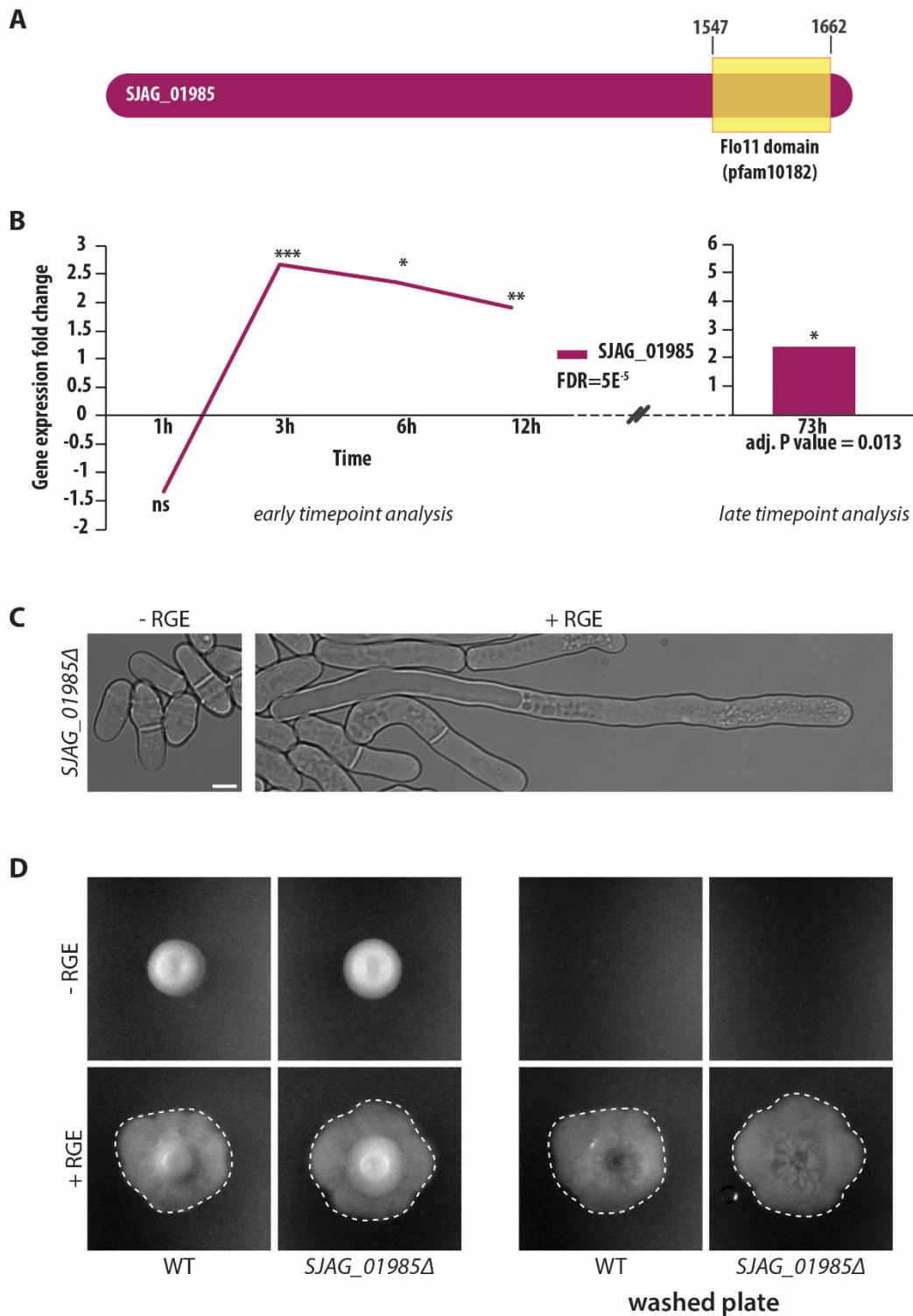


Figure 4.12. Analysis of the deletion of SJAG_01985, a flo11 domain containing protein. **A.** Schematic of the SJAG_01985 protein showing the location of the Flo11 domain between residues 1547 and 1662 (E-value: 4.7×10^{-8}). **B.** Gene expression of SJAG_01985 over the course of the RNA sequencing experiment; adjusted p. value, t test; *** = 6×10^{-4} ; ** = 0.009; * = 0.025; ns = 0.09. FDR is from moderated F-test. **C.** Brightfield images microscopy of mutants for SJAG_01985 growing in microfluidic chambers flowing media with or without RGE. **D.** WT and SJAG_01985 Δ cells growing on solid media supplemented or not with RGE. On the right side panel is the same plate washed to reveal filamentation within the agar. Hyphal growth is highlighted with a dotted line. Scale bar: 5 μ m.

SJAG_01985 – Hypothetical protein. This gene codes for a protein of unknown function but domain analysis predicted a Flo11 domain at the C terminus of the protein. Flo11 is a protein involved in pseudohyphal formation in *S. cerevisiae* (Lo and Dranginis, 1998) (**Fig. 4.12. A**). This gene is significantly downregulated at the beginning of the experiment and upregulated during the transition starting from 3h after induction with RGE. It even remained upregulated at 73h (**Fig. 4.12. B**). Such expression behavior suggests a potential activity necessary during the transition. Deletion of this gene yielded no obvious phenotype as the mutant cells could grow as hyphae on solid and microfluidic environment (**Fig. 4.12. C-D**)

SJAG_00161 – Hypothetical protein. This gene codes for a protein of unknown function but domain analysis revealed it to contain a Vel1 domain (**Fig. 4.13 A**). Vel stands for velum formation, a biofilm formed by some strains of *S. cerevisiae* during wine making (David-Vaizant and Alexandre, 2018). This gene is upregulated starting from 12h after induction and remains heavily upregulated at the late timepoint (**Fig. 4.13 B**). However, deletion of the gene produced no phenotype in hyphal formation in microfluidic chambers or on solid media (**Fig. 4.13 C-D**).

SJAG_00781 – Map2, P-factor. In condition of nitrogen starvation conditions, fission yeast of opposite mating type (haploid M cells (h-) and P cells (h+)) can fuse to form diploids and undergo meiosis to produce four spores. Cells of opposite mating type can grow towards each other prior to fusion by sensing the opposite mating type pheromone, conveniently named P-factor and M-factor. Interestingly, the strain we used for sequencing is h+ and one of the hits in the early timepoint analysis is Map2, gene coding for the P-factor; it is slightly upregulated 12h after RGE induction (**Fig. 4.14 A**). Deletion of Map2 rendered the cells sterile (data not shown) but did not impact hyphal formation in microfluidics or solid media (**Fig. 4.14 B-C**).

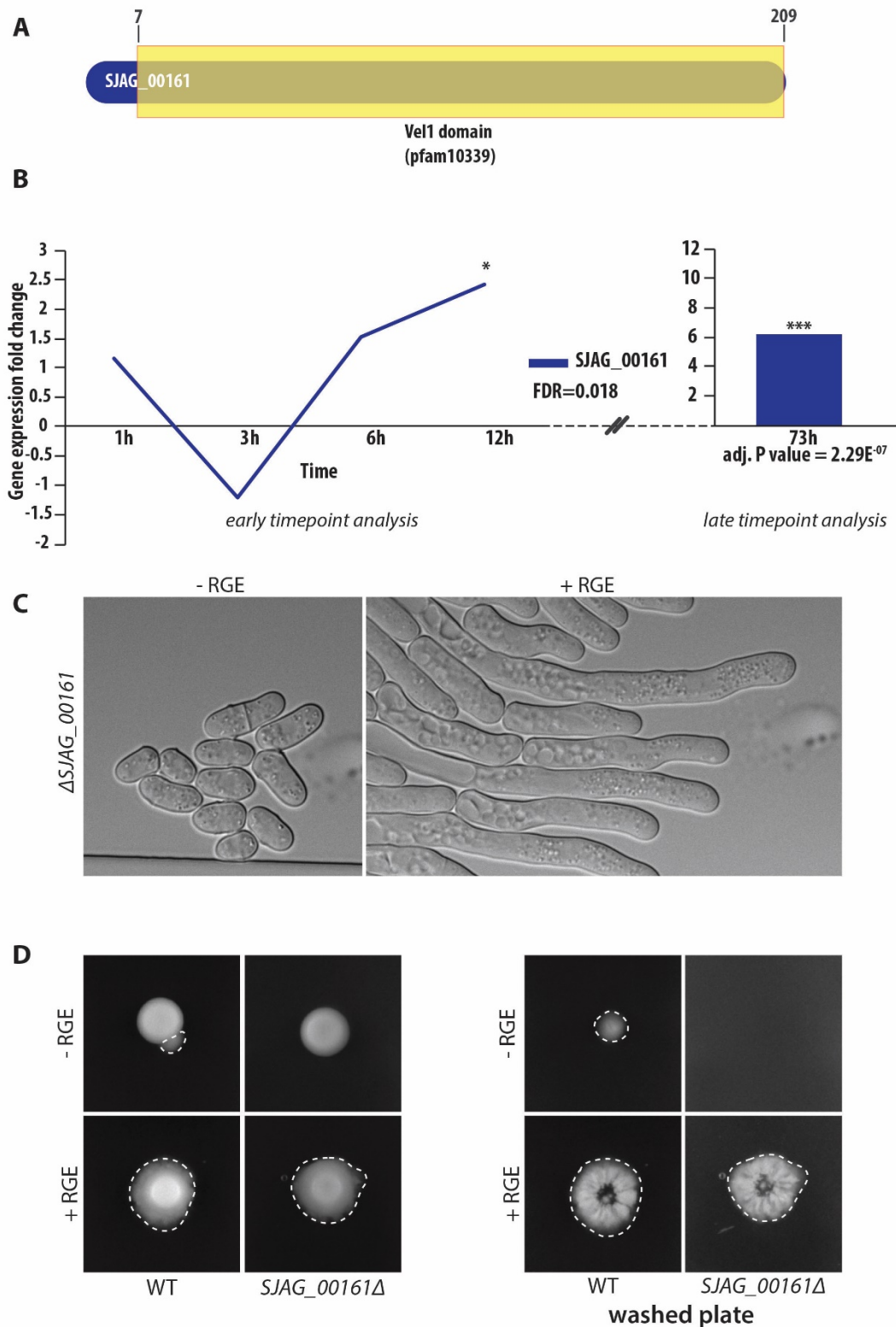


Figure 4.13. Analysis of the deletion of SJAG_00161, a vel1 domain containing protein. **A.** Schematic of the SJAG_00161 protein showing the location of the Vel1 domain between residues 7 and 209 (E-value: 1.09×10^{-127}). **B.** Gene expression of SJAG_00161 over the course of the RNA sequencing experiment, adjusted p. value t.test; * = 0.014. FDR is from moderated F-test. **C.** Brightfield images microscopy of mutants for SJAG_00161 growing in microfluidic chambers flowing media with or without RGE. **D.** WT and SJAG_00161Δ cells growing on solid media supplemented or not with RGE. On the right side panel is the same plate washed to reveal filamentation within the agar. Hyphal growth is highlighted with a dotted line.

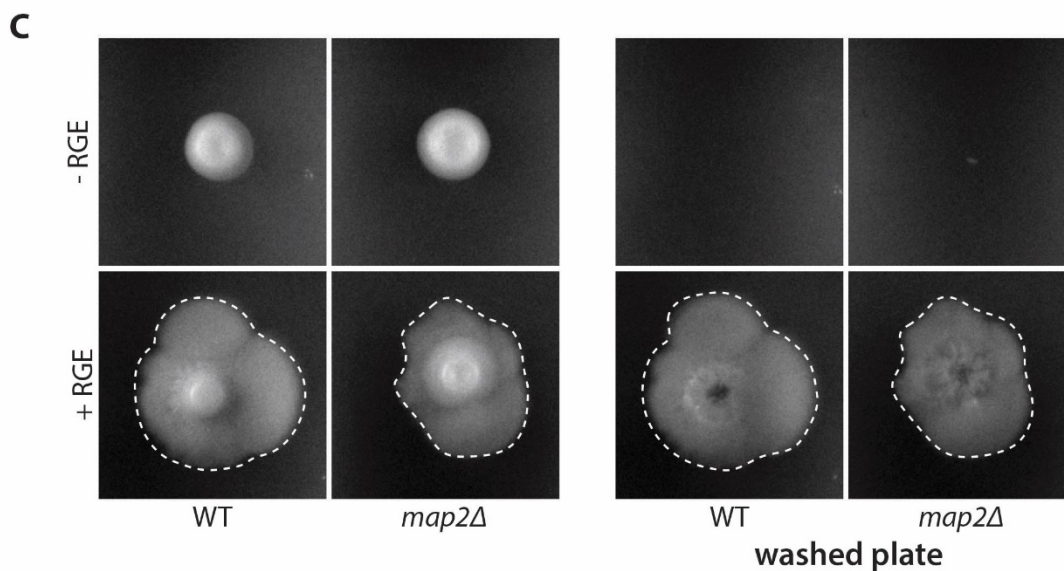
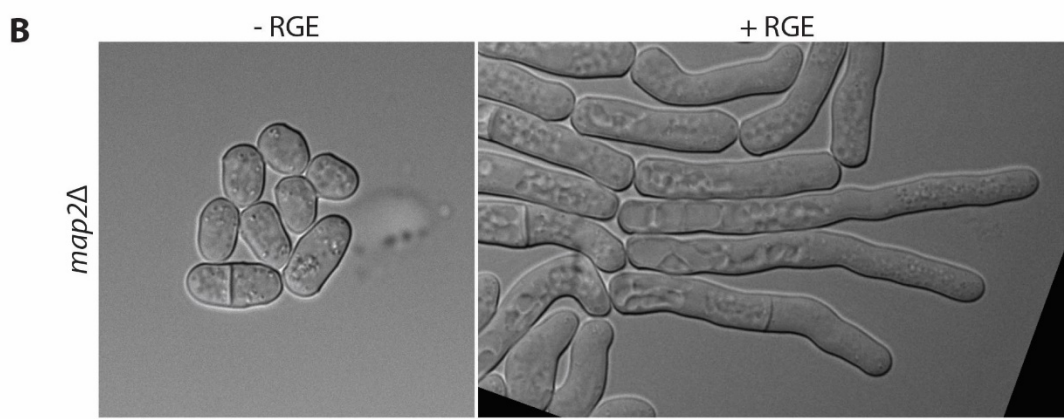
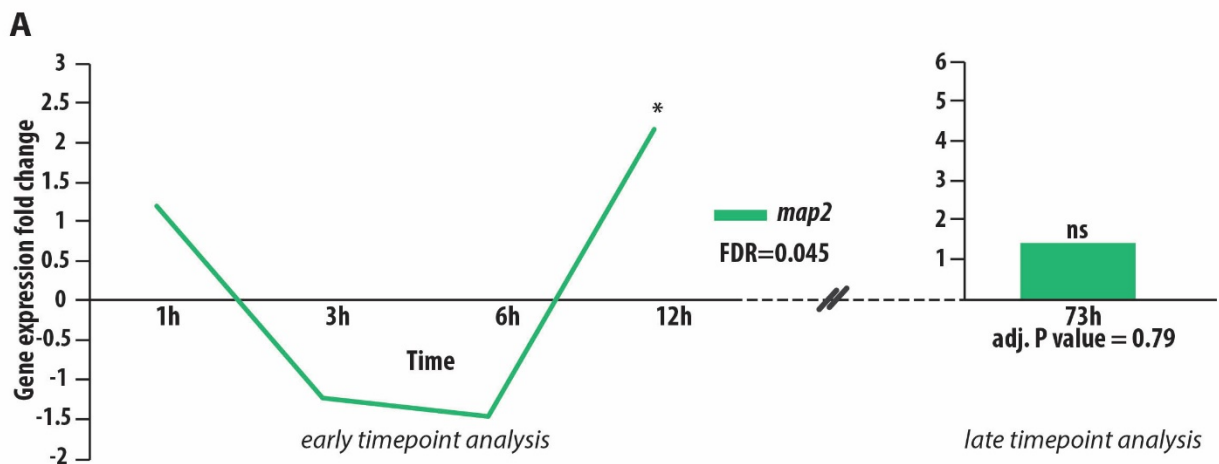


Figure 4.14. Analysis of the deletion of Map2. **A.** Gene expression of *map2* over the course of the RNA sequencing experiment. adjusted p. value; t.test: * = 0.02. FDR is from moderated F-test. **B.** Brightfield images microscopy of *map2* mutants growing in microfluidic chambers flowing media with or without RGE. **C.** WT and *map2* cells growing on solid media supplemented or not with RGE. On the right side panel is the same plate washed to reveal filamentation within the agar. Hyphal growth is highlighted with a dotted line.

3.2.8. RGE does not trigger an oxidative stress response

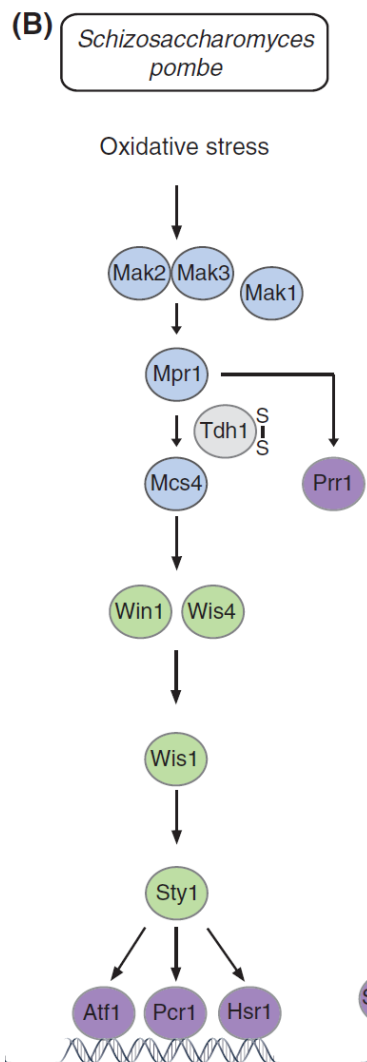


Figure 4.15. Oxidative stress response pathway from *S. pombe* (Papadakis and Workman, 2015).

In **chapter 1**, I mentioned that I could not exclude an oxidative stress when *S. japonicus* when it is put in presence of the RGE. Therefore, I checked if the expression of genes involved in the oxidative response were overexpressed during the dimorphic transition. The MAPK transduction pathway in *S. pombe* involved in oxidative stress response is displayed in **Fig. 4.15** (Papadakis and Workman, 2015). I looked for any variation in gene expression of the *S. japonicus* homologs over the course of the experiment but could only find very few significant ones and most of them were downregulations (**Table 4.3**).

GENE_ID	Description	1H		3H		6H		12H		73H	
		Adj. P Value	Fold change	Adj. P Value	Fold change	Adj. P Value	Fold change	Adj. P Value	Fold change	Adj. P Value	Fold change
SJAG_00331	histidine kinase Mak1	0.102475	-1.19874	0.927007	1.013271	0.34306	-1.11259	0.933761	1.011987	0.101481	-1.27576
SJAG_02183	HisK/Mak2 protein kinase Mak2	0.166009	-1.17387	0.48532	-1.0881	0.079993	-1.22596	0.337387	-1.11638	0.356078	1.150726
SJAG_01587	HisK/Mak3 protein kinase Mak3	0.254185	-1.17224	0.468586	-1.1137	0.990947	1.002076	0.809936	1.036405	0.567929	-1.14231
SJAG_06592	Regulator phosphotransferase Mpr1	0.518204	1.113817	0.537185	1.105994	0.959965	1.009793	0.839844	1.03845	0.001706	-2.21058
SJAG_00318	response regulator Mcs4	0.64336	-1.05233	0.923803	-1.01252	0.465167	-1.08012	0.612924	-1.05967	0.0011	-1.68963
SJAG_01532	transcription factor prr1	0.270339	-1.10216	0.740191	1.033736	0.846138	-1.0209	0.028089	-1.21971	2.29E-05	-1.67017
SJAG_04777	STE/STE11 protein kinase	0.820074	-1.02846	0.520989	1.068894	0.628314	1.054318	0.835736	-1.02585	0.473044	-1.16826
SJAG_03384	STE/STE11 protein kinase	0.197223	-1.13585	0.85158	-1.02276	0.873174	-1.0196	0.69617	1.043857	0.000495	-1.5668
SJAG_02342	STE/STE7 protein kinase Wis1	0.859998	1.017537	0.741969	-1.03058	0.780234	-1.02624	0.267445	-1.093	0.384435	-1.10471
SJAG_02592	CMGC/MAPK/P38 protein kinase Sty1	0.248888	1.106737	0.12684	-1.14228	0.868074	-1.01818	0.056059	-1.18281	0.000204	-1.49449
SJAG_03388	transcription factor Hsr1	0.547855	-1.13031	0.658152	-1.09744	0.666785	1.094875	0.383596	1.189811	0.000984	2.081002
SJAG_00266	transcription factor Atf1	0.377135	1.075359	0.144306	-1.12751	0.101868	-1.14807	0.34275	-1.08355	0.000588	1.64751
SJAG_02311	transcription factor Pcr1	0.998576	1.00013	0.350729	-1.0683	0.180379	-1.09806	0.051081	-1.14744	0.384435	-1.13647

Table 4.3. Expression levels of genes involved in the oxidative stress response in fission yeast during the entire experiment. Bolded, are the significant genes expression variations taking into account a 5% FDR.

I also note that glycolic enzyme glyceraldehyde-3-phosphate dehydrogenase, Tdh1, is highly repetitive in the genome of *S. japonicus*. In *S. pombe*, Tdh1 has two copies and is transiently oxidized during oxidative stress to promote cell response (Morigasaki et al., 2008). I identified 7 repetitions of the gene and observed their fold change at 73h. Three isoforms showed a significant downregulation (**Table 4.4**).

Gene	Adj. P value	Fold change	Description
SJAG_00027	0.664096	-1.123109381	glyceraldehyde-3-phosphate dehydrogenase Tdh1
SJAG_06621	0.001863	-2.840833358	glyceraldehyde-3-phosphate dehydrogenase Tdh1
SJAG_02945	0.141021	-1.549153322	glyceraldehyde-3-phosphate dehydrogenase Tdh1
SJAG_02135	0.318385	-1.491527184	glyceraldehyde-3-phosphate dehydrogenase Tdh1
SJAG_03828	0.239941	-1.331687702	glyceraldehyde-3-phosphate dehydrogenase Tdh1
SJAG_06622	4.83E-06	-2.939468438	glyceraldehyde-3-phosphate dehydrogenase Tdh1
SJAG_03903	8.70E-05	-2.137294587	glyceraldehyde-3-phosphate dehydrogenase Tdh1

Table 4.4. Expression levels of dehydrogenase Tdh1. Bolded are the significant genes expression variations taking into account 5% FDR.

In conclusion, the hypothesis that RGE oxidative properties are not what trigger hyphal formation in the cells (see **Chapter 1**) still stands. There is something else in the fruit extracts that is responsible for the morphological switch.

3.3. Discussion and perspectives

In this chapter, I analyzed the transcriptome of the yeast-to-hypha transition in *S. japonicus*. This study had never been done before in this organism and I had to develop a suitable protocol for RNA extraction in this invasive species. I successfully managed to extract extremely pure total RNA and worked in collaboration with bioinformaticians for the analysis of the sequencing data.

Several steps of controls were performed to ensure the quality of the data and it showed very clear correlations between the different replicates and differences between timepoints and conditions. Even though this indicates that the experiment is valid from a technical point of view, I note several discrepancies in the data set from a biological standpoint.

One of the most striking of hyphal formation in *S. japonicus* is the development at the back of the cell of a gigantic vacuole. From mutagenesis experiments we also know correct vacuole development is necessary to induce proper hyphal growth (Bozsik et al., 2002; Enczi et al., 2007). I therefore expected to see upregulation of genes linked to vacuole biogenesis in this assay (Rains et al., 2017). Moreover, almost no genes pertaining to cell polarity showed up in the screen. Finally, the variance analysis (**Fig. 4.5**) revealed that that early and late timepoints clustered separately regardless of their induction with RGE. This indicates that the transcriptomic changes observed are not only due to the induction of dimorphism but also to the fact that the cells have been growing on plates for a longer period of time in the late timepoint analysis. These reasons are why I doubt the biological validity of the experiment I performed.

One could argue that the regulation of the hyphal transition might occur solely at the proteomics level, altering for example protein half-life rather than transcriptomics but this is not what has been observed in other filamentous species (Martin et al., 2013b).

Another, more plausible explanation for this could be that *S. japonicus* does not transition to hypha as a population, it seems to factor in diverse environmental cues and only a fraction of the population will transition. Even though, I incorporated a step to have the cleanest populations possible, it probably was not enough. There is currently no way to have completely pure cell populations – for example only yeast induced for 1h, as it will always be mixed with non-responding yeasts. This heterogeneity in cellular response potentially adds a lot of noise in the analysis and it probably masks important information. The uncertainty focuses particularly on the early timepoints because not all cells will react to the RGE. To circumvent this issue time could be invested in developing single cell transcriptomics analysis in *S. japonicus*. The main issue is that *S. japonicus* can only undergo transition on solid substrate, but if we could couple an automated single cell

transcriptomic platform like the C1 Single-Cell Auto Prep System (Fluidigm) to a microfluidic perfusion system we could technically achieve single cell transcriptomic analysis of *S. japonicus*.

The cleanest populations in the analysis are at 73 hours because in the control experiment they are mostly yeast and in the RGE experiment the macroscopic state of hyphal growth makes it easy to extract hypha only from the plate. The dataset pertaining to the late timepoint 73h indicates a tremendous transcriptomics alteration between control and RGE conditions with half the genes of *S. japonicus* showing significant expression change. This very clearly indicates that the hyphal form exhibits a strikingly different transcriptome profile but because it represents over 2000 genes it makes it difficult to sort manually through that amount of data. A good portion of those genes were coding for proteins of unknown function and/or hypothetical proteins which could potentially be interesting candidates to study.

Preliminary analysis based on protein analysis and gene expression behavior revealed a strong candidate in SJAG_01985 as it possesses a Flo11 domain. Flo11 is required for pseudohyphal growth and invasion in *S. cerevisiae* (Lo and Dranginis, 1998). Interestingly, its deletion yielded no phenotype on hyphal formation in *S. japonicus*. Through protein blast and domain analysis I have identified a second gene in *S. japonicus* genome to contain a putative Flo11 domain (SJAG_16452). This gene showed no expression change during the experiment explaining why I did not focus on it immediately but future focus could be on deleting it and obtaining the double mutant (SJAG_01985 Δ SJAG_16452 Δ) which might yield polarity phenotype.

Future focus could also be on deleting genes coding for hypothetical proteins and continue to assess hyphal growth capabilities.

3.4. Material and Methods

Strains and media. The strain used for the RNA sequencing experiment is JSM20 (Okamoto et al., 2013). This strain is knocked down for the white collar receptor and is insensitive to blue light. Blue light has a negative impact on hyphal formation, generally breaking down the filamentation process. JSM20 was cultured in 20 mL of rich media (YE) overnight before plating on rich solid media. Cells growing either in liquid or solid are cultured at 30°C. The deletions of genes of interest were obtained through homologous recombination and replacement with URA cassette as described in the material and methods of **Chapter 1**. Strains were grown as described in **Chapter 1**.

Figure	Strain	Genotype	Source
all	JSM20	<i>h- mat-2017 wcs1::natMX6 wcs2::kanMX6</i>	(Okamoto et al., 2013)
4.11D, 4.12D, 4.13D, 4.14C	JSM23	<i>h+ ade6sj-domE ura4sj-D3 ura4-</i>	(Furuya and Niki, 2009)
4.14B-C	JCK081	<i>h- map2::ura4 ade6sj-domE</i>	This study
4.13C-D	JCK078	<i>h+ SJAG_00161::ura4 ade6sj-domE ura4sj-D3</i>	This study
4.12C-D	JCK085	<i>h+ SJAG_01985::ura4 ade6sj-domE</i>	This study
4.11C-D	JCK094	<i>h+ SJAG_04365::ura4 ade6sj-domE</i>	This study

Table 4.5. Table of strains used in this chapter.

mRNA sequencing. Total RNA was extracted following the protocol I developed in the results. Shortly, after cell recuperation I performed a mechanical disruption of the cells and total RNA extraction with the NucleoSpin® RNA kit (Macherey-Nagel). The quality of the RNA was assessed with a Bioanalyzer platform (Agilent) (**Annexe 1**).

From the total RNA samples I extracted, RT-PCR was performed with poly T primers to enrich for mRNA sequences and filter out the ribosomal sequences. Illumina sequencing was performed on the resulting cDNA amplicons with the following parameters: single read 100 with the 24 samples multiplexed in a single lane (performed by the GTF).

Sequencing data analysis. Purity-filtered reads were adapters and quality trimmed with Cutadapt (v. 1.3, (Martin, 2011)) and filtered for low complexity with seq_crumbs (v. 0.1.8). Reads were aligned against *Schizosaccharomyces japonicus* (version GCA 000149845.2) genome using STAR (v. 2.4.2a, (Dobin et al., 2013)). The number of read counts per gene locus was summarized with htseq-count (v. 0.6.1, (Anders et al., 2015)) using *S. japonicus* (Ensembl version GCA 000149845.2.31) gene annotation. Quality of the RNA-seq data alignment was assessed using RSeQC (v. 2.3.7, (Wang et al., 2012)). Sequencing data is high quality with 18-25 million total reads per sample. All samples showed high alignment rate (>98%) on the *S. japonicus* reference genome, except for samples 23 and 24 (94% and 93% respectively). Unmapped sequences in these two samples correspond to ribosomal RNA

sequences principally. Gene body coverage is rather uniform and consistent among samples except for sample 08, which is slightly 3' end biased. This is usually related to the quality of the RNA. All other metrics are within the expected values (**Annexe 2**) (performed by the GTF).

Statistics. Statistical analysis was performed for genes in R (R version 3.2.3). Genes with low counts were filtered out according to the rule of 1 count per million (cpm) in at least 1 sample. Library sizes were scaled using TMM normalization (EdgeR package version 3.12.0; Robinson et al. 2010) and log-transformed with limma voom function (Limma package version 3.26.9 ; Law et al. 2014) (performed by the GTF).

The generated excel file for the early timepoint analysis contains the gene ID, average gene expression during the experiment, the fold change in gene expression control vs induced at each timepoint, the false discovery rate (FDR) associated with the moderated F-test, the group which indicates at which timepoint(s) the significant fold change occurred and a gene description (Rhind et al., 2011). The file also contains *S. pombe* and *S. cerevisiae* orthologs when available (**Annexe 3**).

The generated excel file for the late timepoint analysis contain gene ID, average gene expression during the experiment, the expression in the control and induced experiments (as Log2Exp), the logFC (fold change calculated as $\text{Log2Exp}_{\text{induced}} - \text{Log2Exp}_{\text{control}}$), the P value associated with the T-test, a P value adjusted for this test, the fold change in gene expression and a gene description (Rhind et al., 2011) (**Annexe 4**).

Heatmap generation. The cluster analysis and heatmap were generated using TreeView3. Clustering was performed with the following parameters: hierarchical clustering with uncentered Pearson correlation and average linkage. Average linkage uses the average value of the pairwise links within a cluster based upon all objects in the cluster. 122 genes chosen for the analysis were selected with a False Discovery Rate < 5% and at least one significant expression change over time in the early timepoint analysis. The heatmap was color-coded as follows: red for downregulation and green for upregulation, the darker shade are for values closer to 0, the brightest colors are for fold change of at least |5|.

Domain and protein identification. Protein annotation was extracted from protein data for *S. japonicus* and/or *S. pombe* (taken from fungidb website) (Rhind et al., 2011). Domain analysis was performed on ExpASY and NCBI protein. Protein blasts were performed using the NCBI platform.

Gene ontology analysis. Gene ontology analysis was performed on *S. pombe* orthologs using this online tool <https://go.princeton.edu/cgi-bin/GOTermMapper>

General conclusions and perspectives

In this work I provided an extensive description of the dimorphism in growth pattern exhibited by a fairly unstudied filamentous organism. Interestingly, the filamentous behavior triggered in *S. japonicus* adopts characteristics from both true hyphal filamentation as well as pseudohyphal growth. Indeed, the formation of a vacuolated compartment at the back of the cell is reminiscent of what we observe in the dimorphic pathogen *C. albicans* and in the filamentous fungi *N. crassa*. On the other hand, the absence of the specific filamentous organelle, the Spitzenkörper and the constricting septa are similar to what we can observe during the pseudohyphal growth of *S. cerevisiae*.

One of the fascinating aspects of filamentation in *S. japonicus* is that it is more prone to transition on solid or solid-like medium (i.e. microfluidics) than in liquid. From an evolutionary point of view, growth as yeast is typically associated with life in aquatic places while filamentation and invasiveness behaviors are associated with food foraging on land. This underlies the putative existence of mechanisms of mechanosensation to probe the surroundings of the cell and signal transduction triggering a new mode of growth to adapt to the environment. Interestingly, while growth of *S. japonicus* in presence of the red grape extract on agar medium or in microfluidics always triggered a similar cellular response; i.e. growth as hyphae, we identified a mutant that can seemingly tell both surfaces apart. Indeed, in a mutant lacking Exo70, the dimorphic switch is only activated in the microfluidic devices but not on agar plates. This could indicate defects in mechanosensation or signal transduction and could implicate the existence different signals depending on the type of substrate the cells are exposed to. Geometrical constraints might also be in play in the mechanosensation cascade as the cells are mechanically constrained in a very narrow space (4-8 μ m in height) in the microfluidics chambers.

My initial observations of *S. japonicus* growth behavior in liquid showed it was very difficult to restart a culture after the previous round had reached the saturating concentration (data not shown). This indicates *S. japonicus* produces signaling molecules inhibiting yeast growth in conditions of nutrient depletion. I also noticed during my years of imaging this species that the hyphal cells exhibit negative tropism and grow away from each other.

S. japonicus therefore appears to be able to read different cues from the environment and from itself. Fungal language in the form of small informative molecules, similar to quorum sensing in bacteria, is a rapidly emerging field in fungal research (Leeder et al., 2011). Heterogeneity in the dimorphic transition (i.e. amount of cells initiating the transition as well as the difficulty in replicating

identical responses on different agar plates) might reflect the cell to cell variation of the different cues integration. *S. japonicus* could therefore represent an attractive model to study the mechanics and chemistry of fungal interaction and behavior in response to the environment.

References

- Akashi, T., T. Kanbe, and K. Tanaka. 1994. The role of the cytoskeleton in the polarized growth of the germ tube in *Candida albicans*. *Microbiology*. 140 (Pt 2):271-280.
- Alfa, C.E., and J.S. Hyams. 1990. Distribution of tubulin and actin through the cell division cycle of the fission yeast *Schizosaccharomyces japonicus* var. *versatilis*: a comparison with *Schizosaccharomyces pombe*. *Journal of cell science*. 96 (Pt 1):71-77.
- Almonacid, M., J.B. Moseley, J. Janvoren, A. Mayeux, V. Fraissier, P. Nurse, and A. Paoletti. 2009. Spatial control of cytokinesis by Cdr2 kinase and Mid1/anillin nuclear export. *Current biology : CB*. 19:961-966.
- Amoah-Buahin, E., N. Bone, and J. Armstrong. 2005. Hyphal Growth in the Fission Yeast *Schizosaccharomyces pombe*. *Eukaryotic cell*. 4:1287-1297.
- Anders, S., P.T. Pyl, and W. Huber. 2015. HTSeq--a Python framework to work with high-throughput sequencing data. *Bioinformatics*. 31:166-169.
- Aoki, K., K. Furuya, and H. Niki. 2017. *Schizosaccharomyces japonicus*: A Distinct Dimorphic Yeast among the Fission Yeasts. *Cold Spring Harbor protocols*. 2017:pdb top082651.
- Aoki, K., R. Nakajima, K. Furuya, and H. Niki. 2010. Novel episomal vectors and a highly efficient transformation procedure for the fission yeast *Schizosaccharomyces japonicus*. *Yeast*. 27:1049-1060.
- Aoki, K., and H. Niki. 2017. Transformation of *Schizosaccharomyces japonicus*. *Cold Spring Harbor protocols*. 2017:pdb prot091850.
- Araujo-Palomares, C.L., M. Riquelme, and E. Castro-Longoria. 2009. The polarisome component SPA-2 localizes at the apex of *Neurospora crassa* and partially colocalizes with the Spitzenkorper. *Fungal genetics and biology : FG & B*. 46:551-563.
- Bahn, Y.S., and P. Sundstrom. 2001. CAP1, an adenylate cyclase-associated protein gene, regulates bud-hypha transitions, filamentous growth, and cyclic AMP levels and is required for virulence of *Candida albicans*. *Journal of bacteriology*. 183:3211-3223.
- Bassilana, M., J. Blyth, and R.A. Arkowitz. 2003. Cdc24, the GDP-GTP exchange factor for Cdc42, is required for invasive hyphal growth of *Candida albicans*. *Eukaryotic cell*. 2:9-18.
- Bendezu, F.O., and S.G. Martin. 2011. Actin cables and the exocyst form two independent morphogenesis pathways in the fission yeast. *Molecular biology of the cell*. 22:44-53.
- Bendezu, F.O., V. Vincenzetti, and S.G. Martin. 2012. Fission yeast Sec3 and Exo70 are transported on actin cables and localize the exocyst complex to cell poles. *PLoS One*. 7:e40248.
- Berbee, M.L., and J.W. Taylor. 1993. Dating the evolutionary radiations of the true fungi. *Canadian Journal of Botany*. 71:1114-1127.
- Berepiki, A., A. Lichius, and N.D. Read. 2011. Actin organization and dynamics in filamentous fungi. *Nature reviews. Microbiology*. 9:876-887.
- Bhatia, P., O. Hachet, M. Hersch, S.A. Rincon, M. Berthelot-Grosjean, S. Dalessi, L. Basterra, S. Bergmann, A. Paoletti, and S.G. Martin. 2014. Distinct levels in Pom1 gradients limit Cdr2 activity and localization to time and position division. *Cell cycle*. 13:538-552.
- Bi, E., and H.O. Park. 2012. Cell polarization and cytokinesis in budding yeast. *Genetics*. 191:347-387.
- Bleichrodt, R.J., M. Hulsman, H.A. Wosten, and M.J. Reinders. 2015. Switching from a unicellular to multicellular organization in an *Aspergillus niger* hypha. *mBio*. 6:e00111.
- Boyce, K.J., M.J. Hynes, and A. Andrianopoulos. 2003. Control of morphogenesis and actin localization by the *Penicillium marneffei* RAC homolog. *Journal of cell science*. 116:1249-1260.
- Bozsik, A., Z. Szilagy, Z. Benko, and M. Sipiczki. 2002. Marker construction and cloning of a cut1-like sequence with ARS activity in the fission yeast *Schizosaccharomyces japonicus*. *Yeast*. 19:485-498.

- Brown, S.S. 1999. Cooperation between microtubule- and actin-based motor proteins. *Annual review of cell and developmental biology*. 15:63-80.
- Brunner, D., and P. Nurse. 2000. CLIP170-like tip1p spatially organizes microtubular dynamics in fission yeast. *Cell*. 102:695-704.
- Busch, K.E., and D. Brunner. 2004. The microtubule plus end-tracking proteins mal3p and tip1p cooperate for cell-end targeting of interphase microtubules. *Current biology : CB*. 14:548-559.
- Cao, C., R. Li, Z. Wan, W. Liu, X. Wang, J. Qiao, D. Wang, G. Bulmer, and R. Calderone. 2007. The effects of temperature, pH, and salinity on the growth and dimorphism of *Penicillium marneffei*. *Medical mycology*. 45:401-407.
- Celton-Morizur, S., V. Racine, J.B. Sibarita, and A. Paoletti. 2006. Pom1 kinase links division plane position to cell polarity by regulating Mid1p cortical distribution. *J Cell Sci*. 119:4710-4718.
- Chang, F., D. Drubin, and P. Nurse. 1997. cdc12p, a protein required for cytokinesis in fission yeast, is a component of the cell division ring and interacts with profilin. *J Cell Biol*. 137:169-182.
- Chang, F., and S.G. Martin. 2009. Shaping fission yeast with microtubules. *Cold Spring Harbor perspectives in biology*. 1:a001347.
- Cheng, H., R. Sugiura, W. Wu, M. Fujita, Y. Lu, S.O. Sio, R. Kawai, K. Takegawa, H. Shuntoh, and T. Kuno. 2002. Role of the Rab GTP-binding protein Ypt3 in the fission yeast exocytic pathway and its connection to calcineurin function. *Molecular biology of the cell*. 13:2963-2976.
- Choi, J., and S.-H. Kim. 2017. A genome Tree of Life for the Fungi kingdom. *Proceedings of the National Academy of Sciences*. 114:9391.
- Coll, P.M., Y. Trillo, A. Ametzazurra, and P. Perez. 2003. Gef1p, a new guanine nucleotide exchange factor for Cdc42p, regulates polarity in *Schizosaccharomyces pombe*. *Molecular biology of the cell*. 14:313-323.
- Crampin, H., K. Finley, M. Gerami-Nejad, H. Court, C. Gale, J. Berman, and P. Sudbery. 2005. *Candida albicans* hyphae have a Spitzenkorper that is distinct from the polarisome found in yeast and pseudohyphae. *Journal of cell science*. 118:2935-2947.
- Cullen, P.J., and G.F. Sprague, Jr. 2012. The regulation of filamentous growth in yeast. *Genetics*. 190:23-49.
- Daga, R.R., A. Yonetani, and F. Chang. 2006. Asymmetric microtubule pushing forces in nuclear centering. *Curr Biol*. 16:1544-1550.
- Das, M., T. Drake, D.J. Wiley, P. Buchwald, D. Vavylonis, and F. Verde. 2012. Oscillatory dynamics of Cdc42 GTPase in the control of polarized growth. *Science*. 337:239-243.
- David-Vaizant, V., and H. Alexandre. 2018. Flor Yeast Diversity and Dynamics in Biologically Aged Wines. *Frontiers in microbiology*. 9:2235.
- Dobin, A., C.A. Davis, F. Schlesinger, J. Drenkow, C. Zaleski, S. Jha, P. Batut, M. Chaisson, and T.R. Gingeras. 2013. STAR: ultrafast universal RNA-seq aligner. *Bioinformatics*. 29:15-21.
- Edwards, J.A., C. Chen, M.M. Kemski, J. Hu, T.K. Mitchell, and C.A. Rappleye. 2013. *Histoplasma* yeast and mycelial transcriptomes reveal pathogenic-phase and lineage-specific gene expression profiles. *BMC genomics*. 14:695.
- Egan, M.J., M.A. McClintock, and S.L. Reck-Peterson. 2012. Microtubule-based transport in filamentous fungi. *Current opinion in microbiology*. 15:637-645.
- Enczi, K., M. Yamaguchi, and M. Sipiczki. 2007. Morphology transition genes in the dimorphic fission yeast *Schizosaccharomyces japonicus*. *Antonie van Leeuwenhoek*. 92:143-154.
- Etienne-Manneville, S. 2004. Cdc42--the centre of polarity. *Journal of cell science*. 117:1291-1300.
- Feierbach, B., and F. Chang. 2001. Roles of the fission yeast formin for3p in cell polarity, actin cable formation and symmetric cell division. *Curr Biol*. 11:1656-1665.
- Fischer-Parton, S., R.M. Parton, P.C. Hickey, J. Dijksterhuis, H.A. Atkinson, and N.D. Read. 2000. Confocal microscopy of FM4-64 as a tool for analysing endocytosis and vesicle trafficking in living fungal hyphae. *Journal of microscopy*. 198:246-259.

- Fischer, R., N. Zekert, and N. Takeshita. 2008. Polarized growth in fungi--interplay between the cytoskeleton, positional markers and membrane domains. *Molecular microbiology*. 68:813-826.
- Fisher, K.E., I. Romberger, D. Lowry, P. Shange, and R.W. Roberson. 2018. Hyphal tip growth and cytoplasmic characters of *Conidiobolus coronatus* (Zoopagomycota, Entomophthoromycotina). *Mycologia*. 110:31-38.
- Fuller, K.K., J.J. Loros, and J.C. Dunlap. 2015. Fungal photobiology: visible light as a signal for stress, space and time. *Current genetics*. 61:275-288.
- Furuya, K., and H. Niki. 2009. Isolation of heterothallic haploid and auxotrophic mutants of *Schizosaccharomyces japonicus*. *Yeast*. 26:221-233.
- Furuya, K., and H. Niki. 2010. The DNA damage checkpoint regulates a transition between yeast and hyphal growth in *Schizosaccharomyces japonicus*. *Molecular and cellular biology*. 30:2909-2917.
- Furuya, K., and H. Niki. 2011. Construction of diploid zygotes by interallelic complementation of *ade6* in *Schizosaccharomyces japonicus*. *Yeast*. 28:747-754.
- Furuya, K., and H. Niki. 2012. Hyphal differentiation induced via a DNA damage checkpoint-dependent pathway engaged in crosstalk with nutrient stress signaling in *Schizosaccharomyces japonicus*. *Current genetics*. 58:291-303.
- Gallo Castro, D., and S.G. Martin. 2018. Differential GAP requirement for Cdc42-GTP polarization during proliferation and sexual reproduction. *The Journal of cell biology*. 217:4215-4229.
- Gimeno, C.J., P.O. Ljungdahl, C.A. Styles, and G.R. Fink. 1992. Unipolar cell divisions in the yeast *S. cerevisiae* lead to filamentous growth: Regulation by starvation and RAS. *Cell*. 68:1077-1090.
- Girbardt, M. 1957. Der Spitzenkörper von *Polystictus versicolor*. *Planta*. 50.: 47-59.
- Gladfelter, A.S. 2006. Control of filamentous fungal cell shape by septins and formins. *Nature reviews. Microbiology*. 4:223-229.
- Goode, B.L., D.G. Drubin, and G. Barnes. 2000. Functional cooperation between the microtubule and actin cytoskeletons. *Current opinion in cell biology*. 12:63-71.
- Gow, N.A., and G.W. Gooday. 1982a. Growth kinetics and morphology of colonies of the filamentous form of *Candida albicans*. *Journal of general microbiology*. 128:2187-2194.
- Gow, N.A., and G.W. Gooday. 1982b. Vacuolation, branch production and linear growth of germ tubes in *Candida albicans*. *Journal of general microbiology*. 128:2195-2198.
- Grove, S.N., and C.E. Bracker. 1970. Protoplasmic organization of hyphal tips among fungi: vesicles and Spitzenkörper. *Journal of bacteriology*. 104:989-1009.
- Gu, Y., and S. Oliferenko. 2015. Comparative biology of cell division in the fission yeast clade. *Current opinion in microbiology*. 28:18-25.
- Gu, Y., C. Yam, and S. Oliferenko. 2012. Divergence of mitotic strategies in fission yeasts. *Nucleus*. 3:220-225.
- Gu, Y., C. Yam, and S. Oliferenko. 2015. Rewiring of cellular division site selection in evolution of fission yeasts. *Current biology : CB*. 25:1187-1194.
- Hachet, O., M. Berthelot-Grosjean, K. Kokkoris, V. Vincenzetti, J. Moosbrugger, and S.G. Martin. 2011. A phosphorylation cycle shapes gradients of the DYRK family kinase Pom1 at the plasma membrane. *Cell*. 145:1116-1128.
- Hagan, I.M. 1998. The fission yeast microtubule cytoskeleton. *Journal of cell science*. 111 (Pt 12):1603-1612.
- Halary, S., S.B. Malik, L. Lildhar, C.H. Slamovits, M. Hijri, and N. Corradi. 2011. Conserved meiotic machinery in *Glomus* spp., a putatively ancient asexual fungal lineage. *Genome biology and evolution*. 3:950-958.
- Harris, S.D., L. Hamer, K.E. Sharpless, and J.E. Hamer. 1997. The *Aspergillus nidulans* *sepA* gene encodes an FH1/2 protein involved in cytokinesis and the maintenance of cellular polarity. *The EMBO journal*. 16:3474-3483.

- Harris, S.D., N.D. Read, R.W. Roberson, B. Shaw, S. Seiler, M. Plamann, and M. Momany. 2005. Polarisome meets Spitzenkörper: microscopy, genetics, and genomics converge. *Eukaryotic cell*. 4:225-229.
- Hawksworth, D.L., and R. Lucking. 2017. Fungal Diversity Revisited: 2.2 to 3.8 Million Species. *Microbiology spectrum*. 5.
- Heaton, L., B. Obara, V. Grau, N. Jones, T. Nakagaki, L. Boddy, and M.D. Fricker. 2012. Analysis of fungal networks. *Fungal Biology Reviews*. 26:12-29.
- Helston, R.M., J.A. Box, W. Tang, and P. Baumann. 2010. *Schizosaccharomyces cryophilus* sp. nov., a new species of fission yeast. *FEMS yeast research*. 10:779-786.
- Hirota, K., K. Tanaka, K. Ohta, and M. Yamamoto. 2003. Gef1p and Scd1p, the Two GDP-GTP exchange factors for Cdc42p, form a ring structure that shrinks during cytokinesis in *Schizosaccharomyces pombe*. *Molecular biology of the cell*. 14:3617-3627.
- Horio, T., and B.R. Oakley. 2005. The role of microtubules in rapid hyphal tip growth of *Aspergillus nidulans*. *Molecular biology of the cell*. 16:918-926.
- Huang, Y., T.G. Chew, W. Ge, and M.K. Balasubramanian. 2007. Polarity determinants Tea1p, Tea4p, and Pom1p inhibit division-septum assembly at cell ends in fission yeast. *Developmental cell*. 12:987-996.
- Islam, M.R., G. Tudryn, R. Bucinell, L. Schadler, and R.C. Picu. 2017. Morphology and mechanics of fungal mycelium. *Scientific Reports*. 7:13070.
- Johnston, D.A., K.E. Eberle, J.E. Sturtevant, and G.E. Palmer. 2009. Role for endosomal and vacuolar GTPases in *Candida albicans* pathogenesis. *Infection and immunity*. 77:2343-2355.
- Johnston, D.A., A.L. Tapia, K.E. Eberle, and G.E. Palmer. 2013. Three prevacuolar compartment Rab GTPases impact *Candida albicans* hyphal growth. *Eukaryotic cell*. 12:1039-1050.
- Jorgensen, P., N.P. Edgington, B.L. Schneider, I. Rupes, M. Tyers, and B. Fitcher. 2007. The size of the nucleus increases as yeast cells grow. *Molecular biology of the cell*. 18:3523-3532.
- King, N. 2004. The unicellular ancestry of animal development. *Developmental cell*. 7:313-325.
- Klar, A.J. 2013. *Schizosaccharomyces japonicus* yeast poised to become a favorite experimental organism for eukaryotic research. *G3*. 3:1869-1873.
- Kohli, M., V. Galati, K. Boudier, R.W. Roberson, and P. Philippsen. 2008. Growth-speed-correlated localization of exocyst and polarisome components in growth zones of *Ashbya gossypii* hyphal tips. *Journal of cell science*. 121:3878-3889.
- Konzack, S., P.E. Rischitor, C. Enke, and R. Fischer. 2005. The role of the kinesin motor KipA in microtubule organization and polarized growth of *Aspergillus nidulans*. *Molecular biology of the cell*. 16:497-506.
- Kovar, D.R., V. Sirotkin, and M. Lord. 2011. Three's company: the fission yeast actin cytoskeleton. *Trends in cell biology*. 21:177-187.
- Kwon, M.J., M. Arentshorst, E.D. Roos, C.A. van den Hondel, V. Meyer, and A.F. Ram. 2011. Functional characterization of Rho GTPases in *Aspergillus niger* uncovers conserved and diverged roles of Rho proteins within filamentous fungi. *Molecular microbiology*. 79:1151-1167.
- Lee, P.J., N.C. Helman, W.A. Lim, and P.J. Hung. 2008. A microfluidic system for dynamic yeast cell imaging. *BioTechniques*. 44:91-95.
- Leeder, A.C., J. Palma-Guerrero, and N.L. Glass. 2011. The social network: deciphering fungal language. *Nature reviews. Microbiology*. 9:440-451.
- Lehmler, C., G. Steinberg, K.M. Snetselaar, M. Schliwa, R. Kahmann, and M. Bolker. 1997. Identification of a motor protein required for filamentous growth in *Ustilago maydis*. *The EMBO journal*. 16:3464-3473.
- Liakopoulos, D., J. Kusch, S. Grava, J. Vogel, and Y. Barral. 2003. Asymmetric loading of Kar9 onto spindle poles and microtubules ensures proper spindle alignment. *Cell*. 112:561-574.
- Lips, K.R., F. Brem, R. Brenes, J.D. Reeve, R.A. Alford, J. Voyles, C. Carey, L. Livo, A.P. Pessier, and J.P. Collins. 2006. Emerging infectious disease and the loss of biodiversity in a Neotropical

- amphibian community. *Proceedings of the National Academy of Sciences of the United States of America*. 103:3165-3170.
- Lo Presti, L., F. Chang, and S.G. Martin. 2012. Myosin Vs organize actin cables in fission yeast. *Molecular biology of the cell*. 23:4579-4591.
- Lo Presti, L., and S.G. Martin. 2011. Shaping fission yeast cells by rerouting actin-based transport on microtubules. *Current biology : CB*. 21:2064-2069.
- Lo, W.S., and A.M. Dranginis. 1998. The cell surface flocculin Flo11 is required for pseudohyphae formation and invasion by *Saccharomyces cerevisiae*. *Molecular biology of the cell*. 9:161-171.
- Mahlert, M., L. Leveleki, A. Hlubek, B. Sandrock, and M. Bolker. 2006. Rac1 and Cdc42 regulate hyphal growth and cytokinesis in the dimorphic fungus *Ustilago maydis*. *Molecular microbiology*. 59:567-578.
- Manck, R., Y. Ishitsuka, S. Herrero, N. Takeshita, G.U. Nienhaus, and R. Fischer. 2015. Genetic evidence for a microtubule-capture mechanism during polarised growth of *Aspergillus nidulans*. *Journal of cell science*. 128:3569-3582.
- Martin, M. 2011. Cutadapt removes adapter sequences from high-throughput sequencing reads. 2011. 17:3.
- Martin, R., D. Albrecht-Eckardt, S. Brunke, B. Hube, K. Hünninger, and O. Kurzai. 2013a. A core filamentation response network in *Candida albicans* is restricted to eight genes. *PLoS one*. 8:e58613.
- Martin, R., D. Albrecht-Eckardt, S. Brunke, B. Hube, K. Hünninger, and O. Kurzai. 2013b. A Core Filamentation Response Network in *Candida albicans* Is Restricted to Eight Genes. *PLoS one*. 8:e58613.
- Martin, S.G. 2009. Microtubule-dependent cell morphogenesis in the fission yeast. *Trends in cell biology*. 19:447-454.
- Martin, S.G., and R.A. Arkowitz. 2014. Cell polarization in budding and fission yeasts. *FEMS microbiology reviews*. 38:228-253.
- Martin, S.G., and F. Chang. 2005. New end take off: regulating cell polarity during the fission yeast cell cycle. *Cell cycle*. 4:1046-1049.
- Martin, S.G., and F. Chang. 2006. Dynamics of the formin for3p in actin cable assembly. *Current biology : CB*. 16:1161-1170.
- Martin, S.G., W.H. McDonald, J.R. Yates, 3rd, and F. Chang. 2005. Tea4p links microtubule plus ends with the formin for3p in the establishment of cell polarity. *Dev Cell*. 8:479-491.
- Martin, S.G., S.A. Rincon, R. Basu, P. Perez, and F. Chang. 2007. Regulation of the formin for3p by cdc42p and bud6p. *Molecular biology of the cell*. 18:4155-4167.
- McClure, W.K., D. Park, and P.M. Robinson. 1968. Apical organization in the somatic hyphae of fungi. *Journal of general microbiology*. 50:177-182.
- Menasche, G., C.H. Ho, O. Sanal, J. Feldmann, I. Tezcan, F. Ersoy, A. Houdusse, A. Fischer, and G. de Saint Basile. 2003. Griscelli syndrome restricted to hypopigmentation results from a melanophilin defect (GS3) or a MYO5A F-exon deletion (GS1). *The Journal of clinical investigation*. 112:450-456.
- Miller, P.J., and D.I. Johnson. 1994. Cdc42p GTPase is involved in controlling polarized cell growth in *Schizosaccharomyces pombe*. *Molecular and cellular biology*. 14:1075-1083.
- Minc, N., A. Boudaoud, and F. Chang. 2014. Mechanical Forces of Fission Yeast Growth. *Current biology : CB*. 24:1436.
- Minke, P.F., I.H. Lee, J.H. Tinsley, K.S. Bruno, and M. Plamann. 1999. *Neurospora crassa* ro-10 and ro-11 genes encode novel proteins required for nuclear distribution. *Molecular microbiology*. 32:1065-1076.
- Mitchison, J.M., and P. Nurse. 1985. Growth in cell length in the fission yeast *Schizosaccharomyces pombe*. *Journal of cell science*. 75:357-376.

- Morigasaki, S., K. Shimada, A. Ikner, M. Yanagida, and K. Shiozaki. 2008. Glycolytic enzyme GAPDH promotes peroxide stress signaling through multistep phosphorelay to a MAPK cascade. *Molecular cell*. 30:108-113.
- Motegi, F., R. Arai, and I. Mabuchi. 2001. Identification of two type V myosins in fission yeast, one of which functions in polarized cell growth and moves rapidly in the cell. *Molecular biology of the cell*. 12:1367-1380.
- Mourino-Perez, R.R., and M. Riquelme. 2013. Recent advances in septum biogenesis in *Neurospora crassa*. *Advances in genetics*. 83:99-134.
- Nadal, M., M.D. Garcia-Pedrajas, and S.E. Gold. 2008. Dimorphism in fungal plant pathogens. *FEMS microbiology letters*. 284:127-134.
- Nakano, K., J. Imai, R. Arai, E.A. Toh, Y. Matsui, and I. Mabuchi. 2002. The small GTPase Rho3 and the diaphanous/formin For3 function in polarized cell growth in fission yeast. *Journal of cell science*. 115:4629-4639.
- Nelson, W.J. 2003. Adaptation of core mechanisms to generate cell polarity. *Nature*. 422:766-774.
- Nemecek, J.C., M. Wuthrich, and B.S. Klein. 2006. Global control of dimorphism and virulence in fungi. *Science*. 312:583-588.
- Neumann, F.R., and P. Nurse. 2007. Nuclear size control in fission yeast. *J Cell Biol*. 179:593-600.
- Nigg, M., and L. Bernier. 2016. From yeast to hypha: defining transcriptomic signatures of the morphological switch in the dimorphic fungal pathogen *Ophiostoma novo-ulmi*. *BMC genomics*. 17:920.
- Niki, H. 2014. *Schizosaccharomyces japonicus*: the fission yeast is a fusion of yeast and hyphae. *Yeast*. 31:83-90.
- Nozaki, S., K. Furuya, and H. Niki. 2018. The Ras1-Cdc42 pathway is involved in hyphal development of *Schizosaccharomyces japonicus*. *FEMS yeast research*. 18.
- Okamoto, S., K. Furuya, S. Nozaki, K. Aoki, and H. Niki. 2013. Synchronous activation of cell division by light or temperature stimuli in the dimorphic yeast *Schizosaccharomyces japonicus*. *Eukaryotic cell*. 12:1235-1243.
- Oliferenko, S., T.G. Chew, and M.K. Balasubramanian. 2009. Positioning cytokinesis. *Genes & development*. 23:660-674.
- Padte, N.N., S.G. Martin, M. Howard, and F. Chang. 2006. The cell-end factor pom1p inhibits mid1p in specification of the cell division plane in fission yeast. *Curr Biol*. 16:2480-2487.
- Pan, K.Z., T.E. Saunders, I. Flor-Parra, M. Howard, and F. Chang. 2014. Cortical regulation of cell size by a sizer cdr2p. *eLife*. 3:e02040.
- Papadakis, M.A., and C.T. Workman. 2015. Oxidative stress response pathways: Fission yeast as archetype. *Critical Reviews in Microbiology*. 41:520-535.
- Papp, L., M. Sipiczki, I.J. Holb, and I. Miklos. 2014. Optimal conditions for mycelial growth of *Schizosaccharomyces japonicus* cells in liquid medium: it enables the molecular investigation of dimorphism. *Yeast*. 31:475-482.
- Parfrey, L.W., and D.J. Lahr. 2013. Multicellularity arose several times in the evolution of eukaryotes (response to DOI 10.1002/bies.201100187). *BioEssays : news and reviews in molecular, cellular and developmental biology*. 35:339-347.
- Park, H.O., and E. Bi. 2007. Central roles of small GTPases in the development of cell polarity in yeast and beyond. *Microbiology and molecular biology reviews : MMBR*. 71:48-96.
- Rains, A., Y. Bryant, K.A. Dorsett, A. Culver, J. Egbaria, A. Williams, M. Barnes, R. Lamere, A.R. Rossi, S.C. Waldrep, C. Wilder, E. Kliossis, and M.L. Styers. 2017. Ypt4 and lvs1 regulate vacuolar size and function in *Schizosaccharomyces pombe*. *Cellular logistics*. 7:e1335270.
- Ralsler, M., H. Kuhl, M. Ralsler, M. Werber, H. Lehrach, M. Breitenbach, and B. Timmermann. 2012. The *Saccharomyces cerevisiae* W303-K6001 cross-platform genome sequence: insights into ancestry and physiology of a laboratory mutt. *Open biology*. 2:120093.
- Ray, S., K. Kume, S. Gupta, W. Ge, M. Balasubramanian, D. Hirata, and D. McCollum. 2010. The mitosis-to-interphase transition is coordinated by cross talk between the SIN and MOR pathways in *Schizosaccharomyces pombe*. *The Journal of cell biology*. 190:793-805.

- Read, N.D., A. Fleißner, M.G. Roca, and N.L. Glass. 2010. Hyphal Fusion. *In Cellular and Molecular Biology of Filamentous Fungi*. American Society of Microbiology.
- Read, N.D., A. Lichius, J.Y. Shoji, and A.B. Goryachev. 2009. Self-signalling and self-fusion in filamentous fungi. *Current opinion in microbiology*. 12:608-615.
- Requena, N., C. Alberti-Segui, E. Winzenburg, C. Horn, M. Schliwa, P. Philippsen, R. Liese, and R. Fischer. 2001. Genetic evidence for a microtubule-destabilizing effect of conventional kinesin and analysis of its consequences for the control of nuclear distribution in *Aspergillus nidulans*. *Molecular microbiology*. 42:121-132.
- Revilla-Guarinos, M.T., R. Martin-Garcia, M.A. Villar-Tajadura, M. Estravis, P.M. Coll, and P. Perez. 2016. Rga6 is a Fission Yeast Rho GAP Involved in Cdc42 Regulation of Polarized Growth. *Molecular biology of the cell*.
- Rhind, N., Z. Chen, M. Yassour, D.A. Thompson, B.J. Haas, N. Habib, I. Wapinski, S. Roy, M.F. Lin, D.I. Heiman, S.K. Young, K. Furuya, Y. Guo, A. Pidoux, H.M. Chen, B. Robbertse, J.M. Goldberg, K. Aoki, E.H. Bayne, A.M. Berlin, C.A. Desjardins, E. Dobbs, L. Dukaj, L. Fan, M.G. FitzGerald, C. French, S. Gujja, K. Hansen, D. Keifenheim, J.Z. Levin, R.A. Mosher, C.A. Muller, J. Pfiffner, M. Priest, C. Russ, A. Smialowska, P. Swoboda, S.M. Sykes, M. Vaughn, S. Vengrova, R. Yoder, Q. Zeng, R. Allshire, D. Baulcombe, B.W. Birren, W. Brown, K. Ekwall, M. Kellis, J. Leatherwood, H. Levin, H. Margalit, R. Martienssen, C.A. Nieduszynski, J.W. Spatafora, N. Friedman, J.Z. Dalgaard, P. Baumann, H. Niki, A. Regev, and C. Nusbaum. 2011. Comparative functional genomics of the fission yeasts. *Science*. 332:930-936.
- Rincon, S.A., P. Bhatia, C. Bicho, M. Guzman-Vendrell, V. Fraiser, W.E. Borek, L. Alves Fde, F. Dingli, D. Loew, J. Rappsilber, K.E. Sawin, S.G. Martin, and A. Paoletti. 2014. Pom1 regulates the assembly of Cdr2-Mid1 cortical nodes for robust spatial control of cytokinesis. *The Journal of cell biology*. 206:61-77.
- Riquelme, M. 2013. Tip growth in filamentous fungi: a road trip to the apex. *Annual review of microbiology*. 67:587-609.
- Riquelme, M., J. Aguirre, S. Bartnicki-Garcia, G.H. Braus, M. Feldbrugge, U. Fleig, W. Hansberg, A. Herrera-Estrella, J. Kamper, U. Kuck, R.R. Mourino-Perez, N. Takeshita, and R. Fischer. 2018. Fungal Morphogenesis, from the Polarized Growth of Hyphae to Complex Reproduction and Infection Structures. *Microbiology and molecular biology reviews : MMBR*. 82.
- Riquelme, M., R. Fischer, and S. Bartnicki-Garcia. 2003. Apical growth and mitosis are independent processes in *Aspergillus nidulans*. *Protospasma*. 222:211-215.
- Riquelme, M., and L. Martinez-Nunez. 2016. Hyphal ontogeny in *Neurospora crassa*: a model organism for all seasons. *F1000Research*. 5:2801.
- Riquelme, M., C.G. Reynaga-Pena, G. Gierz, and S. Bartnicki-Garcia. 1998. What determines growth direction in fungal hyphae? *Fungal genetics and biology : FG & B*. 24:101-109.
- Riquelme, M., and E. Sanchez-Leon. 2014. The Spitzenkorper: a choreographer of fungal growth and morphogenesis. *Current opinion in microbiology*. 20:27-33.
- Roberson, R.W., M. Abril, M. Blackwell, P. Letcher, D.J. McLaughlin, R.R. Mouri ÑO-PÉrez, M. Riquelme, and M. Uchida. 2010. Hyphal Structure. *In Cellular and Molecular Biology of Filamentous Fungi*. American Society of Microbiology.
- Rodriguez, O.C., A.W. Schaefer, C.A. Mandato, P. Forscher, W.M. Bement, and C.M. Waterman-Storer. 2003. Conserved microtubule-actin interactions in cell movement and morphogenesis. *Nature cell biology*. 5:599-609.
- Sanchez-Leon, E., B. Bowman, C. Seidel, R. Fischer, P. Novick, and M. Riquelme. 2015. The Rab GTPase YPT-1 associates with Golgi cisternae and Spitzenkorper microvesicles in *Neurospora crassa*. *Molecular microbiology*. 95:472-490.
- Sanchez-Martinez, C., and J. Perez-Martin. 2001. Dimorphism in fungal pathogens: *Candida albicans* and *Ustilago maydis*--similar inputs, different outputs. *Current opinion in microbiology*. 4:214-221.

- Schuchardt, I., D. Assmann, E. Thines, C. Schuberth, and G. Steinberg. 2005. Myosin-V, Kinesin-1, and Kinesin-3 cooperate in hyphal growth of the fungus *Ustilago maydis*. *Molecular biology of the cell*. 16:5191-5201.
- Seiler, S., F.E. Nargang, G. Steinberg, and M. Schliwa. 1997. Kinesin is essential for cell morphogenesis and polarized secretion in *Neurospora crassa*. *The EMBO journal*. 16:3025-3034.
- Silverman-Gavrila, L.B., and R.R. Lew. 2003. Calcium gradient dependence of *Neurospora crassa* hyphal growth. *Microbiology*. 149:2475-2485.
- Simonin, A., J. Palma-Guerrero, M. Fricker, and N.L. Glass. 2012. Physiological significance of network organization in fungi. *Eukaryotic cell*. 11:1345-1352.
- Sipiczki, M. 2000. Where does fission yeast sit on the tree of life? *Genome biology*. 1:REVIEWS1011.
- Sipiczki, M., K. Takeo, and A. Grallert. 1998a. Growth polarity transitions in a dimorphic fission yeast. *Microbiology*. 144 (Pt 12):3475-3485.
- Sipiczki, M., K. Takeo, M. Yamaguchi, S. Yoshida, and I. Miklos. 1998b. Environmentally controlled dimorphic cycle in a fission yeast. *Microbiology*. 144 (Pt 5):1319-1330.
- Smith, M.L., J.N. Bruhn, and J.B. Anderson. 1992. The fungus *Armillaria bulbosa* is among the largest and oldest living organisms. *Nature*. 356:428.
- Sohrmann, M., C. Fankhauser, C. Brodbeck, and V. Simanis. 1996. The *dmf1/mid1* gene is essential for correct positioning of the division septum in fission yeast. *Genes & development*. 10:2707-2719.
- Steinberg, G., M.A. Penalva, M. Riquelme, H.A. Wosten, and S.D. Harris. 2017. Cell Biology of Hyphal Growth. *Microbiology spectrum*. 5.
- Steinberg, G., and J. Perez-Martin. 2008. *Ustilago maydis*, a new fungal model system for cell biology. *Trends in cell biology*. 18:61-67.
- Sudbery, P.E. 2011. Growth of *Candida albicans* hyphae. *Nature reviews. Microbiology*. 9:737-748.
- Taheri-Talesh, N., Y. Xiong, and B.R. Oakley. 2012. The functions of myosin II and myosin V homologs in tip growth and septation in *Aspergillus nidulans*. *PLoS one*. 7:e31218.
- Takeshita, N. 2016. Coordinated process of polarized growth in filamentous fungi. *Bioscience, biotechnology, and biochemistry*. 80:1693-1699.
- Takeshita, N., M. Evangelinos, L. Zhou, T. Serizawa, R.A. Somera-Fajardo, L. Lu, N. Takaya, G.U. Nienhaus, and R. Fischer. 2017. Pulses of Ca²⁺ coordinate actin assembly and exocytosis for stepwise cell extension. *Proceedings of the National Academy of Sciences of the United States of America*. 114:5701-5706.
- Takeshita, N., Y. Higashitsuji, S. Konzack, and R. Fischer. 2008. Apical sterol-rich membranes are essential for localizing cell end markers that determine growth directionality in the filamentous fungus *Aspergillus nidulans*. *Molecular biology of the cell*. 19:339-351.
- Tatebe, H., K. Nakano, R. Maximo, and K. Shiozaki. 2008. Pom1 DYRK regulates localization of the Rga4 GAP to ensure bipolar activation of Cdc42 in fission yeast. *Current biology : CB*. 18:322-330.
- Tolic-Norrelykke, I.M., L. Sacconi, C. Stringari, I. Raabe, and F.S. Pavone. 2005. Nuclear and division-plane positioning revealed by optical micromanipulation. *Current biology : CB*. 15:1212-1216.
- Torralba, S., M. Raudaskoski, A.M. Pedregosa, and F. Laborda. 1998. Effect of cytochalasin A on apical growth, actin cytoskeleton organization and enzyme secretion in *Aspergillus nidulans*. *Microbiology*. 144 (Pt 1):45-53.
- Tran, P.T., L. Marsh, V. Doye, S. Inoue, and F. Chang. 2001. A mechanism for nuclear positioning in fission yeast based on microtubule pushing. *J Cell Biol*. 153:397-411.
- Trybus, K.M. 2008. Myosin V from head to tail. *Cellular and molecular life sciences : CMLS*. 65:1378-1389.
- van Peer, A.F., F. Wang, K.G. van Driel, J.F. de Jong, E.G. van Donselaar, W.H. Muller, T. Boekhout, L.G. Lugones, and H.A. Wosten. 2010. The septal pore cap is an organelle that functions in vegetative growth and mushroom formation of the wood-rot fungus *Schizophyllum commune*. *Environmental microbiology*. 12:833-844.

- Vargas, M.M., J.M. Aronson, and R.W. Roberson. 1993. The cytoplasmic organization of hyphal tip cells in the fungus *Allomyces macrogynus*. *Protoplasma*. 176:43-52.
- Virag, A., and S.D. Harris. 2006. The Spitzenkorper: a molecular perspective. *Mycological research*. 110:4-13.
- Virag, A., M.P. Lee, H. Si, and S.D. Harris. 2007. Regulation of hyphal morphogenesis by *cdc42* and *rac1* homologues in *Aspergillus nidulans*. *Molecular microbiology*. 66:1579-1596.
- Wang, D.Y., S. Kumar, and S.B. Hedges. 1999. Divergence time estimates for the early history of animal phyla and the origin of plants, animals and fungi. *Proceedings. Biological sciences*. 266:163-171.
- Wang, L., S. Wang, and W. Li. 2012. RSeQC: quality control of RNA-seq experiments. *Bioinformatics*. 28:2184-2185.
- Wang, N., L. Lo Presti, Y.H. Zhu, M. Kang, Z. Wu, S.G. Martin, and J.Q. Wu. 2014. The novel proteins Rng8 and Rng9 regulate the myosin-V Myo51 during fission yeast cytokinesis. *The Journal of cell biology*. 205:357-375.
- Weber, I., C. Gruber, and G. Steinberg. 2003. A class-V myosin required for mating, hyphal growth, and pathogenicity in the dimorphic plant pathogen *Ustilago maydis*. *The Plant cell*. 15:2826-2842.
- Weber, R.W.S. 2002. Vacuoles and the fungal lifestyle. *Mycologist*. 16:10-20.
- Webster, M., K.L. Witkin, and O. Cohen-Fix. 2009. Sizing up the nucleus: nuclear shape, size and nuclear-envelope assembly. *Journal of cell science*. 122:1477-1486.
- Wickerham, L.J., and E. Duprat. 1945. A remarkable fission yeast, *Schizosaccharomyces versatilis* nov. sp. *Journal of bacteriology*. 50:597-607.
- Win, T.Z., Y. Gachet, D.P. Mulvihill, K.M. May, and J.S. Hyams. 2001. Two type V myosins with non-overlapping functions in the fission yeast *Schizosaccharomyces pombe*: Myo52 is concerned with growth polarity and cytokinesis, Myo51 is a component of the cytokinetic actin ring. *Journal of cell science*. 114:69-79.
- Wood, E., and P. Nurse. 2015. Sizing up to divide: mitotic cell-size control in fission yeast. *Annual review of cell and developmental biology*. 31:11-29.
- Woolner, S., and W.M. Bement. 2009. Unconventional myosins acting unconventionally. *Trends in cell biology*. 19:245-252.
- Wu, Y., Y.H. Li, S.B. Yu, W.G. Li, X.S. Liu, L. Zhao, and J.X. Lu. 2016. A Genome-Wide Transcriptional Analysis of Yeast-Hyphal Transition in *Candida tropicalis* by RNA-Seq. *PLoS one*. 11:e0166645.
- Xiang, X., S.M. Beckwith, and N.R. Morris. 1994. Cytoplasmic dynein is involved in nuclear migration in *Aspergillus nidulans*. *Proceedings of the National Academy of Sciences of the United States of America*. 91:2100-2104.
- Xiang, X., and R. Fischer. 2004. Nuclear migration and positioning in filamentous fungi. *Fungal genetics and biology : FG & B*. 41:411-419.
- Yam, C., Y. He, D. Zhang, K.H. Chiam, and S. Oliferenko. 2011. Divergent strategies for controlling the nuclear membrane satisfy geometric constraints during nuclear division. *Current biology : CB*. 21:1314-1319.
- Yokoyama, K., H. Kaji, K. Nishimura, and M. Miyaji. 1990. The role of microfilaments and microtubules in apical growth and dimorphism of *Candida albicans*. *Journal of general microbiology*. 136:1067-1075.
- Yukawa, M., and T. Maki. 1931. Regarding the new fission yeast *Schizosaccharomyces japonicus*. *Kyushu Daigaku Kiyou [in Japanese]*:218-226.

Annexes

Annexe 1: Quality control of the RNA sent for sequencing (32 pages)

Annexe 2: Quality control of the RNA sequencing data (11 pages)

Annexe 3: Early timepoint analysis (3 pages)

Annexe 4: Late timepoint analysis (24 pages)

Fragment Analyzer Run Summary:

Filename and Data Path: \\nas.unil.ch\cig\GROUPS\GTF\common\Fragment_Analyzer\hr\2016 05

Filename and Data Path: 31\09-24-40\2016 05 31 09H 24M.raw

Created: 31 May, 2016 9:47:23

of Capillaries: 12

Array Serial #: 011713-05SFS

Effect Length: 33 cm

Array Usage Count: 1135

FA Version #: 1.1.0.11

Device Serial #: 2710

METHOD INFORMATION

Method Name: DNF-472T33 - HS Total RNA 15nt.mthds

Gel Prime: No

Full Conditioning: Yes

Gel Prime to Buffer: Yes

Gel Selection: Gel 1

Perform Prerun: 8.0 kV, 30 sec.

Rinse: No

Marker 1: No

Rinse: Tray: 3, Row: A, # Dips: 2

Sample Injection: 7.0 kV, 150 sec.

Separation: 8.0 kV, 40.0 min.

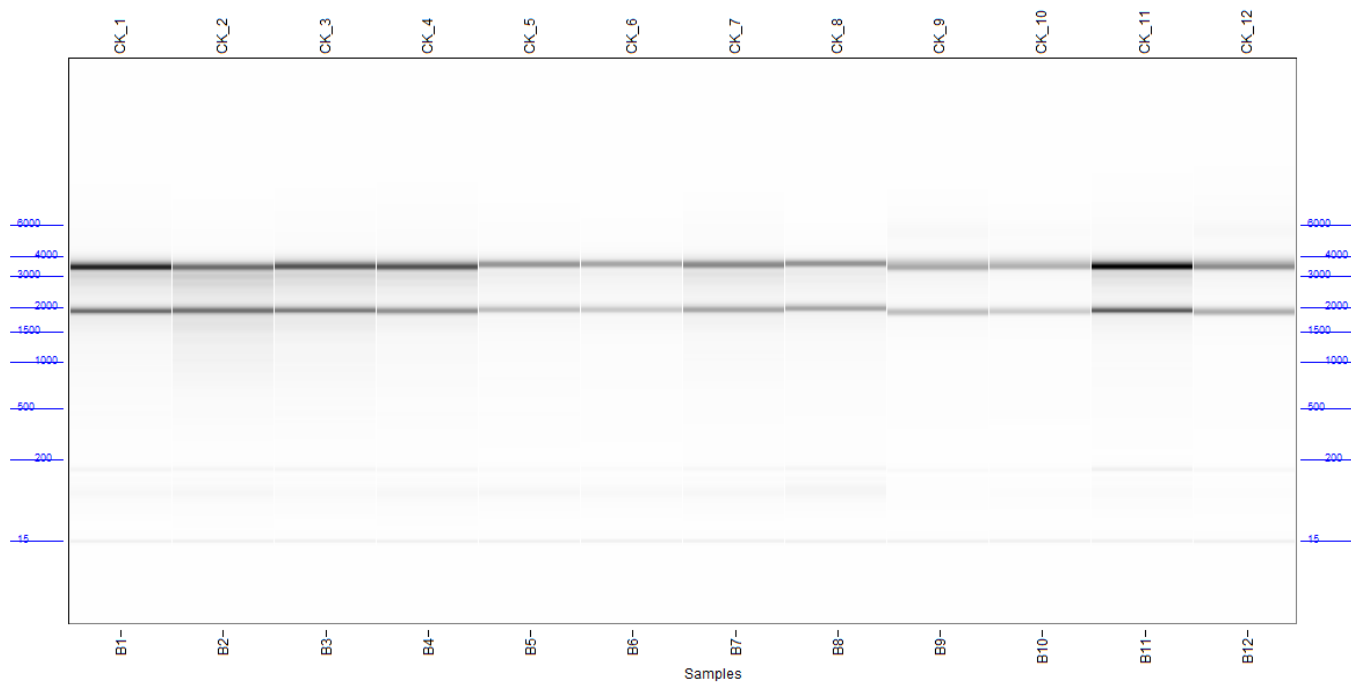
Tray Name: Tray-1

Analysis Mode: RNA (Eukaryotic)

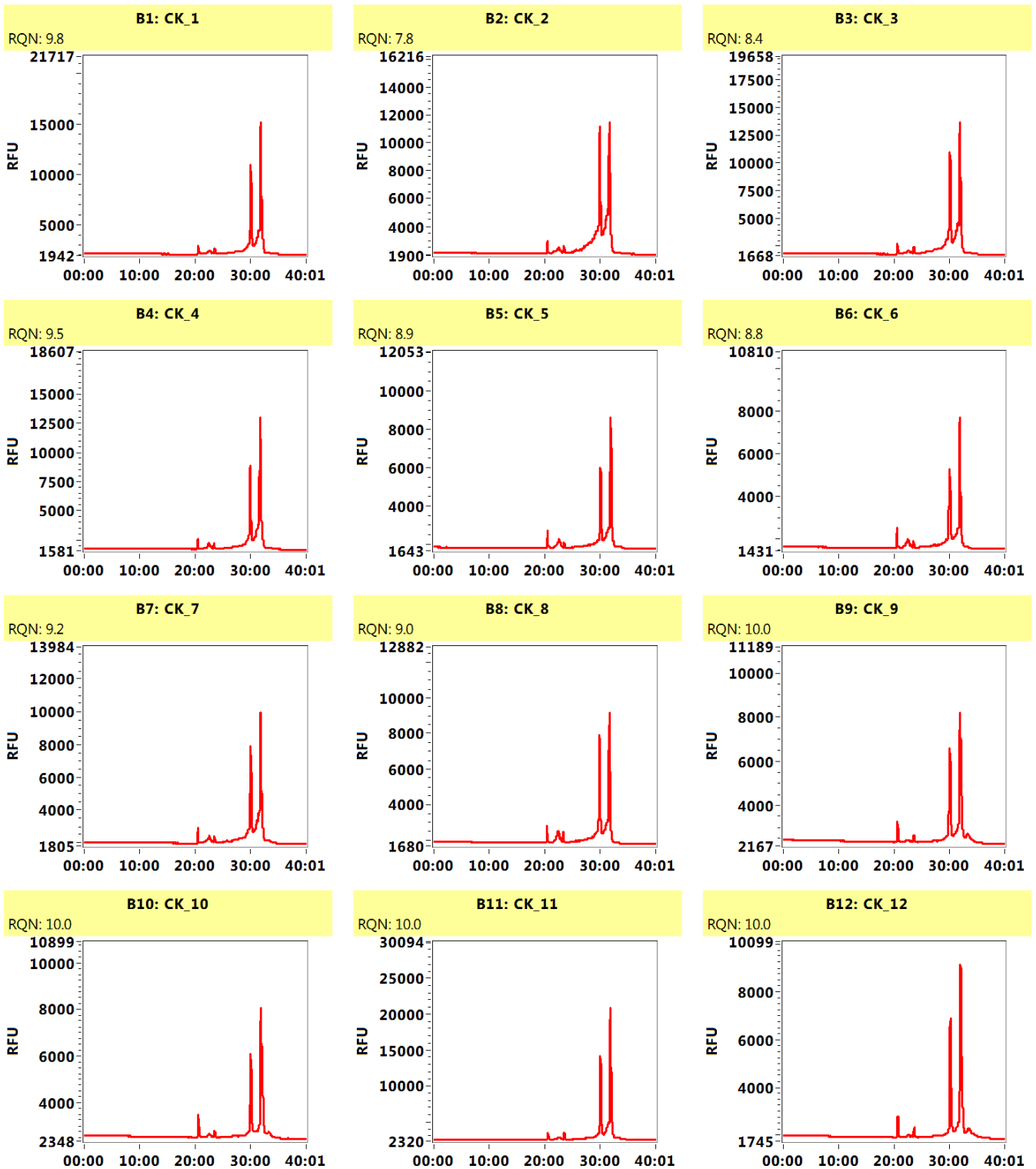
NOTE

Kinnaer

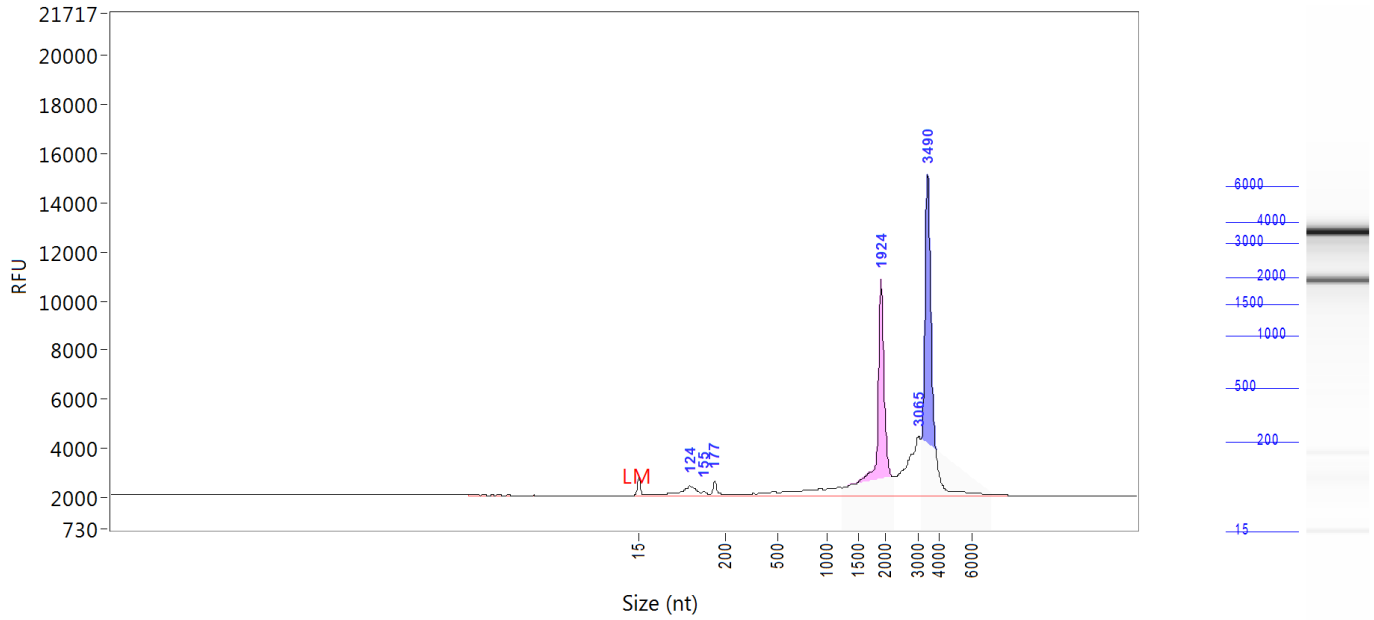
Gel Image



Filename and Data Path: \\nas.unil.ch\cig\GROUPS\GTF\common\Fragment_Analyzer\hr\2016 05 31\09-24-40\2016 05 31 09H 24M.raw



Sample: CK_1
Well Location: B1
Created: 31 May, 2016 9:47:23

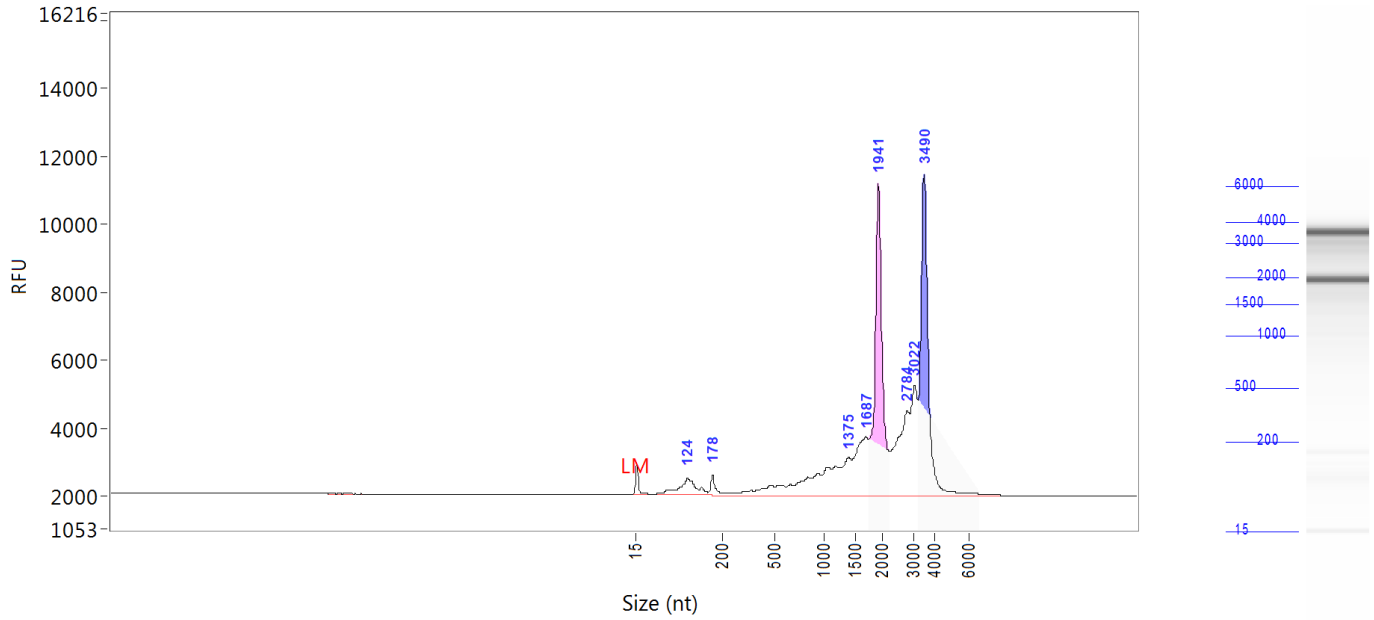


Peak	Size (nt)	Conc. (ng/uL)
1	15 (LM)	0.0224
2	124	0.4844
3	155	0.0725
4	177	0.2145
5	1924	4.2603
6	3065	1.9781
7	3490	5.2869

TIC: 12.2967 ng/uL
 TIM: 31.001 nmole/L
 Total Conc.: 13.3813 ng/uL
 28S/18S: 1.1
 RQN 9.8

Sample Peak Width (sec): 6 Sample Min Peak Height: 150 Sample Baseline V to V?: Y Sample Baseline V to V pts: 3
 Sample Filter: Binomial # of Pts for Filter: 9 Sample Start Region (min): 0 Sample End Region (min): 40
 Manual Baseline Start (min): 18 Manual Baseline End (min): 38
 Marker Peak Width (sec): 6 Marker Min Peak Height: 100 Marker Baseline V to V?: Y Marker Baseline V to V pts: 3
 Lower Marker Selection: First Peak > 100 RFU Upper Marker Selection: Last Peak > 100 RFU
 Ladder Size (bp): 15, 200, 500, 1000, 1500, 2000, 3000, 4000, 6000
 Quantification Using: Ladder Final Concentration (ng/uL): 0.2000 Dilution Factor: 10.0

Sample: CK_2
Well Location: B2
Created: 31 May, 2016 9:47:23

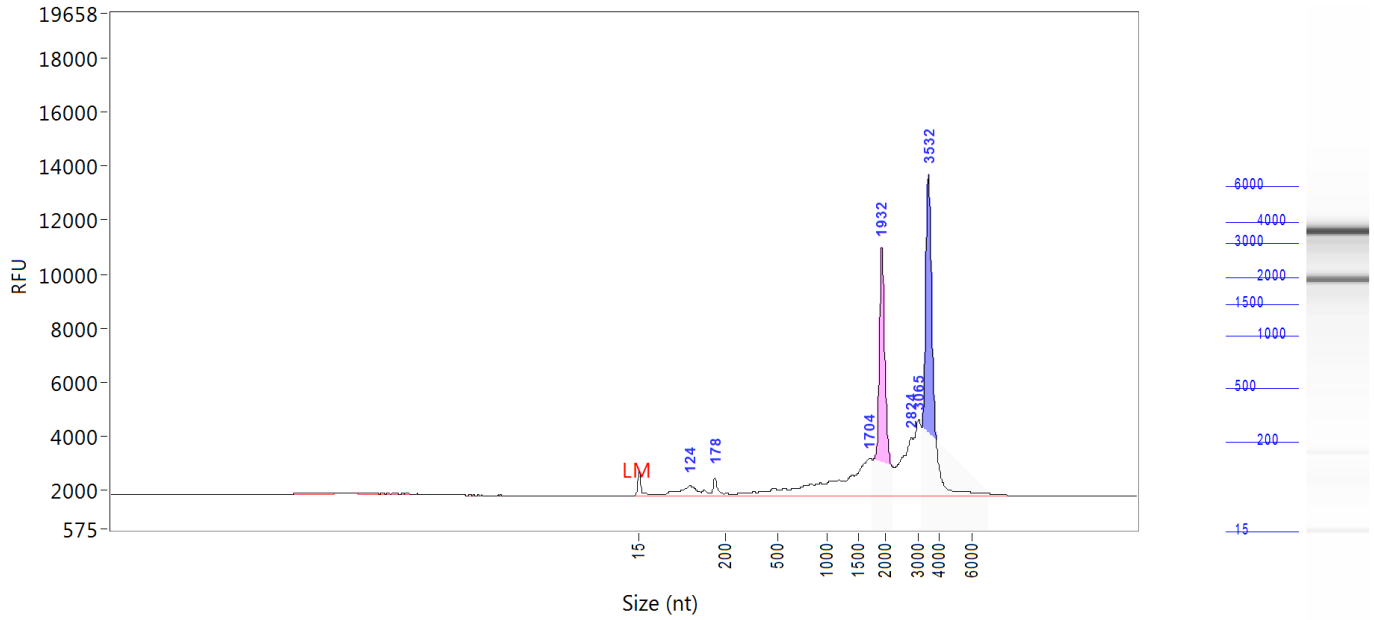


Peak	Size (nt)	Conc. (ng/uL)
1	15 (LM)	0.0224
2	124	0.5708
3	178	0.1846
4	1375	0.5760
5	1687	1.2051
6	1941	3.5632
7	2784	1.7069
8	3022	1.1377
9	3490	3.5330

TIC: 12.4773 ng/uL
 TIM: 33.021 nmole/L
 Total Conc.: 14.4960 ng/uL
 28S/18S: 0.8
 RQN 7.8

Sample Peak Width (sec): 6 Sample Min Peak Height: 180 Sample Baseline V to V?: Y Sample Baseline V to V pts: 3
 Sample Filter: Binomial # of Pts for Filter: 9 Sample Start Region (min): 0 Sample End Region (min): 40
 Manual Baseline Start (min): 18 Manual Baseline End (min): 38
 Marker Peak Width (sec): 6 Marker Min Peak Height: 100 Marker Baseline V to V?: Y Marker Baseline V to V pts: 3
 Lower Marker Selection: First Peak > 100 RFU Upper Marker Selection: Last Peak > 100 RFU
 Ladder Size (bp): 15, 200, 500, 1000, 1500, 2000, 3000, 4000, 6000
 Quantification Using: Ladder Final Concentration (ng/uL): 0.2000 Dilution Factor: 10.0

Sample: CK_3
Well Location: B3
Created: 31 May, 2016 9:47:23

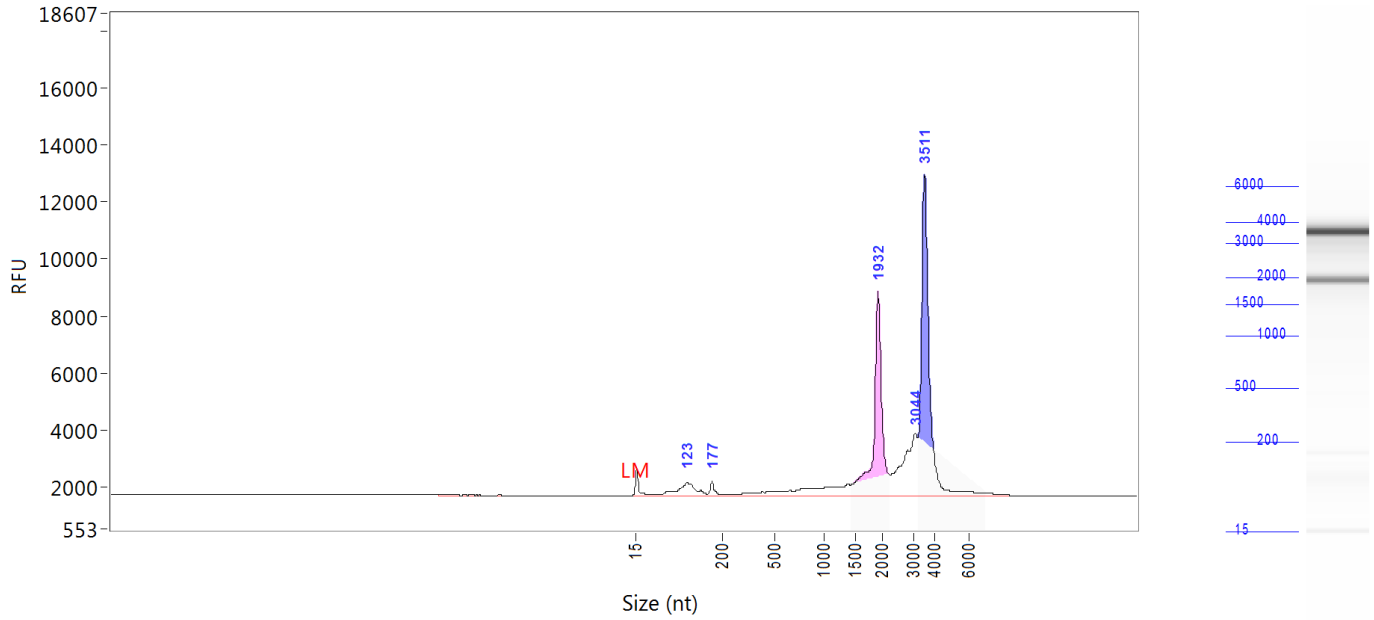


Peak	Size (nt)	Conc. (ng/uL)
1	15 (LM)	0.0224
2	124	0.4084
3	178	0.2247
4	1704	0.8750
5	1932	3.0486
6	2824	1.2649
7	3065	0.8603
8	3532	4.2157

TIC: 10.8976 ng/uL
 TIM: 26.672 nmole/L
 Total Conc.: 12.6998 ng/uL
 28S/18S: 1.2
 RQN 8.4

Sample Peak Width (sec): 6 Sample Min Peak Height: 180 Sample Baseline V to V?: Y Sample Baseline V to V pts: 3
 Sample Filter: Binomial # of Pts for Filter: 9 Sample Start Region (min): 0 Sample End Region (min): 40
 Manual Baseline Start (min): 18 Manual Baseline End (min): 38
 Marker Peak Width (sec): 6 Marker Min Peak Height: 100 Marker Baseline V to V?: Y Marker Baseline V to V pts: 3
 Lower Marker Selection: First Peak > 100 RFU Upper Marker Selection: Last Peak > 100 RFU
 Ladder Size (bp): 15, 200, 500, 1000, 1500, 2000, 3000, 4000, 6000
 Quantification Using: Ladder Final Concentration (ng/uL): 0.2000 Dilution Factor: 10.0

Sample: CK_4
Well Location: B4
Created: 31 May, 2016 9:47:23

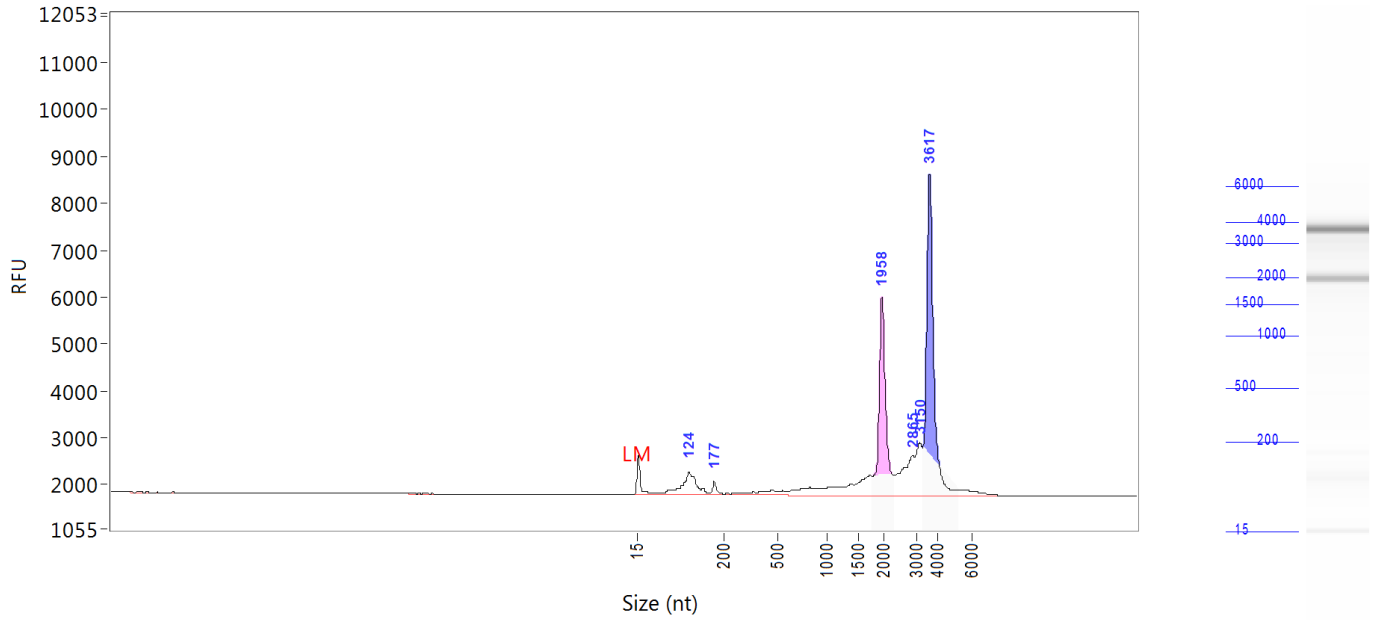


Peak	Size (nt)	Conc. (ng/uL)
1	15 (LM)	0.0224
2	123	0.6052
3	177	0.1666
4	1932	3.0824
5	3044	1.6626
6	3511	4.3674

TIC: 9.8842 ng/uL
 TIM: 28.750 nmole/L
 Total Conc.: 11.0846 ng/uL
 28S/18S: 1.3
 RQN 9.5

Sample Peak Width (sec): 6 Sample Min Peak Height: 150 Sample Baseline V to V?: Y Sample Baseline V to V pts: 3
 Sample Filter: Binomial # of Pts for Filter: 9 Sample Start Region (min): 0 Sample End Region (min): 40
 Manual Baseline Start (min): 18 Manual Baseline End (min): 38
 Marker Peak Width (sec): 6 Marker Min Peak Height: 100 Marker Baseline V to V?: Y Marker Baseline V to V pts: 3
 Lower Marker Selection: First Peak > 100 RFU Upper Marker Selection: Last Peak > 100 RFU
 Ladder Size (bp): 15, 200, 500, 1000, 1500, 2000, 3000, 4000, 6000
 Quantification Using: Ladder Final Concentration (ng/uL): 0.2000 Dilution Factor: 10.0

Sample: CK_5
Well Location: B5
Created: 31 May, 2016 9:47:23

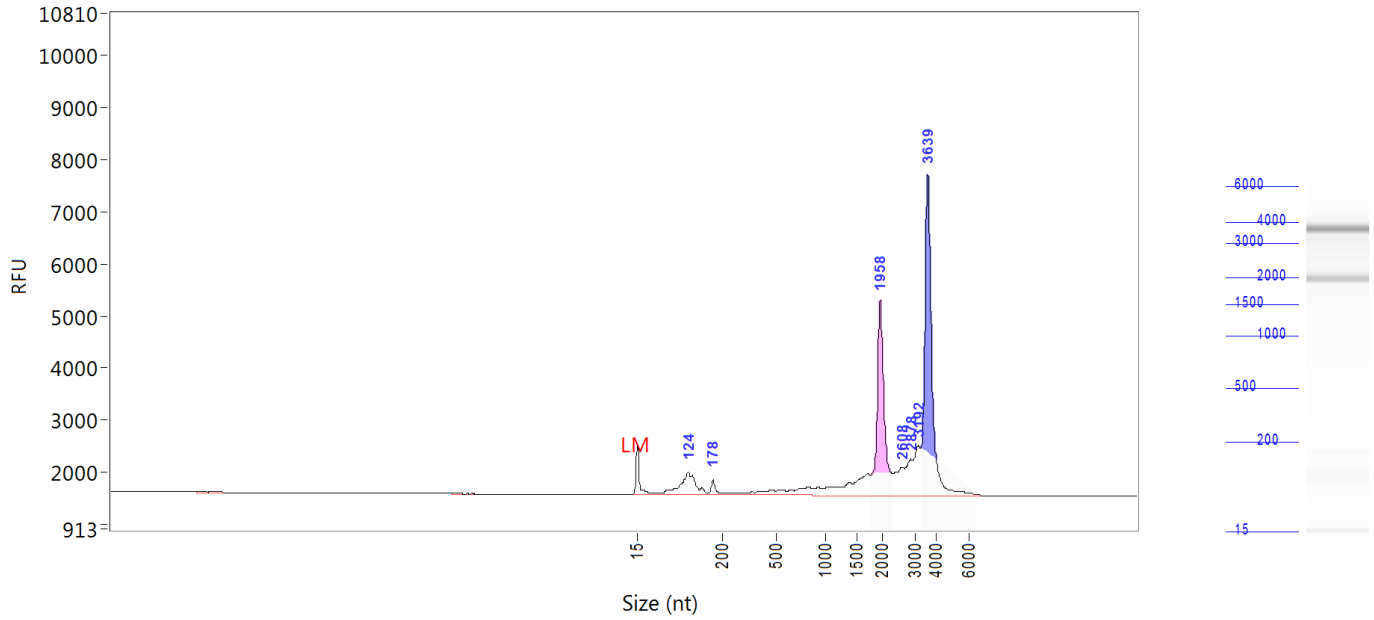


Peak	Size (nt)	Conc. (ng/uL)
1	15 (LM)	0.0224
2	124	0.5241
3	177	0.0831
4	1958	1.4968
5	2865	0.5711
6	3150	0.3728
7	3617	2.3534

TIC: 5.4013 ng/uL
 TIM: 19.985 nmole/L
 Total Conc.: 6.4777 ng/uL
 28S/18S: 1.5
 RQN 8.9

Sample Peak Width (sec): 6 Sample Min Peak Height: 150 Sample Baseline V to V?: Y Sample Baseline V to V pts: 3
 Sample Filter: Binomial # of Pts for Filter: 9 Sample Start Region (min): 0 Sample End Region (min): 40
 Manual Baseline Start (min): 18 Manual Baseline End (min): 38
 Marker Peak Width (sec): 6 Marker Min Peak Height: 100 Marker Baseline V to V?: Y Marker Baseline V to V pts: 3
 Lower Marker Selection: First Peak > 100 RFU Upper Marker Selection: Last Peak > 100 RFU
 Ladder Size (bp): 15, 200, 500, 1000, 1500, 2000, 3000, 4000, 6000
 Quantification Using: Ladder Final Concentration (ng/uL): 0.2000 Dilution Factor: 10.0

Sample: CK_6
Well Location: B6
Created: 31 May, 2016 9:47:23

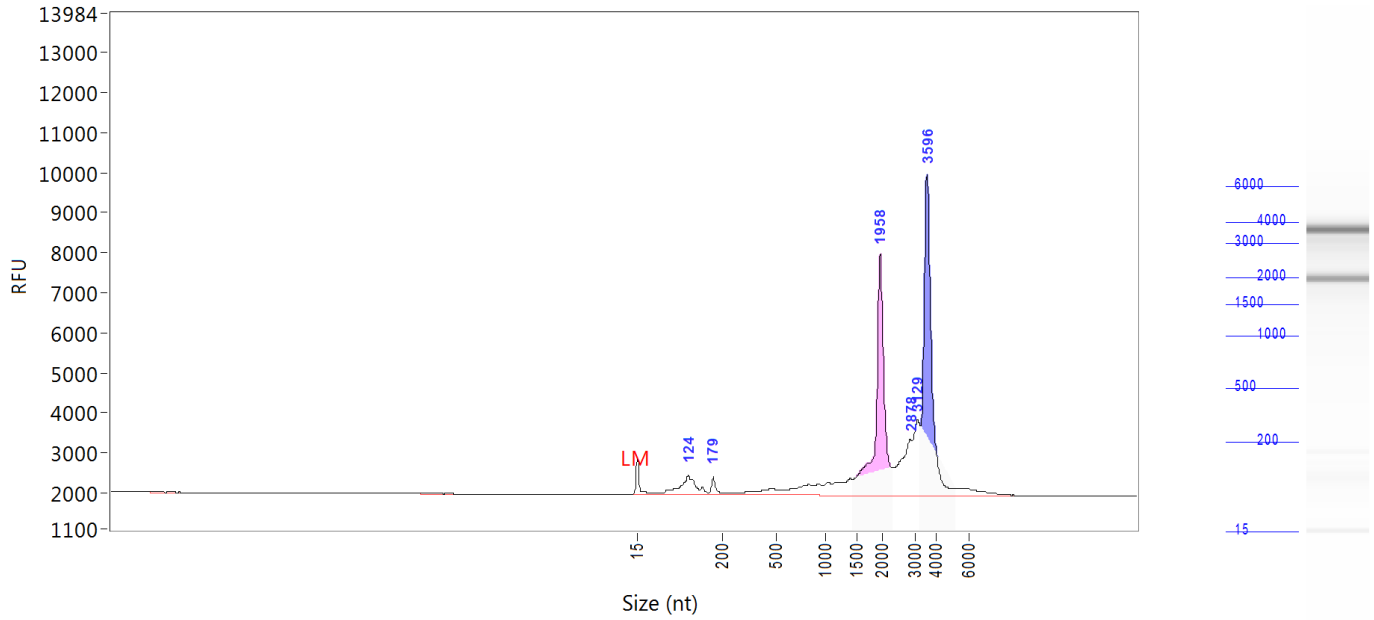


Peak	Size (nt)	Conc. (ng/uL)
1	15 (LM)	0.0224
2	124	0.4535
3	178	0.0800
4	1958	1.2725
5	2608	0.2522
6	2878	0.2151
7	3192	0.2893
8	3639	1.9884

TIC: 4.5510 ng/uL
 TIM: 17.299 nmole/L
 Total Conc.: 5.3759 ng/uL
 28S/18S: 1.5
 RQN 8.8

Sample Peak Width (sec): 6 Sample Min Peak Height: 150 Sample Baseline V to V?: Y Sample Baseline V to V pts: 3
 Sample Filter: Binomial # of Pts for Filter: 9 Sample Start Region (min): 0 Sample End Region (min): 40
 Manual Baseline Start (min): 18 Manual Baseline End (min): 38
 Marker Peak Width (sec): 6 Marker Min Peak Height: 100 Marker Baseline V to V?: Y Marker Baseline V to V pts: 3
 Lower Marker Selection: First Peak > 100 RFU Upper Marker Selection: Last Peak > 100 RFU
 Ladder Size (bp): 15, 200, 500, 1000, 1500, 2000, 3000, 4000, 6000
 Quantification Using: Ladder Final Concentration (ng/uL): 0.2000 Dilution Factor: 10.0

Sample: CK_7
Well Location: B7
Created: 31 May, 2016 9:47:23

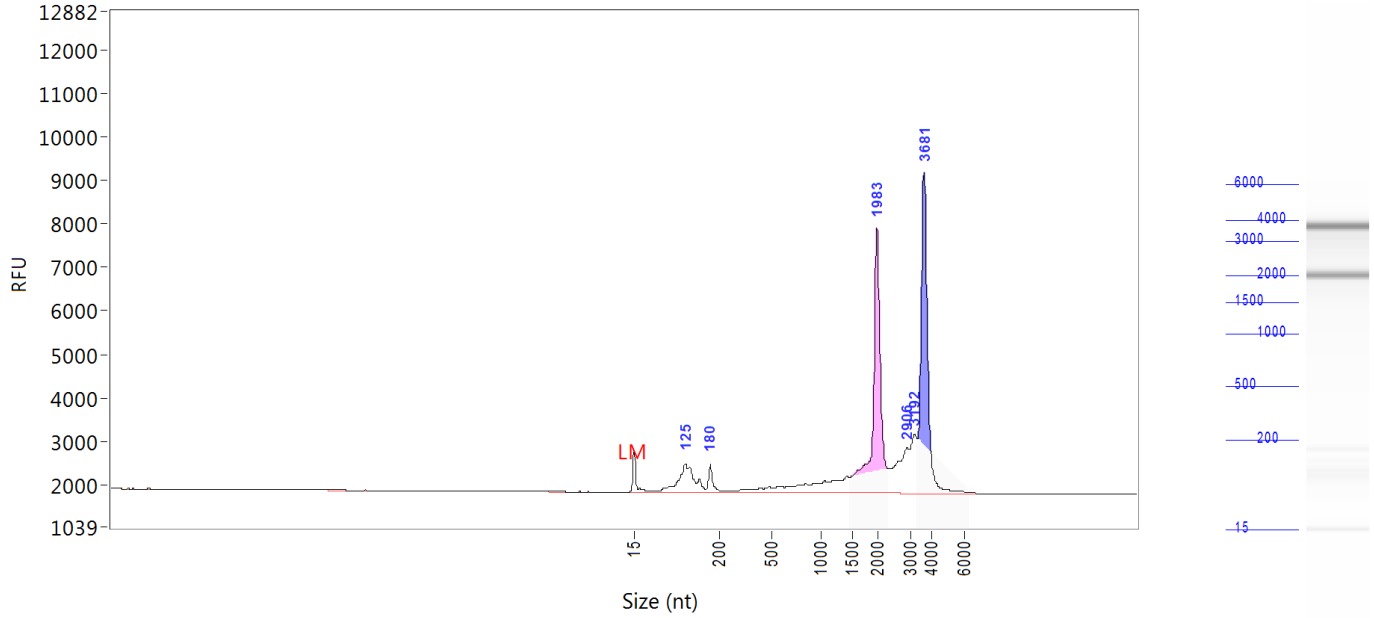


Peak	Size (nt)	Conc. (ng/uL)
1	15 (LM)	0.0224
2	124	0.5541
3	179	0.1256
4	1958	2.6820
5	2878	0.8610
6	3129	0.6041
7	3596	2.9650

TIC: 7.7918 ng/uL
 TIM: 24.436 nmole/L
 Total Conc.: 9.0970 ng/uL
 28S/18S: 1.0
 RQN 9.2

Sample Peak Width (sec): 6 Sample Min Peak Height: 150 Sample Baseline V to V?: Y Sample Baseline V to V pts: 3
 Sample Filter: Binomial # of Pts for Filter: 9 Sample Start Region (min): 0 Sample End Region (min): 40
 Manual Baseline Start (min): 18 Manual Baseline End (min): 38
 Marker Peak Width (sec): 6 Marker Min Peak Height: 100 Marker Baseline V to V?: Y Marker Baseline V to V pts: 3
 Lower Marker Selection: First Peak > 100 RFU Upper Marker Selection: Last Peak > 100 RFU
 Ladder Size (bp): 15, 200, 500, 1000, 1500, 2000, 3000, 4000, 6000
 Quantification Using: Ladder Final Concentration (ng/uL): 0.2000 Dilution Factor: 10.0

Sample: CK_8
Well Location: B8
Created: 31 May, 2016 9:47:23

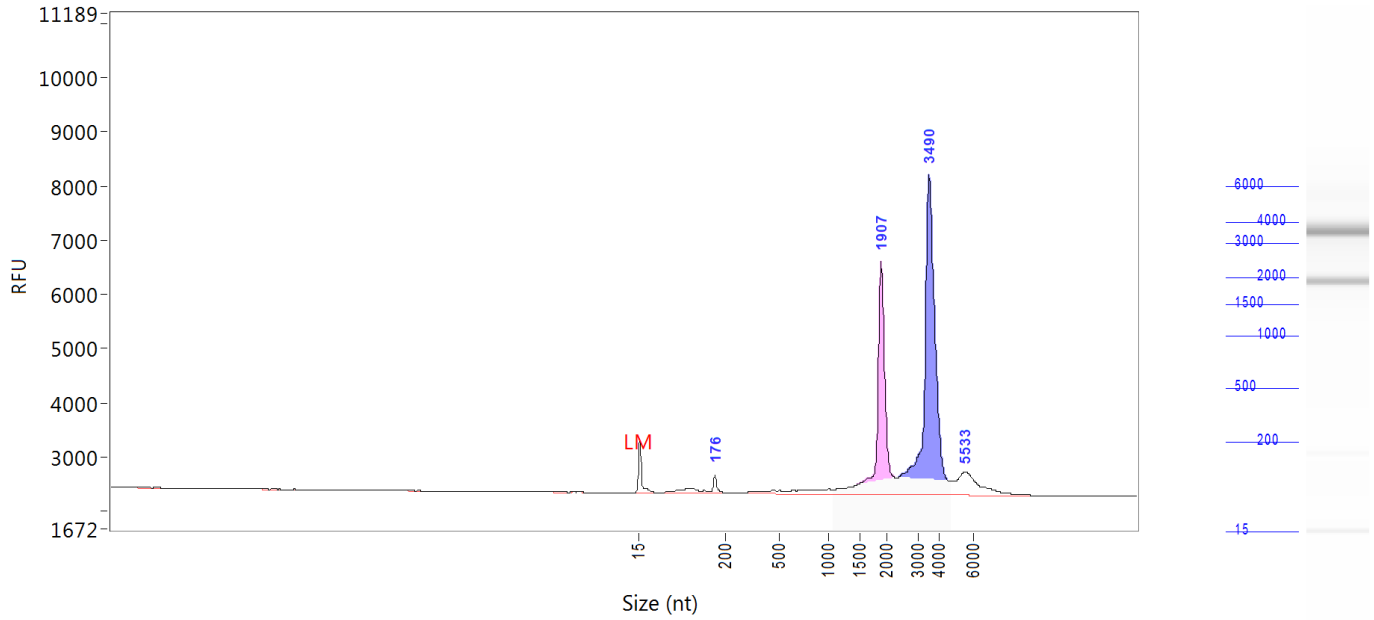


Peak	Size (nt)	Conc. (ng/uL)
1	15 (LM)	0.0224
2	125	0.7141
3	180	0.1783
4	1983	2.3360
5	2906	0.6533
6	3192	0.4186
7	3681	2.2309

TIC: 6.5312 ng/uL
 TIM: 27.503 nmole/L
 Total Conc.: 7.4057 ng/uL
 28S/18S: 0.9
 RQN 9.0

Sample Peak Width (sec): 6 Sample Min Peak Height: 150 Sample Baseline V to V?: Y Sample Baseline V to V pts: 3
 Sample Filter: Binomial # of Pts for Filter: 9 Sample Start Region (min): 0 Sample End Region (min): 40
 Manual Baseline Start (min): 18 Manual Baseline End (min): 38
 Marker Peak Width (sec): 6 Marker Min Peak Height: 100 Marker Baseline V to V?: Y Marker Baseline V to V pts: 3
 Lower Marker Selection: First Peak > 100 RFU Upper Marker Selection: Last Peak > 100 RFU
 Ladder Size (bp): 15, 200, 500, 1000, 1500, 2000, 3000, 4000, 6000
 Quantification Using: Ladder Final Concentration (ng/uL): 0.2000 Dilution Factor: 10.0

Sample: CK_9
Well Location: B9
Created: 31 May, 2016 9:47:23



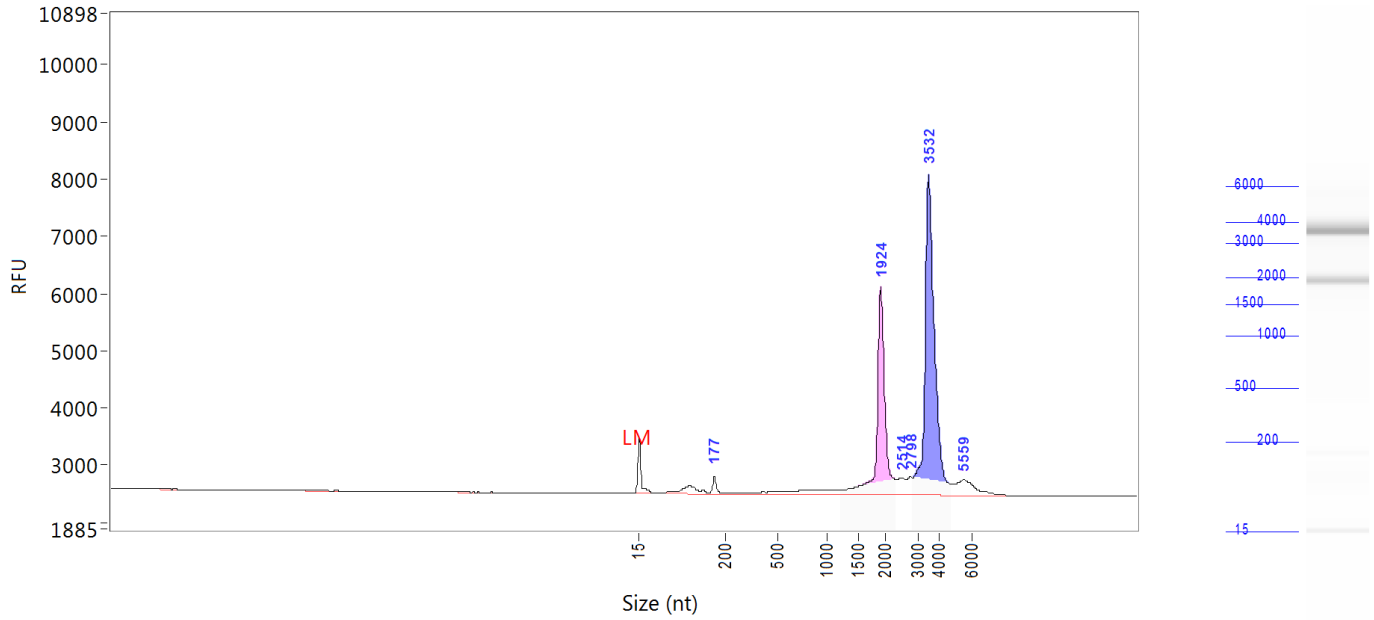
Peak	Size (nt)	Conc. (ng/uL)
1	15 (LM)	0.0224
2	176	0.3590
3	1907	7.2146
4	3490	12.5345
5	5533	1.8784

TIC: 21.9866 ng/uL
 TIM: 30.413 nmole/L
 Total Conc.: 23.5656 ng/uL

 28S/18S: 2.0
 RQN 10.0

Sample Peak Width (sec): 6 Sample Min Peak Height: 150 Sample Baseline V to V?: Y Sample Baseline V to V pts: 3
 Sample Filter: Binomial # of Pts for Filter: 9 Sample Start Region (min): 0 Sample End Region (min): 40
 Manual Baseline Start (min): 18 Manual Baseline End (min): 38
 Marker Peak Width (sec): 6 Marker Min Peak Height: 100 Marker Baseline V to V?: Y Marker Baseline V to V pts: 3
 Lower Marker Selection: First Peak > 100 RFU Upper Marker Selection: Last Peak > 100 RFU
 Ladder Size (bp): 15, 200, 500, 1000, 1500, 2000, 3000, 4000, 6000
 Quantification Using: Ladder Final Concentration (ng/uL): 0.2000 Dilution Factor: 40.0

Sample: CK_10
Well Location: B10
Created: 31 May, 2016 9:47:23

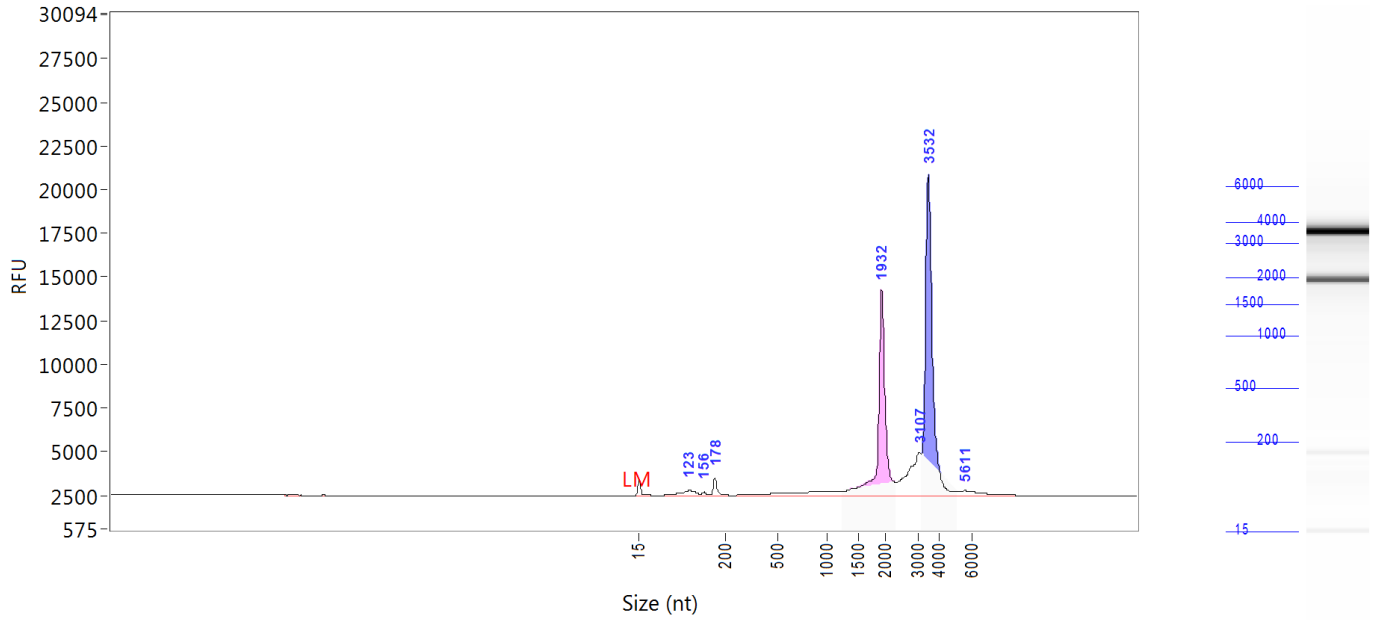


Peak	Size (nt)	Conc. (ng/uL)
1	15 (LM)	0.0224
2	177	0.2963
3	1924	5.5201
4	2514	0.4403
5	2798	0.3355
6	3532	9.2581
7	5559	0.9855

TIC: 16.8358 ng/uL
 TIM: 23.813 nmole/L
 Total Conc.: 18.4193 ng/uL
 28S/18S: 2.0
 RQN 10.0

Sample Peak Width (sec): 6 Sample Min Peak Height: 150 Sample Baseline V to V?: Y Sample Baseline V to V pts: 3
 Sample Filter: Binomial # of Pts for Filter: 9 Sample Start Region (min): 0 Sample End Region (min): 40
 Manual Baseline Start (min): 18 Manual Baseline End (min): 38
 Marker Peak Width (sec): 6 Marker Min Peak Height: 100 Marker Baseline V to V?: Y Marker Baseline V to V pts: 3
 Lower Marker Selection: First Peak > 100 RFU Upper Marker Selection: Last Peak > 100 RFU
 Ladder Size (bp): 15, 200, 500, 1000, 1500, 2000, 3000, 4000, 6000
 Quantification Using: Ladder Final Concentration (ng/uL): 0.2000 Dilution Factor: 40.0

Sample: CK_11
Well Location: B11
Created: 31 May, 2016 9:47:23

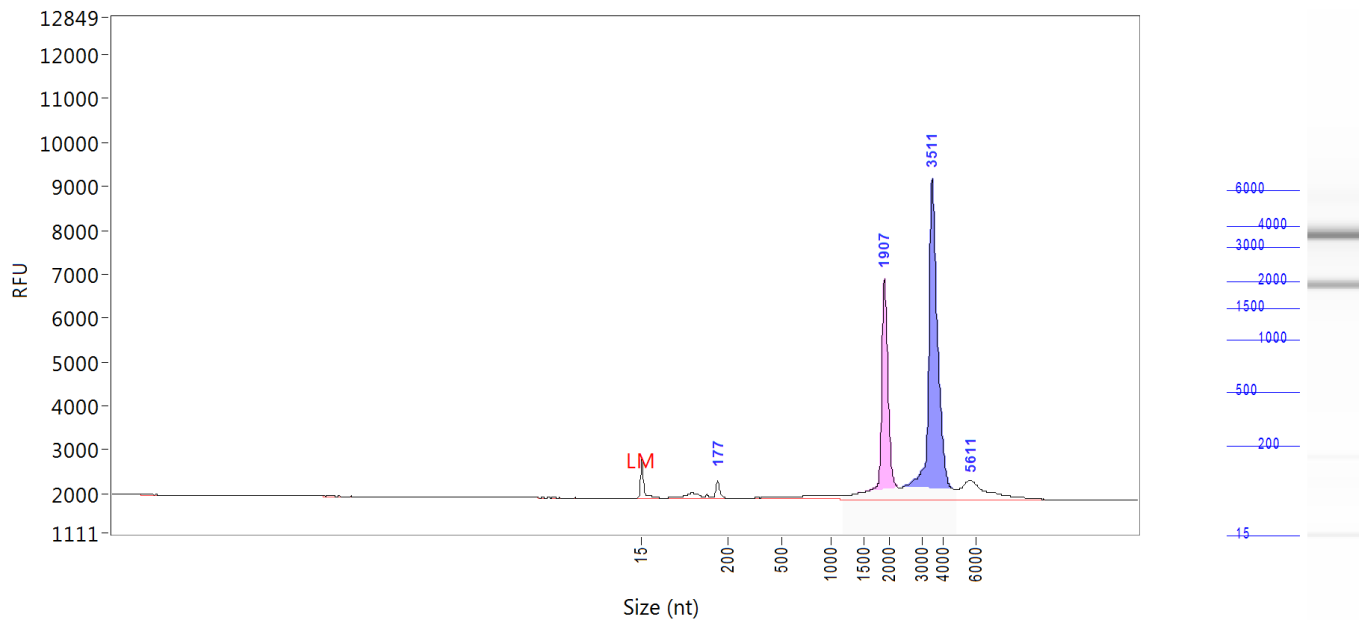


Peak	Size (nt)	Conc. (ng/uL)
1	15 (LM)	0.0224
2	123	0.3241
3	156	0.0618
4	178	0.2496
5	1932	3.9561
6	3107	1.4483
7	3532	5.5768
8	5611	0.3308

TIC: 11.9475 ng/uL
 TIM: 26.724 nmole/L
 Total Conc.: 12.6983 ng/uL
 28S/18S: 1.4
 RQN 10.0

Sample Peak Width (sec): 6 Sample Min Peak Height: 150 Sample Baseline V to V?: Y Sample Baseline V to V pts: 3
 Sample Filter: Binomial # of Pts for Filter: 9 Sample Start Region (min): 0 Sample End Region (min): 40
 Manual Baseline Start (min): 18 Manual Baseline End (min): 38
 Marker Peak Width (sec): 6 Marker Min Peak Height: 100 Marker Baseline V to V?: Y Marker Baseline V to V pts: 3
 Lower Marker Selection: First Peak > 100 RFU Upper Marker Selection: Last Peak > 100 RFU
 Ladder Size (bp): 15, 200, 500, 1000, 1500, 2000, 3000, 4000, 6000
 Quantification Using: Ladder Final Concentration (ng/uL): 0.2000 Dilution Factor: 10.0

Sample: CK_12
Well Location: B12
Created: 31 May, 2016 9:47:23



Peak	Size (nt)	Conc. (ng/uL)
1	15 (LM)	0.0224
2	177	0.4604
3	1907	7.9399
4	3511	14.3733
5	5611	2.1584

TIC: 24.9319 ng/uL
 TIM: 35.056 nmole/L
 Total Conc.: 26.9394 ng/uL

28S/18S: 1.9
 RQN 10.0

Sample Peak Width (sec): 6 Sample Min Peak Height: 150 Sample Baseline V to V?: Y Sample Baseline V to V pts: 3
 Sample Filter: Binomial # of Pts for Filter: 9 Sample Start Region (min): 0 Sample End Region (min): 40
 Manual Baseline Start (min): 18 Manual Baseline End (min): 38
 Marker Peak Width (sec): 6 Marker Min Peak Height: 100 Marker Baseline V to V?: Y Marker Baseline V to V pts: 3
 Lower Marker Selection: First Peak > 100 RFU Upper Marker Selection: Last Peak > 100 RFU
 Ladder Size (bp): 15, 200, 500, 1000, 1500, 2000, 3000, 4000, 6000
 Quantification Using: Ladder Final Concentration (ng/uL): 0.2000 Dilution Factor: 40.0

Sample: DNA Size Ladder

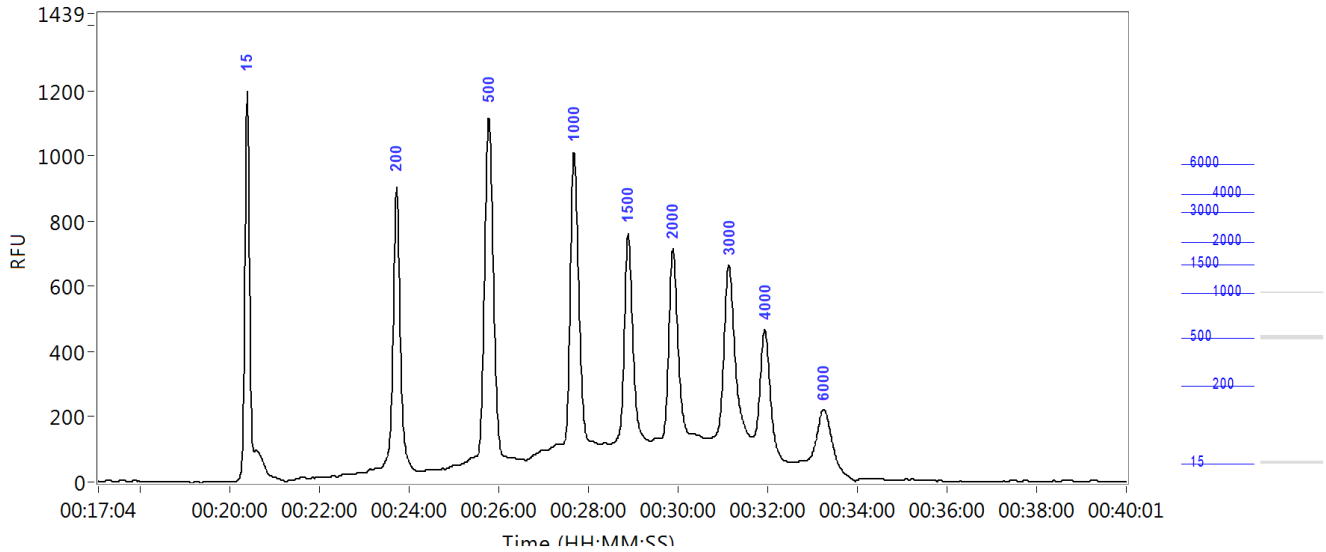
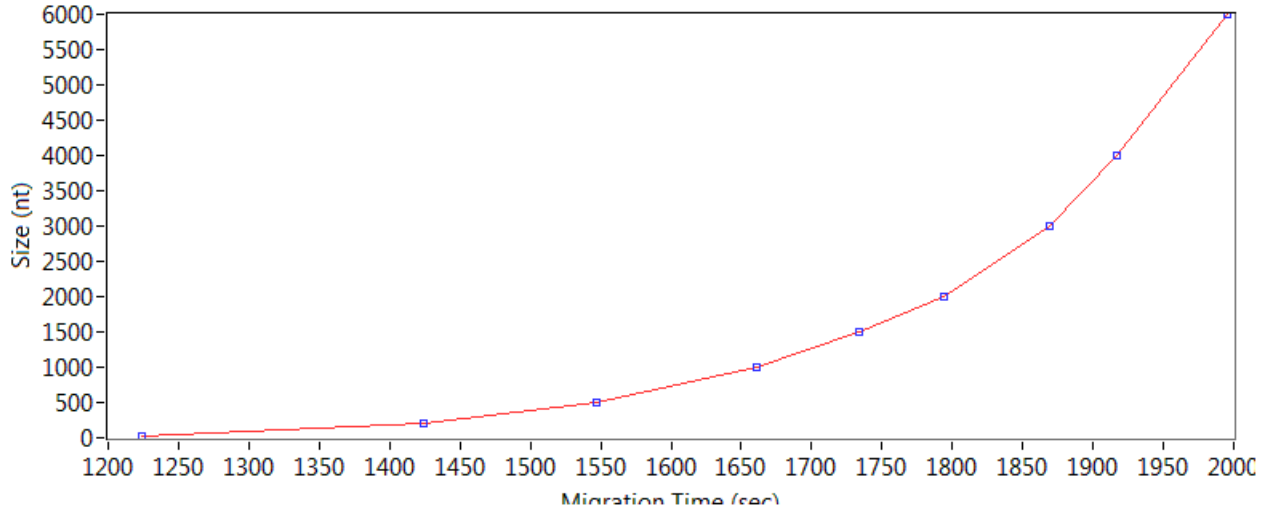
Well Location: A12

Created: 31 May, 2016 9:47:23

Import From: C:\PROSize 2.0\Ladders\ladder RNA HS 15NT 08.03.2016.SCAL

Fit Type: Point to Point

Calibration Curve



Fragment Analyzer Run Summary:

Filename and Data Path: \\nas.unil.ch\cig\GROUPS\GTF\common\Fragment_Analyzer\hr\2016 05

Filename and Data Path: 31\10-27-34\2016 05 31 10H 27M.raw

Created: 31 May, 2016 10:47:01

of Capillaries: 12

Array Serial #: 011713-05SFS

Effect Length: 33 cm

Array Usage Count: 1136

FA Version #: 1.1.0.11

Device Serial #: 2710

METHOD INFORMATION

Method Name: DNF-471-33 - SS Total RNA 15nt.mthds

Gel Prime: No

Full Conditioning: Yes

Gel Prime to Buffer: Yes

Gel Selection: Gel 1

Perform Prerun: 8.0 kV, 30 sec.

Rinse: No

Marker 1: No

Rinse: Tray: 3, Row: A, # Dips: 2

Sample Injection: 5.0 kV, 4 sec.

Separation: 8.0 kV, 40.0 min.

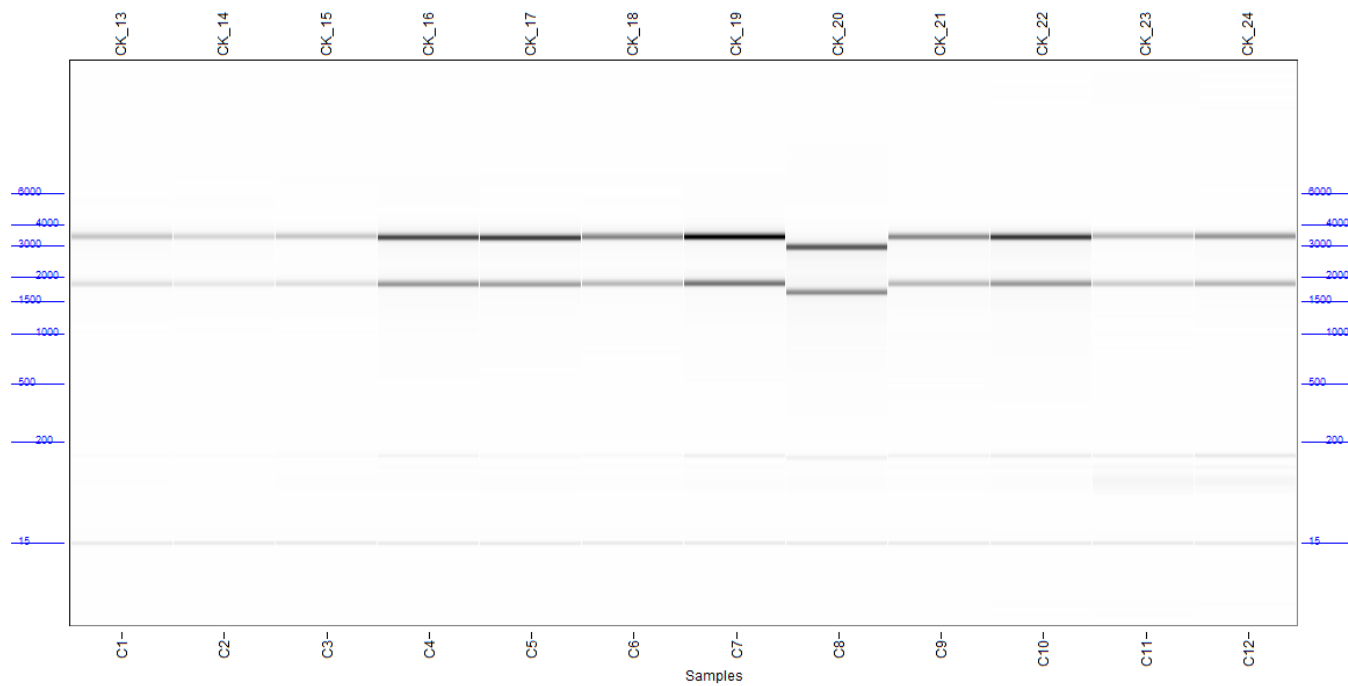
Tray Name: Tray-1

Analysis Mode: RNA (Eukaryotic)

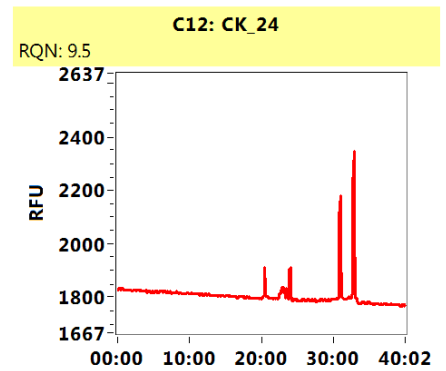
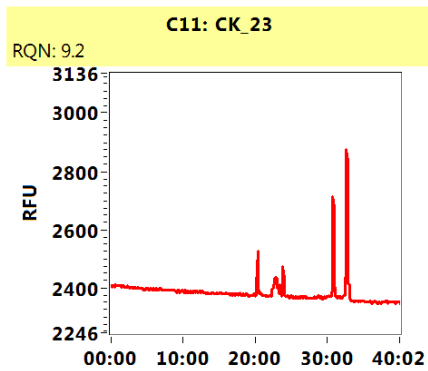
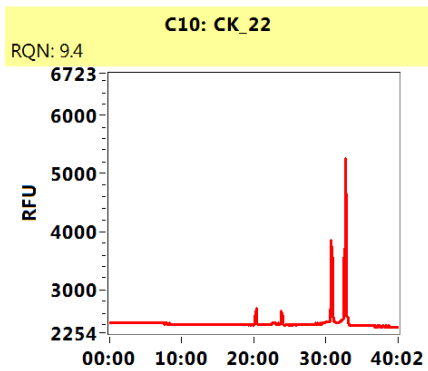
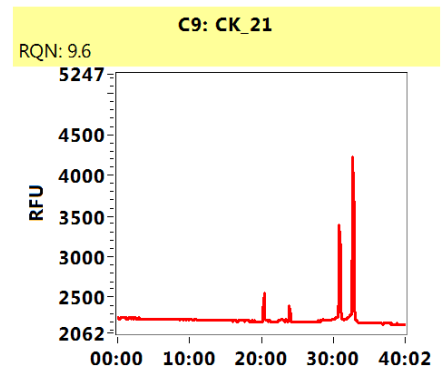
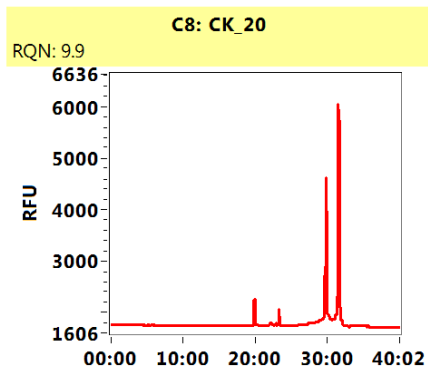
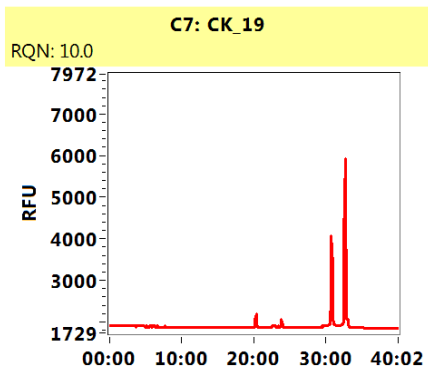
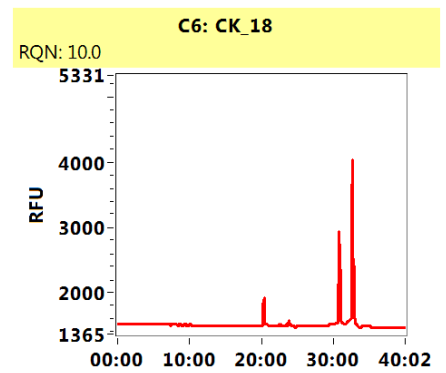
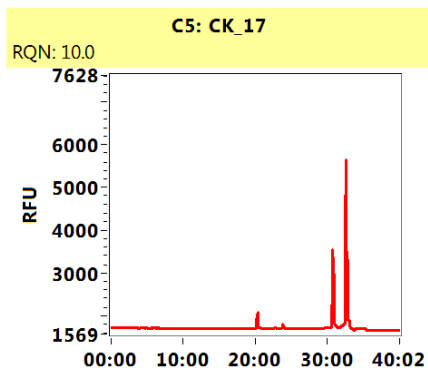
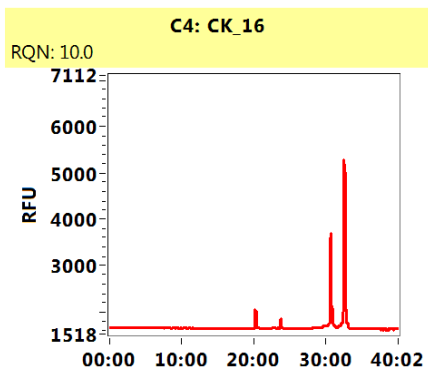
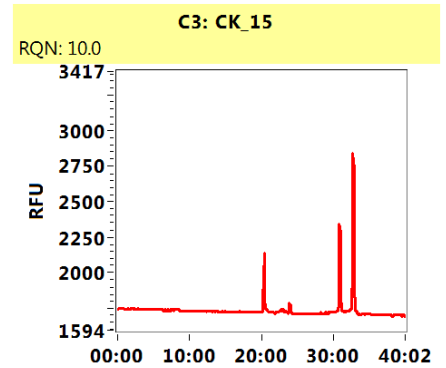
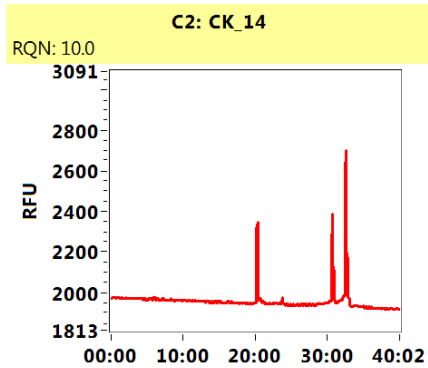
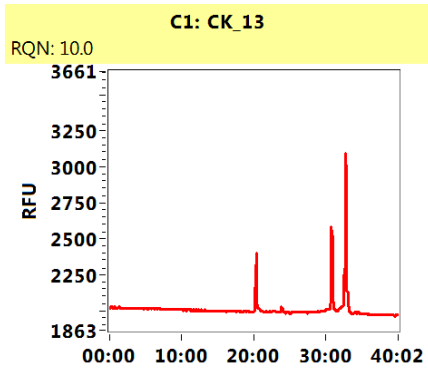
NOTE

Kinnaer

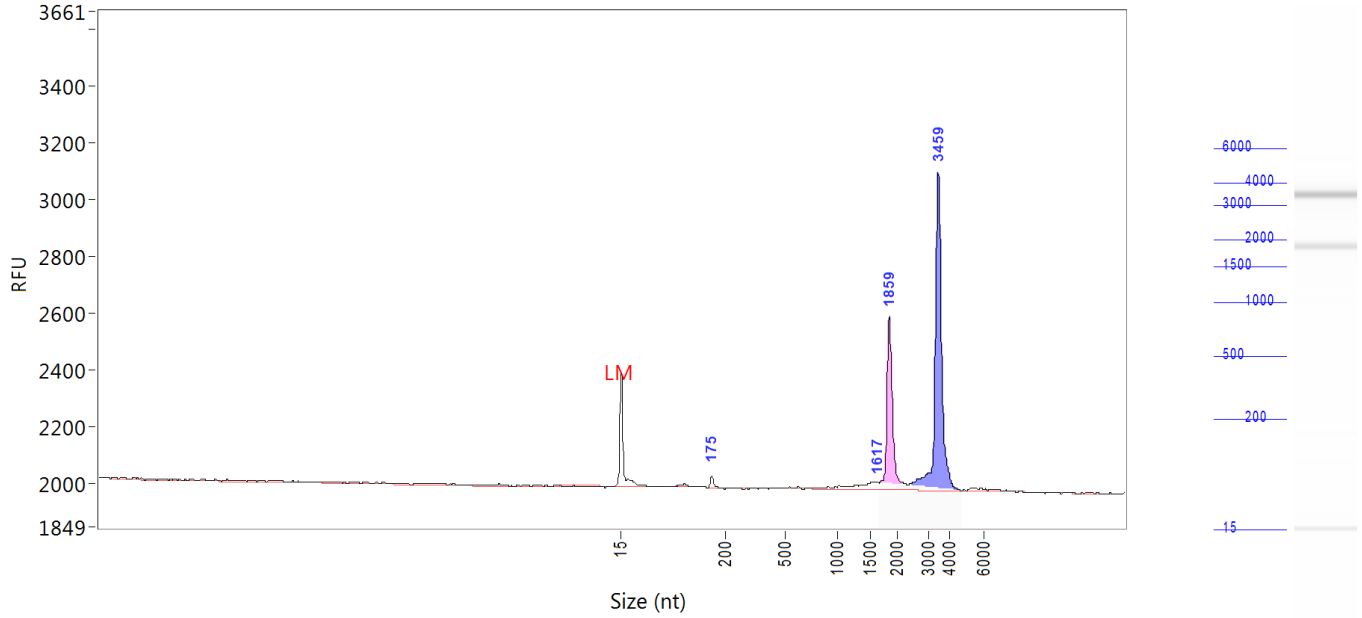
Gel Image



Filename and Data Path: \\nas.unil.ch\cig\GROUPS\GTF\common\Fragment_Analyzer\hr\2016 05 31\10-27-34\2016 05 31 10H 27M.raw



Sample: CK_13
Well Location: C1
Created: 31 May, 2016 10:47:01



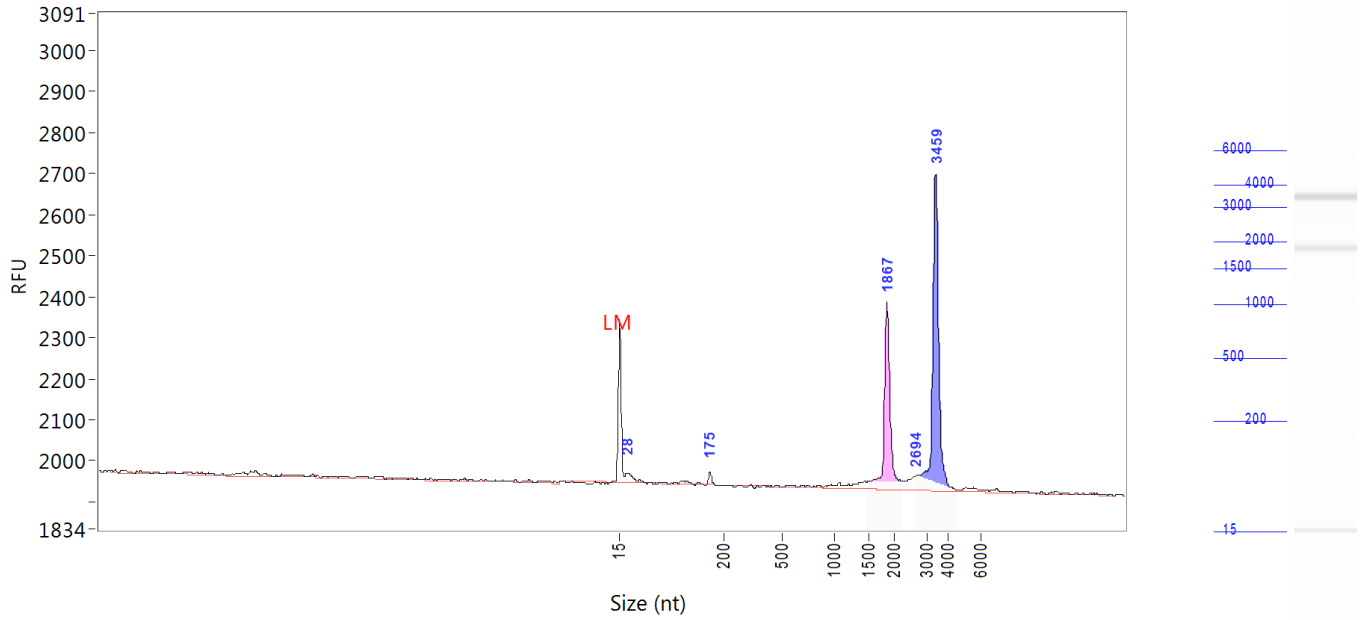
Peak	Size (nt)	Conc. (ng/uL)
1	15 (LM)	0.6462
2	175	0.5426
3	1617	1.3777
4	1859	13.4763
5	3459	26.6154

TIC: 42.0121 ng/uL
 TIM: 58.915 nmole/L
 Total Conc.: 43.9215 ng/uL

 28S/18S: 2.2
 RQN 10.0

Sample Peak Width (sec): 6 Sample Min Peak Height: 20 Sample Baseline V to V?: Y Sample Baseline V to V pts: 3
 Sample Filter: Binomial # of Pts for Filter: 9 Sample Start Region (min): 0 Sample End Region (min): 40
 Manual Baseline Start (min): 18 Manual Baseline End (min): 38
 Marker Peak Width (sec): 6 Marker Min Peak Height: 100 Marker Baseline V to V?: Y Marker Baseline V to V pts: 3
 Lower Marker Selection: First Peak > 100 RFU Upper Marker Selection: Last Peak > 100 RFU
 Ladder Size (bp): 15, 200, 500, 1000, 1500, 2000, 3000, 4000, 6000
 Quantification Using: Ladder Final Concentration (ng/uL): 8.0000 Dilution Factor: 12.0
 Min. RFU for Data Processing: 2

Sample: CK_14
Well Location: C2
Created: 31 May, 2016 10:47:01

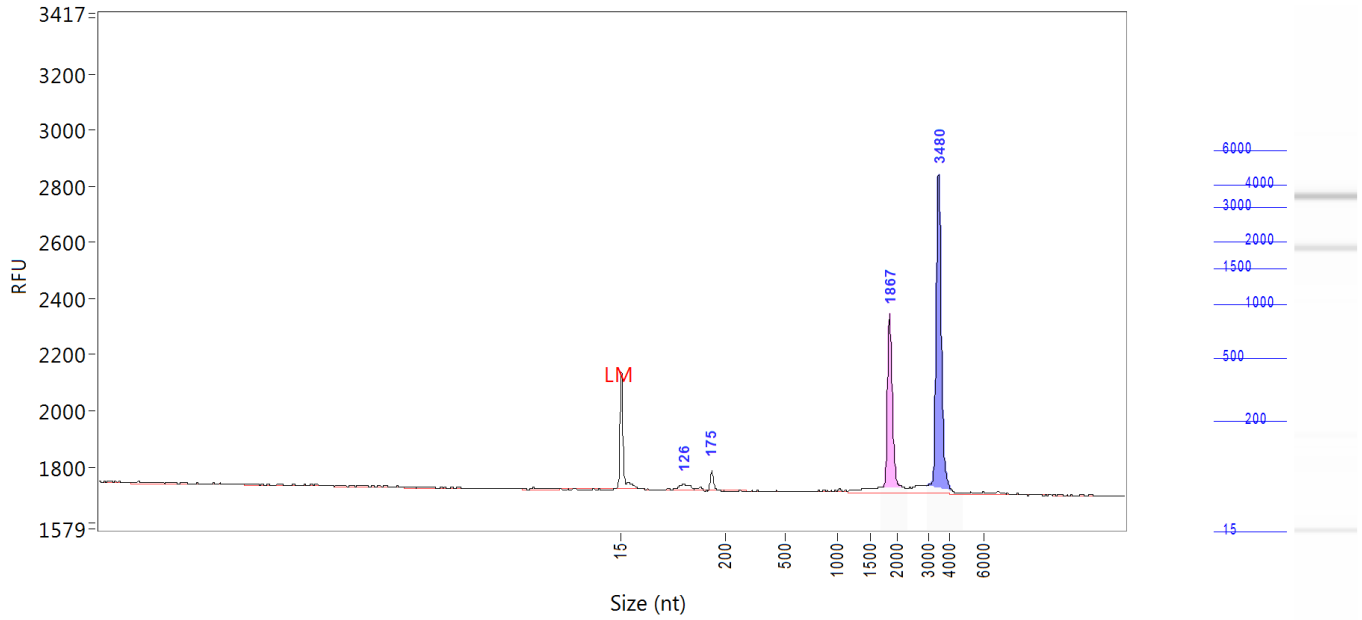


Peak	Size (nt)	Conc. (ng/uL)
1	15 (LM)	0.6462
2	28	1.0417
3	175	0.4833
4	1867	12.3405
5	2694	1.4363
6	3459	20.1268

TIC: 35.4286 ng/uL
 TIM: 163.015 nmole/L
 Total Conc.: 38.3109 ng/uL
 28S/18S: 1.7
 RQN 10.0

Sample Peak Width (sec): 6 Sample Min Peak Height: 20 Sample Baseline V to V?: Y Sample Baseline V to V pts: 3
 Sample Filter: Binomial # of Pts for Filter: 9 Sample Start Region (min): 0 Sample End Region (min): 40
 Manual Baseline Start (min): 18 Manual Baseline End (min): 38
 Marker Peak Width (sec): 6 Marker Min Peak Height: 100 Marker Baseline V to V?: Y Marker Baseline V to V pts: 3
 Lower Marker Selection: First Peak > 100 RFU Upper Marker Selection: Last Peak > 100 RFU
 Ladder Size (bp): 15, 200, 500, 1000, 1500, 2000, 3000, 4000, 6000
 Quantification Using: Ladder Final Concentration (ng/uL): 8.0000 Dilution Factor: 12.0
 Min. RFU for Data Processing: 2

Sample: CK_15
Well Location: C3
Created: 31 May, 2016 10:47:01



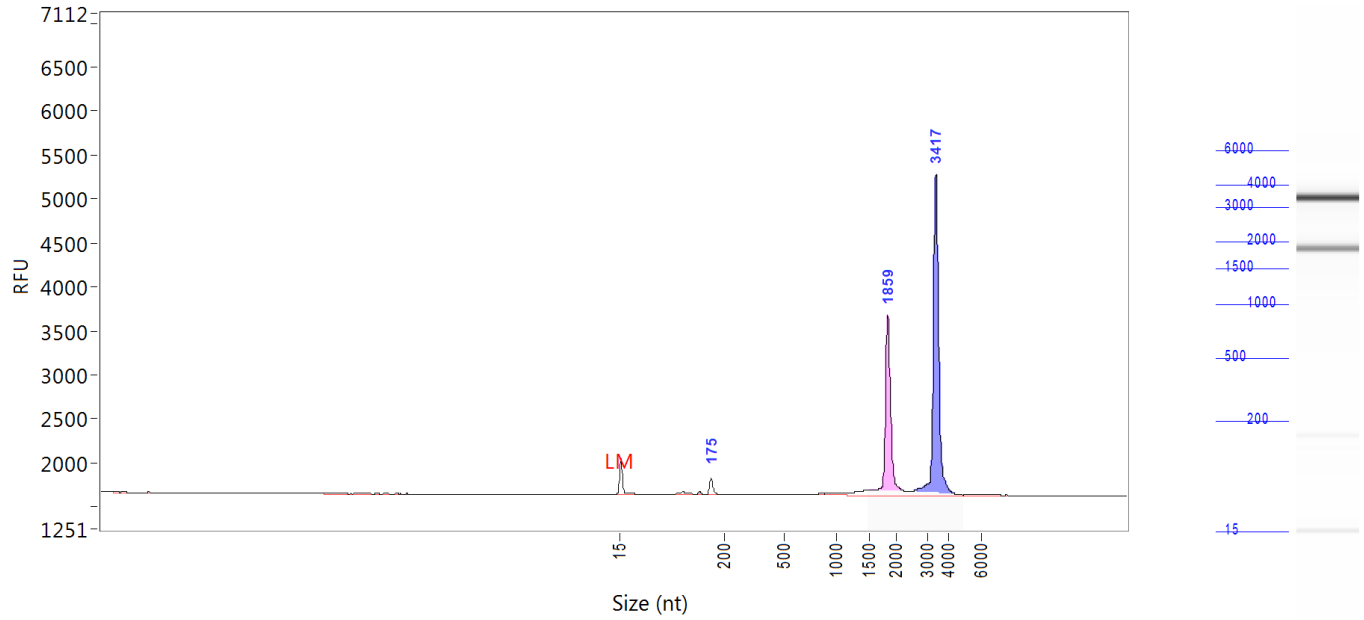
Peak	Size (nt)	Conc. (ng/uL)
1	15 (LM)	0.6462
2	126	0.9786
3	175	1.0156
4	1867	12.8039
5	3480	21.9515

TIC: 36.7497 ng/uL
 TIM: 83.313 nmole/L
 Total Conc.: 40.3540 ng/uL

 28S/18S: 1.8
 RQN 10.0

Sample Peak Width (sec): 6 Sample Min Peak Height: 20 Sample Baseline V to V?: Y Sample Baseline V to V pts: 3
 Sample Filter: Binomial # of Pts for Filter: 9 Sample Start Region (min): 0 Sample End Region (min): 40
 Manual Baseline Start (min): 18 Manual Baseline End (min): 38
 Marker Peak Width (sec): 6 Marker Min Peak Height: 100 Marker Baseline V to V?: Y Marker Baseline V to V pts: 3
 Lower Marker Selection: First Peak > 100 RFU Upper Marker Selection: Last Peak > 100 RFU
 Ladder Size (bp): 15, 200, 500, 1000, 1500, 2000, 3000, 4000, 6000
 Quantification Using: Ladder Final Concentration (ng/uL): 8.0000 Dilution Factor: 12.0
 Min. RFU for Data Processing: 2

Sample: CK_16
Well Location: C4
Created: 31 May, 2016 10:47:01



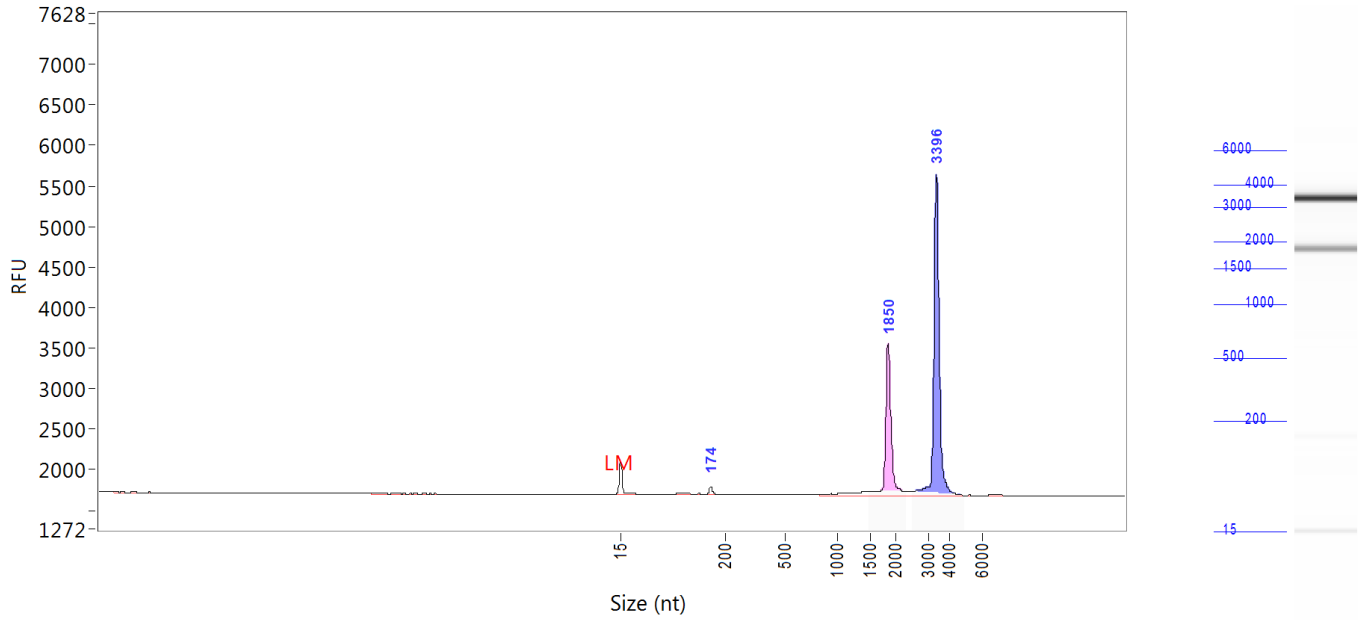
Peak	Size (nt)	Conc. (ng/uL)
1	15 (LM)	0.6462
2	175	3.3686
3	1859	46.4913
4	3417	76.7131

TIC: 126.5731 ng/uL
 TIM: 207.876 nmole/L
 Total Conc.: 136.4312 ng/uL

 28S/18S: 1.8
 RQN: 10.0

Sample Peak Width (sec): 6 Sample Min Peak Height: 50 Sample Baseline V to V?: Y Sample Baseline V to V pts: 3
 Sample Filter: Binomial # of Pts for Filter: 9 Sample Start Region (min): 0 Sample End Region (min): 40
 Manual Baseline Start (min): 18 Manual Baseline End (min): 38
 Marker Peak Width (sec): 6 Marker Min Peak Height: 100 Marker Baseline V to V?: Y Marker Baseline V to V pts: 3
 Lower Marker Selection: First Peak > 100 RFU Upper Marker Selection: Last Peak > 100 RFU
 Ladder Size (bp): 15, 200, 500, 1000, 1500, 2000, 3000, 4000, 6000
 Quantification Using: Ladder Final Concentration (ng/uL): 8.0000 Dilution Factor: 12.0
 Min. RFU for Data Processing: 2

Sample: CK_17
Well Location: C5
Created: 31 May, 2016 10:47:01



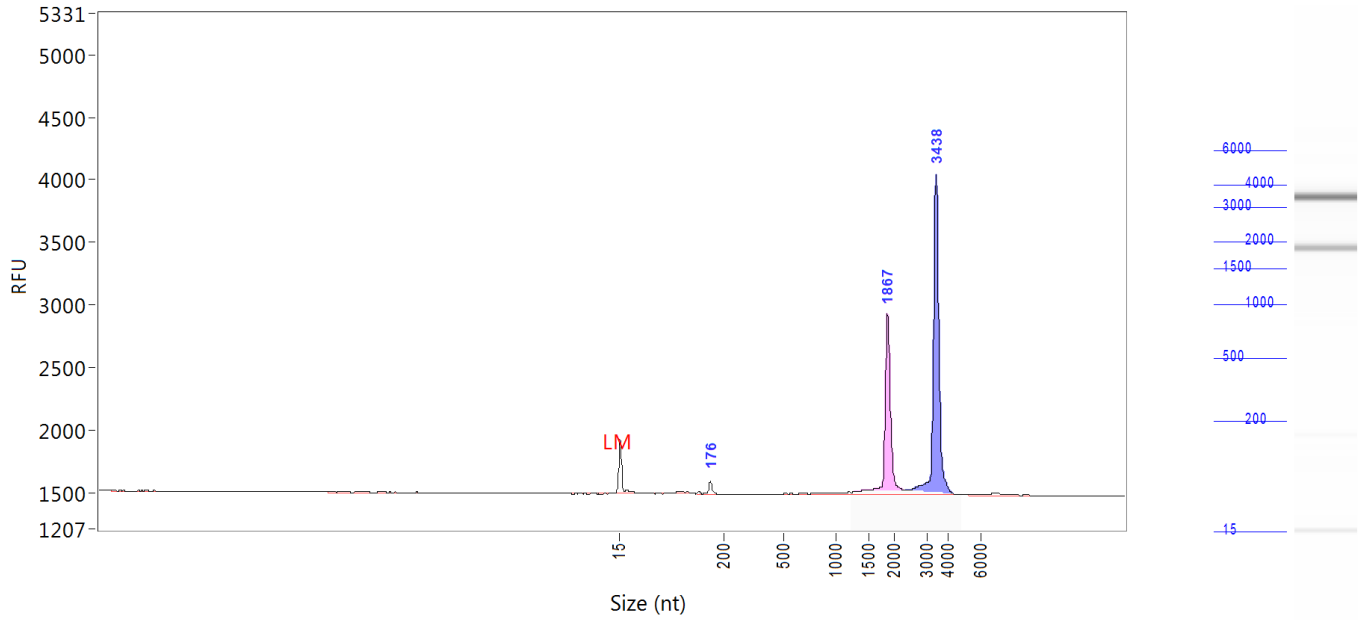
Peak	Size (nt)	Conc. (ng/uL)
1	15 (LM)	0.6462
2	174	1.6495
3	1850	40.0680
4	3396	76.0519

TIC: 117.7694 ng/uL
 TIM: 166.819 nmole/L
 Total Conc.: 126.8043 ng/uL

 28S/18S: 2.1
 RQN 10.0

Sample Peak Width (sec): 6 Sample Min Peak Height: 50 Sample Baseline V to V?: Y Sample Baseline V to V pts: 3
 Sample Filter: Binomial # of Pts for Filter: 9 Sample Start Region (min): 0 Sample End Region (min): 40
 Manual Baseline Start (min): 18 Manual Baseline End (min): 38
 Marker Peak Width (sec): 6 Marker Min Peak Height: 100 Marker Baseline V to V?: Y Marker Baseline V to V pts: 3
 Lower Marker Selection: First Peak > 100 RFU Upper Marker Selection: Last Peak > 100 RFU
 Ladder Size (bp): 15, 200, 500, 1000, 1500, 2000, 3000, 4000, 6000
 Quantification Using: Ladder Final Concentration (ng/uL): 8.0000 Dilution Factor: 12.0
 Min. RFU for Data Processing: 2

Sample: CK_18
Well Location: C6
Created: 31 May, 2016 10:47:01



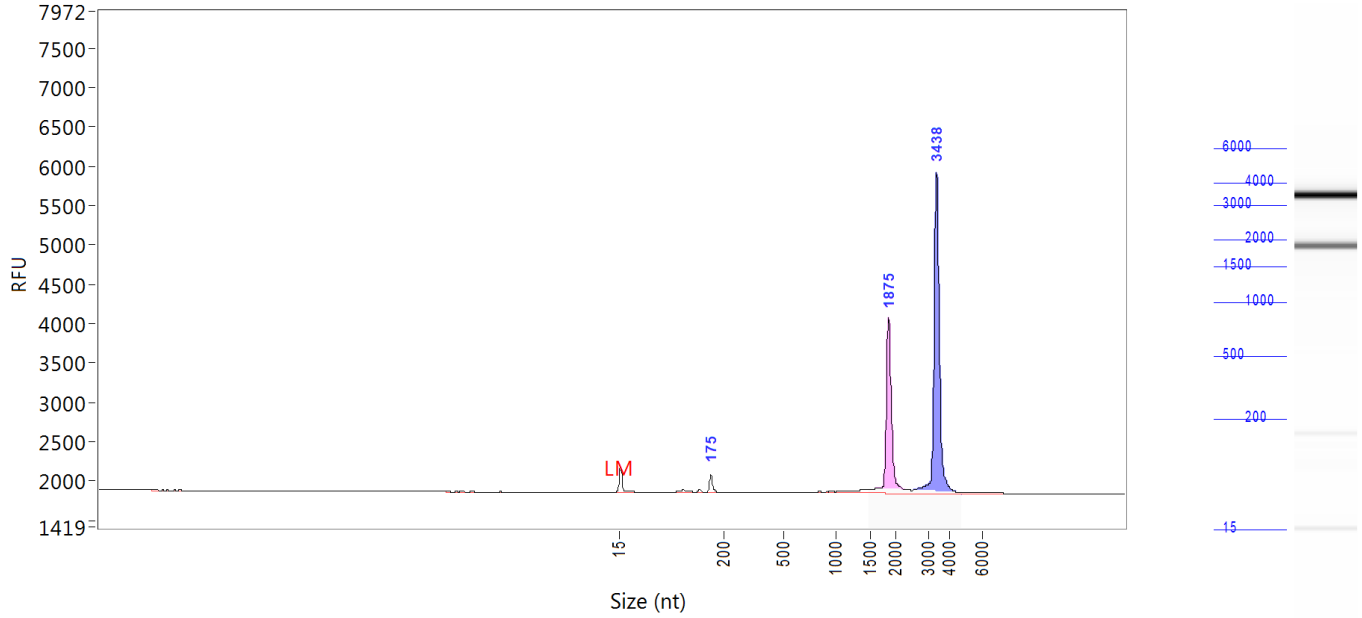
Peak	Size (nt)	Conc. (ng/uL)
1	15 (LM)	0.6462
2	176	1.4527
3	1867	31.9163
4	3438	51.0634

TIC: 84.4324 ng/uL
 TIM: 125.346 nmole/L
 Total Conc.: 88.4268 ng/uL

 28S/18S: 1.7
 RQN: 10.0

Sample Peak Width (sec): 6 Sample Min Peak Height: 50 Sample Baseline V to V?: Y Sample Baseline V to V pts: 3
 Sample Filter: Binomial # of Pts for Filter: 9 Sample Start Region (min): 0 Sample End Region (min): 40
 Manual Baseline Start (min): 18 Manual Baseline End (min): 38
 Marker Peak Width (sec): 6 Marker Min Peak Height: 100 Marker Baseline V to V?: Y Marker Baseline V to V pts: 3
 Lower Marker Selection: First Peak > 100 RFU Upper Marker Selection: Last Peak > 100 RFU
 Ladder Size (bp): 15, 200, 500, 1000, 1500, 2000, 3000, 4000, 6000
 Quantification Using: Ladder Final Concentration (ng/uL): 8.0000 Dilution Factor: 12.0
 Min. RFU for Data Processing: 2

Sample: CK_19
Well Location: C7
Created: 31 May, 2016 10:47:01



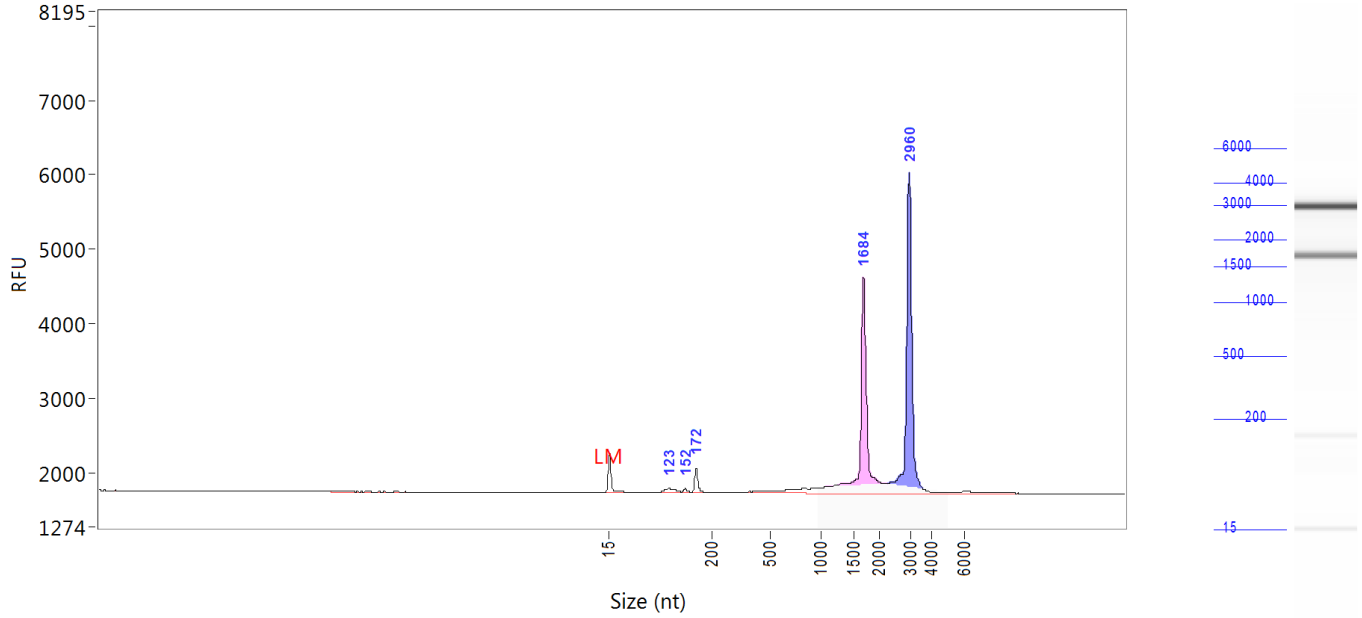
Peak	Size (nt)	Conc. (ng/uL)
1	15 (LM)	0.6462
2	175	4.6773
3	1875	63.4823
4	3438	104.5712

TIC: 172.7308 ng/uL
 TIM: 283.539 nmole/L
 Total Conc.: 184.5994 ng/uL

28S/18S: 1.8
 RQN: 10.0

Sample Peak Width (sec): 6 Sample Min Peak Height: 50 Sample Baseline V to V?: Y Sample Baseline V to V pts: 3
 Sample Filter: Binomial # of Pts for Filter: 9 Sample Start Region (min): 0 Sample End Region (min): 40
 Manual Baseline Start (min): 18 Manual Baseline End (min): 38
 Marker Peak Width (sec): 6 Marker Min Peak Height: 100 Marker Baseline V to V?: Y Marker Baseline V to V pts: 3
 Lower Marker Selection: First Peak > 100 RFU Upper Marker Selection: Last Peak > 100 RFU
 Ladder Size (bp): 15, 200, 500, 1000, 1500, 2000, 3000, 4000, 6000
 Quantification Using: Ladder Final Concentration (ng/uL): 8.0000 Dilution Factor: 12.0
 Min. RFU for Data Processing: 2

Sample: CK_20
Well Location: C8
Created: 31 May, 2016 10:47:01

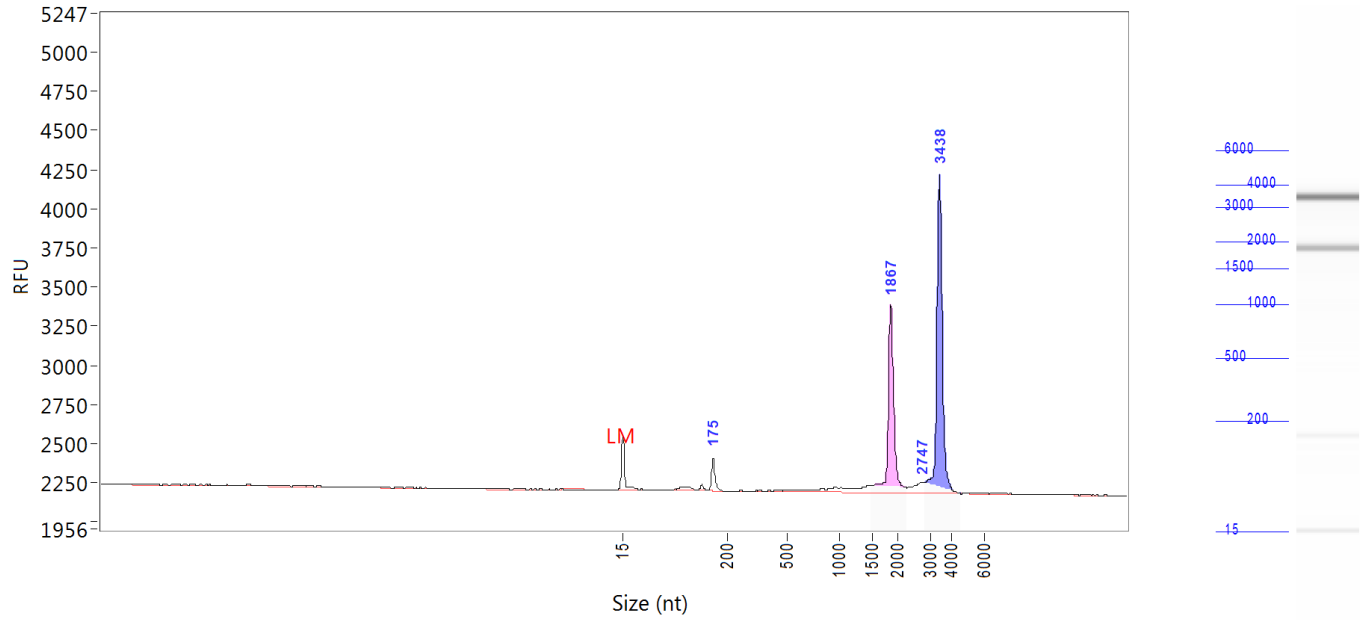


Peak	Size (nt)	Conc. (ng/uL)
1	15 (LM)	0.6462
2	123	2.7317
3	152	0.8733
4	172	4.5584
5	1684	63.8502
6	2960	71.3205

TIC: 143.3341 ng/uL
 TIM: 362.459 nmole/L
 Total Conc.: 155.1891 ng/uL
 28S/18S: 1.4
 RQN 9.9

Sample Peak Width (sec): 6 Sample Min Peak Height: 50 Sample Baseline V to V?: Y Sample Baseline V to V pts: 3
 Sample Filter: Binomial # of Pts for Filter: 9 Sample Start Region (min): 0 Sample End Region (min): 40
 Manual Baseline Start (min): 18 Manual Baseline End (min): 38
 Marker Peak Width (sec): 6 Marker Min Peak Height: 100 Marker Baseline V to V?: Y Marker Baseline V to V pts: 3
 Lower Marker Selection: First Peak > 100 RFU Upper Marker Selection: Last Peak > 100 RFU
 Ladder Size (bp): 15, 200, 500, 1000, 1500, 2000, 3000, 4000, 6000
 Quantification Using: Ladder Final Concentration (ng/uL): 8.0000 Dilution Factor: 12.0
 Min. RFU for Data Processing: 2

Sample: CK_21
Well Location: C9
Created: 31 May, 2016 10:47:01

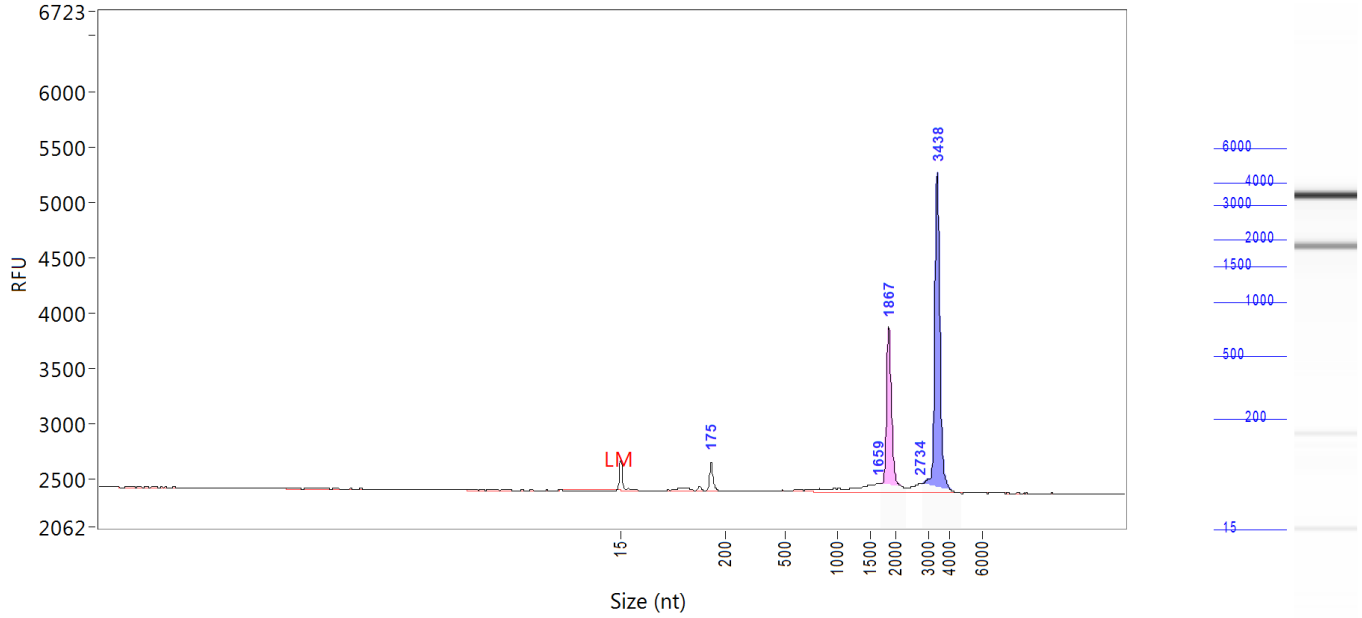


Peak	Size (nt)	Conc. (ng/uL)
1	15 (LM)	0.6462
2	175	4.1691
3	1867	33.0498
4	2747	3.3573
5	3438	49.3568

TIC: 89.9330 ng/uL
 TIM: 177.849 nmole/L
 Total Conc.: 100.1664 ng/uL
 28S/18S: 1.6
 RQN 9.6

Sample Peak Width (sec): 6 Sample Min Peak Height: 50 Sample Baseline V to V?: Y Sample Baseline V to V pts: 3
 Sample Filter: Binomial # of Pts for Filter: 9 Sample Start Region (min): 0 Sample End Region (min): 40
 Manual Baseline Start (min): 18 Manual Baseline End (min): 38
 Marker Peak Width (sec): 6 Marker Min Peak Height: 100 Marker Baseline V to V?: Y Marker Baseline V to V pts: 3
 Lower Marker Selection: First Peak > 100 RFU Upper Marker Selection: Last Peak > 100 RFU
 Ladder Size (bp): 15, 200, 500, 1000, 1500, 2000, 3000, 4000, 6000
 Quantification Using: Ladder Final Concentration (ng/uL): 8.0000 Dilution Factor: 12.0
 Min. RFU for Data Processing: 2

Sample: CK_22
Well Location: C10
Created: 31 May, 2016 10:47:01

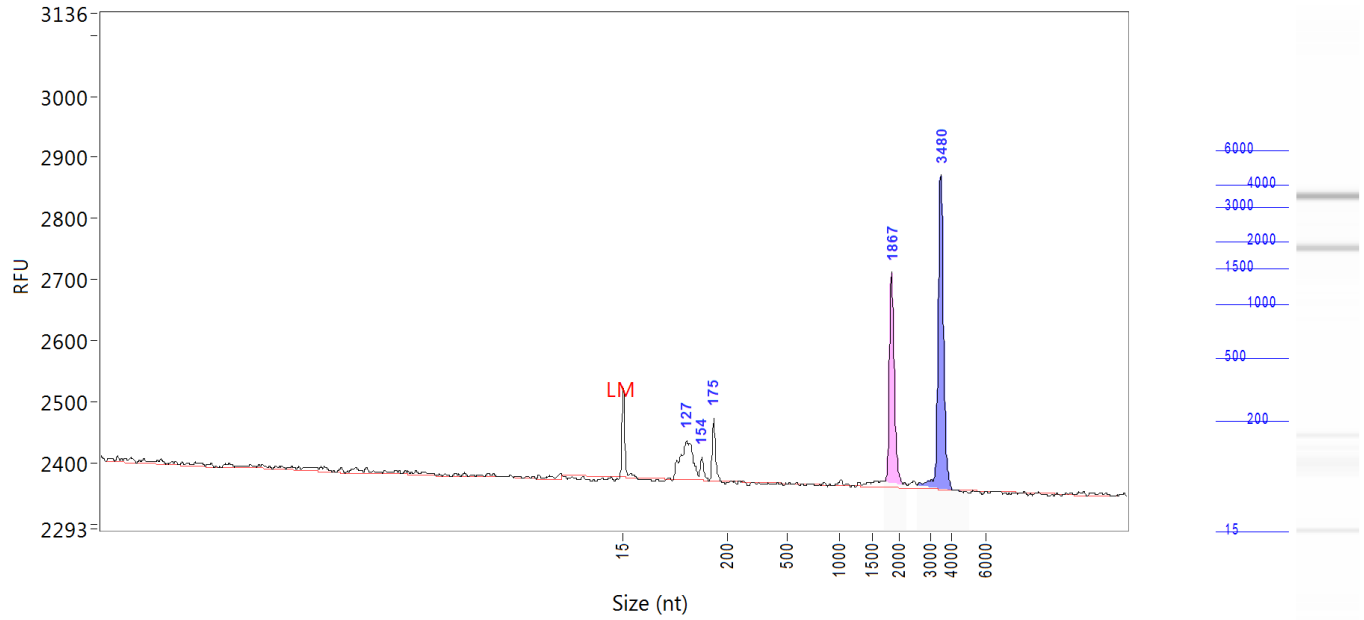


Peak	Size (nt)	Conc. (ng/uL)
1	15 (LM)	0.6462
2	175	6.5608
3	1659	7.7004
4	1867	48.3556
5	2734	4.4858
6	3438	85.5062

TIC: 152.6087 ng/uL
 TIM: 294.477 nmole/L
 Total Conc.: 164.0927 ng/uL
 28S/18S: 1.9
 RQN 9.4

Sample Peak Width (sec): 6 Sample Min Peak Height: 50 Sample Baseline V to V?: Y Sample Baseline V to V pts: 3
 Sample Filter: Binomial # of Pts for Filter: 9 Sample Start Region (min): 0 Sample End Region (min): 40
 Manual Baseline Start (min): 18 Manual Baseline End (min): 38
 Marker Peak Width (sec): 6 Marker Min Peak Height: 100 Marker Baseline V to V?: Y Marker Baseline V to V pts: 3
 Lower Marker Selection: First Peak > 100 RFU Upper Marker Selection: Last Peak > 100 RFU
 Ladder Size (bp): 15, 200, 500, 1000, 1500, 2000, 3000, 4000, 6000
 Quantification Using: Ladder Final Concentration (ng/uL): 8.0000 Dilution Factor: 12.0
 Min. RFU for Data Processing: 2

Sample: CK_23
Well Location: C11
Created: 31 May, 2016 10:47:01

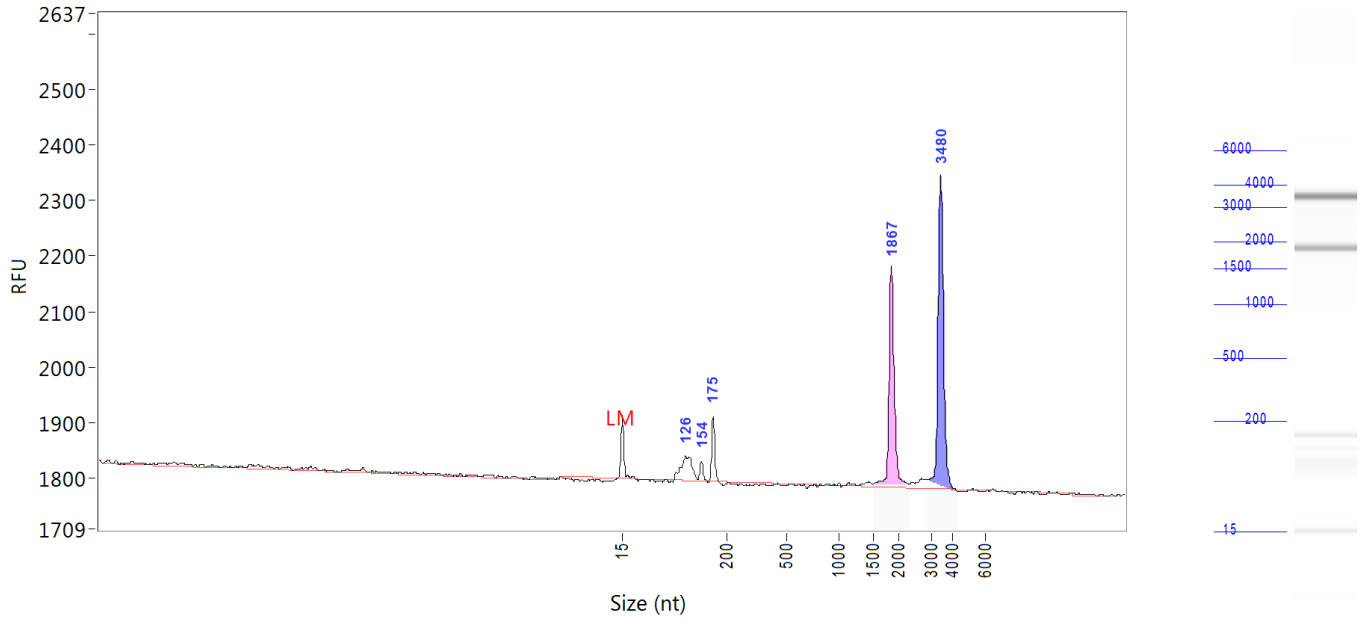


Peak	Size (nt)	Conc. (ng/uL)
1	15 (LM)	0.6462
2	127	12.9701
3	154	2.0159
4	175	5.0831
5	1867	22.2338
6	3480	32.4134

TIC: 74.7162 ng/uL
 TIM: 514.163 nmole/L
 Total Conc.: 77.9370 ng/uL
 28S/18S: 1.5
 RQN 9.2

Sample Peak Width (sec): 6 Sample Min Peak Height: 20 Sample Baseline V to V?: Y Sample Baseline V to V pts: 3
 Sample Filter: Binomial # of Pts for Filter: 9 Sample Start Region (min): 0 Sample End Region (min): 40
 Manual Baseline Start (min): 18 Manual Baseline End (min): 38
 Marker Peak Width (sec): 6 Marker Min Peak Height: 100 Marker Baseline V to V?: Y Marker Baseline V to V pts: 3
 Lower Marker Selection: First Peak > 100 RFU Upper Marker Selection: Last Peak > 100 RFU
 Ladder Size (bp): 15, 200, 500, 1000, 1500, 2000, 3000, 4000, 6000
 Quantification Using: Ladder Final Concentration (ng/uL): 8.0000 Dilution Factor: 12.0
 Min. RFU for Data Processing: 2

Sample: CK_24
Well Location: C12
Created: 31 May, 2016 10:47:01



Peak	Size (nt)	Conc. (ng/uL)
1	15 (LM)	0.6462
2	126	10.2270
3	154	2.1953
4	175	7.3261
5	1867	34.1743
6	3480	46.5755

TIC: 100.4982 ng/uL
 TIM: 524.689 nmole/L
 Total Conc.: 104.2878 ng/uL
 28S/18S: 1.4
 RQN 9.5

Sample Peak Width (sec): 6 Sample Min Peak Height: 40 Sample Baseline V to V?: Y Sample Baseline V to V pts: 3
 Sample Filter: Binomial # of Pts for Filter: 9 Sample Start Region (min): 0 Sample End Region (min): 40
 Manual Baseline Start (min): 18 Manual Baseline End (min): 38
 Marker Peak Width (sec): 6 Marker Min Peak Height: 100 Marker Baseline V to V?: Y Marker Baseline V to V pts: 3
 Lower Marker Selection: First Peak > 100 RFU Upper Marker Selection: Last Peak > 100 RFU
 Ladder Size (bp): 15, 200, 500, 1000, 1500, 2000, 3000, 4000, 6000
 Quantification Using: Ladder Final Concentration (ng/uL): 8.0000 Dilution Factor: 12.0
 Min. RFU for Data Processing: 2

Sample: DNA Size Ladder

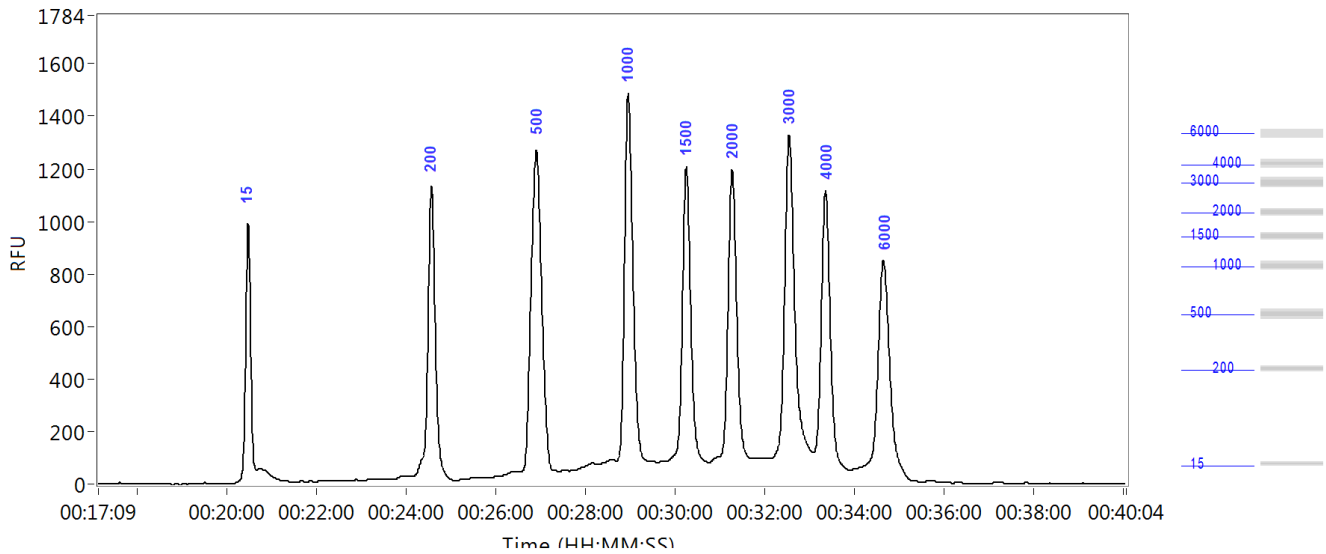
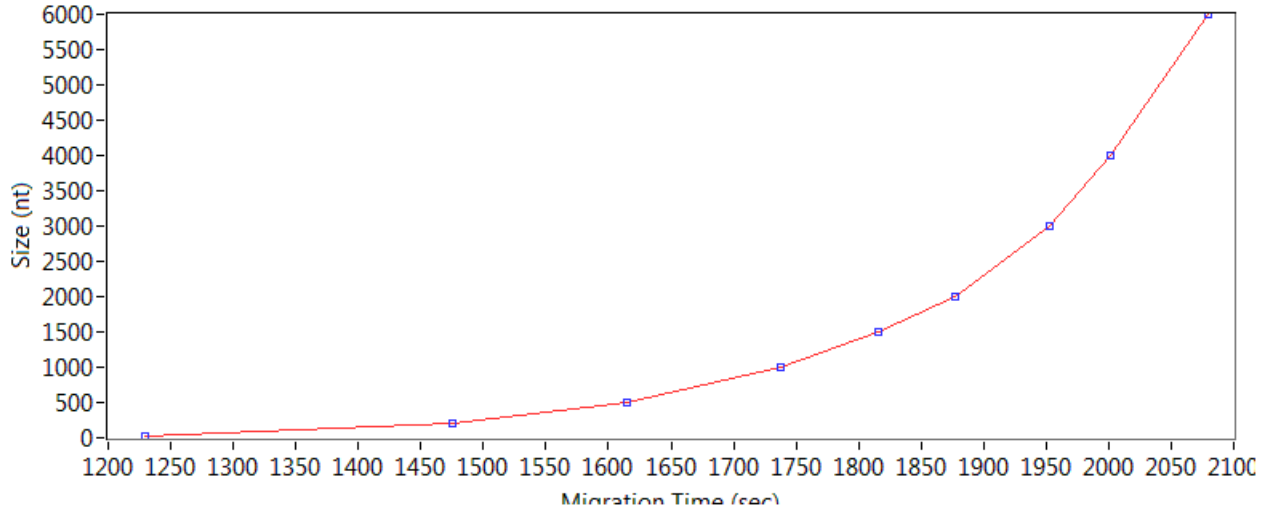
Well Location: A8

Created: 31 May, 2016 10:47:01

Import From: C:\PROSize 2.0\Ladders\ladder RNA standard15 nt 04.11.15.SCAL

Fit Type: Point to Point

Calibration Curve



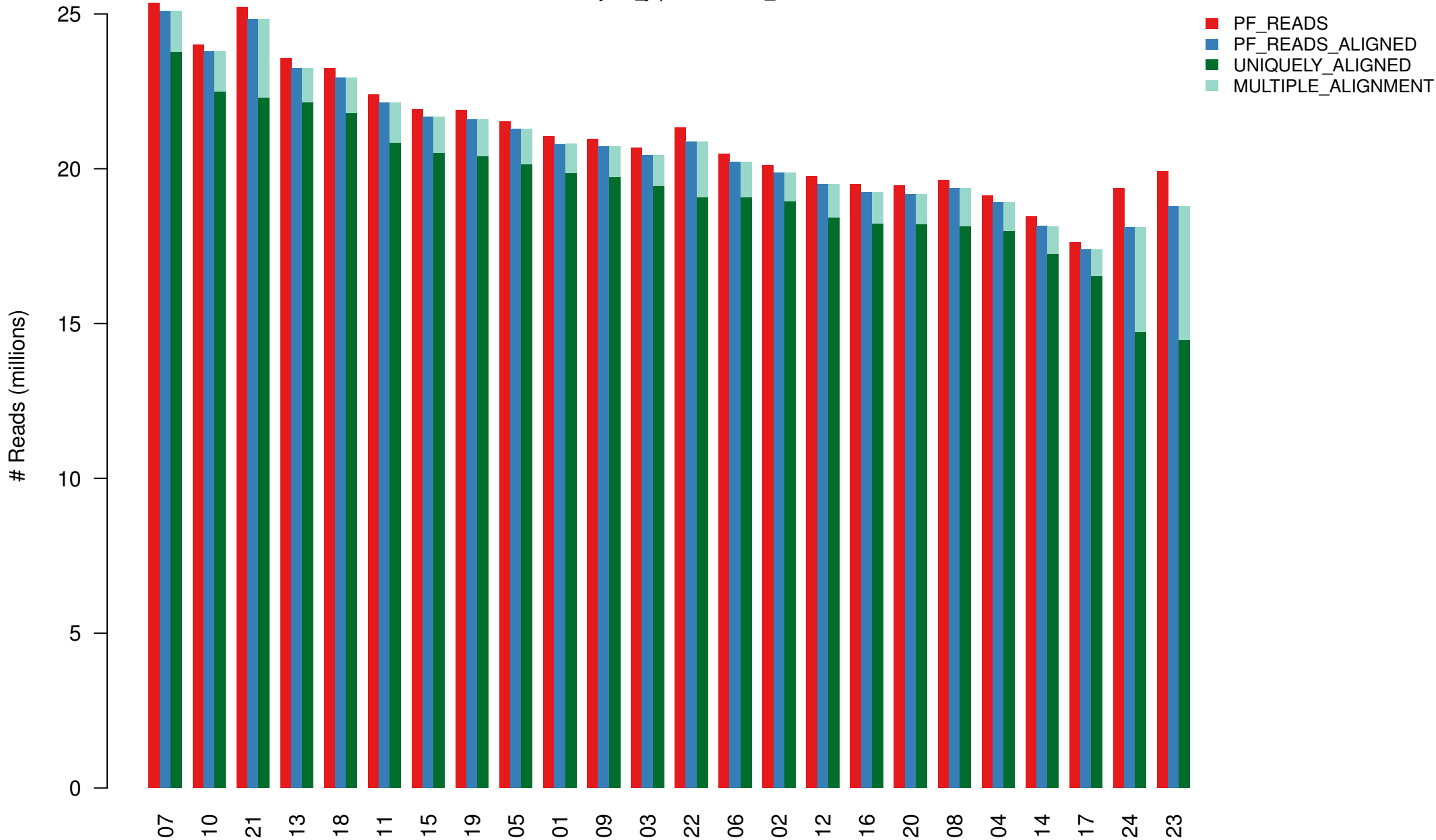
RNA-seq Project QC Report

Project	
Project ID	Project_Sjaponicus_SM
Laboratory	
Submitter	
Ref Organism	
Library Created by	
Protocol	
Run Type	
Number of Cycles	

Alignment Summary

Schizosaccharomyces_japonicus.GCA_000149845.2

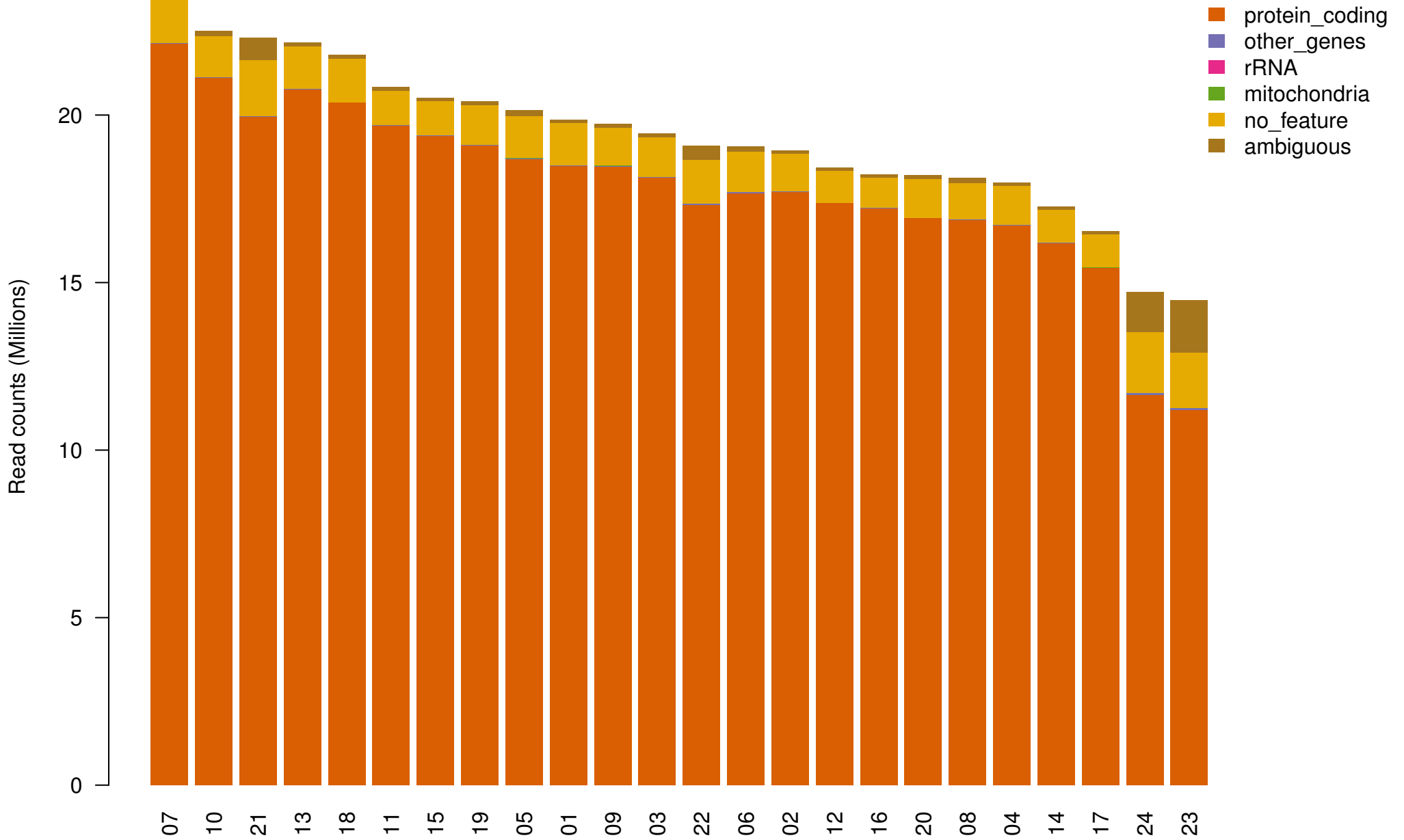
1 / 1



HTSeq-counts distribution

Schizosaccharomyces japonicus.GCA_000149845.2.31

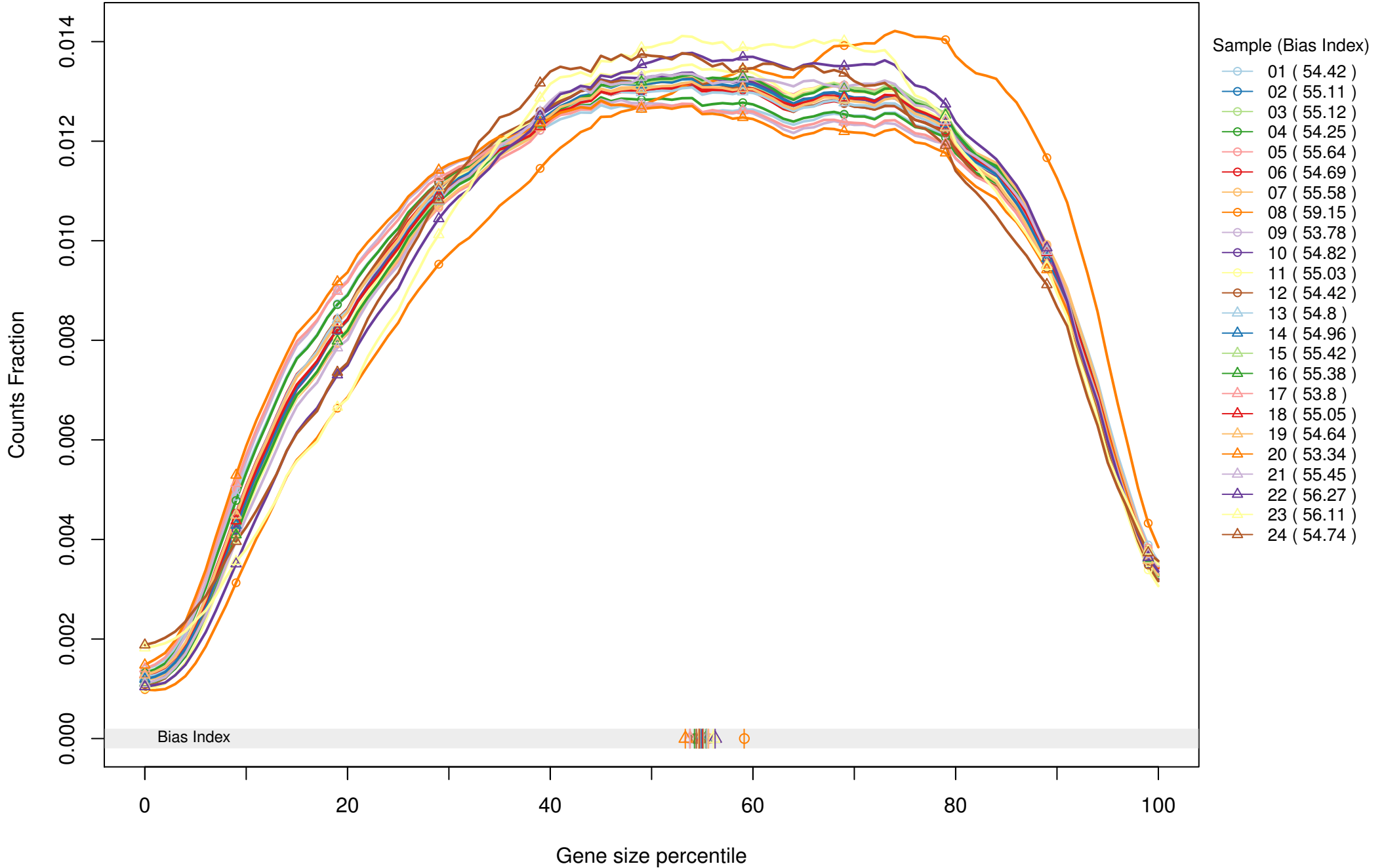
1 / 1



RSeQC gene body coverage

PROTEIN-CODING

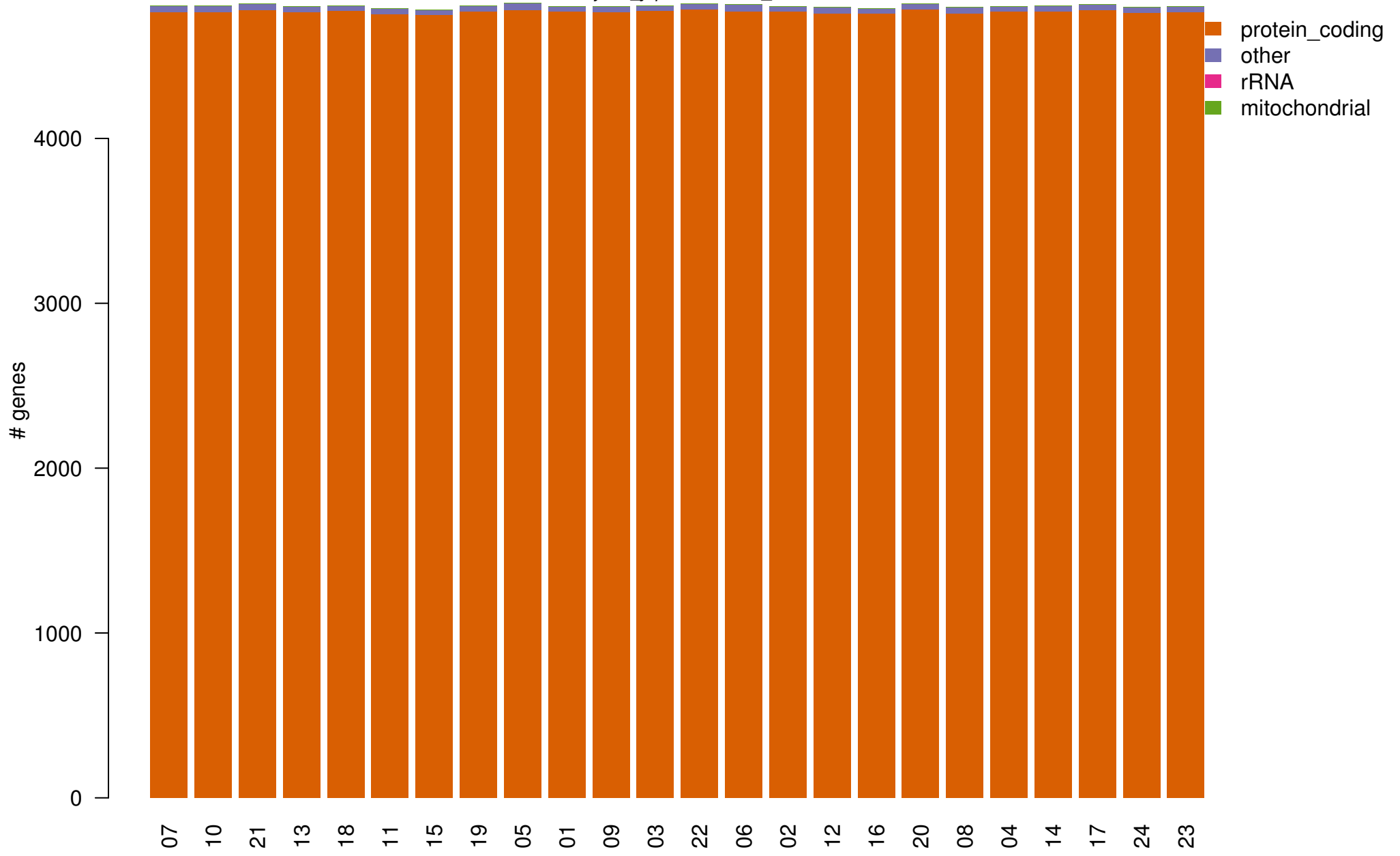
1 / 1



Expressed genes (RPKM >= 1)

Schizosaccharomyces japonicus.GCA_000149845.2.31

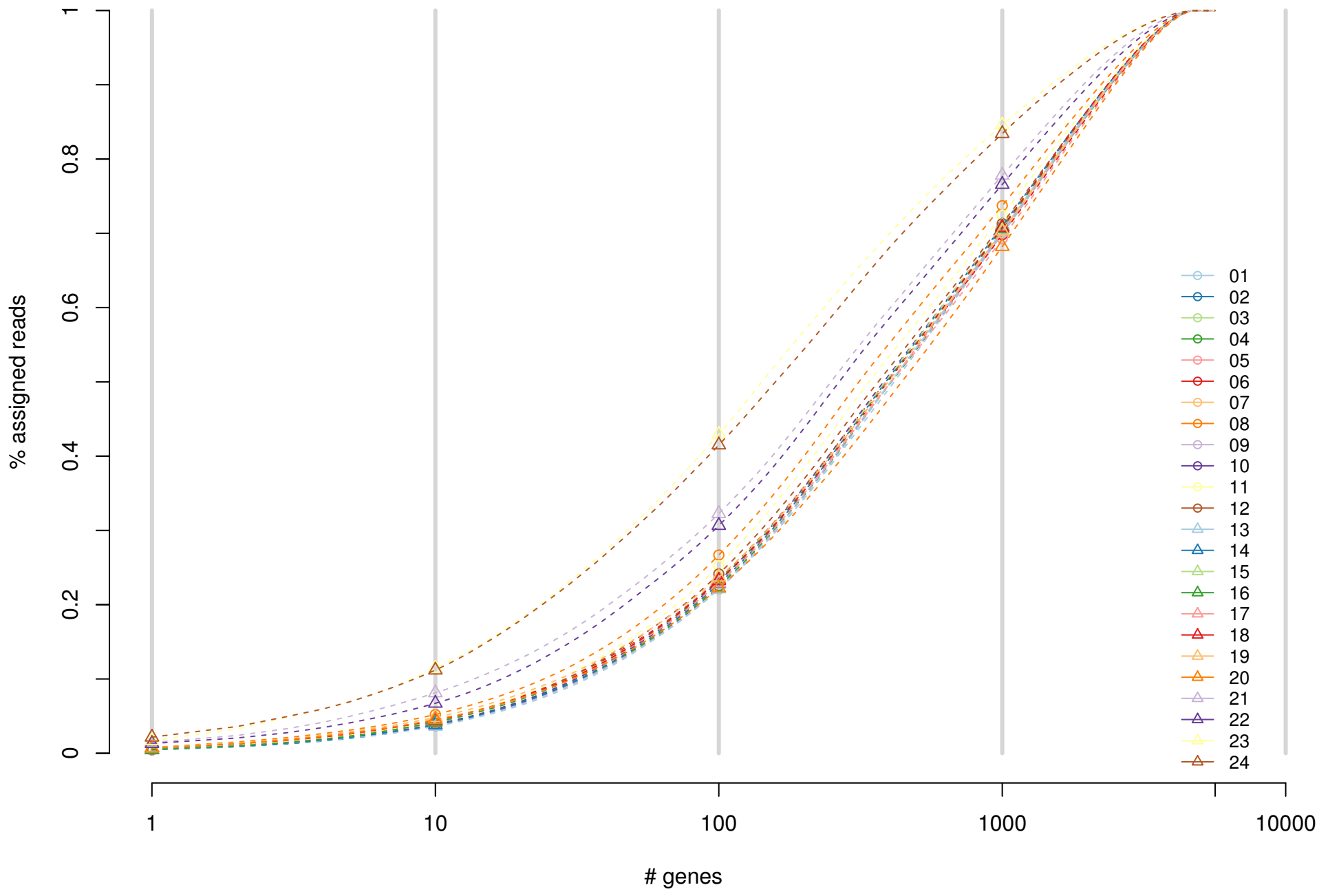
1 / 1



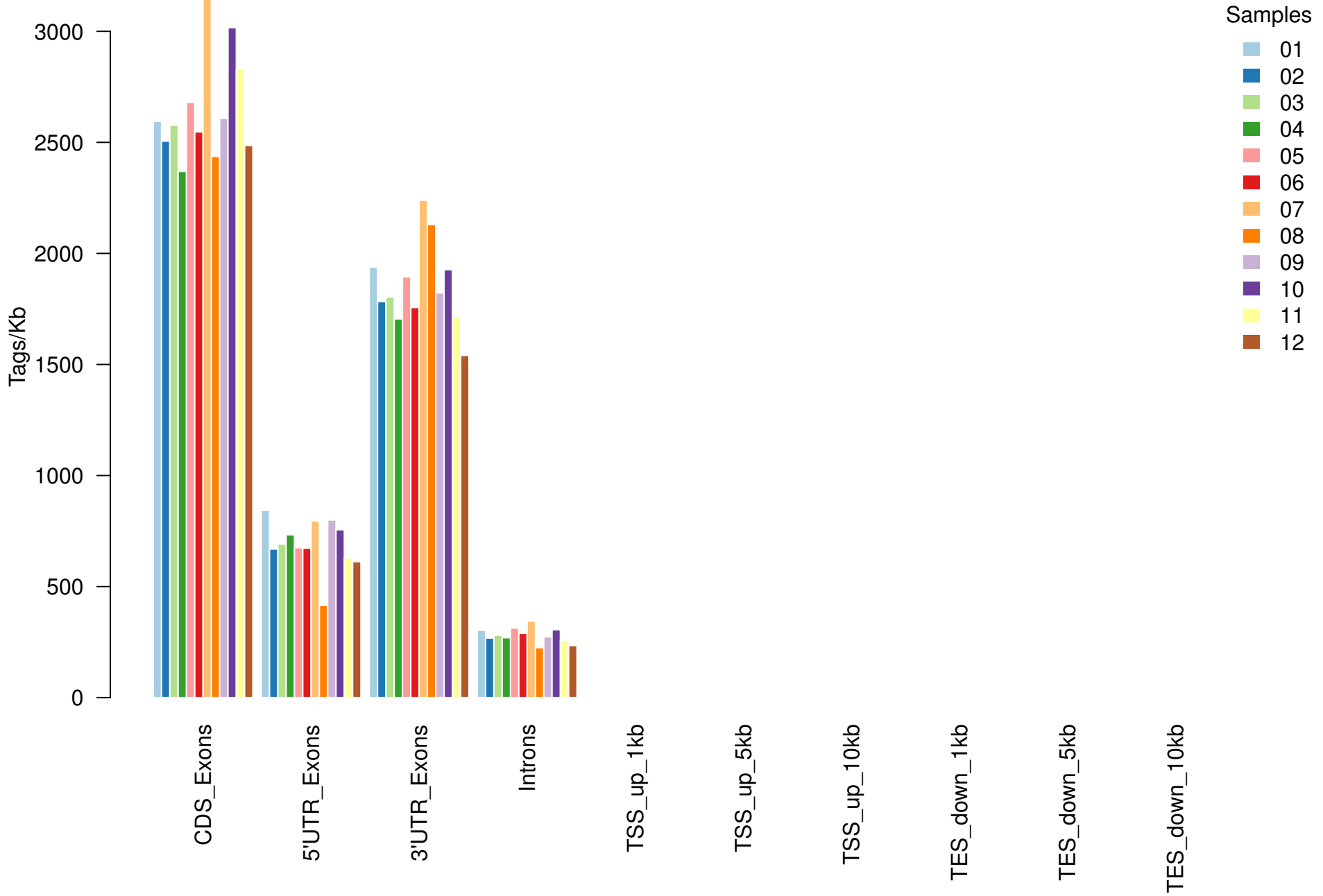
Cumulative Gene Diversity

Schizosaccharomyces japonicus.GCA_000149845.2.31

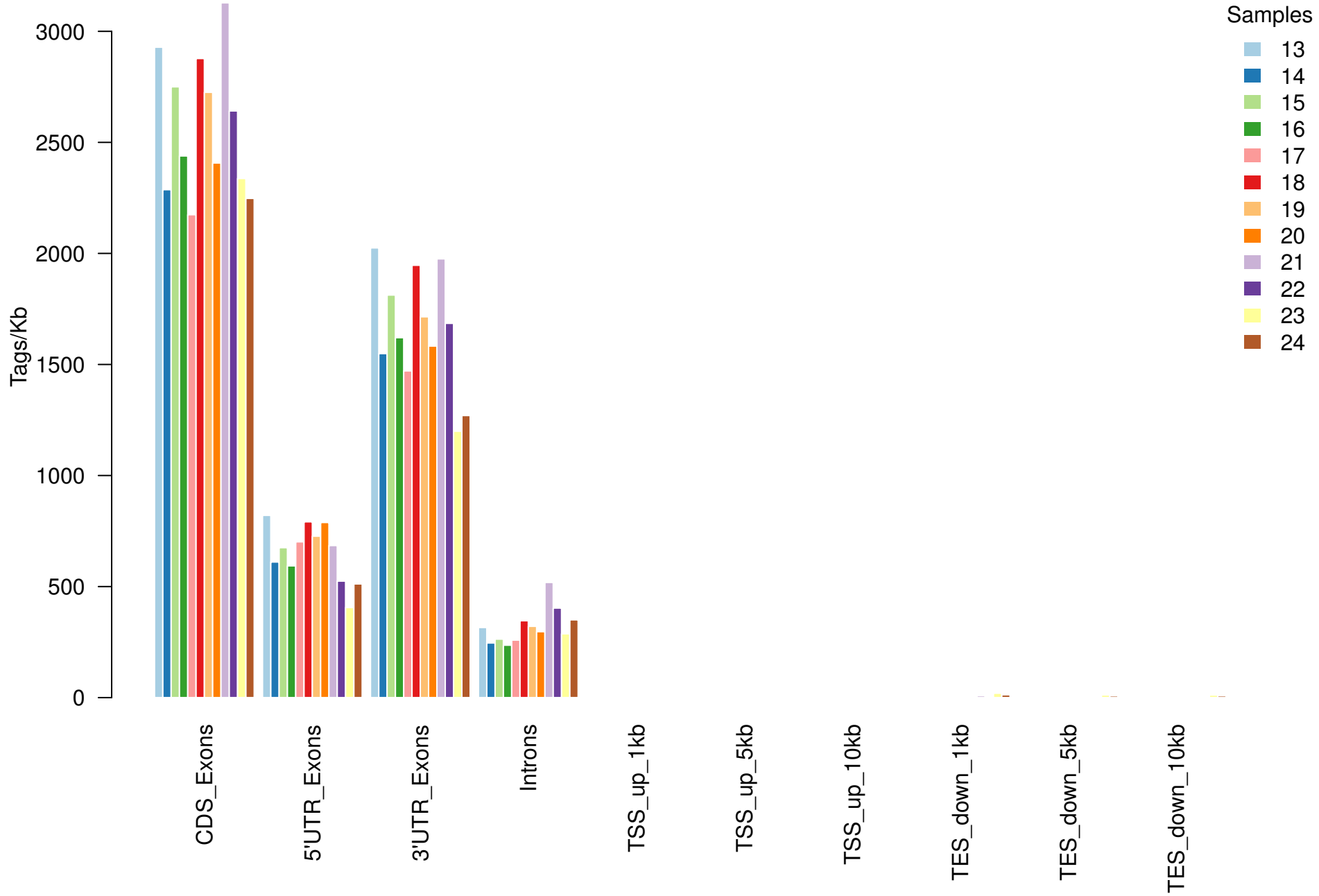
1 / 1



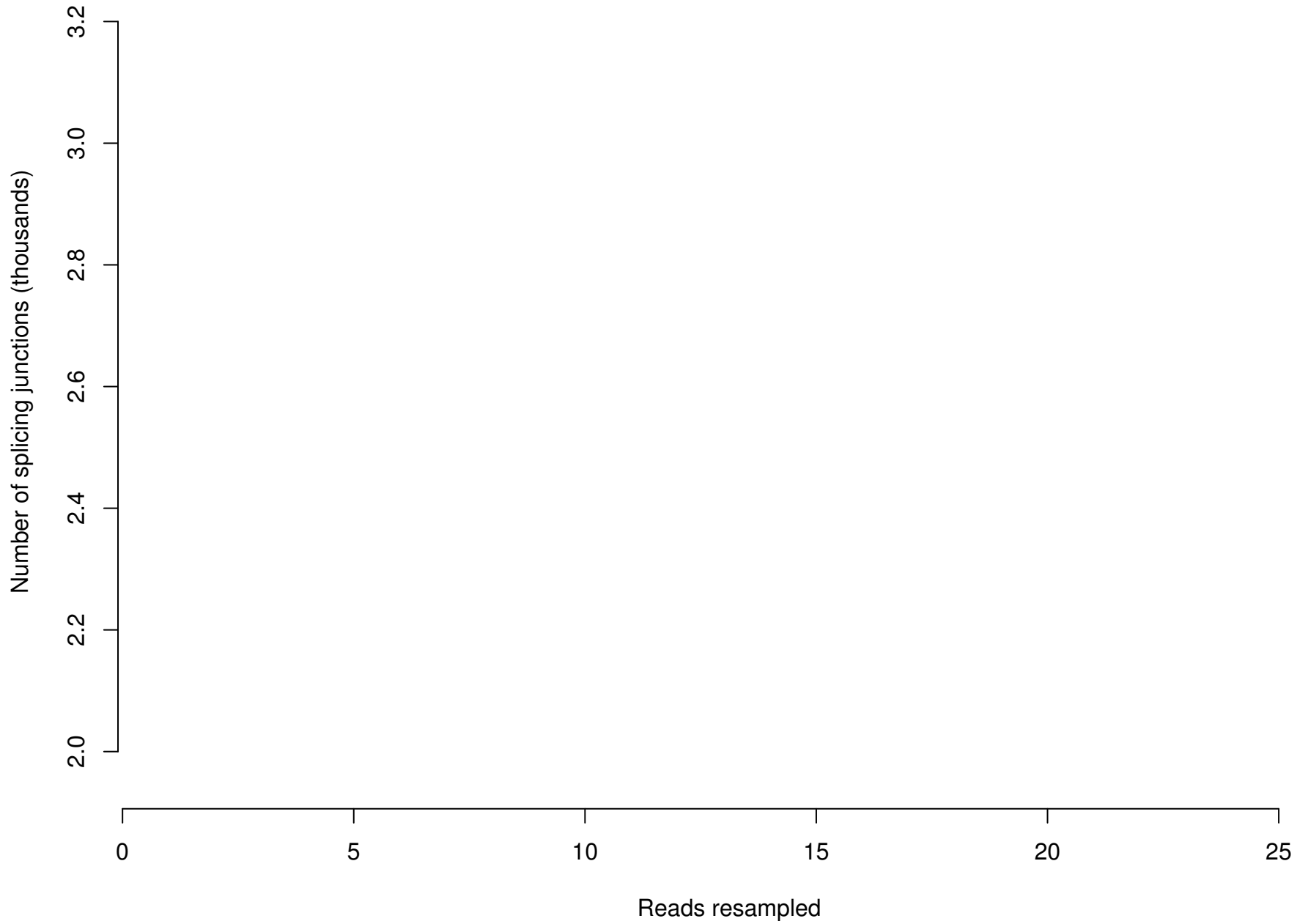
Reads Density (1/2)



Reads Density (2/2)



Known Splicing Junctions Saturation



Project alignment metrics (1/2)

METRIC	01	02	03	04	05	06	07	08	09	10	11	12
TOTAL_READS	21051101	20123023	20683101	19141543	21527072	20474912	25361894	19643224	20957868	24017202	22394290	19774826
PF_READS	21051101	20123023	20683101	19141543	21527072	20474912	25361894	19643224	20957868	24017202	22394290	19774826
PF_READS_ALIGNED	20799439	19875431	20448542	18907541	21291424	20218773	25100912	19366972	20731148	23787185	22131311	19510423
PCT_PF_READS_ALIGNED	98.80	98.77	98.87	98.78	98.91	98.75	98.97	98.59	98.92	99.04	98.83	98.66
PF_ALIGNED_BASES	1910077148	1826727000	1879595108	1736818006	1955097631	1856953365	2306406356	1778621796	1902907618	2190496915	2034353622	1793052047
MEAN_READ_LENGTH	92.08	92.13	92.15	92.10	92.07	92.08	92.11	92.10	92.04	92.31	92.15	92.13
READS_ALIGNED_IN_PAIRS	0	0	0	0	0	0	0	0	0	0	0	0
PCT_READS_ALIGNED_IN_PAIRS	0	0	0	0	0	0	0	0	0	0	0	0
STRAND_BALANCE	0.51	0.51	0.51	0.51	0.51	0.51	0.51	0.51	0.51	0.51	0.51	0.51
UNPAIRED_READ_DUPLICATES	17245638	16457459	17017445	15523286	17626899	16713125	21311057	16280229	17276650	20207593	18758553	16325046
READ_PAIR_DUPLICATES	0	0	0	0	0	0	0	0	0	0	0	0
PERCENT_DUPLICATION	82.91	82.80	83.22	82.10	82.79	82.66	84.90	84.06	83.34	84.95	84.76	83.67
UNIQUELY_ALIGNED	19862555	18940835	19450103	17986827	20139257	19070009	23779757	18131021	19738048	22499521	20840770	18424892
MULTIPLE_ALIGNMENT	936884	934596	998439	920714	1152167	1148764	1321155	1235951	993100	1287664	1290541	1085531
READ_ALIGNED_TO_REF_EXONS	18502280	17723568	18157504	16730976	18718423	17706813	22159705	16895076	18490324	21133848	19711190	17387425
NO_FEATURE	1262239	1129894	1189801	1153850	1256635	1208547	1463718	1085364	1135526	1221881	1016562	942042
AMBIGUOUS	98036	87373	102798	102001	164199	154649	156334	150581	112198	143792	113018	95425
TOO_LOW_AQUAL	0	0	0	0	0	0	0	0	0	0	0	0
NOT_ALIGNED	0	0	0	0	0	0	0	0	0	0	0	0
ALIGNMENT_NOT_UNIQUE	2361160	2380236	2526395	2324531	2851792	2850214	3294749	3109224	2458923	3241219	3295220	2778074
READS_ALIGNED_TO_rRNA	385911	368847	411979	398350	596394	628361	561506	587955	436914	540552	486244	441745
READS_ALIGNED_TO_rRNA_%	1.83	1.83	1.99	2.08	2.77	3.07	2.21	2.99	2.08	2.25	2.17	2.23
READS_ALIGNED_TO_MITOCHONDRIA	7606	7030	8074	8329	13192	13630	12505	13182	9362	11397	9620	8280
READS_ALIGNED_TO_MITOCHONDRIA_%	0.04	0.03	0.04	0.04	0.06	0.07	0.05	0.07	0.04	0.05	0.04	0.04
bias_index_50	54.42	55.11	55.12	54.25	55.64	54.69	55.58	59.15	53.78	54.82	55.03	54.42
5over3_cov_ratio	0.65	0.60	0.60	0.65	0.57	0.63	0.57	0.41	0.68	0.60	0.59	0.63

Project alignment metrics (2/2)

METRIC	13	14	15	16	17	18	19	20	21	22	23	24
TOTAL_READS	23583500	18453330	21931237	19498300	17634932	23251976	21898591	19465081	25217092	21330424	19923768	19383992
PF_READS	23583500	18453330	21931237	19498300	17634932	23251976	21898591	19465081	25217092	21330424	19923768	19383992
PF_READS_ALIGNED	23254924	18147516	21685723	19244428	17395441	22942617	21600948	19189648	24826943	20884727	18785535	18104885
PCT_PF_READS_ALIGNED	98.61	98.34	98.88	98.70	98.64	98.67	98.64	98.58	98.45	97.91	94.29	93.40
PF_ALIGNED_BASES	2135083188	1666957006	1992418378	1769380596	1595483690	2111952561	1985523257	1762483673	2277482180	1917286574	1722155675	1659481467
MEAN_READ_LENGTH	92.07	92.10	92.12	92.17	91.97	92.28	92.14	92.08	91.98	92.07	91.97	91.94
READS_ALIGNED_IN_PAIRS	0	0	0	0	0	0	0	0	0	0	0	0
PCT_READS_ALIGNED_IN_PAIRS	0	0	0	0	0	0	0	0	0	0	0	0
STRAND_BALANCE	0.51	0.51	0.51	0.51	0.51	0.51	0.51	0.51	0.56	0.54	0.65	0.63
UNPAIRED_READ_DUPLICATES	19677172	14908788	18194192	15948790	14119251	19309834	18017444	15762593	21606606	17837856	16872532	16278081
READ_PAIR_DUPLICATES	0	0	0	0	0	0	0	0	0	0	0	0
PERCENT_DUPLICATION	84.62	82.15	83.90	82.87	81.17	84.17	83.41	82.14	87.03	85.41	89.82	89.91
UNIQUELY_ALIGNED	22156347	17258468	20513535	18227974	16535304	21791523	20410958	18212324	22300178	19087994	14466358	14717097
MULTIPLE_ALIGNMENT	1098577	889048	1172188	1016454	860137	1151094	1189990	977324	2526765	1796733	4319177	3387788
READ_ALIGNED_TO_REF_EXONS	20783169	16197074	19396875	17232792	15453463	20387281	19110926	16936837	19985024	17355631	11260579	11710942
NO_FEATURE	1265554	977883	1019074	910449	991670	1285460	1179177	1155617	1654440	1315922	1642298	1816351
AMBIGUOUS	107624	83511	97586	84733	90171	118782	120855	119870	660714	416441	1563481	1189804
TOO_LOW_AQUAL	0	0	0	0	0	0	0	0	0	0	0	0
NOT_ALIGNED	0	0	0	0	0	0	0	0	0	0	0	0
ALIGNMENT_NOT_UNIQUE	2769084	2238584	3030688	2612960	2157790	2895656	3032610	2487203	6368362	4491523	11097773	8628277
READS_ALIGNED_TO_rRNA	494041	436084	404668	386906	382969	505660	533705	511393	2406436	1614708	6060960	5009395
READS_ALIGNED_TO_rRNA_%	2.09	2.36	1.85	1.98	2.17	2.17	2.44	2.63	9.54	7.57	30.42	25.84
READS_ALIGNED_TO_MITOCHONDRIA	9444	8118	8328	7579	7591	9746	10131	9949	44289	30298	114920	81313
READS_ALIGNED_TO_MITOCHONDRIA_%	0.04	0.04	0.04	0.04	0.04	0.04	0.05	0.05	0.18	0.14	0.58	0.42
bias_index_50	54.80	54.96	55.42	55.38	53.80	55.05	54.64	53.34	55.45	56.27	56.11	54.74
5over3_cov_ratio	0.62	0.60	0.58	0.58	0.69	0.60	0.63	0.72	0.57	0.52	0.52	0.60

Annexe 3: Early timepoint analysis

Gene_ID	AveExpr	FC_ind_vs_ctr.	FC_ind_vs_ctr.	FC_ind_vs_ctr.	FC_ind_vs_ctr.	FDR	Groups	Description	Spombe_GeneID	Scerevisiae_GeneID
SIAG_02435	5.527198533	1.065432809	1.334246407	1.667115692	3.19515205	0.003274181	ind_vs_ctr.12h	alpha-amylase Mde5	SPAC25H1.09	
SIAG_00240	6.634195617	-1.344516886	1.867023908	2.894141715	5.586624408	0.04033424	ind_vs_ctr.12h	alcohol dehydrogenase Adh4	SPAC5H10.06c	YGL256W
SIAG_01368	6.773724546	1.080304768	1.162600656	1.356635515	2.008537325	0.027210765	ind_vs_ctr.12h	methionyl-tRNA formyltransferase Fmt1	SPAC1805.09c	YBL013W
SIAG_01306	6.989666051	1.093107607	-1.365512779	1.250184587	2.851822457	0.002280074	ind_vs_ctr.12h	hypothetical protein		
SIAG_00246	7.110579977	1.567204492	-1.530939324	-1.412894767	-3.676117648	0.009224475	ind_vs_ctr.12h	acetyltransferase		
SIAG_00217	7.19451431	1.100654664	1.478513814	1.373337587	2.186108829	0.009679622	ind_vs_ctr.12h	eukaryotic protein	SPAC11E3.12	
SIAG_02124	7.486524055	-1.740707686	-1.754827246	1.307272648	4.276370526	0.023022547	ind_vs_ctr.12h	cobW		
SIAG_00922	8.264667854	-1.123407213	1.361585376	1.435087995	2.25136698	0.003903818	ind_vs_ctr.12h	OPT oligopeptide transporter Isp4	SPBC29B5.02c	
SIAG_00781	8.6432588	1.210582383	-1.209161741	-1.440132464	2.181527816	0.045496532	ind_vs_ctr.12h	P-factor pheromone Map2	SPCC1795.06	
SIAG_00161	9.598700014	1.120814939	-1.255933167	1.489593044	2.384707974	0.018401334	ind_vs_ctr.12h	hypothetical protein	SPBPB2B2.15,SPAC977.05c,SPBC1348.06c	YGL258W,YOR387C
SIAG_00827	10.29154329	1.305911922	1.154789034	1.373210581	-2.93139884	0.041701958	ind_vs_ctr.12h	thiazole biosynthetic enzyme	SPBC26H8.01	YGR144W
SIAG_04258	4.789148297	2.407564704	1.004883369	-1.07111722	1.882860124	0.043703461	ind_vs_ctr.1h	P-type proton ATPase Pma2	SPCC1020.01c	YPL036W,YGL008C
SIAG_04365	6.334597706	-2.006260294	1.154353431	-1.828684276	-1.180796171	0.005704267	ind_vs_ctr.1h	hypothetical protein		
SIAG_03999	7.336113873	-2.03052015	1.151160432	1.387636839	1.741652345	0.018309403	ind_vs_ctr.1h_ind_vs_ctr.12h	meiotically upregulated Mug97	SPBC146.11c	
SIAG_02945	11.50376368	1.448668439	2.435302791	1.921574115	1.361510399	0.0009048	ind_vs_ctr.1h_ind_vs_ctr.3h_ind_vs_ctr.6h	glyceraldehyde-3-phosphate dehydrogenase Tdh1	SPBC354.12,SPBC32F12.11	YGR192C,YIR009C,YIL052W
SIAG_05896	11.65089053	1.327893268	-2.576641101	-2.088526134	-1.165279589	6.36E-05	ind_vs_ctr.1h_ind_vs_ctr.3h_ind_vs_ctr.6h	hypothetical protein	SPBC30B4.09	
SIAG_05181	12.39117667	1.542923778	-2.417233001	-1.804336944	1.206114627	0.000780867	ind_vs_ctr.1h_ind_vs_ctr.3h_ind_vs_ctr.6h	glutathione S-transferase Gst3	SPAC688.04c	
SIAG_00372	12.47710068	1.424929641	-2.34217926	-1.476134111	-1.146520267	0.000631925	ind_vs_ctr.1h_ind_vs_ctr.3h_ind_vs_ctr.6h	plasma membrane proteolipid Pmp3	SPBC713.11c	
SIAG_02135	8.438275569	1.589724691	2.839175053	2.2865724	1.695453834	0.00056197	ind_vs_ctr.1h_ind_vs_ctr.3h_ind_vs_ctr.6h_ind_vs_ctr.12h	glyceraldehyde-3-phosphate dehydrogenase Tdh1	SPBC354.12,SPBC32F12.11	YGR192C,YIR009C,YIL052W
SIAG_01029	10.32376639	1.202901073	-1.361090834	-1.461193222	-2.2319618	5.30E-06	ind_vs_ctr.1h_ind_vs_ctr.3h_ind_vs_ctr.6h_ind_vs_ctr.12h	alpha-amylase Aah2	SPAC23D3.14c	
SIAG_04042	10.90099939	1.277352404	-2.059178747	-1.954788549	-1.830665318	1.09E-05	ind_vs_ctr.1h_ind_vs_ctr.3h_ind_vs_ctr.6h_ind_vs_ctr.12h	FAD binding protein	SPAC1783.01	YPR048W
SIAG_04823	11.22123555	1.334009187	-1.34813366	-1.492317008	-1.497117317	0.000365614	ind_vs_ctr.1h_ind_vs_ctr.3h_ind_vs_ctr.6h_ind_vs_ctr.12h	catalase	SPCC757.07c	YDR256C
SIAG_02142	11.63076607	1.28872228	-2.414685865	-1.820716344	-1.34187818	6.13E-05	ind_vs_ctr.1h_ind_vs_ctr.3h_ind_vs_ctr.6h_ind_vs_ctr.12h	cytochrome b2		
SIAG_02107	12.21511602	1.509899686	2.327612096	1.552003174	1.45595423	0.000697254	ind_vs_ctr.1h_ind_vs_ctr.3h_ind_vs_ctr.6h_ind_vs_ctr.12h	enolase	SPBC1815.01	YPL281C,YMR323W,YOR393W
SIAG_04608	12.33508649	1.226017825	-1.677492732	-2.109592939	-2.436582299	7.01E-07	ind_vs_ctr.1h_ind_vs_ctr.3h_ind_vs_ctr.6h_ind_vs_ctr.12h	flavin dependent monooxygenase	SPBP16F5.08c	YHR176W
SIAG_00308	12.46227407	1.302023214	-1.791277344	-2.699400507	-1.507817979	2.75E-07	ind_vs_ctr.1h_ind_vs_ctr.3h_ind_vs_ctr.6h_ind_vs_ctr.12h	peptide release factor	SPBC1105.18c	YLR281C
SIAG_01432	12.59685352	1.574260835	-1.724514397	-1.520344156	-2.382076284	6.13E-05	ind_vs_ctr.1h_ind_vs_ctr.3h_ind_vs_ctr.6h_ind_vs_ctr.12h	hydroxyacid dehydrogenase	SPACUNK4.10	
SIAG_03475	12.67097248	1.713437472	2.806489098	2.744956506	1.667310045	7.40E-06	ind_vs_ctr.1h_ind_vs_ctr.3h_ind_vs_ctr.6h_ind_vs_ctr.12h	sulfate adenylyltransferase	SPBC27.08c	YJR010W
SIAG_03815	12.71460048	1.726417572	-2.291506834	-1.455387139	1.479205923	0.000335759	ind_vs_ctr.1h_ind_vs_ctr.3h_ind_vs_ctr.6h_ind_vs_ctr.12h	hsp16-like protein	SPBC3E7.02c	
SIAG_04658	12.82918494	1.597047059	-3.246197737	-4.930094122	-3.539058397	2.27E-07	ind_vs_ctr.1h_ind_vs_ctr.3h_ind_vs_ctr.6h_ind_vs_ctr.12h	methyltransferase	SPCC70.08c	
SIAG_01985	12.97752514	-1.560070584	2.66524329	2.35240351	1.968458543	5.59E-05	ind_vs_ctr.1h_ind_vs_ctr.3h_ind_vs_ctr.6h_ind_vs_ctr.12h	hypothetical protein		
SIAG_00635	13.15829127	1.411063824	-1.755793616	-1.908311083	-2.449089315	3.04E-06	ind_vs_ctr.1h_ind_vs_ctr.3h_ind_vs_ctr.6h_ind_vs_ctr.12h	ornithine carbamoyltransferase Arg3	SPAC469.10	YIL088W
SIAG_03608	13.40914511	-1.375689111	1.271200449	2.294956586	1.593305817	5.98E-05	ind_vs_ctr.1h_ind_vs_ctr.3h_ind_vs_ctr.6h_ind_vs_ctr.12h	hexose transporter Ght5	SPCC548.06c,SPCC1235.14,SPCC548.07c	
SIAG_04577	14.69280875	1.273958126	-1.605172566	-1.938026633	-2.748779778	7.01E-07	ind_vs_ctr.1h_ind_vs_ctr.3h_ind_vs_ctr.6h_ind_vs_ctr.12h	argininosuccinate synthase	SPBC428.05c	YOL058W
SIAG_03312	14.99385405	1.309088097	-1.236584407	-1.500605863	-2.368399208	2.95E-05	ind_vs_ctr.1h_ind_vs_ctr.3h_ind_vs_ctr.6h_ind_vs_ctr.12h	aromatic aminotransferase	SPAC56E4.03,SPCC569.07,SPBC1773.13	YGL202W
EFISIAG0000000	7.157878011	-1.402876885	-1.14477354	-4.6555803	-1.634382451	0.002590447	ind_vs_ctr.1h_ind_vs_ctr.6h	U2 spliceosomal RNA [Source:RFAM;Acc:RF00004]		
SIAG_01095	6.598815068	-1.431300212	-1.477939292	-5.386413252	-3.381268085	4.56E-05	ind_vs_ctr.1h_ind_vs_ctr.6h_ind_vs_ctr.12h	hypothetical protein	SPAC17G6.02c	YOR049C
EFISIAG0000000	7.784125861	-1.395649939	-1.1477112	-4.466264469	-2.141572719	0.001159263	ind_vs_ctr.1h_ind_vs_ctr.6h_ind_vs_ctr.12h	U2 spliceosomal RNA [Source:RFAM;Acc:RF00004]		
EFISIAG0000000	8.129275137	-1.427254192	1.100691474	-14.50298142	-11.01328159	0.000147563	ind_vs_ctr.1h_ind_vs_ctr.6h_ind_vs_ctr.12h	U1 spliceosomal RNA [Source:RFAM;Acc:RF00003]		
EFISIAG0000000	9.664008188	-1.256270039	-1.087110949	-2.351269452	-1.939530959	0.005136942	ind_vs_ctr.1h_ind_vs_ctr.6h_ind_vs_ctr.12h	Nuclear RNase P [Source:RFAM;Acc:RF00009]		
SIAG_02568	10.27745684	1.915640845	1.034794575	2.054272824	1.542905632	0.00239627	ind_vs_ctr.1h_ind_vs_ctr.6h_ind_vs_ctr.12h	hypothetical protein		
SIAG_01363	10.41634745	1.41583219	-1.212563264	-2.205870958	-1.598316585	0.00010525	ind_vs_ctr.1h_ind_vs_ctr.6h_ind_vs_ctr.12h	trichothecene 3-O-acetyltransferase		YLL063C
SIAG_00310	11.83229825	1.551471651	1.053982148	2.031867573	2.12217869	7.31E-07	ind_vs_ctr.1h_ind_vs_ctr.6h_ind_vs_ctr.12h	mannan endo-1,6-alpha-mannosidase DCW1	SPBC1198.07c	
SIAG_00691	11.91292895	-1.260768306	-1.204083628	-2.073150951	-1.28441754	0.00067901	ind_vs_ctr.1h_ind_vs_ctr.6h_ind_vs_ctr.12h	glutamine aminotransferase subunit	SPAC222.08c	YMR095C,YNL334C,YFL060C
SIAG_03420	12.33752775	1.44594968	-1.161786637	-1.807592718	-3.229295956	8.23E-06	ind_vs_ctr.1h_ind_vs_ctr.6h_ind_vs_ctr.12h	hypothetical protein		
SIAG_06614	5.975810634	-1.104517284	-2.858175781	-1.105299637	-1.448908963	0.036091662	ind_vs_ctr.3h	hypothetical protein		
SIAG_06256	6.682314135	1.233652054	-2.521934356	-1.344439523	1.15345915	0.026941305	ind_vs_ctr.3h	hypothetical protein	SPCC1620.03	
SIAG_01690	7.293271502	1.556511873	2.083255728	-1.859046269	1.055032907	0.036501191	ind_vs_ctr.3h	NADP-dependent L-serine/L-allo-threonine dehydrogenase	SPAC521.03	
SIAG_03432	8.70383332	1.04434275	-2.529049918	-1.144827664	1.352140161	0.037786945	ind_vs_ctr.3h	WDR44 family WD repeat protein	SPBC18H10.05	YMR102C,YKL121W
SIAG_03830	9.262897999	1.054981367	-2.588782843	-1.498818424	1.190791181	0.022334859	ind_vs_ctr.3h	hypothetical protein		
SIAG_06471	10.76023985	1.188315939	-2.720410999	-1.525747608	-1.080453101	0.032746405	ind_vs_ctr.3h	hypothetical protein		
SIAG_00165	11.68369565	1.337022454	-2.492976034	-1.092775352	1.41582772	0.020982096	ind_vs_ctr.3h	hypothetical protein		
SIAG_04072	11.77711993	1.140869148	-2.585566668	-1.281663577	1.003403511	0.01031466	ind_vs_ctr.3h	hypothetical protein	SPBC11C11.06c	
SIAG_03132	12.55257192	-1.087512982	-2.417372057	-1.567862304	-1.141860233	0.048065637	ind_vs_ctr.3h	ribonuclease II family protein	SPBC609.01	YDR293C
SIAG_03253	12.64555587	1.270810296	-2.631827803	-1.543349959	-1.026928208	0.007293895	ind_vs_ctr.3h	hypothetical protein	SPAC19A8.16	
SIAG_02230	12.92380354	1.046400142	-2.175719283	-1.210149789	1.126900808	0.022976164	ind_vs_ctr.3h	phosphoketolase	SPBC24C6.09c	

Annexe 3: Early timepoint analysis

SIAG_02696	13.5034216	1.082094914	-2.812048513	-1.564850103	-1.045920207	0.005862572	ind_vs_ctr.3h	glucose-6-phosphate 1-dehydrogenase	SPAC3C7.13c	
SIAG_04567	13.6182695	1.519123469	-2.369608688	-1.274787598	1.264867117	0.009623574	ind_vs_ctr.3h	hsp16-like protein	SPBC3E7.02c	
SIAG_04764	13.76023711	-1.174508957	-2.289946728	-1.504820216	-1.086629292	0.023298261	ind_vs_ctr.3h	hypothetical protein		
SIAG_05005	13.88511295	-1.131820355	-2.493538081	-1.493049098	-1.106691947	0.00852869	ind_vs_ctr.3h	fungus protein	SPAC32A11.02c	
SIAG_00625	14.25658823	1.232284762	-2.868458051	-1.610711294	-1.128796046	0.001818829	ind_vs_ctr.3h	hypothetical protein		
SIAG_03824	11.39123817	1.515315198	-3.543306181	1.120499248	1.966149493	0.015666738	ind_vs_ctr.3h_ind_vs_ctr.12h	alpha-glucosidase	SPAC30D11.01c,SPAPB24D3.10c,SPAC1039.11c	
SIAG_00709	5.21121814	-1.472632324	2.80300347	3.27250527	1.741482696	0.022172487	ind_vs_ctr.3h_ind_vs_ctr.6h	hypothetical protein		
SIAG_00708	5.59202663	1.416001734	1.822147526	2.591474495	1.69427268	0.023409003	ind_vs_ctr.3h_ind_vs_ctr.6h	hypothetical protein		
SIAG_06595	5.977270825	-1.094233541	-4.744366252	-2.778453845	-1.8143788	0.002303671	ind_vs_ctr.3h_ind_vs_ctr.6h	hypothetical protein		
SIAG_02047	8.381754917	1.090693146	2.306507865	2.701324663	-1.231419501	5.59E-05	ind_vs_ctr.3h_ind_vs_ctr.6h	TENA/THI domain-containing protein	SPBC530.07c	
SIAG_01742	8.553774758	-1.190018016	4.109657872	4.941060656	1.349445221	9.99E-05	ind_vs_ctr.3h_ind_vs_ctr.6h	TENA/THI domain-containing protein	SPBC530.07c	
SIAG_01845	8.657344881	1.09626945	-1.922592942	-2.54284401	1.012262813	0.001284078	ind_vs_ctr.3h_ind_vs_ctr.6h	glutamine synthetase		
SIAG_04167	10.62563989	-1.269609655	-2.575244612	-1.826971594	-1.518525466	0.031591735	ind_vs_ctr.3h_ind_vs_ctr.6h	P-type ATPase	SPBC839.06	
SIAG_04359	10.73830358	1.110329576	-2.389680561	-1.44218899	-1.035694822	0.001104184	ind_vs_ctr.3h_ind_vs_ctr.6h	cytoplasm protein	SPAC6G10.06	YHR009C
SIAG_04450	10.79968357	-1.0396112	-2.773052198	-1.728076136	1.015678842	0.018196791	ind_vs_ctr.3h_ind_vs_ctr.6h	fungus protein	SPBC3H7.08c	
SIAG_00084	11.16302464	1.085682758	2.225286017	1.493314378	1.102844715	0.00164368	ind_vs_ctr.3h_ind_vs_ctr.6h	adenylyl-sulfate kinase	SPAC1782.11	YKL001C
SIAG_04861	11.91290085	1.310524144	-2.141030917	-1.518965003	-1.069857578	0.003654472	ind_vs_ctr.3h_ind_vs_ctr.6h	hypothetical protein		
SIAG_00223	12.18873143	1.46684683	-2.717672797	-1.726285433	-1.229649155	0.006254341	ind_vs_ctr.3h_ind_vs_ctr.6h	hsp9-like protein	SPAP8A3.04c	
SIAG_04625	12.20854933	1.289743955	-2.143979081	-1.544941689	-1.202257691	0.001330464	ind_vs_ctr.3h_ind_vs_ctr.6h	DUF1761 family protein	SPAC15E1.02c	
SIAG_02122	12.23685165	1.312513449	-2.655189326	-2.256837465	-1.110136085	0.000320976	ind_vs_ctr.3h_ind_vs_ctr.6h	hypothetical protein		
SIAG_00788	12.27890819	1.061418967	-2.696119987	-2.064936329	-1.094733262	0.026250743	ind_vs_ctr.3h_ind_vs_ctr.6h	hypothetical protein		
SIAG_03509	12.52063563	1.196567778	-2.809557922	-2.473036298	-1.27006237	1.57E-05	ind_vs_ctr.3h_ind_vs_ctr.6h	C-5 sterol desaturase Erg32	SPBC27B12.03c	
SIAG_04243	12.58402155	1.182944641	-2.278645813	-1.672041482	-1.033027475	0.008619351	ind_vs_ctr.3h_ind_vs_ctr.6h	hypothetical protein	SPCC1393.12	
SIAG_01869	13.12019063	1.265368677	-2.019608828	-1.617340126	1.009373889	0.000476476	ind_vs_ctr.3h_ind_vs_ctr.6h	NADH/NADPH dependent indole-3-acetaldehyde reductase	SPAC19G12.09	
SIAG_01084	13.22633485	-1.195945328	-2.176163968	-1.573440128	-1.281338745	0.003549077	ind_vs_ctr.3h_ind_vs_ctr.6h	CAMK/CAMK1 protein kinase Srk1	SPCC1322.08	YLR248W,YGL158W
SIAG_02744	13.24368864	1.247983436	-2.155222805	-1.657969633	-1.192216678	0.000643625	ind_vs_ctr.3h_ind_vs_ctr.6h	cytochrome c	SPCC191.07	YJR048W,YEL039C
SIAG_01815	13.2699323	1.318748106	-2.502160482	-1.962794481	-1.066586595	0.000171951	ind_vs_ctr.3h_ind_vs_ctr.6h	hypothetical protein		
SIAG_00487	13.74397891	1.124704525	-2.972447835	-2.286844006	-1.068568184	0.000224531	ind_vs_ctr.3h_ind_vs_ctr.6h	SBDS family protein Rtc3	SPBC21C3.19	
SIAG_02442	14.98709973	1.164250934	-2.729080335	-1.916460786	-1.205460683	0.005316321	ind_vs_ctr.3h_ind_vs_ctr.6h	hypothetical protein		
SIAG_03743	15.78901437	1.236010225	-2.575237047	-2.062021262	-1.051969067	0.001538873	ind_vs_ctr.3h_ind_vs_ctr.6h	pyruvate decarboxylase	SPAC13A11.06	YLR134W,YLR044C,YDL080C,YGR087C
SIAG_03778	3.730500873	-1.040721003	-2.883588466	-5.141626648	-3.549444291	0.00891581	ind_vs_ctr.3h_ind_vs_ctr.6h_ind_vs_ctr.12h	hypothetical protein		
SIAG_00216	6.118195824	1.039882652	-1.878262044	-3.513533828	-3.263983121	0.000404945	ind_vs_ctr.3h_ind_vs_ctr.6h_ind_vs_ctr.12h	trichothecene 3-O-acetyltransferase	YLL063C	
SIAG_00025	6.606099517	1.067804276	-1.629113915	-2.326943886	-1.627969328	0.004934391	ind_vs_ctr.3h_ind_vs_ctr.6h_ind_vs_ctr.12h	hypothetical protein		
SIAG_01971	9.109939448	1.206924321	-2.272853212	-1.454436933	1.215537732	0.001298126	ind_vs_ctr.3h_ind_vs_ctr.6h_ind_vs_ctr.12h	DNA-3-methyladenine glycosylase Mag1	SPAPB24D3.04c	YER142C
SIAG_00981	9.239488761	-1.358430688	-1.568924071	-2.255703305	-3.709877202	0.001209727	ind_vs_ctr.3h_ind_vs_ctr.6h_ind_vs_ctr.12h	fungus cellulose binding domain-containing protein	SPAC2E1P3.05c	
SIAG_02946	9.645524153	1.008776581	-1.645777015	-3.96532412	-3.200679784	0.0001206	ind_vs_ctr.3h_ind_vs_ctr.6h_ind_vs_ctr.12h	amino acid permease	SPBPB2B2.01	YLL061W,YOL020W,YCL025C,YBR069C,YDR046C,YPL274W,YBR068C,YDR508C
SIAG_00262	10.61300442	1.093116149	-1.583173613	-2.323480712	-1.832608576	1.66E-05	ind_vs_ctr.3h_ind_vs_ctr.6h_ind_vs_ctr.12h	F-box protein	SPAPB1A10.14	
SIAG_04866	11.06470932	1.542010418	1.871604972	3.027635951	-1.61544683	0.001209727	ind_vs_ctr.3h_ind_vs_ctr.6h_ind_vs_ctr.12h	hypothetical protein	SPCC1223.02	YJR156C,YNL323W,YDL244W,YFL058W
SIAG_04787	11.0943296	-1.012148429	-1.522007517	-2.09844201	-1.880560001	4.70E-05	ind_vs_ctr.3h_ind_vs_ctr.6h_ind_vs_ctr.12h	PQ loop protein	SPAC2E12.03c	YDR090C
SIAG_01911	11.30125911	1.088719695	-2.077087933	-2.621935423	-2.251390529	7.40E-06	ind_vs_ctr.3h_ind_vs_ctr.6h_ind_vs_ctr.12h	hexaprenyldihydroxybenzoate methyltransferase	SPBC1347.09	
SIAG_04828	11.56406644	1.074572773	-1.954416306	-2.928004661	-2.29826406	2.79E-05	ind_vs_ctr.3h_ind_vs_ctr.6h_ind_vs_ctr.12h	membrane transporter	SPCC757.11c	
SIAG_03652	11.64767133	-1.229931393	2.030009991	1.649622343	-1.676686728	0.000644663	ind_vs_ctr.3h_ind_vs_ctr.6h_ind_vs_ctr.12h	high-affinity import carrier for pyridoxine	SPAC17A2.01	
SIAG_04983	11.69233683	-1.033355783	-1.426150158	-2.288481693	-1.99678151	0.000206826	ind_vs_ctr.3h_ind_vs_ctr.6h_ind_vs_ctr.12h	inner membrane transport protein yieO	SPBC16A3.17c	
SIAG_03288	13.27064827	1.184357894	-1.37544626	-1.757086054	-2.081875349	6.13E-05	ind_vs_ctr.3h_ind_vs_ctr.6h_ind_vs_ctr.12h	N-acetyltransferase Ats1	SPAC1002.07c	
SIAG_05889	13.48841746	1.031743053	-2.213100464	-2.254253111	-1.578554046	2.75E-07	ind_vs_ctr.3h_ind_vs_ctr.6h_ind_vs_ctr.12h	hypothetical protein		
EFSAAG0000000	2.370573693	-1.074779882	-1.830745074	-5.972155847	-3.182925883	0.04346624	ind_vs_ctr.6h	ACEA small nucleolar RNA U3 [Source:RFAM;Acc:RF01848]		
EFSAAG0000000	6.225302842	-1.343536006	-1.333083949	-3.617210919	-2.472223512	0.034141372	ind_vs_ctr.6h	U4 spliceosomal RNA [Source:RFAM;Acc:RF00015]		
SIAG_02113	7.273189375	1.028778957	-1.396251208	-2.088224335	-1.011822655	0.027785829	ind_vs_ctr.6h	amino acid permease	SPAC1039.01,SPCC74.04	
EFSAAG0000000	7.591716697	1.312500611	-1.231574002	-2.101558353	-1.227863568	0.031591735	ind_vs_ctr.6h	Small nucleolar RNA Z13/snR52 [Source:RFAM;Acc:RF00335]		
SIAG_00587	8.637397834	1.161750176	1.06162534	-2.513639217	-2.494337416	0.047446059	ind_vs_ctr.6h	sphingoid long-chain base transporter RSB1	SPAC17G6.02c	YOR049C
EFSAAG0000000	9.774403971	1.134197815	-1.199991038	-2.571382655	-1.434584048	0.02141596	ind_vs_ctr.6h	small nucleolar RNA snR3 [Source:RFAM;Acc:RF01434]		
SIAG_04048	13.2362684	1.015470882	-1.644910376	1.985199624	2.037975639	0.047446059	ind_vs_ctr.6h	glycerol dehydrogenase Gld1	SPAC13F5.03c	
SIAG_03446	5.591852215	1.429534451	-1.719501054	-2.450743649	-3.736897232	0.009623574	ind_vs_ctr.6h_ind_vs_ctr.12h	hypothetical protein		
SIAG_03099	5.79411401	1.620890721	-1.347874229	2.692386458	1.857818535	0.012694958	ind_vs_ctr.6h_ind_vs_ctr.12h	hypothetical protein	SPBC30D10.21	
SIAG_01096	6.216302043	-1.041568235	-1.265389153	-3.554392892	-2.55583082	0.009883384	ind_vs_ctr.6h_ind_vs_ctr.12h	amino acid permease	SPAC1039.01,SPCC74.04	
SIAG_00658	8.709902053	-1.184198806	1.451133746	2.048474109	1.892139067	0.001256208	ind_vs_ctr.6h_ind_vs_ctr.12h	hypothetical protein		
SIAG_02515	9.844899934	1.153365613	-1.129005752	-1.647045875	-3.699226046	0.000278024	ind_vs_ctr.6h_ind_vs_ctr.12h	thioredoxin peroxidase	SPBC1773.02c	YIL010W

Annexe 3: Early timepoint analysis

EFSJAG000000	10.32742154	-1.062007983	-1.101799919	-2.083027607	1.296748186	6.14E-05	ind_vs_ctr.6h_ind_vs_ctr.12h
SJAG_02834	11.26696073	-1.243677896	-1.333079421	-1.850111122	-2.142494681	0.029028073	ind_vs_ctr.6h_ind_vs_ctr.12h
SJAG_00493	11.34145563	1.178299848	-1.117512711	-1.456717693	-2.232949678	0.000295365	ind_vs_ctr.6h_ind_vs_ctr.12h
SJAG_03818	11.40149271	-1.023204217	-1.525134475	1.826314146	3.630900431	0.001201662	ind_vs_ctr.6h_ind_vs_ctr.12h
SJAG_04905	11.43072069	-1.17610783	1.01922042	-2.292513357	-3.50980132	2.29E-06	ind_vs_ctr.6h_ind_vs_ctr.12h
SJAG_02150	12.58454763	-1.046216546	1.042382673	-1.432250103	-2.038492438	0.001045289	ind_vs_ctr.6h_ind_vs_ctr.12h
SJAG_00923	13.2156073	-1.285729055	-1.149623491	-2.80107221	-1.775160875	1.57E-05	ind_vs_ctr.6h_ind_vs_ctr.12h
SJAG_00885	14.11131168	-1.126761809	1.040145166	-1.398309507	-2.082666049	0.000138526	ind_vs_ctr.6h_ind_vs_ctr.12h
SJAG_03398	14.31908034	1.133046621	-1.111345338	-1.452062095	-2.114133846	8.86E-05	ind_vs_ctr.6h_ind_vs_ctr.12h

Small nucleolar RNA SNORD14 [Source:RFAM;Acc:RF00016]		
siderophore iron transporter 1	SPBC4F6.09	YOL158C
fumarylacetoacetate hydrolase	SPBC21C3.09c	YNL168C
gal10		
hexose transporter Ght6	SPAC1F8.01, SPBC1683.08	
amino acid permease inda1		YLL061W, YOL020W, YCL025C, YBR069C, YDR046C, YPL274W, YBR068C, YDR508C
CobW/HypB/UreG nucleotide binding domain-containing pr	SPBC15D4.05	YNR029C
ribonucleotide reductase small subunit Suc22	SPBC25D12.04	YJL026W
arginase	SPBP26C9.02c, SPAC3H1.07	YPL111W

Annexe 4: Late timepoint analysis

Gene_ID	AveExpr	log2Exp_induced	log2Exp_control	logFC	P.Value	adj.P.Val	Fold_Change	Description
SJAG_02132	4.238600296	2.686125015	5.752848293	-3.066723278	0.000291231	0.003318725	-8.378681757	hypothetical protein
SJAG_01589	6.520242264	3.021845726	5.279068742	-2.257223016	0.006033304	0.040479436	-4.780703777	tricarboxylate transporter
SJAG_00809	8.564664262	6.207909169	8.460598794	-2.252689625	0.000196715	0.002380794	-4.765704914	DNA replication protein Dre4
SJAG_04303	9.118620279	8.040337147	10.28435819	-2.244021043	8.34E-06	0.000169032	-4.737155542	meiotic recombination protein Rec25
SJAG_03526	14.32839235	12.44629428	14.65830256	-2.212008281	0.000921523	0.008864294	-4.633197818	Lsd90 protein
SJAG_02515	10.31968023	6.943549209	8.963335098	-2.019785889	4.50E-05	0.000687106	-4.055236035	thioredoxin peroxidase
SJAG_03331	9.14897182	7.90087542	9.911994486	-2.011119066	4.00E-07	1.34E-05	-4.030947703	hypothetical protein
SJAG_05182	12.33511244	7.942545383	9.861006732	-1.918461349	0.000798324	0.007830645	-3.780196812	allantoate permease
SJAG_04603	8.504337712	7.235537695	9.09454788	-1.859010185	0.000182166	0.002223485	-3.627586925	inner membrane protein
SJAG_01622	11.38140691	9.021451496	10.86912944	-1.847677944	1.43E-10	1.94E-08	-3.599204171	RSC complex subunit Rsc9
SJAG_04580	13.47661446	10.40279561	12.21753161	-1.814736	5.09E-06	0.000112508	-3.517952491	2-OG-Fe(II) oxygenase superfamily protein
SJAG_04711	16.16961028	11.78320712	13.57529432	-1.792087202	1.97E-07	7.29E-06	-3.463155583	GTP cyclohydrolase II
SJAG_01451	9.417167857	7.521370873	9.300836776	-1.779465903	5.48E-07	1.73E-05	-3.43299059	hypothetical protein
SJAG_01093	4.672683718	7.980218339	9.61267954	-1.632461201	4.44E-06	9.98E-05	-3.100414707	hypothetical protein
SJAG_00715	10.13008666	8.425682178	9.992353464	-1.566671286	2.26E-07	8.18E-06	-2.96220459	hypothetical protein
SJAG_06622	16.05570885	13.82152038	15.37707567	-1.55555287	1.22E-07	4.83E-06	-2.939468438	glyceraldehyde-3-phosphate dehydrogenase Tdh1
SJAG_05196	10.6932764	9.02006267	10.54942771	-1.529365035	2.41E-07	8.59E-06	-2.886587655	spindle pole body protein Sad1
SJAG_05231	8.643341873	6.554513734	8.079579981	-1.525066247	0.000199625	0.002413617	-2.877999312	CMGC/SRPK protein kinase
SJAG_06621	12.43793422	10.29196581	11.79828002	-1.506314206	0.000146399	0.001863429	-2.840833358	glyceraldehyde-3-phosphate dehydrogenase Tdh1
SJAG_01169	13.4130492	12.74237051	14.2193934	-1.477022891	2.67E-09	2.04E-07	-2.783736953	RNA-binding protein Mrd1
SJAG_00524	9.725094044	7.243657696	8.720528825	-1.47687113	0.000253617	0.002969219	-2.783444139	prefoldin subunit 4
SJAG_04575	10.55064448	10.08684168	11.55502869	-1.468187015	7.24E-07	2.17E-05	-2.766739883	meiotic chromosome segregation protein Meu6
SJAG_04301	14.51698145	13.59381844	15.02995565	-1.436137211	0.002436546	0.019698441	-2.705953807	invertase
SJAG_00987	11.1305815	9.32553824	10.75899815	-1.433459912	4.79E-06	0.000106869	-2.700936855	MBF transcription factor complex subunit Res2
SJAG_02332	10.78458905	9.880740236	11.31279479	-1.432054555	3.42E-05	0.000548416	-2.698307102	spindle pole body protein Cut12
SJAG_02997	10.91017334	8.563370946	9.981352841	-1.417981895	0.000151286	0.001911658	-2.672114624	peroxin-6
SJAG_01764	13.38810791	12.69705228	14.10921944	-1.412167158	2.40E-09	1.88E-07	-2.661366424	U3 snoRNP-associated protein Nan1
SJAG_00139	13.45026383	12.4227188	13.83053576	-1.407816959	2.62E-09	2.02E-07	-2.653353618	RNA polymerase II associated Paf1 complex subunit Tpr1
SJAG_04558	10.85517158	9.636063243	11.02864762	-1.392584376	2.80E-05	0.000463849	-2.62548577	spindle pole body protein Kms2
SJAG_02084	12.34530733	11.57711763	12.95823549	-1.381117861	1.08E-06	3.09E-05	-2.604701162	moeb/ThiF domain-containing protein
SJAG_04126	11.67027341	10.20190834	11.57190426	-1.369995928	1.41E-07	5.47E-06	-2.584698365	TTK protein kinase Mph1
SJAG_01664	16.91236804	16.17785256	17.54636836	-1.368515796	6.92E-08	3.01E-06	-2.582047957	hsp90-like protein
SJAG_02720	11.98748249	10.68726261	12.05533093	-1.368068322	2.00E-10	2.51E-08	-2.581247219	poly(A) polymerase Pla1
SJAG_02446	10.22737465	8.793049276	10.15121312	-1.358163848	2.02E-06	5.12E-05	-2.56358698	glucosidase
SJAG_02150	12.86579835	8.641937166	9.994073248	-1.352136082	0.001627373	0.014216222	-2.552898328	amino acid permease inda1
SJAG_03370	16.57089462	15.18032929	16.52745028	-1.347120991	2.58E-07	9.13E-06	-2.54403936	alcohol dehydrogenase Adh1

Annexe 4: Late timepoint analysis

SJAG_02733	9.430299284	6.92920636	8.27570306	-1.346496701	0.00011246	0.001488357	-2.542938728	chitin synthase regulatory factor Chr2
SJAG_00141	11.88275781	9.290133198	10.63479904	-1.344665843	3.68E-06	8.53E-05	-2.539713648	neddylation pathway protein But1
SJAG_04318	10.90870137	9.100336414	10.44360478	-1.343268368	1.38E-08	7.92E-07	-2.537254731	splicing factor Sap114
SJAG_05257	7.473118674	6.727897754	8.069747673	-1.341849919	0.001186325	0.010957431	-2.534761344	DNA-3-methyladenine glycosidase Mag2
SJAG_02776	10.06856375	8.243476489	9.578127427	-1.334650938	0.000207018	0.00248738	-2.522144507	pig-U
SJAG_04713	13.36041116	10.13166493	11.46556913	-1.333904206	1.78E-05	0.000315892	-2.520839395	uracil phosphoribosyltransferase
SJAG_01380	8.816197184	7.278673264	8.60668557	-1.328012305	0.000474548	0.005029182	-2.510565396	RNA-binding protein
SJAG_01936	12.28665913	11.98355146	13.3084816	-1.324930145	2.04E-11	4.06E-09	-2.505207573	SMR domain-containing protein
SJAG_02445	8.322091594	6.875267481	8.187109667	-1.311842186	0.004905317	0.034437527	-2.482583403	hypothetical protein
SJAG_00882	14.04279833	12.55938346	13.87049365	-1.311110194	1.67E-08	9.20E-07	-2.481324114	pescadillo-family BRCT domain-containing protein
SJAG_02143	12.53340931	11.16736114	12.47504543	-1.307684289	2.69E-08	1.36E-06	-2.475438812	hypothetical protein
SJAG_04718	11.28098642	8.382073052	9.68763619	-1.305563138	0.000435838	0.004679974	-2.471801923	proline specific permease
SJAG_02252	11.89513006	8.737185028	10.04170118	-1.30451615	0.000186447	0.00227232	-2.470008745	transcription factor Ace2
SJAG_04862	10.88860988	9.180370568	10.4846391	-1.304268533	9.35E-05	0.001277614	-2.469584842	translation elongation factor G
SJAG_04145	12.24694511	10.15569761	11.45593255	-1.300234938	9.58E-09	5.75E-07	-2.462689835	alanine aminotransferase
SJAG_05185	8.048087392	8.325124845	9.608066571	-1.282941726	0.000255742	0.002984061	-2.433346426	actin-like protein Arp10
SJAG_00042	8.537681163	6.680193407	7.962565242	-1.282371835	0.00422861	0.030612523	-2.4323854	hypothetical protein
SJAG_01001	10.30303036	7.657508822	8.939538859	-1.282030037	0.000303336	0.003437381	-2.431809196	Erd1
SJAG_00440	10.48220262	8.855569723	10.13702937	-1.281459648	9.68E-06	0.000192406	-2.430847937	RSC complex subunit Rsc4
SJAG_02059	14.26816375	14.56683121	15.84044438	-1.273613168	3.89E-08	1.83E-06	-2.417663013	spermidine family transporter
SJAG_01352	13.7967837	11.78066329	13.04332668	-1.262663394	1.58E-07	6.03E-06	-2.399382881	cytoplasmic glycine-tRNA ligase Grs1
SJAG_04462	10.39203061	9.202317574	10.46172876	-1.259411188	9.61E-05	0.001304959	-2.393980146	rho-type GTPase activating protein Rga5
SJAG_02419	12.63595431	10.42511608	11.68276493	-1.257648851	6.64E-08	2.90E-06	-2.391057544	ubiquitin carboxy terminal hydrolase Ubp3
SJAG_02180	17.73183936	16.81537598	18.07079156	-1.255415583	1.87E-05	0.000328315	-2.387359091	translation elongation factor EF-1 alpha Ef1a-c
SJAG_04995	8.685474677	6.739251705	7.990585574	-1.25133387	0.004685467	0.033197082	-2.380614253	DNA replication checkpoint protein Drc1
SJAG_04789	9.540458075	8.704039958	9.953459466	-1.249419508	0.00050029	0.005254015	-2.377457429	alpha-amylase Aah4
SJAG_03777	13.78215805	13.08004354	14.32237973	-1.242336192	1.31E-08	7.54E-07	-2.365813243	transmembrane transporter
SJAG_01707	11.76820534	10.42992985	11.66389822	-1.233968371	1.73E-08	9.45E-07	-2.352130933	transcription elongation regulator
SJAG_00913	11.5428418	10.48404136	11.71561268	-1.231571316	2.22E-08	1.17E-06	-2.348226085	hira protein
SJAG_02118	10.92378305	9.670086472	10.90078696	-1.23070049	4.40E-07	1.46E-05	-2.346809098	pheromone-regulated membrane protein
SJAG_00102	11.00548236	9.10375313	10.32964004	-1.22588691	8.69E-05	0.001209665	-2.338991972	N-myristoyltransferase 1
SJAG_03606	15.33650939	14.70087491	15.92562511	-1.224750193	0.004729189	0.033441825	-2.337149778	hexose transporter Ght6
SJAG_03668	9.946695858	8.914785826	10.12859329	-1.213807461	9.82E-06	0.000193671	-2.319489734	SAGA complex subunit Spt3
SJAG_01440	10.99154739	9.720423479	10.93286535	-1.212441875	2.26E-06	5.65E-05	-2.317295255	U1 snRNP-associated protein Usp109
SJAG_00875	12.03810184	10.88323026	12.09461712	-1.211386857	1.39E-09	1.22E-07	-2.315601276	SCY1 protein kinase Ppk32
SJAG_01965	12.65545984	9.121632402	10.33032221	-1.208689806	0.001238055	0.011359641	-2.311276413	hypothetical protein
SJAG_02922	12.08218111	11.57106314	12.77682038	-1.205757242	7.92E-09	4.89E-07	-2.306583056	myb family protein Eta2

Annexe 4: Late timepoint analysis

SJAG_04677	15.59486738	13.01510736	14.22049895	-1.205391591	2.06E-08	1.09E-06	-2.305998526 iron transport multicopper oxidase Fio1
SJAG_04068	15.33396172	11.64691402	12.8480704	-1.201156379	0.006613376	0.043509051	-2.299238906 high-affinity fructose transporter ght6
SJAG_01185	12.70713281	11.50557135	12.70455932	-1.198987967	1.94E-07	7.23E-06	-2.295785679 nucleoporin Npp106
SJAG_01699	12.57480127	11.02884881	12.22746013	-1.198611317	3.31E-05	0.00053422	-2.295186388 G-protein coupled receptor Git3
SJAG_01298	16.74372403	16.63766399	17.83571382	-1.198049837	1.74E-09	1.46E-07	-2.294293301 IMP dehydrogenase Gua1
SJAG_03633	10.36675735	8.02955538	9.227263379	-1.197708	8.76E-06	0.000175957	-2.293749748 inner membrane translocase Oxa102
SJAG_00886	11.71336217	11.06248047	12.26010019	-1.197619719	1.12E-06	3.17E-05	-2.293609395 N2,N2-dimethylguanosine tRNA methyltransferase
SJAG_01026	12.65648184	11.28558432	12.47944443	-1.19386011	2.08E-06	5.26E-05	-2.287640115 RNA-binding protein
SJAG_04943	10.85900301	9.292662807	10.485802	-1.193139197	5.49E-07	1.73E-05	-2.28649727 two-component GAP Byr4
SJAG_04456	10.25602799	8.918247354	10.10922603	-1.190978679	2.62E-06	6.42E-05	-2.283075674 BRCT domain-containing protein
SJAG_04424	13.00083008	11.38448741	12.56936504	-1.184877636	3.98E-08	1.86E-06	-2.273441114 U3 snoRNP protein Utp14
SJAG_03267	10.8297962	9.626960816	10.80821585	-1.181255034	1.20E-05	0.000227135	-2.267739672 tel Two Interacting protein 1
SJAG_03846	14.03753946	13.4480877	14.62528405	-1.177196344	3.67E-08	1.74E-06	-2.261368875 GTP binding protein Bms1
SJAG_04694	10.87737043	9.747679117	10.92207704	-1.17439792	4.20E-06	9.58E-05	-2.256986705 WD repeat protein Prp5
SJAG_02079	10.66611586	8.659299146	9.828246688	-1.168947543	0.000445624	0.004762359	-2.24847609 DNA recombination protein Rad22
SJAG_00604	11.55423711	9.531912142	10.70067345	-1.168761304	1.14E-05	0.000218611	-2.248185851 SUMO E1-like activator enzyme Fub2
SJAG_04874	15.13445575	14.82096262	15.98090897	-1.159946347	2.36E-08	1.22E-06	-2.234491175 GTP binding protein
SJAG_01320	10.03113463	9.274418219	10.42508914	-1.150670922	3.69E-05	0.000583223	-2.22017119 WD repeat protein Pop3
SJAG_05006	9.06063959	9.184912736	10.33425278	-1.149340045	5.56E-07	1.74E-05	-2.21812404 homeobox transcription factor Phx1
SJAG_01063	9.992945419	8.642348201	9.788568382	-1.146220181	2.90E-05	0.000479922	-2.213332475 NADPH-adrenodoxin reductase Arh1
SJAG_06592	9.845474139	8.495179547	9.639602608	-1.14442306	0.000131926	0.001705936	-2.210577111 histidine-containing response regulator phosphotransferase Mpr1
SJAG_00044	14.6346209	13.01828688	14.16150229	-1.143215409	1.37E-07	5.33E-06	-2.208727455 adenylosuccinate synthetase Ade2
SJAG_16455	13.50407903	12.13762491	13.27777247	-1.140147562	6.89E-08	3.00E-06	-2.204035654 hypothetical protein
SJAG_02097	13.25659948	12.2477374	13.38745965	-1.139722244	4.72E-10	5.07E-08	-2.203385982 transcription elongation factor Spt5
SJAG_00746	11.10293202	9.550937507	10.68950093	-1.138563426	3.58E-06	8.34E-05	-2.201616864 Ino80 complex subunit Ies4
SJAG_02540	13.2004967	12.62925647	13.76603169	-1.136775215	6.50E-10	6.60E-08	-2.198889665 CCR4-Not complex subunit Ccr4
SJAG_01291	12.49187966	11.36532668	12.49668007	-1.131353388	8.35E-08	3.49E-06	-2.190641473 TTC27 family TPR repeat protein
SJAG_01777	11.98457059	11.00068122	12.13033714	-1.12965592	2.11E-06	5.30E-05	-2.188065491 TRF Taz1
SJAG_04766	12.09045405	11.24875996	12.37715097	-1.128391005	1.05E-07	4.25E-06	-2.186147897 RNA polymerase I upstream activation factor complex subunit Rrn5
SJAG_02250	12.36878894	11.02515965	12.15308308	-1.127923425	8.32E-09	5.09E-07	-2.185439476 RNA-binding protein Nop9
SJAG_04385	13.76455966	14.54345488	15.66951388	-1.126059002	1.22E-07	4.81E-06	-2.182617015 RNA-binding protein Cip1
SJAG_00104	11.66817056	10.31750983	11.43870242	-1.121192593	6.61E-09	4.27E-07	-2.175267151 AP-2 adaptor complex subunit Apl1
SJAG_00720	9.677024686	7.854210786	8.971915563	-1.117704776	0.00021741	0.002595183	-2.170014641 COP9/signalosome complex subunit Csn5
SJAG_03959	13.24495322	11.72731155	12.84366391	-1.116352366	5.27E-06	0.000115531	-2.16798138 karyopherin Kap104
SJAG_01374	12.63802041	11.00729549	12.12155714	-1.114261649	2.71E-09	2.05E-07	-2.164841872 nucleoporin Nup132
SJAG_02856	11.76468466	10.90885993	12.0229118	-1.11405187	0.00062075	0.006308906	-2.16452711 translation initiation factor IF-2Mt
SJAG_04916	10.06321303	7.878623792	8.991371833	-1.112748041	0.005712229	0.038838378	-2.162571813 RNase P and RNase MRP subunit p30

Annexe 4: Late timepoint analysis

SJAG_02667	11.37887043	9.324847609	10.43583684	-1.110989231	9.31E-05	0.001276313	-2.159936997 DNA polymerase epsilon catalytic subunit B
SJAG_05343	11.84065053	11.34264076	12.44957113	-1.106930376	3.37E-06	7.91E-05	-2.153868804 transcription factor
SJAG_04687	12.38617943	11.18119433	12.28416006	-1.102965726	2.76E-09	2.06E-07	-2.147957913 rRNA processing protein Rrp12-like protein
SJAG_00637	13.51893335	12.90496095	14.00204755	-1.097086605	8.85E-08	3.66E-06	-2.139222589 DNA-directed RNA polymerase III complex subunit Rpc2
SJAG_04351	10.19416922	9.528446007	10.62524289	-1.096796884	7.49E-05	0.001068182	-2.138793035 GTPase
SJAG_03903	14.15779816	13.45580718	14.55159295	-1.095785771	3.77E-06	8.70E-05	-2.137294587 glyceraldehyde-3-phosphate dehydrogenase Tdh1
SJAG_03664	11.49846937	10.2416389	11.33681425	-1.095175356	1.39E-06	3.80E-05	-2.136390473 jmjC domain chromatin associated protein Epe1
SJAG_04749	14.4034614	12.66217329	13.75480939	-1.0926361	4.89E-10	5.20E-08	-2.132633567 transcription factor Zip1
SJAG_03069	11.11511354	9.235560493	10.32742583	-1.091865337	1.84E-06	4.73E-05	-2.131494506 biotin-protein ligase
SJAG_01654	13.06100863	12.40952582	13.49997434	-1.090448513	2.58E-11	5.00E-09	-2.129402262 U1 snRNP-associated protein Usp104
SJAG_03097	11.2645501	10.00350578	11.09100945	-1.087503677	1.28E-05	0.00023904	-2.12506015 replication fork protection complex subunit Swi3
SJAG_05192	9.75079822	8.984840835	10.06885972	-1.084018881	0.000119207	0.001562188	-2.119933311 Swr1 complex subunit Vps71
SJAG_01340	9.790648974	8.727464573	9.81015097	-1.082686398	1.31E-05	0.000243676	-2.117976229 hypothetical protein
SJAG_01761	10.90355055	9.530283479	10.60659116	-1.076307677	4.32E-06	9.78E-05	-2.108632498 meiotically upregulated Mug174
SJAG_01420	13.02299263	11.43366616	12.50543583	-1.071769675	1.92E-06	4.93E-05	-2.102010207 U3 snoRNP-associated protein Cic1/Utp30 family protein
SJAG_02647	12.72097803	12.06012234	13.12932151	-1.069199174	7.44E-10	7.40E-08	-2.098268316 cycloisomerase 2 family protein
SJAG_04065	12.33873116	11.2064859	12.27534386	-1.068857968	3.02E-10	3.51E-08	-2.097772122 tRNA pseudouridine synthase
SJAG_01612	12.24753962	11.13848818	12.20730032	-1.068812143	1.23E-07	4.86E-06	-2.09770549 gamma-glutamyltranspeptidase Ggt1
SJAG_04372	10.17483516	8.770345071	9.835208109	-1.064863037	0.000100957	0.001362588	-2.091971268 Ku domain-containing protein Pku80
SJAG_00197	16.93574757	17.74777026	18.81091515	-1.06314489	4.95E-07	1.60E-05	-2.089481363 dihydroorotate dehydrogenase Ura3
SJAG_00917	10.83197369	9.770659131	10.82833014	-1.057671011	0.000146897	0.001867819	-2.081568465 hypothetical protein
SJAG_03578	14.84127675	13.92112653	14.97807085	-1.05694432	6.34E-06	0.000135362	-2.080520234 DNA-directed RNA polymerase I complex subunit Rpa2
SJAG_04205	11.14858448	11.71225175	12.76691193	-1.054660184	1.68E-08	9.25E-07	-2.077228873 SAGA complex subunit Ada2
SJAG_01441	12.0299028	11.14785089	12.20233261	-1.054481716	3.96E-09	2.78E-07	-2.076971926 transcription factor
SJAG_04628	12.25700265	11.32995702	12.38202509	-1.052068068	2.99E-09	2.22E-07	-2.073500029 ethanolamine-phosphate cytidyltransferase
SJAG_03459	9.783726607	7.831452893	8.882581709	-1.051128816	0.000828602	0.008091821	-2.072150537 ribosomal protein subunit L15
SJAG_03356	11.54484937	10.1485466	11.1977848	-1.049238202	1.72E-06	4.50E-05	-2.069436817 RNA-directed RNA polymerase Rdp1
SJAG_00443	14.57983254	13.77350536	14.82145743	-1.047952071	3.96E-08	1.86E-06	-2.067592783 cytoplasmic valine-tRNA ligase Vrs1/Vas1
SJAG_02172	10.26245974	7.966096044	9.013729448	-1.047633404	0.00053643	0.005573517	-2.067136136 DNA polymerase alpha B-subunit
SJAG_04768	12.25331765	12.21737733	13.26365242	-1.046275083	7.87E-08	3.31E-06	-2.065190809 hypothetical protein
SJAG_04265	12.95314488	11.95535912	13.00123359	-1.045874468	3.08E-05	0.00050296	-2.064617416 wybutosine biosynthesis protein Tyw1
SJAG_05007	14.23470896	13.45593766	14.50153077	-1.045593109	2.26E-07	8.18E-06	-2.064214807 tryptophan synthase
SJAG_01325	10.15974217	10.78330114	11.82438172	-1.041080581	0.000115676	0.001521641	-2.057768349 Set1C PHD Finger protein Spf1
SJAG_03494	14.17727928	12.10521283	13.14549592	-1.040283093	3.20E-07	1.11E-05	-2.056631177 glutamate-cysteine ligase regulatory subunit
SJAG_03538	12.03011522	10.96274564	12.00003857	-1.037292931	5.67E-08	2.52E-06	-2.052372971 transcription factor Thi1
SJAG_05315	10.65790952	8.987767609	10.02479686	-1.037029251	0.000665952	0.00667733	-2.051997895 hypothetical protein
SJAG_16454	10.97106619	10.53463937	11.57018168	-1.035542303	3.25E-08	1.58E-06	-2.049884044 hypothetical protein

Annexe 4: Late timepoint analysis

SJAG_04464	11.96358986	10.6560058	11.69105986	-1.035054066	0.000393626	0.004290986	-2.04919044	ran GDP/GTP exchange factor
SJAG_03787	11.72329274	11.19084329	12.22454343	-1.033700144	2.81E-08	1.41E-06	-2.047268243	RSC complex subunit Rsc1
SJAG_00972	12.18916917	11.51430295	12.54768875	-1.033385809	6.67E-09	4.29E-07	-2.046822233	NADPH-dependent diflavin oxidoreductase
SJAG_00077	9.961947471	9.575050968	10.6081285	-1.033077536	0.000255207	0.002979249	-2.046384916	hypothetical protein
SJAG_04141	11.09694175	9.726318067	10.75747722	-1.031159154	0.000253765	0.002969527	-2.043665604	fungal protein
SJAG_02471	12.27172581	10.79156124	11.82199174	-1.0304305	3.59E-06	8.35E-05	-2.042633681	translation initiation factor eIF2B epsilon subunit
SJAG_04426	13.01915917	12.63050251	13.65812632	-1.027623813	1.83E-10	2.35E-08	-2.03866371	serine/threonine protein phosphatase Pzh1
SJAG_01746	15.67990251	16.26267735	17.29011647	-1.027439119	3.05E-08	1.51E-06	-2.038402735	hypothetical protein
SJAG_02757	13.47131225	12.03393389	13.06081662	-1.026882732	4.28E-06	9.72E-05	-2.037616761	nucleoporin Nup157/170
SJAG_02545	11.78299727	10.3847888	11.41099124	-1.026202435	8.44E-08	3.52E-06	-2.036656158	Smc5-6 complex SMC subunit Smc6
SJAG_00859	12.05639496	11.39474457	12.42043575	-1.025691179	4.51E-07	1.49E-05	-2.035934545	complexed with Cdc5 protein Cwf3
SJAG_04745	11.79125487	10.38779889	11.41276892	-1.024970029	5.73E-07	1.78E-05	-2.03491711	kinesin-like protein Cut7
SJAG_02518	10.57921522	9.042477887	10.06574226	-1.023264375	7.84E-05	0.001107295	-2.032512711	meiotically upregulated Mug184
SJAG_03945	11.75715451	12.03467505	13.05607427	-1.021399222	5.51E-08	2.47E-06	-2.029886725	PHD finger containing protein Phf2
SJAG_01453	12.14879359	10.98513264	12.0061759	-1.021043255	2.47E-07	8.80E-06	-2.029385937	1,3-beta-glucan synthase regulatory factor Chf3/Chr4
SJAG_04712	11.51177416	10.19036181	11.21012908	-1.019767261	0.000395893	0.004309909	-2.027591838	transcription factor
SJAG_03897	12.88195506	13.0870701	14.10565314	-1.01858304	2.01E-09	1.63E-07	-2.025928193	ATP-dependent RNA helicase Prh1
SJAG_02841	15.78134639	15.97095749	16.98645805	-1.01550056	9.35E-08	3.85E-06	-2.021604191	2-isopropylmalate synthase
SJAG_02509	13.61641656	12.31764758	13.32976525	-1.01211767	6.09E-06	0.000130693	-2.016869404	tubulin alpha 2
SJAG_01506	9.59793437	8.366569626	9.376956104	-1.010386478	5.41E-05	0.000810798	-2.014450672	meiotically up-regulated 132 protein
SJAG_00693	9.949021375	8.920492301	9.929340072	-1.008847772	0.000120586	0.001579305	-2.012303304	MBF transcription factor complex subunit Res1
SJAG_02663	11.30355373	10.03507449	11.04220429	-1.007129809	0.000867854	0.008414451	-2.009908478	ubiquitin protease cofactor
SJAG_02628	15.19658109	14.85879524	15.86507985	-1.006284609	8.37E-07	2.47E-05	-2.008731322	translation initiation factor eIF3a
SJAG_01953	11.31377047	9.450880326	10.45622991	-1.005349588	0.00010606	0.00141889	-2.00742987	ATP-dependent RNA helicase A-like protein
SJAG_04036	13.59523719	13.23684023	14.23937085	-1.002530616	3.71E-08	1.76E-06	-2.003511257	transcription factor Pap1/Caf3
SJAG_02321	13.19009551	12.89559384	13.89783223	-1.002238386	7.82E-08	3.30E-06	-2.00310547	inositol polyphosphate kinase
SJAG_00311	12.56574414	11.22170578	12.22336715	-1.001661364	9.48E-08	3.89E-06	-2.002304466	Noc2p-Noc3p complex subunit Noc3
SJAG_01970	12.67314487	13.27091825	14.27125226	-1.000334008	3.24E-05	0.000524724	-2.000463086	thiamine-repressible acid phosphatase pho4
SJAG_00544	16.04958115	17.74136473	16.74010723	1.001257501	5.31E-06	0.000116189	2.001744027	40S ribosomal protein S9
SJAG_04611	11.58935511	12.50757039	11.50610606	1.001464336	4.23E-08	1.95E-06	2.002031032	ribosome biogenesis protein Nop8
SJAG_00940	15.78462245	17.80623557	16.80377117	1.002464402	3.02E-08	1.50E-06	2.003419307	60S ribosomal protein L17
SJAG_00235	12.69486641	13.1615375	12.15776156	1.003775939	1.43E-10	1.94E-08	2.00524142	cytochrome b5 reductase
SJAG_05746	13.84134017	15.46282292	14.45887349	1.00394943	2.68E-05	0.000447253	2.005482573	hypothetical protein
SJAG_03782	12.73912701	14.95455391	13.9501126	1.004441311	8.79E-08	3.64E-06	2.006166452	CIA30 family protein
SJAG_00959	12.44612203	13.5268834	12.52130526	1.00557814	3.86E-09	2.73E-07	2.007747913	translocon gamma subunit Sss1
SJAG_00562	11.53021815	12.35884769	11.3521427	1.00670499	5.97E-07	1.84E-05	2.009316723	rRNA processing protein
SJAG_05349	10.72023943	12.61180413	11.60413862	1.00766551	1.72E-06	4.50E-05	2.010654935	complexed with Cdc5 protein Cwf21

Annexe 4: Late timepoint analysis

SJAG_00373	11.66413838	13.4370404	12.42920361	1.007836784	3.61E-08	1.73E-06	2.01089365 TIM23 translocase complex subunit Tim16
SJAG_00233	9.051682999	10.44641943	9.438175159	1.008244269	0.000152359	0.001921517	2.011461701 SPX/EXS domain-containing protein
SJAG_02547	9.101141584	10.3820872	9.373524778	1.008562417	1.11E-06	3.14E-05	2.011905325 RNase MRP
SJAG_02605	13.13384624	15.52366357	14.51438548	1.009278091	2.36E-06	5.86E-05	2.012903613 rheb GTPase Rhb1
SJAG_00097	10.16782508	11.98939202	10.97648925	1.012902771	1.18E-05	0.000224988	2.017967265 5-aminolevulinate synthase
SJAG_05236	10.82378686	11.78149155	10.76478482	1.016706735	7.32E-09	4.60E-07	2.023295073 anaphase-promoting complex subunit Apc11
SJAG_00748	16.02038124	17.79981028	16.78226602	1.017544261	1.10E-07	4.40E-06	2.024469995 60S ribosomal protein L9
SJAG_04656	12.43773453	14.37432024	13.35541084	1.0189094	1.51E-09	1.31E-07	2.026386541 nuclear export factor
SJAG_02405	10.47357545	10.85564637	9.835047828	1.020598543	8.29E-06	0.000168365	2.028760474 acid phosphatase
SJAG_03049	16.75899551	17.10804618	16.08485119	1.023194985	1.60E-06	4.26E-05	2.032414955 fungal protein
SJAG_05009	12.70449047	14.5104465	13.48630293	1.024143564	2.88E-10	3.41E-08	2.033751717 U1 snRNP-associated protein Usp101
SJAG_01860	12.00983437	12.74357845	11.71878996	1.024788485	3.06E-10	3.54E-08	2.034661059 phosphoprotein phosphatase
SJAG_05273	10.16660461	11.72951348	10.70460512	1.024908362	6.03E-06	0.00012976	2.034830131 kinetochore protein Mis18
SJAG_03368	13.41937277	14.80600014	13.78007818	1.025921964	1.63E-06	4.31E-05	2.036260254 COPI-coated vesicle associated protein
SJAG_04850	12.75312836	15.06647428	14.04032245	1.026151829	4.08E-09	2.85E-07	2.036584718 mannan endo-1,6-alpha-mannosidase
SJAG_02387	9.549856575	10.59869715	9.570778447	1.027918703	2.51E-05	0.000423588	2.039080459 hypothetical protein
SJAG_02425	13.5902929	14.00798502	12.97812639	1.029858635	1.46E-09	1.28E-07	2.04182417 nuclear transport factor Nxt2
SJAG_04222	11.65633922	13.83083303	12.80058836	1.030244666	1.68E-05	0.000301123	2.042370586 U4/U6 X U5 tri-snRNP complex subunit Dim1
SJAG_01524	12.74181024	12.31909485	11.28696056	1.03213429	6.20E-06	0.000132844	2.045047411 succinate-CoA ligase alpha subunit
SJAG_04086	8.677444926	11.10434095	10.07069212	1.033648828	7.59E-06	0.000156709	2.047195424 transcriptional regulatory protein Spp41
SJAG_02224	14.44687203	15.8940634	14.85500579	1.039057615	1.11E-09	1.03E-07	2.054884941 40S ribosomal protein S30
SJAG_05198	11.99738591	13.07086388	12.03058883	1.040275048	4.89E-09	3.30E-07	2.056619708 hypothetical protein
SJAG_01409	11.86872406	13.08126742	12.04091119	1.040356236	5.25E-07	1.67E-05	2.056735448 rab GTPase binding protein
SJAG_04879	11.97660825	12.85417387	11.81340955	1.040764325	2.00E-05	0.000349118	2.057317311 DNA polymerase epsilon subunit Dpb4
SJAG_05896	13.0116255	15.43475161	14.39383202	1.040919586	0.000116712	0.001532516	2.057538728 hypothetical protein
SJAG_01959	16.92186284	16.50687594	15.46581561	1.041060328	0.001349964	0.012231206	2.057739461 Uba3-binding protein but2
SJAG_01744	12.75304432	14.58627328	13.54420417	1.042069104	7.72E-10	7.62E-08	2.059178797 ribosomal DNA transcription factor Rrn3
SJAG_01810	11.10905693	12.5352968	11.49320662	1.04232306	6.27E-06	0.000134285	2.059541304 complexed with Cdc5 protein Cwf18
SJAG_03990	13.04173938	16.56830716	15.52536227	1.042944886	6.90E-05	0.000996908	2.060429192 proteasome interacting protein
SJAG_00280	11.24917227	13.09193826	12.04812686	1.043811395	4.52E-07	1.49E-05	2.061667096 fungal protein
SJAG_05230	12.64447555	13.78078804	12.73614442	1.044643624	3.31E-10	3.77E-08	2.062856727 alanine racemase
SJAG_03610	8.326920154	9.973080455	8.928093608	1.044986848	1.16E-05	0.00022103	2.063347548 hypothetical protein
SJAG_01783	12.08487417	13.94258948	12.89696484	1.04562464	3.88E-08	1.83E-06	2.064259922 WD repeat protein
SJAG_00812	13.26394243	13.93373015	12.88793862	1.045791525	3.81E-09	2.70E-07	2.064498721 phosphatidyl-N-methylethanolamine N-methyltransferase
SJAG_03010	7.467978092	8.844671595	7.795373277	1.049298318	2.66E-05	0.000444054	2.069523051 BAR adaptor protein
SJAG_00083	15.2690566	17.15923954	16.10624153	1.05299801	4.24E-08	1.95E-06	2.074837011 RNA-binding protein Nhp2
SJAG_00666	11.67593381	10.68369308	9.630257945	1.053435131	0.000168675	0.002087033	2.075465759 sleepy Slp1

Annexe 4: Late timepoint analysis

SJAG_04982	13.61691012	14.10905326	13.05488784	1.05416542	1.12E-09	1.03E-07	2.076516622 profilin
SJAG_01864	9.787892874	10.80485905	9.749434172	1.055424874	7.21E-07	2.16E-05	2.078330185 Pot1 associated protein Poz1
SJAG_04978	12.23176341	14.0621871	13.00616796	1.056019136	0.000396222	0.004311562	2.079186449 SNARE Tlg2
SJAG_02010	14.32795219	16.21352849	15.15661193	1.056916558	1.61E-06	4.27E-05	2.0804802 glucose 1-dehydrogenase
SJAG_03388	13.51963232	14.77491593	13.71763785	1.057278078	6.79E-05	0.000984369	2.081001606 transcription factor Hsr1
SJAG_02474	11.30611995	12.46557913	11.40825573	1.057323402	6.06E-07	1.87E-05	2.081066983 BoA domain-containing protein
SJAG_01238	12.05088686	14.10547376	13.04713557	1.058338188	3.49E-08	1.69E-06	2.082531312 type II fatty acid synthase component
SJAG_04223	8.416835612	9.605602934	8.547183504	1.05841943	2.15E-05	0.000372169	2.082648589 ubiquinone binding protein Coq10
SJAG_01873	14.38911008	14.90944517	13.85052122	1.058923955	8.55E-08	3.56E-06	2.083377039 histone H2A alpha
SJAG_02126	7.644520048	11.1218537	10.06277779	1.059075913	1.03E-05	0.000201638	2.083596491 trichothecene 3-O-acetyltransferase
SJAG_01710	13.38285115	15.21451808	14.15484387	1.059674213	5.06E-07	1.63E-05	2.08446076 transcription factor TFIIA complex large subunit
SJAG_02803	16.21701257	17.8500359	16.7903365	1.059699408	4.95E-06	0.00010998	2.084497162 40S ribosomal protein S0A
SJAG_04261	13.33234301	14.3084763	13.24736588	1.061110428	1.74E-10	2.30E-08	2.08653689 DNA-directed RNA polymerase I
SJAG_00538	13.56931676	15.23993694	14.17793172	1.062005221	3.55E-09	2.55E-07	2.08783141 CGI-48 family protein
SJAG_01780	10.66458658	10.91155292	9.849538224	1.062014691	2.05E-07	7.52E-06	2.087845116 metaxin 1
SJAG_03028	13.37081308	15.27917531	14.21614493	1.063030378	8.33E-09	5.09E-07	2.089315519 U3 snoRNP-associated protein Rrp9
SJAG_02891	15.41756822	16.8419631	15.77640221	1.065560883	1.03E-08	6.09E-07	2.09298342 ribosomal-ubiquitin fusion protein Ubi1
SJAG_01894	13.2856257	15.29302479	14.22717943	1.065845355	5.56E-08	2.48E-06	2.093396157 F-actin capping protein alpha subunit
SJAG_02894	15.62442035	17.15097005	16.08504768	1.065922372	7.17E-08	3.08E-06	2.093507914 40S ribosomal protein S26
SJAG_01223	11.52627112	13.36081823	12.29399226	1.066825969	2.20E-09	1.75E-07	2.094819543 protein involved in protein folding in the ER
SJAG_02749	15.38377907	16.68799266	15.61875159	1.069241074	9.18E-09	5.54E-07	2.098329256 40S ribosomal protein S28
SJAG_03510	11.70423697	12.68356903	11.61410966	1.069459373	1.79E-07	6.71E-06	2.098646786 hypothetical protein
SJAG_02805	11.64321021	13.04228911	11.97170892	1.070580185	2.85E-07	1.00E-05	2.100277831 AP-2 adaptor complex subunit Aps2
SJAG_04422	11.60624357	12.55772502	11.48493891	1.072786105	7.96E-06	0.000162573	2.10349167 hypothetical protein
SJAG_01826	12.3054637	14.22743274	13.15318227	1.074250475	5.19E-09	3.48E-07	2.105627848 NatB N-acetyltransferase complex catalytic subunit Nat3
SJAG_04277	13.46619478	13.2071365	12.13262389	1.074512611	2.51E-05	0.000423588	2.106010473 brefeldin A resistance protein
SJAG_04332	13.2924318	13.09228062	12.01533919	1.076941424	2.92E-08	1.46E-06	2.109558981 M phase inducer phosphatase Cdc25
SJAG_03796	10.10562492	10.6505307	9.571006562	1.07952414	2.28E-05	0.000390878	2.1133389 RNase P and RNase MRP subunit
SJAG_04672	16.25418427	17.33758372	16.25787135	1.07971237	2.66E-08	1.35E-06	2.113614648 40S ribosomal protein S25
SJAG_01172	11.1885245	12.41125313	11.3300188	1.081234322	1.43E-08	8.07E-07	2.115845555 tRNA pseudouridylylase synthase
SJAG_03201	11.11786449	12.37786238	11.29636631	1.081496073	4.25E-07	1.42E-05	2.116229471 hypothetical protein
SJAG_03080	14.62530025	17.47789163	16.39560667	1.082284963	3.27E-07	1.13E-05	2.117386977 fungal protein
SJAG_03458	13.05932019	14.59843705	13.51563627	1.082800778	1.48E-06	4.01E-05	2.118144154 nucleolar protein Nop52 family protein
SJAG_03351	11.5750103	12.29355971	11.20894112	1.084618597	2.49E-08	1.28E-06	2.120814733 anaphase-promoting complex subunit Apc8
SJAG_04390	12.43296354	13.60762178	12.52008882	1.087532958	1.68E-08	9.25E-07	2.12510328 fungal protein
SJAG_01666	11.24988443	12.8310268	11.74338026	1.087646537	1.26E-06	3.51E-05	2.12527059 fungal protein
SJAG_03365	12.35841986	15.23805978	14.14879506	1.089264721	8.02E-09	4.94E-07	2.127655714 hypothetical protein

Annexe 4: Late timepoint analysis

SJAG_01190	11.82309246	13.77858165	12.68798284	1.090598816	5.23E-09	3.49E-07	2.12962412 cytochrome c oxidase subunit VIa
SJAG_06309	10.98650713	14.06433424	12.97184769	1.092486551	3.48E-07	1.19E-05	2.13241251 autophagy associated ubiquitin-like modifier Atg12
SJAG_02065	9.968152938	10.22952817	9.13535271	1.094175458	1.74E-05	0.000309822	2.134910305 TPR repeat protein Oca3/ER membrane protein complex Ecm2
SJAG_04305	13.71937185	14.44786145	13.35013147	1.097729982	8.33E-10	8.02E-08	2.1401768 homoserine O-acetyltransferase
SJAG_01087	15.91140419	17.65545935	16.55650144	1.098957905	1.32E-08	7.57E-07	2.141999147 60S ribosomal protein L23
SJAG_00921	16.41913485	17.66151423	16.5624642	1.099050031	3.66E-08	1.74E-06	2.142135931 60S ribosomal protein L26
SJAG_00360	11.78815341	13.23163092	12.13137199	1.100258932	4.01E-10	4.44E-08	2.143931678 signal recognition particle receptor beta subunit Srp102
SJAG_04125	12.46433757	12.64828831	11.54364633	1.104641979	3.26E-07	1.13E-05	2.150455055 sulfiredoxin
SJAG_00306	9.67537671	10.89506123	9.7901621	1.104899129	5.47E-07	1.73E-05	2.150838393 RNase P subunit Rpr2
SJAG_00566	14.03737141	15.57573398	14.47024005	1.105493932	1.29E-09	1.14E-07	2.151725335 small nucleolar ribonucleoprotein Nop10
SJAG_03284	9.658829557	10.19430605	9.086741601	1.107564446	9.69E-06	0.000192452	2.154815646 ribosomal protein subunit L1
SJAG_00410	10.38740752	11.57725722	10.46917262	1.108084598	3.98E-06	9.12E-05	2.155592689 hypothetical protein
SJAG_00458	12.90404557	13.91520248	12.80449628	1.110706205	5.01E-11	8.31E-09	2.159513305 DNA-directed RNA polymerase II complex subunit Rpb4
SJAG_00332	9.984283485	10.99704827	9.884623621	1.112424649	7.44E-05	0.001062818	2.162087108 kinesin-like protein Klp3
SJAG_00634	13.26863328	13.98009903	12.86696125	1.11313778	3.43E-08	1.67E-06	2.163156102 hypothetical protein
SJAG_04404	13.90123665	15.28198576	14.16804341	1.113942353	2.99E-10	3.48E-08	2.164362804 Thij domain-containing protein
SJAG_02225	9.797813018	10.94179468	9.827025109	1.114769574	3.42E-07	1.17E-05	2.165604175 4-amino-4-deoxychorismate lyase
SJAG_01784	13.52939038	14.66933035	13.55414931	1.115181042	5.43E-11	8.76E-09	2.166221911 UDP-glucose 4-epimerase Gal10
SJAG_03051	9.982649627	11.23281111	10.11619725	1.116613859	1.52E-07	5.83E-06	2.16837437 SWIM domain containing-Srs2 interacting protein 1
SJAG_00759	9.584043087	11.40002903	10.28321039	1.11681864	3.16E-05	0.000512749	2.168682177 RNA-binding protein Mcp2
SJAG_03611	10.4607508	11.28599517	10.16870149	1.117293679	0.000230457	0.002728466	2.169396382 hypothetical protein
SJAG_04286	10.31947478	11.12958891	10.00999808	1.119590835	4.28E-07	1.42E-05	2.172853391 hypothetical protein
SJAG_03425	16.68403195	18.27828433	17.15799424	1.120290097	3.52E-08	1.70E-06	2.173906811 60S ribosomal protein L7
SJAG_00772	13.54159708	15.98501992	14.86414386	1.120876065	0.000107362	0.001433158	2.174789949 rRNA processing protein Fcf1
SJAG_04719	10.55953008	9.990756504	8.869783585	1.12097292	0.000665915	0.00667733	2.174935956 ornithine cyclodeaminase family protein
SJAG_02280	15.28949915	16.75918236	15.63690931	1.122273059	3.17E-06	7.51E-05	2.176896865 60S ribosomal protein L11
SJAG_04553	10.63925332	12.17420459	11.0508709	1.123333693	4.99E-06	0.000110545	2.178497856 copper chaperone Sco1
SJAG_00453	12.59503282	13.71130334	12.58614376	1.12515958	2.36E-08	1.22E-06	2.181256726 Erg28 protein
SJAG_02073	12.4718248	13.04346507	11.91817323	1.125291848	1.69E-07	6.42E-06	2.181456715 hypothetical protein
SJAG_03461	12.59879924	13.18139892	12.05518953	1.126209384	5.60E-09	3.70E-07	2.182844537 translation elongation factor EF-Tu Tuf1
SJAG_01818	12.5357791	13.28498114	12.15789016	1.127090978	7.47E-09	4.67E-07	2.184178824 exosome subunit Csl4
SJAG_01116	12.10374421	14.18101324	13.05282935	1.128183895	5.28E-08	2.36E-06	2.18583408 eukaryotic protein
SJAG_06355	7.266617512	7.562648261	6.433169947	1.129478314	0.001741371	0.015023519	2.187796141 hypothetical protein
SJAG_01662	11.55340016	12.82052889	11.6905387	1.129990194	1.63E-09	1.39E-07	2.188572526 dynein light chain Dlc2
SJAG_02243	15.50111861	17.10945548	15.97726478	1.132190704	1.07E-07	4.31E-06	2.191913254 60S ribosomal protein L24
SJAG_02413	14.36297097	15.58122212	14.44888269	1.132339439	1.71E-09	1.45E-07	2.192139242 cyclophilin family peptidyl-prolyl cis-trans isomerase Cyp4
SJAG_03251	12.09143552	14.79895337	13.66601394	1.132939426	2.72E-08	1.37E-06	2.193051096 short chain dehydrogenase

Annexe 4: Late timepoint analysis

SJAG_03358	13.0564643	14.40717628	13.27323433	1.133941947	5.49E-10	5.75E-08	2.194575566 TOM complex subunit Tom20
SJAG_02870	15.2227302	17.221657	16.08437822	1.137278779	5.70E-08	2.53E-06	2.199657308 40S ribosomal protein S15
SJAG_03928	11.95442155	13.76708146	12.62789141	1.139190051	2.13E-10	2.62E-08	2.202573329 hypothetical protein
SJAG_04959	10.74460287	11.65435832	10.51501953	1.139338784	7.66E-06	0.000157662	2.202800413 hypothetical protein
SJAG_02788	6.735879949	6.992825464	5.851658038	1.141167425	0.002052552	0.01720608	2.205594271 fungal protein
SJAG_01588	15.71316343	16.88801269	15.74531078	1.142701915	1.42E-08	8.01E-07	2.207941449 60S ribosomal protein L27
SJAG_00694	14.06939673	15.97043211	14.82741692	1.143015195	3.46E-09	2.49E-07	2.208420955 orotate phosphoribosyltransferase Ura5
SJAG_01271	10.97832448	12.5995502	11.45522212	1.144328085	4.75E-08	2.16E-06	2.210431589 lipoate-protein ligase
SJAG_02600	11.31009421	13.10474612	11.9554012	1.149344924	2.13E-06	5.34E-05	2.218131541 DNA-directed RNA polymerase III complex subunit Rpc25
SJAG_00358	9.390812144	8.751450032	7.601085872	1.15036416	0.003633969	0.027146181	2.219699162 tRNA(5-methylaminomethyl-2-thiouridylate)-methyltransferase
SJAG_01669	14.43495477	14.54827337	13.39776606	1.150507311	5.74E-06	0.000124447	2.219919422 P-type proton ATPase Pma1
SJAG_01548	13.95270838	15.72212822	14.56996525	1.152162968	2.85E-06	6.88E-05	2.222468494 40S ribosomal protein S14
SJAG_04428	10.7549929	11.83492552	10.68118621	1.153739311	7.78E-09	4.82E-07	2.224898175 hypothetical protein
SJAG_00629	15.75681596	17.20462543	16.05086046	1.153764972	4.09E-07	1.37E-05	2.224937749 60S ribosomal protein L9
SJAG_05200	11.43518544	12.84062634	11.68613822	1.15448812	3.14E-10	3.61E-08	2.226053275 3-methyl-2-oxobutanoatehydroxymethyltransferase
SJAG_01347	11.04025799	12.46314882	11.30760716	1.155541662	3.07E-09	2.26E-07	2.227679465 rRNA processing protein Faf1
SJAG_05268	8.590968053	10.52253595	9.366481117	1.156054832	1.89E-06	4.85E-05	2.228471997 hypothetical protein
SJAG_03636	10.0356365	11.28046225	10.12361706	1.156845192	2.67E-08	1.36E-06	2.229693169 ribosomal protein subunit L27
SJAG_00091	10.08053689	10.05611272	8.898970291	1.157142432	5.25E-06	0.000115166	2.230152602 fungal protein
SJAG_03937	10.56794667	11.11268872	9.952780718	1.159908	2.32E-07	8.37E-06	2.234431783 RNA-binding protein
SJAG_04861	13.27762749	15.90532355	14.74317597	1.162147582	3.09E-05	0.000504003	2.237903119 hypothetical protein
SJAG_01985	13.79737022	13.4740501	12.3101269	1.163923203	0.00142959	0.012764198	2.240659151 hypothetical protein
SJAG_03524	10.60926281	11.2639122	10.09902609	1.16488611	1.74E-08	9.50E-07	2.242155147 phosphatidylserine decarboxylase Psd1
SJAG_02843	11.6054055	12.21529959	11.04968378	1.165615815	4.45E-08	2.04E-06	2.243289501 Sm snRNP core protein Smf1
SJAG_04830	12.54407407	12.24096532	11.07419221	1.166773107	5.97E-08	2.64E-06	2.24508973 NiCoT heavy metal ion transporter Nic1
SJAG_00060	8.540489608	9.325252629	8.157638424	1.167614205	0.000148887	0.001888195	2.24639901 fungal protein
SJAG_02910	11.89339181	13.26959217	12.10145218	1.16813999	2.87E-06	6.91E-05	2.247217852 UNC-50 family protein
SJAG_06428	11.26646425	12.66172487	11.49309016	1.168634707	2.32E-08	1.21E-06	2.247988581 hypothetical protein
SJAG_01241	11.21750132	11.21096399	10.0415505	1.169413486	1.54E-06	4.13E-05	2.249202391 alkaline phosphatase
SJAG_04987	9.753299661	10.14430372	8.974824692	1.169479029	3.61E-06	8.38E-05	2.249304577 HbrB family protein
SJAG_01691	11.48634944	12.02696649	10.85681664	1.170149846	8.17E-05	0.001148311	2.25035069 hypothetical protein
SJAG_03257	7.219704457	7.894243939	6.722804048	1.171439891	0.004787212	0.033729155	2.252363833 Poly(A) RNA polymerase cid11
SJAG_02857	12.78271927	14.49310891	13.32097869	1.172130221	1.31E-10	1.83E-08	2.253441849 hypothetical protein
SJAG_00018	5.280714583	8.702188391	7.528062458	1.174125932	0.000338356	0.003765951	2.256561241 hypothetical protein
SJAG_00902	11.18961995	13.20468964	12.0295464	1.175143233	5.12E-09	3.44E-07	2.258152992 acyl-CoA thioesterase
SJAG_02783	14.25587424	15.25322412	14.07626503	1.176959085	6.14E-10	6.26E-08	2.260997011 phosphomannomutase Pmm1
SJAG_04871	9.612360758	11.26283495	10.085605	1.177229947	7.14E-09	4.53E-07	2.261421547 calcipressin

Annexe 4: Late timepoint analysis

SJAG_03318	11.34460444	12.04043214	10.86015893	1.18027321	2.20E-05	0.000380568	2.266196891 N-acetyltransferase
SJAG_00269	13.98347417	15.70309144	14.52232528	1.180766158	2.53E-08	1.29E-06	2.26697135 transcriptional coactivator
SJAG_04543	12.89746955	14.30598111	13.1251378	1.180843311	2.74E-09	2.06E-07	2.267092587 DUF3074 family protein
SJAG_02113	8.724178697	12.00638529	10.82529102	1.181094267	8.57E-08	3.56E-06	2.26748698 amino acid permease
SJAG_01157	10.25284169	10.35581178	9.173365086	1.182446698	1.27E-06	3.54E-05	2.269613596 MBF complex negative regulatory component Yox1
SJAG_00307	9.192488973	9.564786166	8.381982844	1.182803322	1.46E-06	3.97E-05	2.270174697 centromere-specific histone H3 CENP-A
SJAG_05208	9.146400239	9.60001978	8.417192364	1.182827416	0.00027394	0.003156911	2.270212611 splicing factor 3B
SJAG_04281	10.25450459	10.10932839	8.925503836	1.183824557	4.76E-08	2.16E-06	2.271782247 ribosomal protein subunit S18
SJAG_04890	11.76956014	13.47243712	12.28848909	1.183948038	6.94E-08	3.01E-06	2.271976697 tRNA (guanine-N2-)-methyltransferase regulatory subunit Trm112
SJAG_06613	10.83194807	12.40042131	11.21513898	1.185282324	7.20E-08	3.09E-06	2.274078922 RNaseP RNase MRP subunit Pop6
SJAG_00454	10.86276643	13.12993907	11.9438907	1.186048362	1.76E-10	2.31E-08	2.275286727 hypothetical protein
SJAG_01296	15.41102969	17.71085586	16.51783717	1.193018692	1.10E-09	1.03E-07	2.286306292 40S ribosomal protein S19
SJAG_03759	11.6599474	11.20190919	10.00830069	1.193608499	6.86E-05	0.000991989	2.287241179 phosphoglycerate mutase
SJAG_04420	9.405199567	10.16697167	8.972318809	1.194652857	5.07E-05	0.000765616	2.288897498 hypothetical protein
SJAG_03989	7.79163123	8.519130871	7.322648021	1.19648285	0.000270139	0.003128093	2.291802703 shugoshin Sgo1
SJAG_00970	13.59819029	14.92854203	13.73123159	1.197310435	1.77E-10	2.31E-08	2.293117745 actin cortical patch component Lsb4
SJAG_04396	11.09192831	13.16209304	11.96305722	1.199035822	8.76E-05	0.001215553	2.295861833 histone lysine methyltransferase Set3
SJAG_02778	11.15484428	12.57552073	11.37635298	1.199167756	2.50E-09	1.95E-07	2.296071798 chromatin silencing protein Clr2
SJAG_04999	11.21151288	12.75806664	11.55753943	1.200527213	9.49E-08	3.89E-06	2.298236416 protein phosphatase inhibitor
SJAG_05250	4.522527289	8.923224636	7.719664593	1.203560043	0.00123806	0.011359641	2.303072844 hypothetical protein
SJAG_03598	12.7341885	13.28531643	12.08150731	1.203809119	1.00E-10	1.47E-08	2.303470496 C-8 sterol isomerase Erg2
SJAG_00384	15.61521583	17.18023819	15.97619541	1.20404278	1.85E-09	1.53E-07	2.303843599 60S ribosomal protein L19
SJAG_03037	9.104015539	10.52030028	9.316118574	1.20418171	5.22E-07	1.67E-05	2.304065467 anaphase-promoting complex subunit Apc15
SJAG_01155	8.725756756	8.489931579	7.285134375	1.204797204	0.000146577	0.001864726	2.305048656 fungal protein
SJAG_04901	14.20489012	15.48859976	14.28303634	1.205563419	1.18E-11	2.69E-09	2.306273192 calmodulin Cam1
SJAG_02653	12.92040185	13.55947854	12.35169417	1.207784361	1.81E-09	1.51E-07	2.309826295 DNA-directed RNA polymerase I complex subunit Ker1
SJAG_01750	11.38472075	13.07674484	11.86739493	1.209349913	8.17E-10	7.97E-08	2.312334182 hypothetical protein
SJAG_01466	13.88170596	15.49479484	14.28538145	1.209413393	1.71E-07	6.46E-06	2.312435928 methylenetetrahydrofolate reductase Met11
SJAG_00480	13.75123947	15.53881408	14.3268572	1.211956879	1.75E-10	2.31E-08	2.316516373 3,4-dihydroxy-2-butanone 4-phosphate synthase
SJAG_02114	7.789791404	9.685341908	8.473348155	1.211993754	1.39E-05	0.000255906	2.316575583 hypothetical protein
SJAG_01364	16.6421635	18.54955579	17.33311858	1.216437213	7.08E-10	7.14E-08	2.323721568 60S ribosomal protein L14
SJAG_00785	12.49253309	13.788178	12.57100802	1.21716998	2.75E-07	9.70E-06	2.324902122 Sed5 Vesicle protein Svp26
SJAG_00187	9.875208834	9.951349794	8.7336749	1.217674894	7.56E-07	2.25E-05	2.325715932 bromodomain containing protein 1
SJAG_02477	16.79945603	18.74273951	17.52329928	1.21944023	1.57E-09	1.35E-07	2.328563508 40S ribosomal protein S5
SJAG_00909	11.18004619	13.23728803	12.01754131	1.219746724	1.51E-09	1.31E-07	2.329058253 mediator complex subunit Med10
SJAG_04304	16.39637023	18.15840447	16.93689577	1.221508705	6.59E-09	4.27E-07	2.331904497 60S ribosomal protein L25
SJAG_03287	8.219287876	9.761410625	8.53871181	1.222698816	1.81E-06	4.68E-05	2.333828931 bouquet formation protein Bqt2

Annexe 4: Late timepoint analysis

SJAG_05181	13.74979906	16.20412631	14.97675352	1.22737279	1.40E-05	0.000257036	2.341402219 glutathione S-transferase Gst3
SJAG_03762	16.57922924	18.40823859	17.17990471	1.228333881	1.25E-10	1.78E-08	2.342962528 40S ribosomal protein S15a
SJAG_04164	9.438580605	9.887314529	8.657539906	1.229774623	2.81E-06	6.81E-05	2.345303488 ribosomal protein subunit Mrp21
SJAG_03232	10.03581994	12.12046556	10.89035321	1.230112347	7.06E-07	2.13E-05	2.345852569 translation termination factor Rrf1
SJAG_02524	11.54976413	12.85917851	11.62819176	1.230986757	1.39E-08	7.92E-07	2.34727481 TIM22 inner membrane protein import complex subunit Tim8
SJAG_01714	15.38765703	17.36734588	16.13301455	1.234331334	1.01E-07	4.13E-06	2.352722773 cyclophilin family peptidyl-prolyl cis-trans isomerase Cyp2
SJAG_03326	14.55206014	16.35008194	15.11374721	1.236334736	2.64E-09	2.02E-07	2.355992156 60S ribosomal protein L37
SJAG_03922	14.54628501	15.58498444	14.34619876	1.238785683	4.82E-08	2.18E-06	2.359998075 60S ribosomal protein L24
SJAG_02726	12.06100882	14.50580644	13.26680802	1.238998423	4.18E-08	1.94E-06	2.360346106 N-acetyltransferase
SJAG_01273	7.156368648	7.911587367	6.671174719	1.240412649	0.001664482	0.014469239	2.362661009 hypothetical protein
SJAG_03309	14.11603455	15.28950646	14.04664221	1.24286425	4.19E-11	7.25E-09	2.36667934 endosulphine family protein
SJAG_01066	12.24382352	13.60453568	12.35982799	1.244707695	5.45E-07	1.72E-05	2.369705366 hypothetical protein
SJAG_03164	12.72291263	13.40161132	12.15548056	1.246130755	1.13E-07	4.50E-06	2.372043973 orotidine 5'-phosphate decarboxylase Ura4
SJAG_03848	12.45954903	14.03975757	12.78962164	1.250135936	3.82E-07	1.29E-05	2.378638344 SNARE Pep12
SJAG_00792	13.92950058	16.56033663	15.31001486	1.250321768	4.23E-08	1.95E-06	2.378944753 iron-sensing transcription factor Fep1
SJAG_03962	13.2132309	14.82250767	13.57047178	1.252035888	9.05E-10	8.55E-08	2.381772945 hypothetical protein
SJAG_00084	11.82033176	10.7859798	9.531172806	1.254806992	0.000137315	0.001766253	2.386352211 adenylyl-sulfate kinase
SJAG_04751	8.523159808	9.089554949	7.831451835	1.258103114	0.000239205	0.002819453	2.391810537 ELLA family acetyltransferase
SJAG_02442	16.39564023	18.93849988	17.67987517	1.258624705	0.001203872	0.011102678	2.392675427 hypothetical protein
SJAG_01941	11.51368372	12.17828586	10.91825564	1.260030223	2.54E-09	1.97E-07	2.395007582 sulfate transporter
SJAG_02675	5.057413836	7.956097837	6.695933139	1.260164698	0.004431864	0.031725898	2.395230833 hypothetical protein
SJAG_00026	8.034947522	10.1764911	8.914501982	1.261989123	6.12E-07	1.88E-05	2.398261746 hypothetical protein
EF SJAG000000000	11.97710329	15.3044518	14.04188298	1.262568819	1.17E-11	2.69E-09	2.399225597 Small nucleolar RNA SNORD14 [Source:RFAM;Acc:RF00016]
SJAG_00836	11.7038455	13.6712203	12.40782094	1.263399356	5.08E-11	8.31E-09	2.400607192 F0-ATPase subunit
SJAG_03079	11.31483046	12.86166996	11.59550339	1.266166569	7.73E-06	0.000158552	2.405216181 membrane transporter
SJAG_03043	15.1581501	17.45644366	16.18970325	1.266740405	8.27E-10	8.00E-08	2.406173052 60S ribosomal protein L43-B
SJAG_04106	9.634503924	11.15288957	9.881868341	1.271021228	1.63E-06	4.32E-05	2.413323349 DNA-directed RNA polymerase complex I subunit Rpa12
SJAG_02871	15.83254933	17.43301298	16.15869588	1.274317107	4.58E-09	3.11E-07	2.418842959 60S acidic ribosomal protein P2-alpha
SJAG_04324	16.73960568	18.58521523	17.31081021	1.274405021	5.61E-08	2.50E-06	2.418990361 40S ribosomal protein S4
SJAG_03468	12.6601866	14.47294792	13.19834077	1.274607153	1.90E-09	1.56E-07	2.419329304 DNA-directed RNA polymerase I complex subunit Rpa34
SJAG_01660	14.28471988	14.01188053	12.73621037	1.275670163	1.55E-10	2.07E-08	2.421112577 glutathione transporter Pgt1
SJAG_00855	12.44361331	15.015165	13.73822434	1.276940653	1.18E-07	4.68E-06	2.423245636 ubiquitin conjugating enzyme Ubc8
SJAG_04759	8.279722528	9.332648857	8.05330763	1.279341227	4.47E-05	0.000685484	2.427281155 mitochondrial FUN14 family protein
SJAG_05211	9.522689424	12.65260424	11.37096071	1.281643533	2.52E-06	6.21E-05	2.431157791 hypothetical protein
SJAG_03270	12.93442558	14.12092989	12.83608884	1.284841044	9.09E-11	1.35E-08	2.436552053 COPII-coated vesicle component Erp2/3/4
SJAG_01206	12.69757967	14.40937242	13.12143469	1.287937727	1.87E-10	2.40E-08	2.441787626 hypothetical protein
SJAG_02944	3.557527864	7.890762289	6.601931807	1.288830482	0.003388343	0.025697219	2.443299096 hypothetical protein

Annexe 4: Late timepoint analysis

SJAG_00580	10.76051705	11.9971708	10.70833834	1.288832462	1.31E-06	3.63E-05	2.44330245 farnesyl pyrophosphate synthetase
SJAG_00983	10.38797954	12.61314868	11.32161828	1.291530395	7.23E-09	4.56E-07	2.447875858 ADP-ribosylation factor Alp41
SJAG_06420	7.929632611	10.43987109	9.1468949	1.292976187	4.82E-06	0.000107396	2.450330218 hypothetical protein
SJAG_04009	13.70456785	13.7217404	12.4260311	1.295709303	1.06E-06	3.03E-05	2.45497665 transcription factor Ste11
SJAG_03607	3.81167029	7.09186242	5.795827205	1.296035215	0.002778567	0.02190852	2.455531305 hypothetical protein
SJAG_03430	10.28287372	11.30911231	10.01254382	1.29656849	2.04E-06	5.17E-05	2.456439131 WW domain-binding protein 4
SJAG_03297	10.19164375	12.36612387	11.06406927	1.302054602	5.81E-10	6.03E-08	2.465797973 ribosomal protein subunit L19
SJAG_01551	16.33104539	17.90651724	16.59828102	1.308236221	5.21E-08	2.35E-06	2.476386022 60S ribosomal protein L7
SJAG_04880	12.35424799	14.0121863	12.70383726	1.308349044	3.47E-09	2.49E-07	2.476579689 mRNA decapping complex subunit
SJAG_04112	10.25038257	10.46837721	9.159405097	1.308972109	5.65E-07	1.76E-05	2.477649496 hypothetical protein
SJAG_04290	12.62967402	14.41079058	13.1010359	1.309754676	2.16E-07	7.90E-06	2.478993823 proteasome maturation factor Ump1
SJAG_02682	10.18893034	11.95527606	10.64451723	1.310758826	4.17E-05	0.000647543	2.480719861 40S ribosomal protein S23
SJAG_03537	11.02157355	12.76083542	11.44975942	1.311076002	5.43E-10	5.70E-08	2.481265306 histone N-acetyltransferase
SJAG_01567	11.30296788	14.1463358	12.83331672	1.313019077	2.27E-05	0.000390102	2.484609418 hypothetical protein
SJAG_01139	11.05958454	12.0482727	10.7338954	1.314377299	9.04E-08	3.72E-06	2.486949649 phosphopantothenate-cysteine ligase
SJAG_04155	14.68089284	15.67109865	14.35399811	1.317100539	1.69E-11	3.55E-09	2.491648464 FKBP-type peptidyl-prolyl cis-trans isomerase Fkh1
SJAG_06002	9.970654039	12.15697779	10.83972546	1.31725233	1.23E-07	4.85E-06	2.491910633 hypothetical protein
SJAG_04212	11.94765163	13.58590792	12.2649849	1.320923024	5.60E-05	0.000835097	2.498258952 hypothetical protein
SJAG_05216	13.5840798	15.19540854	13.87332562	1.322082923	5.34E-11	8.67E-09	2.500268311 60S ribosomal protein L34
SJAG_01246	11.56926758	12.53554276	11.21299701	1.322545746	2.72E-08	1.37E-06	2.501070537 cyclophilin family peptidyl-prolyl cis-trans isomerase Cyp2
SJAG_01199	15.85026908	15.60556294	14.28285825	1.322704694	2.80E-07	9.87E-06	2.501346105 thioredoxin peroxidase Tpx1
SJAG_02786	16.66998533	19.31977061	17.99656537	1.323205241	1.54E-08	8.59E-07	2.502214105 translationally controlled tumor protein
SJAG_00950	11.54556176	12.74851692	11.42414335	1.324373576	1.52E-09	1.31E-07	2.50424129 peptidyl-prolyl cis-trans isomerase NIMA-interacting 4
SJAG_01261	11.58571211	12.39602523	11.06913944	1.32688579	0.000132984	0.001716894	2.508605809 leucine carboxyl methyltransferase
SJAG_03245	13.110402	15.49571666	14.1688033	1.326913363	4.14E-08	1.93E-06	2.508653755 RING finger-like protein Ini1
SJAG_01014	13.56899146	15.38187776	14.05267318	1.329204583	1.29E-11	2.86E-09	2.512641044 20S proteasome component beta 2
SJAG_03483	7.280400101	10.08314426	8.753116522	1.330027743	3.86E-06	8.87E-05	2.514075094 GPI anchored cell surface protein
SJAG_02462	12.46965596	15.14703139	13.81565936	1.331372023	6.45E-09	4.20E-07	2.516418761 YjeF family protein
SJAG_01251	9.295793083	11.20992678	9.878283502	1.331643282	2.90E-06	6.99E-05	2.516891949 autophagy C terminal domain family protein
EFSJAG00000000	8.93211767	10.49264644	9.160884643	1.331761794	9.43E-06	0.000187996	2.51709871 Small nucleolar RNA snR87 [Source:RFAM;Acc:RF01216]
SJAG_04836	5.427653569	8.946180781	7.6114056	1.334775181	4.75E-05	0.000721094	2.522361721 hypothetical protein
SJAG_03984	12.05928096	14.32855238	12.99369677	1.334855616	5.64E-11	9.00E-09	2.522502355 zinc knuckle TRAMP complex subunit Air1
SJAG_05292	10.6222224	11.59111588	10.25503469	1.336081182	3.76E-09	2.68E-07	2.524646125 hypothetical protein
SJAG_00601	10.28389735	11.98137675	10.6406832	1.340693545	5.75E-06	0.000124497	2.532730451 ubiquinol-cytochrome-c reductase complex subunit 5
SJAG_04174	15.96139376	18.09012551	16.74900361	1.341121893	9.09E-09	5.51E-07	2.533482551 40S ribosomal protein S21
SJAG_04015	12.36989544	13.6147365	12.26825126	1.346485234	1.97E-11	3.97E-09	2.542918516 V-type ATPase V1 subunit F
SJAG_01996	10.4049773	11.3152131	9.96768292	1.347530177	7.33E-07	2.19E-05	2.544761017 copper chaperone

Annexe 4: Late timepoint analysis

SJAG_02740	13.45269806	15.16849396	13.82014205	1.348351907	1.83E-05	0.00032228	2.546210874	hypothetical protein
SJAG_05246	7.247216518	9.445706196	8.096611975	1.349094221	6.12E-07	1.88E-05	2.547521321	hypothetical protein
SJAG_00194	12.07524986	14.61594792	13.2662538	1.349694118	1.30E-08	7.49E-07	2.548580844	hypothetical protein
SJAG_02531	17.09191145	18.69605468	17.34380718	1.352247502	2.90E-09	2.17E-07	2.553095498	60S ribosomal protein L10a
SJAG_03062	13.67141242	14.67035098	13.31573819	1.35461279	5.09E-07	1.64E-05	2.557284712	WDR8 family WD repeat protein
SJAG_02480	9.449291602	12.5280988	11.17290334	1.35519546	9.16E-09	5.54E-07	2.558317747	hypothetical protein
SJAG_02189	16.95573676	17.91740527	16.56110009	1.35630518	2.99E-08	1.49E-06	2.560286359	translation elongation factor eIF5A
SJAG_04007	11.6408709	14.89985741	13.54067704	1.359180362	1.49E-07	5.72E-06	2.565393905	fungus protein
SJAG_01149	11.0488565	12.20659965	10.84648755	1.360112098	1.51E-10	2.04E-08	2.567051248	domain kinase I gamma subunit
SJAG_01721	14.89953829	16.08930185	14.72834538	1.360956465	3.11E-08	1.53E-06	2.568554107	60S ribosomal protein L17
SJAG_02170	10.40324334	11.69274668	10.32974202	1.363004656	1.02E-07	4.15E-06	2.572203268	Set1C complex subunit Shg1
SJAG_04953	15.1418736	15.75457675	14.38888227	1.365694483	7.52E-12	1.84E-09	2.577003475	cytosolic thioredoxin Trx1
SJAG_04612	12.6522789	14.36594042	12.99374766	1.372192761	1.61E-13	1.15E-10	2.588637159	ubiquitin conjugating enzyme Ubc7/UbcP3
SJAG_02192	14.83936016	16.58932875	15.21688472	1.372444026	5.92E-08	2.62E-06	2.589088044	glucan 1,3-beta-glucosidase Bgl2
SJAG_04430	14.19535657	15.99290636	14.61809868	1.374807676	1.97E-08	1.05E-06	2.593333373	hypothetical protein
SJAG_03476	11.216525	13.44057627	12.06534896	1.375227305	4.33E-09	2.97E-07	2.594087792	NADPH quinone oxidoreductase/ARE-binding protein
SJAG_00147	11.53469678	12.86214824	11.48402712	1.378121117	4.17E-09	2.90E-07	2.599296332	Sm snRNP core protein Smd1
SJAG_03931	12.87544567	14.28519855	12.90561121	1.37958734	8.66E-12	2.07E-09	2.60193936	CK2 family regulatory subunit
SJAG_03669	11.51123025	12.70286716	11.32072028	1.382146878	8.94E-09	5.43E-07	2.606559654	hypothetical protein
SJAG_04474	13.42442905	15.41485757	14.03241499	1.382442581	2.82E-11	5.21E-09	2.607093964	coatamer zeta subunit
SJAG_04998	16.50731989	18.95285639	17.56987193	1.382984467	2.94E-11	5.38E-09	2.60807339	40S ribosomal protein S27
SJAG_01747	10.66769531	12.6614934	11.2777643	1.383729095	4.88E-07	1.58E-05	2.60941986	nuclear distribution protein NUDC
SJAG_00450	10.3638649	11.8441141	10.46017603	1.383938065	4.07E-10	4.49E-08	2.609797855	hypothetical protein
SJAG_04131	10.64726518	12.0229002	10.63675046	1.386149738	5.03E-11	8.31E-09	2.613801782	NatC N-acetyltransferase complex catalytic subunit
SJAG_04867	11.7233448	12.70357109	11.31159993	1.391971158	8.65E-10	8.21E-08	2.624370042	ferrous iron transporter Pcl1
SJAG_00751	12.57218341	15.33083166	13.93835894	1.392472723	1.92E-10	2.45E-08	2.625282585	fungus protein
SJAG_04196	13.62932672	15.22899649	13.83480573	1.394190759	2.17E-13	1.27E-10	2.62841077	COPII-coated vesicle component Emp24
SJAG_05301	11.95860388	13.17837942	11.78384323	1.394536189	6.33E-06	0.000135362	2.629040176	origin recognition complex subunit Orp3
SJAG_01051	11.40267841	13.46342524	12.06652668	1.396898563	2.17E-10	2.65E-08	2.633348684	CUE domain-containing protein Cue1/4 family protein
SJAG_04654	11.48411204	13.66733426	12.26913171	1.398202545	1.27E-11	2.83E-09	2.635729917	transcription factor TFIID complex subunit Taf13
SJAG_02046	17.0492783	18.93126781	17.53146717	1.399800647	2.21E-09	1.75E-07	2.638651185	40S ribosomal protein S7
SJAG_05279	12.45170163	14.67791686	13.27774026	1.400176594	0.000287464	0.003285018	2.639338872	hypothetical protein
EF SJAG000000000	7.138330911	8.138653389	6.738292078	1.400361311	2.37E-05	0.00040273	2.639676825	Small nucleolar RNA snR75 [Source:RFAM;Acc:RF01185]
SJAG_04344	12.7768991	15.89391171	14.49279105	1.401120658	4.84E-05	0.000734733	2.641066556	hypothetical protein
SJAG_03362	12.56745242	14.97906873	13.57742902	1.401639701	4.78E-09	3.23E-07	2.642016912	thiamine diphosphokinase Tnr3
SJAG_00931	12.22183298	13.79619615	12.39409847	1.402097686	2.17E-08	1.14E-06	2.642855755	ubiquitin conjugating enzyme Ubc1
SJAG_00449	9.088899647	10.31531722	8.910063182	1.405254036	1.19E-05	0.000226439	2.648644165	cytochrome C oxidase copper chaperone Cox17

Annexe 4: Late timepoint analysis

SJAG_06135	7.834308326	8.656550762	7.249019567	1.407531195	3.59E-05	0.00056978	2.652828103	hypothetical protein
SJAG_03821	15.37415414	17.59384652	16.18561923	1.408227288	1.88E-06	4.85E-05	2.654108387	hypothetical protein
SJAG_00765	15.81563037	17.42044126	16.01205626	1.408384999	1.27E-10	1.79E-08	2.654398541	60S ribosomal protein L19
SJAG_00310	12.44677441	11.24951853	9.837015436	1.412503094	0.000163018	0.002031759	2.661986204	mannan endo-1,6-alpha-mannosidase DCW1
SJAG_02860	10.77967096	13.6911318	12.27784016	1.413291637	1.24E-09	1.11E-07	2.66344158	PAS family protein
SJAG_01216	15.19409321	16.26646463	14.85189926	1.414565368	2.70E-05	0.000450644	2.665794125	glutathione peroxidase Gpx1
SJAG_00020	9.408092134	12.45385281	11.03758041	1.416272405	1.05E-09	9.89E-08	2.668950235	trichothecene 3-O-acetyltransferase
SJAG_06600	3.783543711	8.499951956	7.082648079	1.417303877	0.001653235	0.014392002	2.670859115	hypothetical protein
SJAG_05221	9.847705362	12.66387833	11.24088965	1.422988681	1.23E-08	7.14E-07	2.681404145	translation release factor
SJAG_04487	10.28947563	10.16720317	8.743686333	1.423516835	9.60E-09	5.75E-07	2.682385956	deoxyuridine 5'-triphosphate nucleotidohydrolase
SJAG_03166	15.35266613	14.80229675	13.37727999	1.425016759	4.00E-08	1.87E-06	2.685176198	thioredoxin peroxidase
SJAG_02581	9.447497411	12.49555218	11.06841465	1.427137528	2.75E-09	2.06E-07	2.689126323	hypothetical protein
SJAG_03252	13.42523947	16.29443137	14.86686342	1.42756795	4.20E-10	4.59E-08	2.689928731	U3 snoRNP-associated protein Imp4
SJAG_01018	10.1788168	11.5052296	10.07713211	1.428097493	3.96E-08	1.86E-06	2.690916254	NEDD8-conjugating enzyme Ubc12
SJAG_04204	15.30292877	17.59149415	16.15593423	1.435559923	4.23E-09	2.94E-07	2.704871247	40S ribosomal protein S17
SJAG_03955	12.61525098	14.37418682	12.93820311	1.435983711	2.04E-10	2.55E-08	2.705665913	ER protein translocation subcomplex subunit Sec72
SJAG_00808	13.96672046	15.77577641	14.33891171	1.436864699	5.17E-07	1.65E-05	2.707318645	20S proteasome component alpha 3
SJAG_06595	7.246592186	8.534930036	7.096725259	1.438204778	0.00037125	0.004079896	2.709834565	hypothetical protein
SJAG_04799	8.869283232	9.748526157	8.308293862	1.440232295	1.37E-05	0.000253507	2.713645557	hypothetical protein
SJAG_04626	16.91111614	18.98057902	17.53732119	1.443257835	3.41E-10	3.85E-08	2.719342435	60S ribosomal protein L36/L42
SJAG_02469	11.27915372	12.90736188	11.4557693	1.451592582	7.92E-10	7.79E-08	2.735098106	U6 snRNP-associated protein core protein
SJAG_05237	12.59556753	15.37127619	13.91661704	1.454659148	6.67E-09	4.29E-07	2.740917963	structure-specific endonuclease catalytic subunit
SJAG_03929	12.27647634	14.42347438	12.9675885	1.455885882	6.93E-10	7.01E-08	2.743249576	cytochrome b5
SJAG_01355	12.13625318	13.77736866	12.3186798	1.458688858	5.21E-09	3.48E-07	2.748584547	cytochrome c oxidase subunit VI
SJAG_00300	12.8666045	15.89936237	14.44031445	1.459047911	1.88E-08	1.01E-06	2.749268692	ubiquitin conjugating enzyme Ubc15
SJAG_01218	12.48742825	14.14056312	12.6799862	1.460576919	1.16E-12	4.79E-10	2.752183987	ski complex subunit Rec14
SJAG_00507	14.54059938	17.08699886	15.62522962	1.46176924	5.94E-10	6.10E-08	2.75445948	translation initiation factor eIF4E
SJAG_06383	9.0857039	10.0928202	8.629407582	1.463412622	3.36E-07	1.15E-05	2.757598888	hypothetical protein
SJAG_01853	16.61788645	18.68511519	17.22034991	1.464765282	5.83E-09	3.83E-07	2.760185604	60S ribosomal protein L34
SJAG_04625	13.30079319	14.63704727	13.17039082	1.46665645	3.47E-07	1.18E-05	2.763806187	DUF1761 family protein
SJAG_05153	13.09199463	13.56095611	12.09424838	1.466707733	3.62E-06	8.39E-05	2.763904433	mating-type m-specific polypeptide mc
SJAG_01054	9.203424852	9.87649316	8.409172545	1.467320615	4.90E-07	1.59E-05	2.765078838	CMP/dCMP deaminase family protein
SJAG_02890	13.96068244	15.37439816	13.90479531	1.469602856	1.32E-10	1.83E-08	2.769456458	60S ribosomal protein L14
SJAG_00550	11.65465689	13.39180657	11.92053592	1.47127065	6.51E-11	1.00E-08	2.772659874	WD40/YVTN repeat-like protein
SJAG_04601	12.72304298	14.49069117	13.01778625	1.47290492	3.51E-10	3.93E-08	2.775802494	poly(A) binding protein Pab2
SJAG_05199	9.963103904	11.50674441	10.03293911	1.473805308	9.85E-06	0.000194028	2.777535417	inner membrane protein
SJAG_00138	13.90992652	15.83776492	14.35354397	1.48422095	3.47E-09	2.49E-07	2.797660597	fungal protein

Annexe 4: Late timepoint analysis

SJAG_00316	11.29204619	13.59335744	12.10724488	1.486112561	3.44E-10	3.87E-08	2.801331197	hypothetical protein
SJAG_04026	10.99366823	12.84114803	11.35412711	1.487020923	1.57E-09	1.35E-07	2.80309555	hypothetical protein
SJAG_02510	15.64200417	17.30121507	15.81197676	1.489238311	3.70E-09	2.64E-07	2.807407154	60S ribosomal protein L43-B
SJAG_03068	11.65865667	12.11018215	10.61528868	1.494893466	6.34E-09	4.13E-07	2.818433379	DNA repair protein
SJAG_01458	12.78863478	14.64111434	13.14258331	1.498531028	1.28E-10	1.79E-08	2.825548646	acyl-coenzyme A binding protein
SJAG_01624	11.79428906	13.4650834	11.96208255	1.503000847	3.26E-11	5.84E-09	2.834316456	GINS complex subunit Sld5
SJAG_04918	8.543925542	10.20796883	8.699698504	1.508270322	1.12E-07	4.49E-06	2.844687789	ribosomal protein subunit S19
SJAG_03171	6.359700874	8.785884765	7.276597769	1.509286996	1.33E-05	0.00024747	2.84669316	hypothetical protein
SJAG_03954	11.37535423	13.43194311	11.92166132	1.510281788	1.20E-09	1.09E-07	2.848656738	U6 snRNP-associated protein Lsm6
SJAG_00341	9.678328075	10.4768058	8.966288458	1.510517345	4.40E-07	1.46E-05	2.849121893	RING-box protein 1
SJAG_04506	13.42416825	16.20323387	14.69242749	1.510806381	8.27E-10	8.00E-08	2.849692756	myo-inositol transporter Itr1
SJAG_04838	13.19375493	15.85748597	14.34439	1.513095974	2.30E-09	1.81E-07	2.85421888	rRNA processing protein Fcf2
SJAG_03773	10.56198628	12.25445894	10.74025095	1.514207989	1.74E-09	1.46E-07	2.85641973	2' O-ribose methyltransferase Mrm2
SJAG_01545	12.17668084	14.39377411	12.87799038	1.515783733	7.24E-09	4.56E-07	2.859541281	prefoldin subunit 6
SJAG_03438	8.650128142	9.597277317	8.080988839	1.516288477	2.89E-05	0.000478919	2.860541901	CAMK/RAD53 protein kinase Mek1
SJAG_05154	11.45194359	11.57261145	10.04818463	1.524426827	0.002475788	0.019929767	2.87672403	hypothetical protein
SJAG_01526	10.73965176	12.27522806	10.7442785	1.530949559	3.32E-11	5.91E-09	2.88975976	tubulin specific chaperone cofactor C
SJAG_01000	10.97138749	12.6916324	11.15952414	1.532108256	1.39E-07	5.39E-06	2.892081596	CMGC/CDK protein kinase Csk1
SJAG_02504	11.2020082	13.92106277	12.38837209	1.532690681	4.17E-10	4.58E-08	2.893249381	cytochrome c oxidase subunit Vlb
SJAG_03472	15.41004473	18.49340497	16.95688795	1.536517013	7.08E-11	1.08E-08	2.900933076	translation initiation factor eIF3g
SJAG_04674	11.21011924	12.31690486	10.77706179	1.539843072	0.000686568	0.006861458	2.907628742	hypothetical protein
SJAG_06591	2.214948918	8.056059684	6.515620755	1.540438929	0.000400797	0.004351638	2.908829889	hypothetical protein
SJAG_06468	10.40734617	11.8526745	10.30999556	1.542678936	3.69E-11	6.52E-09	2.913349806	hypothetical protein
SJAG_00273	13.92453481	17.77780097	16.23447777	1.5433232	4.16E-06	9.49E-05	2.914651109	hypothetical protein
SJAG_00064	13.00317474	14.7025165	13.15892985	1.543586642	2.51E-13	1.39E-10	2.915183385	translocon beta subunit Sbh1
SJAG_04908	13.30711117	15.32901789	13.78152003	1.547497858	1.77E-11	3.68E-09	2.923097312	U3 snoRNP-associated protein Utp7
SJAG_03253	13.91879223	16.0952785	14.54620759	1.549070908	1.73E-05	0.000308182	2.926286263	hypothetical protein
SJAG_04746	16.3196095	18.92567128	17.37430801	1.551363273	4.45E-10	4.80E-08	2.930939671	40S ribosomal protein S28
SJAG_00593	12.02884976	14.27141859	12.71941817	1.552000418	2.73E-11	5.07E-09	2.932234364	short chain dehydrogenase DHRS family protein
SJAG_04909	12.94505851	14.62379799	13.06591359	1.557884406	2.59E-12	8.25E-10	2.944217814	alpha SNAP
SJAG_02745	10.92644034	12.90022711	11.33929925	1.560927863	6.15E-12	1.58E-09	2.950435385	DUF1715 family protein
SJAG_01330	11.41615075	13.43522874	11.87316919	1.562059546	6.08E-11	9.50E-09	2.952750681	spindle checkpoint protein Mad2
SJAG_05223	11.0273802	13.67214498	12.10758205	1.564562932	6.14E-14	6.24E-11	2.957878786	zf-HIT protein Hit1
SJAG_02081	15.36112548	17.78088527	16.21483485	1.566050419	9.97E-10	9.38E-08	2.960930072	60S ribosomal protein L38
SJAG_00960	12.6256446	14.88044612	13.31420115	1.566244963	0.000594323	0.006086821	2.961329373	fungus protein
SJAG_00179	9.108249217	10.91367067	9.346821728	1.566848944	2.11E-07	7.72E-06	2.962569387	glutathione S-transferase Gst2
SJAG_00113	8.662882656	10.49113541	8.922704778	1.568430632	1.56E-06	4.17E-05	2.965819159	hypothetical protein

Annexe 4: Late timepoint analysis

SJAG_00389	14.55601983	17.78092968	16.21232606	1.568603617	0.000279448	0.003206946	2.966174794	hypothetical protein
SJAG_01670	11.94664353	13.01101399	11.44132555	1.569688435	3.76E-08	1.78E-06	2.968406014	DNAJC9 family DNAJ domain-containing protein
SJAG_01665	12.16394762	13.49233274	11.92250414	1.569828606	2.91E-10	3.42E-08	2.968694435	myosin II regulatory light chain Rlc1
SJAG_01839	13.23055876	15.47132553	13.89984457	1.571480961	9.73E-12	2.30E-09	2.972096504	RNA-binding protein
SJAG_03149	11.1557362	12.24443085	10.67111128	1.573318048	5.89E-10	6.08E-08	2.975883498	acetylglucosaminyltransferase
SJAG_03133	15.13333261	16.93121654	15.34806279	1.583153755	1.43E-09	1.25E-07	2.996241177	60S ribosomal protein L36
SJAG_04690	11.3856646	12.82436094	11.23940544	1.584955505	4.28E-09	2.95E-07	2.999985453	beta-glucan synthesis-associated protein
SJAG_03254	15.25866856	17.73332431	16.14686558	1.586458726	1.71E-08	9.36E-07	3.003112927	40S ribosomal protein S29
SJAG_02708	12.2335448	14.60700332	13.01337661	1.59362671	7.62E-09	4.73E-07	3.018070925	RecA family ATPase Rhp55
SJAG_03118	12.83310944	14.34062193	12.74597083	1.594651101	1.36E-13	1.10E-10	3.020214678	RNA polymerase II associated Paf1 complex
SJAG_01280	13.45746118	16.3156619	14.71959881	1.596063086	1.39E-11	3.05E-09	3.023172051	zinc finger protein
SJAG_02887	12.08091608	12.34280947	10.74288793	1.599921542	7.53E-09	4.69E-07	3.03126828	nucleoside diphosphate kinase Ndk1
SJAG_02218	12.53784167	13.43562014	11.83332159	1.602298555	3.46E-12	1.01E-09	3.036266773	MADS-box transcription factor Mbx1
SJAG_04364	11.69252615	12.0700332	10.46368321	1.606349986	8.42E-10	8.08E-08	3.044805317	hypothetical protein
EF SJAG00000000	10.1769829	11.60561265	9.994917165	1.610695485	2.35E-08	1.22E-06	3.05399031	Small nucleolar RNA SNORD24 [Source:RFAM;Acc:RF00069]
SJAG_04776	7.540008809	8.713240565	7.099068337	1.614172228	6.49E-06	0.000137751	3.061358981	hypothetical protein
SJAG_06392	10.73591091	12.23602665	10.619559	1.616467646	2.05E-09	1.65E-07	3.066233672	hypothetical protein
SJAG_04984	10.7144532	13.07342034	11.4453594	1.628060943	4.54E-09	3.09E-07	3.090972766	carrier with solute carrier repeats
SJAG_04450	12.50021438	16.90637205	15.27199814	1.634373905	5.14E-06	0.000113161	3.104527917	fungus protein
SJAG_05872	9.631202606	11.42541665	9.789357834	1.636058812	2.09E-10	2.60E-08	3.108155778	hypothetical protein
SJAG_04217	14.36699565	15.99685698	14.35824956	1.638607421	2.36E-13	1.34E-10	3.113651378	cytochrome b5
SJAG_03460	11.93021576	14.03933274	12.39764649	1.641686245	8.64E-11	1.29E-08	3.120303249	U6 snRNP-associated protein Lsm3
SJAG_03793	13.65804442	15.52027408	13.87664533	1.643628749	2.07E-14	2.97E-11	3.124507383	calcineurin regulatory subunit
SJAG_01282	11.83653229	13.08950181	11.44449989	1.645001925	2.05E-11	4.06E-09	3.127482746	signal recognition particle subunit Srp14
SJAG_04939	10.38382276	12.81069945	11.16152154	1.649177909	2.48E-10	3.01E-08	3.136548583	bis(5'-adenosyl)-triphosphatase
SJAG_02002	10.97643387	12.37625638	10.72684964	1.64940674	6.19E-09	4.04E-07	3.13704612	eukaryotic protein
SJAG_03739	11.54918481	14.07133532	12.42183775	1.64949757	3.48E-12	1.01E-09	3.137243632	inositol monophosphatase
SJAG_04195	13.10132224	16.18549567	14.53544101	1.650054663	2.40E-10	2.93E-08	3.138455304	leydig cell tumor protein
SJAG_00569	11.41677219	13.12111488	11.4676971	1.65341778	4.87E-08	2.20E-06	3.14578	TOM complex assembly protein Mim1
SJAG_01413	10.64742156	12.84374524	11.18751139	1.656233857	5.65E-11	9.00E-09	3.151926421	ribosomal protein subunit L9
SJAG_00365	10.47552052	13.02507121	11.36870292	1.656368281	1.21E-09	1.09E-07	3.152220119	methionine sulfoxide
SJAG_01407	14.6013453	16.05601306	14.39941645	1.656596615	1.12E-12	4.73E-10	3.152719056	niemann-Pick disease type C2 protein hE1
SJAG_00080	10.32512771	14.93997008	13.27845352	1.661516568	3.88E-09	2.74E-07	3.163488975	ubiquinol-cytochrome-c reductase complex subunit 7
SJAG_03766	3.370229593	7.789158407	6.124410783	1.664747624	0.001493333	0.013221938	3.170581856	hypothetical protein
SJAG_02664	15.07931553	17.155145	15.48311445	1.672030553	8.57E-13	3.98E-10	3.186627869	CENP-H Fta3
SJAG_04964	13.02048509	14.99524921	13.32295534	1.672293863	2.05E-13	1.25E-10	3.187209524	phosphoric monoester hydrolase
SJAG_03104	8.120818348	8.62561415	6.952211727	1.673402423	0.001535384	0.013545054	3.189659501	Mam33 family protein

Annexe 4: Late timepoint analysis

SJAG_03490	11.15863167	12.97154986	11.29794376	1.673606103	2.10E-06	5.30E-05	3.190109849	ubiquinol-cytochrome-c reductase complex subunit 6
SJAG_00264	10.60265402	11.39899263	9.725174794	1.673817839	7.20E-08	3.09E-06	3.190578077	hypothetical protein
SJAG_02003	12.10820001	15.64380453	13.96621557	1.677588969	3.65E-08	1.74E-06	3.198928993	yippee-like protein
SJAG_02731	9.938666288	10.24378043	8.566115128	1.677665303	1.76E-06	4.56E-05	3.199098254	DASH complex subunit Dad5
SJAG_03334	11.15150005	13.50357612	11.82426524	1.679310882	8.74E-14	7.89E-11	3.20274932	coenzyme A/diphosphate transporter
SJAG_03142	9.888024842	11.70280881	10.02273329	1.680075518	2.87E-10	3.41E-08	3.204447242	guanyl-nucleotide exchange factor
SJAG_04448	3.956195032	7.563690942	5.883458966	1.680231977	0.000257022	0.002996128	3.204794781	hypothetical protein
SJAG_03996	11.8447836	13.01362839	11.33172286	1.681905525	7.63E-12	1.84E-09	3.208514548	translation initiation factor eIF1A-like protein
SJAG_00688	10.66812458	12.13198849	10.44476527	1.687223216	1.71E-12	5.86E-10	3.220362771	hypothetical protein
SJAG_04403	11.75880286	13.75078055	12.06100432	1.689776229	1.30E-12	4.95E-10	3.226066615	metallochaperone Ccs1
SJAG_05322	11.41256357	13.08309222	11.39190286	1.691189362	3.46E-09	2.49E-07	3.229228125	RNA-binding protein
SJAG_02106	9.685893245	10.42274356	8.73112242	1.691621142	6.19E-09	4.04E-07	3.230194735	hypothetical protein
SJAG_00115	11.2545166	13.44206621	11.74136613	1.700700079	4.91E-10	5.20E-08	3.250586576	WD repeat protein
SJAG_06111	6.596426777	8.593598557	6.881483069	1.712115487	0.000187302	0.002281604	3.276409057	hypothetical protein
SJAG_03047	12.21944643	15.58144828	13.86776908	1.713679198	3.43E-09	2.49E-07	3.279962221	histone H2A variant H2A.Z
SJAG_00120	13.9501097	16.02678143	14.31289912	1.713882311	2.98E-10	3.48E-08	3.280424031	delta-1-pyrroline-5-carboxylate reductase
SJAG_01239	9.579625706	13.02620752	11.31069406	1.715513458	2.70E-09	2.05E-07	3.284135058	protein phosphatase Fmp31
SJAG_03072	12.3914483	14.49873015	12.77561091	1.723119243	4.22E-10	4.59E-08	3.3014945	GTPase Ypt71
SJAG_05265	12.37836733	13.90101656	12.17547348	1.725543072	8.43E-06	0.000170444	3.307045907	Jmj1 protein
SJAG_02361	10.89143533	13.05115883	11.31511736	1.736041474	1.01E-11	2.38E-09	3.331198847	hypothetical protein
SJAG_01648	11.96221295	14.35536327	12.61902789	1.73633538	4.72E-14	5.23E-11	3.331877547	FEN-1 endonuclease
SJAG_01769	6.194389795	7.464610881	5.719991357	1.744619524	0.000658517	0.006621981	3.351064659	septin Spn5
SJAG_03531	14.36258904	15.37018333	13.62452835	1.745654982	1.02E-13	8.91E-11	3.353470664	sterol 24-C-methyltransferase Erg6
SJAG_06617	5.901584464	6.188596117	4.441141149	1.747454967	0.00225449	0.018546468	3.35765725	LYR family protein
SJAG_00237	6.872527252	9.425345462	7.677668837	1.747676625	1.05E-07	4.26E-06	3.358173166	hexitol dehydrogenase
SJAG_02195	7.711206123	9.928655073	8.178153984	1.750501088	7.47E-08	3.17E-06	3.364754131	hypothetical protein
SJAG_03159	15.95478854	18.39105264	16.6364575	1.754595133	1.09E-10	1.58E-08	3.374316108	60S ribosomal protein L27/L28
SJAG_03411	12.4776468	14.40923537	12.65334383	1.755891542	1.97E-10	2.49E-08	3.37734964	signal recognition particle subunit Srp21
SJAG_04541	13.54095788	15.32520884	13.56472284	1.760486001	2.85E-14	3.86E-11	3.388122414	20S proteasome component beta 7
SJAG_03645	9.083178417	9.263437973	7.498904366	1.764533607	1.99E-08	1.06E-06	3.397641432	hypothetical protein
SJAG_01668	10.66007743	13.83967202	12.07080395	1.768868063	1.97E-09	1.60E-07	3.40786471	NADH-dependent flavin oxidoreductase
SJAG_02359	9.322011593	11.20408538	9.43253429	1.771551088	1.28E-08	7.41E-07	3.414208319	ribosomal protein subunit S17
SJAG_06546	8.285944865	11.06618312	9.292277334	1.773905786	1.38E-09	1.21E-07	3.419785379	hypothetical protein
SJAG_01616	11.69614507	14.96119903	13.18714655	1.774052478	1.92E-12	6.51E-10	3.420133117	5-formyltetrahydrofolate cyclo-ligase
SJAG_02755	15.81891021	18.17395294	16.39956218	1.774390759	8.51E-13	3.98E-10	3.420935159	60S ribosomal protein L31
SJAG_01207	10.02744776	11.86693986	10.08886936	1.778070499	2.95E-12	9.02E-10	3.429671738	transcription factor TFIIH complex subunit Tfb5
SJAG_05637	8.585021844	11.36716291	9.585914182	1.781248725	1.52E-08	8.50E-07	3.437235559	hypothetical protein

Annexe 4: Late timepoint analysis

EFSJAG00000000	3.231532503	7.737846404	5.955691203	1.782155201	0.000350165	0.003876143	3.439395925 Small nucleolar RNA R38 [Source:RFAM;Acc:RF00213]
SJAG_04458	15.73313063	17.54669793	15.76435369	1.782344243	0.000530205	0.005520614	3.439846632 NAD binding dehydrogenase
SJAG_03502	10.91290421	13.5094057	11.72343432	1.785971373	8.19E-09	5.03E-07	3.448505751 TOM complex subunit Tom7
SJAG_01327	11.06836404	13.34597957	11.55950247	1.786477103	1.04E-11	2.42E-09	3.449714821 U6 snRNP-associated protein Lsm5
EFSJAG00000000	5.488400205	9.14876041	7.359923443	1.788836966	3.86E-06	8.87E-05	3.45536225 Small nucleolar RNA Z196/R39/R59 family [Source:RFAM;Acc:RF00134]
SJAG_00904	13.50857895	15.59108721	13.80146569	1.789621525	2.96E-12	9.02E-10	3.457241838 mediator complex subunit Srb4
SJAG_04185	16.00195915	16.58107581	14.78875192	1.792323887	2.83E-12	8.83E-10	3.463723786 ZIP zinc transporter Zrt1
SJAG_04180	12.5526058	14.29045163	12.49624777	1.794203861	2.86E-10	3.41E-08	3.468240302 fungal protein
SJAG_01194	15.96987633	18.00885562	16.21297524	1.795880383	2.66E-11	5.05E-09	3.472273005 60S ribosomal protein L37
SJAG_05118	4.811747337	7.584910373	5.78403854	1.800871833	0.000100675	0.001359532	3.484307213 hypothetical protein
SJAG_00831	12.8521544	15.07189678	13.26759742	1.804299358	1.19E-13	9.96E-11	3.492595 dolichol-phosphate mannosyltransferase subunit 3
SJAG_04820	11.87004348	15.2073357	13.39882185	1.808513849	1.41E-11	3.06E-09	3.502812705 mediator complex subunit Pmc6
SJAG_00703	6.348315897	7.216657106	5.407330918	1.809326188	0.000414821	0.00447996	3.50478559 hypothetical protein
SJAG_01287	15.54816252	18.27766306	16.46537818	1.812284874	1.67E-09	1.41E-07	3.511980596 40S ribosomal protein S30
SJAG_00347	9.854256941	12.74086356	10.91861439	1.82224917	6.76E-12	1.68E-09	3.536320835 hypothetical protein
SJAG_02697	16.26915281	16.89222633	15.06748503	1.824741301	4.16E-08	1.94E-06	3.542434804 ubiquitinated histone-like protein Uhp1
EFSJAG00000000	10.52928727	10.58739657	8.762431125	1.824965447	2.48E-07	8.80E-06	3.542985219 Small nucleolar RNA snR79 [Source:RFAM;Acc:RF01184]
SJAG_02744	14.35654718	15.80411746	13.97890128	1.825216179	6.72E-09	4.31E-07	3.543601024 cytochrome c
SJAG_02248	9.843566936	11.01542518	9.190034239	1.825390945	1.05E-08	6.20E-07	3.544030316 hypothetical protein
SJAG_00844	10.67666157	13.01161285	11.18463869	1.826974157	1.33E-12	4.95E-10	3.547921666 ribosomal protein subunit L32
SJAG_03637	13.35629396	16.04657986	14.21132284	1.835257023	1.14E-10	1.64E-08	3.56834974 morphogenesis protein Mor2
SJAG_00166	14.6364572	17.45385237	15.61848887	1.835363495	5.48E-12	1.44E-09	3.568613096 60S ribosomal protein L35a
SJAG_02458	12.04475097	14.26965723	12.43332869	1.836328536	5.20E-06	0.000114198	3.571000996 transcription factor TFIID complex subunit A/SAGA complex subunit
SJAG_04122	9.645982327	12.00797107	10.17080034	1.837170724	2.17E-09	1.73E-07	3.573086211 F0-ATPase subunit E
SJAG_03894	8.435444577	9.453434678	7.6114056	1.842029078	3.54E-07	1.21E-05	3.585139058 SMN family protein Smn1
SJAG_01553	9.038573841	11.74253271	9.897657091	1.844875619	5.40E-09	3.58E-07	3.592219777 hypothetical protein
SJAG_04349	10.24237335	12.45224708	10.60650841	1.845738678	7.18E-11	1.09E-08	3.594369383 ESCRT I complex subunit Vps28
SJAG_04647	10.99741568	13.20308583	11.35511404	1.847971787	1.18E-10	1.69E-08	3.59993732 mediator complex subunit Med31
SJAG_02495	11.77446065	14.33640974	12.48208822	1.854321521	4.59E-15	1.24E-11	3.615816644 monothiol glutaredoxin Grx3
SJAG_06382	11.54731369	14.63391037	12.7787635	1.855146871	1.04E-14	1.81E-11	3.617885804 hypothetical protein
SJAG_01775	10.86935628	12.98685581	11.13132194	1.855533878	9.45E-11	1.40E-08	3.618856441 DASH complex subunit Dad1
SJAG_00531	10.71016031	10.76425285	8.905681659	1.858571194	4.39E-05	0.000677476	3.626483271 U4/U6 X U5 tri-snRNP complex subunit Prp4 family protein
SJAG_03487	10.30512896	12.78371062	10.92498711	1.858723507	2.42E-11	4.72E-09	3.626866158 histone lysine methyltransferase Set7
SJAG_02441	12.67237087	15.29374692	13.43406856	1.859678363	4.56E-08	2.08E-06	3.629267416 meiotically upregulated Mug66
EFSJAG00000000	4.518056979	8.80883481	6.94860234	1.86023247	1.55E-06	4.14E-05	3.630661605 Fungal signal recognition particle RNA [Source:RFAM;Acc:RF01502]
SJAG_00617	10.92697208	13.09910665	11.23390175	1.865204909	3.49E-12	1.01E-09	3.643196748 fungal family protein
EFSJAG00000000	10.9705018	13.17453088	11.30896949	1.865561396	1.82E-08	9.86E-07	3.644097085 small nucleolar RNA snR3 [Source:RFAM;Acc:RF01434]

Annexe 4: Late timepoint analysis

EFSJAG00000000	12.11735592	16.30520058	14.42778847	1.877412108	2.67E-11	5.05E-09	3.674154026 small nucleolar RNA snR100 [Source:RFAM;Acc:RF01449]
SJAG_02304	11.26252898	12.75028697	10.8717432	1.878543768	2.49E-12	8.19E-10	3.677037189 Sm snRNP core protein Smd2
SJAG_00047	11.82534874	14.50465771	12.62343152	1.881226187	1.29E-09	1.14E-07	3.683880305 hypothetical protein
SJAG_00709	6.420629412	8.445102864	6.562148505	1.882954359	0.000206551	0.002483805	3.688295787 hypothetical protein
SJAG_02236	11.3519513	11.93866438	10.04898855	1.889675829	5.08E-11	8.31E-09	3.70551953 proline-tRNA ligase
SJAG_02812	14.70369175	14.83781812	12.94636757	1.891450559	3.02E-09	2.23E-07	3.710080677 translation elongation factor eIF5A
SJAG_00075	10.02036211	10.52693032	8.630727182	1.89620314	4.85E-07	1.58E-05	3.72232272 trichothecene 3-O-acetyltransferase
SJAG_01649	13.3026591	16.09371637	14.1940898	1.899626563	1.11E-08	6.49E-07	3.731166042 Mvp17/PMP22 family protein 1
SJAG_06449	10.53842034	13.19786786	11.29257704	1.905290815	1.89E-11	3.83E-09	3.745843991 Sm domain-containing protein
SJAG_00699	10.27076058	11.31016151	9.402931077	1.907230431	0.00550295	0.037699385	3.75088344 tspO/peripheral benzodiazepine receptor
SJAG_04515	11.17177287	13.75688761	11.84550056	1.911387048	4.95E-12	1.33E-09	3.761705871 hypothetical protein
SJAG_01127	13.04895327	15.70496579	13.79242556	1.912540227	1.33E-12	4.95E-10	3.764713889 eukaryotic protein
SJAG_04648	10.63755907	13.10813938	11.19103653	1.917102848	4.43E-12	1.21E-09	3.776638899 fungal protein
SJAG_02398	10.02948838	14.80005831	12.87487354	1.925184769	1.21E-09	1.09E-07	3.797854851 TIM22 inner membrane protein import complex anchor subunit Tim18
SJAG_00217	8.225568037	9.126257616	7.189773879	1.936483736	1.54E-06	4.13E-05	3.827715852 eukaryotic protein
EFSJAG00000000	13.28611845	15.45743659	13.51390483	1.943531762	4.23E-11	7.26E-09	3.846461216 Small nucleolar RNA snR61/Z1/Z11 [Source:RFAM;Acc:RF00476]
SJAG_03719	11.73814497	13.77646439	11.82798895	1.948475433	4.97E-11	8.31E-09	3.859664463 hypothetical protein
SJAG_01555	3.015163446	9.30839341	7.354580611	1.953812799	9.53E-05	0.001298807	3.873970047 hypothetical protein
SJAG_06269	10.88637911	13.66430281	11.71015202	1.954150791	6.22E-12	1.58E-09	3.874877739 hypothetical protein
SJAG_00155	16.30944968	18.71399912	16.75961552	1.9543836	4.40E-12	1.21E-09	3.875503083 60S ribosomal protein L21
SJAG_03127	16.50272389	19.21784122	17.2602193	1.957621917	7.25E-10	7.25E-08	3.884211925 60S ribosomal protein L29
SJAG_05242	12.49443581	15.61647771	13.65395678	1.962520929	7.95E-10	7.79E-08	3.897424104 hypothetical protein
EFSJAG00000000	9.269723016	11.08556591	9.121120899	1.964445015	3.59E-08	1.73E-06	3.902625468 Small nucleolar RNA snR60/Z15/Z230/Z193/J17 [Source:RFAM;Acc:RF00309]
SJAG_00707	11.86952601	14.52420017	12.55789658	1.966303596	2.07E-08	1.10E-06	3.907656343 fungal protein
SJAG_05840	5.142850834	7.435036232	5.468572297	1.966463936	0.000123508	0.001614207	3.908090661 hypothetical protein
SJAG_04664	9.268283892	11.75209428	9.783885426	1.968208858	2.62E-10	3.14E-08	3.91282031 protein disulfide isomerase
SJAG_02007	12.52593128	15.08303164	13.11329462	1.969737022	2.61E-10	3.14E-08	3.916967131 enoyl-[acyl-carrier protein] reductase
SJAG_00487	15.01064776	17.42894923	15.45173771	1.977211515	1.29E-07	5.05E-06	3.9373133 SBDS family protein Rtc3
SJAG_03679	11.13032935	13.34034585	11.3583657	1.981980152	6.56E-14	6.24E-11	3.950349099 pantoate-beta-alanine ligase
SJAG_00523	15.83223011	18.15487251	16.16900449	1.985868021	2.19E-13	1.27E-10	3.961009113 40S ribosomal protein S5
SJAG_01815	14.77063489	18.31208279	16.31934417	1.992738625	3.54E-08	1.71E-06	3.979917774 hypothetical protein
SJAG_01763	9.674485663	12.49494238	10.49777227	1.997170104	1.22E-09	1.09E-07	3.992161553 ubiquinol-cytochrome-c reductase complex subunit 9
SJAG_05312	12.5648813	15.33050355	13.33106123	1.999442313	1.58E-12	5.49E-10	3.998454063 hypothetical protein
SJAG_01904	9.043057345	13.90131182	11.90118975	2.000122062	1.12E-12	4.73E-10	4.000338443 hypothetical protein
SJAG_04636	5.604825001	9.54418869	7.543879811	2.000308879	7.17E-06	0.000149588	4.000856485 hypothetical protein
SJAG_02957	6.619798765	9.137672646	7.136733088	2.000939558	1.53E-07	5.87E-06	4.002605857 hypothetical protein
SJAG_00704	11.11786213	14.60295598	12.60143538	2.001520592	5.59E-05	0.000834048	4.004218198 AGC protein kinase Ppk31

Annexe 4: Late timepoint analysis

SJAG_04567	15.44517529	20.58928094	18.57090273	2.018378204	1.72E-05	0.000306648	4.051281137 hsp16-like protein
SJAG_04837	11.82798535	14.62719399	12.60458139	2.022612602	2.60E-12	8.25E-10	4.063189361 TRAPP complex subunit Bet5
SJAG_00176	10.98749596	10.77020447	8.739468497	2.030735978	8.64E-07	2.54E-05	4.086132475 Svf1 family protein Svf2
SJAG_05305	8.723581683	10.44673078	8.415157283	2.031573499	2.33E-07	8.38E-06	4.088505268 membrane protein complex assembly protein
SJAG_03820	11.86993801	13.51462412	11.47366929	2.040954828	3.07E-09	2.26E-07	4.115177979 hexose transporter Ght8
SJAG_01447	13.68107745	16.61037133	14.5656635	2.044707834	1.57E-12	5.49E-10	4.125897081 V-type ATPase subunit G
SJAG_06440	10.70958944	13.711963	11.66360925	2.048353746	1.79E-13	1.15E-10	4.136337042 distribution and morphology protein Mdm35
SJAG_00626	10.97118309	12.66326272	10.61056912	2.052693594	1.11E-09	1.03E-07	4.148798512 carrier with solute carrier repeats
SJAG_04166	12.25025759	13.83370479	11.77609998	2.057604811	1.66E-13	1.15E-10	4.162945904 Cdc25 family phosphatase lbp1
SJAG_00779	11.46678822	12.57802407	10.51817854	2.059845531	6.64E-12	1.67E-09	4.1694166 uridylylate kinase
SJAG_05191	11.24090252	13.31058862	11.24634279	2.064245828	3.10E-11	5.63E-09	4.182152958 prefoldin subunit 2
EFSJAG00000000	9.949099384	14.12347386	12.05918696	2.064286902	1.78E-10	2.31E-08	4.182272028 small nucleolar RNA snR92 [Source:RFAM;Acc:RF01444]
SJAG_02424	12.13403502	14.93664728	12.86406768	2.072579607	3.01E-15	9.18E-12	4.206381223 nucleoporin Seh1
EFSJAG00000000	10.67554997	13.0668207	10.99062142	2.076199277	3.28E-07	1.13E-05	4.216948132 small nucleolar RNA snR99 [Source:RFAM;Acc:RF01452]
SJAG_01418	12.46116146	17.84902154	15.77194082	2.07708072	5.16E-10	5.44E-08	4.219525347 diphthamide biosynthesis protein Dph3
SJAG_01650	13.9769353	16.52025207	14.43922679	2.081025276	1.44E-12	5.23E-10	4.231077984 RNA-binding protein Rnp24
SJAG_06097	10.85357897	13.79007818	11.68877095	2.101307231	4.31E-12	1.21E-09	4.290980161 hypothetical protein
SJAG_03390	9.544498384	12.8224231	10.71480635	2.107616758	2.47E-09	1.93E-07	4.309787563 hypothetical protein
SJAG_02914	10.50069971	12.04912304	9.932463747	2.116659292	2.11E-12	7.06E-10	4.336885313 ER membrane protein complex subunit 4
SJAG_01845	9.921455547	12.47836565	10.34484119	2.133524456	7.58E-10	7.51E-08	4.387881169 glutamine synthetase
SJAG_00468	16.71418704	19.51354955	17.37825915	2.135290395	1.50E-11	3.19E-09	4.393255469 40S ribosomal protein S24
SJAG_00731	12.96568425	16.22122487	14.08300412	2.138220749	1.27E-12	4.95E-10	4.402187971 DNA-directed RNA polymerase I and III subunit Rpc19
SJAG_00827	10.97049104	10.55217115	8.412707691	2.139463463	0.000737949	0.007294207	4.405981579 thiazole biosynthetic enzyme
SJAG_00967	10.53228508	13.0081681	10.86667519	2.141492907	4.37E-14	5.07E-11	4.412183847 hypothetical protein
SJAG_01518	7.397285754	8.785884765	6.639590184	2.146294581	2.39E-07	8.54E-06	4.426893239 peptide chain release factor
SJAG_05105	5.457245219	7.226725604	5.077356074	2.14936953	7.41E-06	0.000153533	4.436338746 hypothetical protein
SJAG_02365	8.34832151	12.13812215	9.98259119	2.155530956	5.76E-11	9.06E-09	4.455325867 hypothetical protein
SJAG_04336	11.08230644	13.44204315	11.26907698	2.172966178	1.31E-12	4.95E-10	4.509495927 TIM23 translocase complex subunit Tim15
SJAG_01117	15.11886259	18.75590066	16.57961962	2.17628104	1.10E-08	6.44E-07	4.519869252 translation initiation factor eIF1
SJAG_05750	11.22148019	16.34474421	14.16780283	2.176941377	3.77E-11	6.62E-09	4.521938518 hypothetical protein
SJAG_00308	14.09989911	18.5108192	16.33383984	2.176979353	4.28E-11	7.29E-09	4.52205755 peptide release factor
SJAG_00789	16.19245317	19.78429397	17.60471352	2.179580446	5.48E-06	0.000119137	4.530217904 hypothetical protein
SJAG_00894	11.71977813	15.18502521	13.00233256	2.18269265	2.68E-11	5.05E-09	4.540001109 iron sulfur cluster assembly protein Isd11
SJAG_03999	8.535820938	10.71716585	8.530190067	2.186975787	1.03E-07	4.19E-06	4.553499693 meiotically upregulated Mug97
SJAG_03616	12.02747789	14.71252434	12.52207922	2.190445117	4.91E-13	2.49E-10	4.564462927 ubiquitin family protein Urm1
SJAG_01226	16.98030394	19.38201153	17.18120659	2.200804932	6.05E-10	6.19E-08	4.597357736 ribomal-ubiquitin fusion protein Ubi5
EFSJAG00000000	3.690084006	8.222723122	6.018007077	2.204716045	0.000319211	0.003592233	4.609837978 U6 spliceosomal RNA [Source:RFAM;Acc:RF00026]

Annexe 4: Late timepoint analysis

SJAG_02696	14.76954347	17.355521	15.14562944	2.209891559	1.72E-06	4.50E-05	4.626404976	glucose-6-phosphate 1-dehydrogenase
SJAG_01801	10.02068483	13.10002037	10.88909367	2.210926706	1.50E-11	3.19E-09	4.629725655	anaphase-promoting complex subunit Hcn1
EFSJAG00000000	2.154730246	7.476045948	5.255296794	2.220749154	7.79E-05	0.001103121	4.661354237	Small nucleolar RNA snR69 [Source:RFAM;Acc:RF00475]
SJAG_03815	13.94619277	16.18510181	13.96315246	2.221949351	1.91E-09	1.56E-07	4.665233694	hsp16-like protein
SJAG_06212	6.633764557	9.726641898	7.497836091	2.228805807	3.99E-09	2.79E-07	4.687458141	hypothetical protein
SJAG_01776	11.1474696	14.45652053	12.2205218	2.235998728	4.03E-13	2.09E-10	4.710887005	Smc5-6 complex non-SMC subunit 2
SJAG_01742	9.579477153	10.68857718	8.444185479	2.244391696	8.18E-06	0.000166388	4.738372756	TENA/THI domain-containing protein
SJAG_00943	16.47902666	20.34733148	18.09404359	2.253287885	5.81E-13	2.89E-10	4.76768158	fibrillarin
SJAG_01079	10.87000448	13.4514647	11.19780354	2.253661162	2.97E-13	1.57E-10	4.768915308	methyltransferase Rrg1
SJAG_05180	8.743003694	9.796897132	7.540797319	2.256099813	1.16E-09	1.06E-07	4.776983234	structure-specific endonuclease subunit
SJAG_01905	10.05042176	15.15741096	12.89102406	2.266386901	2.70E-11	5.05E-09	4.811167079	progesterone binding protein
SJAG_06585	6.08076043	10.62883402	8.357901603	2.270932416	8.59E-10	8.18E-08	4.826349579	hypothetical protein
SJAG_01870	11.89647641	15.31817668	13.03945833	2.278718344	1.79E-11	3.68E-09	4.852466805	Sm snRNP core protein Smg1
SJAG_02047	9.41866961	10.77899147	8.499471672	2.279519795	2.99E-07	1.05E-05	4.855163213	TENA/THI domain-containing protein
EFSJAG00000000	6.088524717	11.32410408	9.044558207	2.27954587	2.31E-09	1.82E-07	4.855250966	Fungal signal recognition particle RNA [Source:RFAM;Acc:RF01502]
SJAG_01164	10.73202437	13.34740899	11.05823921	2.289169786	1.78E-14	2.71E-11	4.887747596	lipote-protein ligase A
SJAG_01032	10.31530417	13.03172611	10.73546497	2.296261146	1.36E-14	2.21E-11	4.911831758	hypothetical protein
SJAG_04243	14.01399867	17.28241168	14.98365987	2.298751809	8.31E-08	3.48E-06	4.920318851	hypothetical protein
SJAG_03871	6.281274181	9.00776293	6.704982559	2.302780371	1.50E-06	4.06E-05	4.934077482	alpha-1,2-galactosyltransferase gmh3
SJAG_01757	9.01104258	10.97044918	8.662642695	2.307806489	2.70E-09	2.05E-07	4.951296994	hypothetical protein
SJAG_00439	12.50275809	15.97854639	13.66285351	2.31569288	3.00E-12	9.02E-10	4.978437024	cyclin-dependent protein kinase regulatory subunit Suc1
SJAG_01975	11.63458617	12.81615956	10.49750706	2.318652498	7.08E-07	2.13E-05	4.988660526	kinetochore protein fta5
EFSJAG00000000	12.51871596	15.38914036	13.06972978	2.319410585	3.63E-14	4.42E-11	4.991282583	Small nucleolar RNA SNORD14 [Source:RFAM;Acc:RF00016]
SJAG_02494	11.12908603	14.89875177	12.57445296	2.324298818	5.72E-15	1.29E-11	5.008223054	mediator complex subunit Med19/Rox3
SJAG_00615	11.2034007	13.90691994	11.57416989	2.332750049	1.23E-12	4.95E-10	5.037647058	ubiquitin-like protein modifier Ned8
SJAG_04764	15.28841395	19.20540694	16.86842661	2.336980327	5.27E-07	1.67E-05	5.052440151	hypothetical protein
SJAG_03367	12.0655132	15.03439755	12.67879219	2.355605364	5.20E-14	5.51E-11	5.118089458	tRNA methyltransferase
SJAG_03818	12.7299784	15.61564684	13.25849999	2.357146843	1.55E-07	5.92E-06	5.123560916	gal10
SJAG_03977	11.11935645	14.06308423	11.7048596	2.358224631	1.90E-09	1.56E-07	5.12738998	ADP-ribose diphosphatase
SJAG_01476	14.1922489	17.96978113	15.61145079	2.358330338	1.84E-09	1.53E-07	5.12776568	RNA 3'-terminal phosphate cyclase
SJAG_04382	3.516332924	7.871504153	5.487424353	2.384079799	9.37E-05	0.001280689	5.220108521	hypothetical protein
EFSJAG00000000	4.162946551	7.976444812	5.59005617	2.386388642	6.71E-05	0.000974816	5.228469303	Fungal signal recognition particle RNA [Source:RFAM;Acc:RF01502]
SJAG_00668	15.5956004	18.18021569	15.79282583	2.387389857	1.50E-12	5.37E-10	5.232099065	superoxide dismutase Sod1
SJAG_00535	5.104685221	8.973158798	6.572851994	2.400306804	8.89E-06	0.000178354	5.279154191	hypothetical protein
SJAG_04742	9.617480827	11.90050104	9.490820105	2.40968094	3.66E-08	1.74E-06	5.313568	hypothetical protein
SJAG_02232	13.13894326	16.24246844	13.82575824	2.416710198	2.42E-15	8.43E-12	5.339520525	SIN component Cdc14
SJAG_02567	11.03007295	13.05733819	10.63915337	2.41818482	7.13E-13	3.48E-10	5.344981	phosphoprotein phosphatase

Annexe 4: Late timepoint analysis

SJAG_04592	13.03976728	15.82254724	13.38763735	2.434909895	6.24E-15	1.29E-11	5.407305603 COPII-coated vesicle component Erv46
SJAG_03683	11.12139397	14.81013688	12.37225402	2.437882855	4.54E-11	7.68E-09	5.418459922 kinetochore protein Spc25
SJAG_06618	4.098530867	6.446962375	4.003677628	2.443284747	0.00206826	0.017306504	5.438786325 hypothetical protein
SJAG_02677	4.960510606	8.212835246	5.767281365	2.445553881	1.59E-05	0.000285588	5.447347416 hypothetical protein
EFSJAG00000000	11.51333729	13.70100718	11.24615832	2.454848856	7.38E-11	1.12E-08	5.48255681 small nucleolar RNA snR90 [Source:RFAM;Acc:RF01442]
SJAG_02928	4.153584613	8.758910651	6.298364665	2.460545986	1.70E-06	4.46E-05	5.504249955 hypothetical protein
SJAG_05558	13.35159447	15.95637041	13.48464131	2.471729101	1.78E-13	1.15E-10	5.547082188 fungal protein
SJAG_02121	14.38883761	17.29096206	14.81855894	2.472403124	1.80E-13	1.15E-10	5.549674374 60S ribosomal protein L36
SJAG_00372	13.66237661	15.91658379	13.4422587	2.474325088	6.29E-11	9.76E-09	5.557072598 plasma membrane proteolipid Pmp3
EFSJAG00000000	10.29820717	13.81861773	11.33983354	2.478784191	1.18E-09	1.08E-07	5.574275049 small nucleolar RNA snR5 [Source:RFAM;Acc:RF01435]
EFSJAG00000000	10.70019984	13.09699241	10.61279639	2.484196016	1.11E-10	1.60E-08	5.595224489 small nucleolar RNA snR42 [Source:RFAM;Acc:RF01440]
SJAG_06046	11.54125239	15.39163404	12.90640516	2.485228881	1.76E-13	1.15E-10	5.599231699 hypothetical protein
SJAG_03155	12.62364886	15.52362641	13.03253512	2.491091288	6.65E-14	6.24E-11	5.622030531 Mam33 family protein
EFSJAG00000000	9.598517324	14.86780421	12.37531758	2.492486628	2.26E-11	4.45E-09	5.627470651 U2 spliceosomal RNA [Source:RFAM;Acc:RF00004]
SJAG_03778	4.679713376	6.154258283	3.660311444	2.493946839	0.000408209	0.004420298	5.633169331 hypothetical protein
SJAG_05629	9.016311429	13.79876214	11.29415354	2.504608601	7.58E-12	1.84E-09	5.674953616 hypothetical protein
SJAG_00708	6.575929156	7.890762289	5.376790327	2.513971963	8.14E-06	0.000165833	5.711904912 hypothetical protein
SJAG_02802	16.65667503	20.23648167	17.71950571	2.51697596	8.64E-13	3.98E-10	5.723810702 60S ribosomal protein L27
SJAG_00919	12.21745753	16.20210703	13.67301588	2.529091143	3.74E-12	1.07E-09	5.77207939 trafficking protein Pga2
SJAG_00007	7.527138104	8.599910479	6.061443694	2.538466784	1.98E-06	5.05E-05	5.809712549 hypothetical protein
SJAG_02360	13.78916922	17.108749	14.56467549	2.544073509	5.28E-17	2.58E-13	5.832334681 6,7-dimethyl-8-ribityllumazine synthase
EFSJAG00000000	9.671067993	13.57300602	11.02292145	2.550084563	1.41E-10	1.93E-08	5.856686062 U1 spliceosomal RNA [Source:RFAM;Acc:RF00003]
SJAG_00973	10.72623158	14.02507762	11.46624315	2.558834479	7.18E-16	2.92E-12	5.892314675 cyclin L family cyclin
SJAG_03765	2.404858057	7.955523089	5.388557072	2.566966017	1.41E-05	0.000258785	5.925619613 hypothetical protein
SJAG_01072	14.78026425	17.67796098	15.09353777	2.584423204	9.75E-13	4.32E-10	5.997757546 subtilisin cleaved region like protein
SJAG_00672	6.9351615	8.717814903	6.126913624	2.590901278	5.53E-08	2.47E-06	6.024749586 hypothetical protein
SJAG_00006	4.153168427	6.177984169	3.578233595	2.599750574	0.000524863	0.005472	6.061818153 hypothetical protein
EFSJAG00000000	3.123761952	8.866531861	6.266446847	2.600085014	1.27E-05	0.000237627	6.063223545 Fungal signal recognition particle RNA [Source:RFAM;Acc:RF01502]
EFSJAG00000000	10.25222126	13.68588832	11.08555866	2.600329661	1.34E-12	4.95E-10	6.064251811 small nucleolar RNA snR35 [Source:RFAM;Acc:RF01438]
SJAG_02339	10.89764709	14.21237647	11.60046952	2.611906952	2.81E-17	1.71E-13	6.113111799 RecA family ATPase Rlp1
SJAG_04436	10.82029417	14.36760584	11.75414156	2.613464286	1.80E-11	3.68E-09	6.119714233 hypothetical protein
EFSJAG00000000	8.028168572	13.29572526	10.67274248	2.622982781	4.81E-10	5.14E-08	6.160223871 U4 spliceosomal RNA [Source:RFAM;Acc:RF00015]
SJAG_02975	8.689782501	11.14864444	8.521574758	2.62706968	1.70E-10	2.26E-08	6.177699432 hypoxia induced family protein
EFSJAG00000000	6.940927274	12.00897147	9.377435436	2.631536037	2.07E-09	1.66E-07	6.19685425 U5 spliceosomal RNA [Source:RFAM;Acc:RF00020]
SJAG_04188	16.08532378	19.55251761	16.91073908	2.641778529	6.36E-15	1.29E-11	6.241005699 40S ribosomal protein S18
SJAG_00161	10.72851122	12.80580787	10.16374846	2.642059413	3.12E-09	2.29E-07	6.242220903 hypothetical protein
SJAG_01091	4.472103601	8.176186144	5.527364158	2.648821986	4.32E-08	1.99E-06	6.271549739 hypothetical protein

Annexe 4: Late timepoint analysis

SJAG_06013	7.755745544	10.47494672	7.810321476	2.664625243	1.88E-09	1.55E-07	6.340625826 hypothetical protein
EFSJAG00000000	9.725063066	11.81768522	9.152294262	2.66539096	1.94E-09	1.58E-07	6.343992036 Small nucleolar RNA snR56 [Source:RFAM;Acc:RF01188]
SJAG_04534	14.84384425	18.23798552	15.57069714	2.66728838	1.54E-13	1.15E-10	6.352341087 60S ribosomal protein L38
SJAG_02234	12.73870192	15.64891013	12.97579166	2.673118469	1.34E-17	1.63E-13	6.378063536 coatomer epsilon subunit
SJAG_02585	16.09082668	19.32949515	16.61338038	2.716114775	1.03E-12	4.50E-10	6.571008349 40S ribosomal protein S24
EFSJAG00000000	9.065124681	14.71499827	11.9454157	2.769582574	4.67E-12	1.26E-09	6.819105826 U2 spliceosomal RNA [Source:RFAM;Acc:RF00004]
SJAG_01636	4.075627734	7.389147278	4.615445451	2.773701828	4.50E-05	0.000687106	6.838603892 azole resistance protein
SJAG_02982	11.36301922	14.17195755	11.36474862	2.807208931	8.26E-15	1.55E-11	6.999291683 cytochrome P450 regulator Dap1
EFSJAG00000000	9.033863332	12.11716583	9.299217288	2.817948543	5.41E-12	1.43E-09	7.051589746 Small nucleolar RNA SNORD18 [Source:RFAM;Acc:RF00093]
EFSJAG00000000	11.10935465	14.62954249	11.79643317	2.833109321	9.11E-13	4.11E-10	7.126083167 Nuclear RNase P [Source:RFAM;Acc:RF00009]
SJAG_00023	5.675953518	10.60785302	7.76172477	2.846128248	1.50E-11	3.19E-09	7.190680197 hypothetical protein
SJAG_04796	4.286634907	7.625622502	4.778876347	2.846746155	8.95E-06	0.00017949	7.193760629 hypothetical protein
SJAG_05404	5.699489384	8.91888484	6.052177661	2.866707179	1.42E-08	8.01E-07	7.293984727 hypothetical protein
EFSJAG00000000	9.077027257	12.9849325	10.10384771	2.881084786	1.20E-11	2.72E-09	7.367038521 Small nucleolar RNA Z13/snr52 [Source:RFAM;Acc:RF00335]
SJAG_00994	9.565747415	13.86685957	10.97654523	2.890314341	1.96E-13	1.23E-10	7.414319785 hypothetical protein
SJAG_01477	13.85960409	18.33025764	15.397193	2.933064642	1.06E-09	9.89E-08	7.637310307 fungal protein
SJAG_05358	6.727906856	11.20342936	8.242657077	2.960772282	3.51E-14	4.42E-11	7.785406031 hypothetical protein
SJAG_01869	14.72704625	19.40160962	16.43660487	2.965004749	5.68E-11	9.00E-09	7.80827979 NADH/NADPH dependent indole-3-acetaldehyde reductase AKR3C2
SJAG_02357	6.476512871	9.755439596	6.757306803	2.998132793	2.58E-12	8.25E-10	7.989652705 DUF1769 family protein
SJAG_01396	5.713906107	8.969411737	5.967650558	3.001761179	7.38E-08	3.14E-06	8.009772011 hypothetical protein
SJAG_03830	10.8950859	15.53925239	12.52623658	3.013015817	2.76E-13	1.49E-10	8.072501571 hypothetical protein
SJAG_00388	6.516531138	11.47048607	8.427546272	3.042939797	3.38E-10	3.83E-08	8.2416877 hypothetical protein
EFSJAG00000000	6.434888342	11.13461462	8.082661813	3.051952808	8.48E-10	8.10E-08	8.293337517 U5 spliceosomal RNA [Source:RFAM;Acc:RF00020]
SJAG_06471	12.21187518	16.18359382	13.12326788	3.060325936	1.97E-10	2.49E-08	8.341610421 hypothetical protein
SJAG_00976	10.55814552	14.17868841	11.1113916	3.067296813	1.49E-13	1.15E-10	8.382013312 cytochrome c oxidase subunit IV
SJAG_00927	3.761204196	6.849869939	3.775308059	3.07456188	2.24E-06	5.61E-05	8.424329586 hypothetical protein
SJAG_03361	12.85295111	16.45595422	13.36737626	3.088577964	2.46E-17	1.71E-13	8.506572563 rho GDP dissociation inhibitor Rdi1
SJAG_04365	7.855288907	11.80434989	8.693349277	3.111000616	4.01E-12	1.14E-09	8.63981617 hypothetical protein
SJAG_02105	8.10239009	11.20980457	8.085230225	3.124574344	7.48E-11	1.12E-08	8.721488272 F0-ATPase subunit J
SJAG_02683	11.34784605	14.79994664	11.63108929	3.168857344	4.04E-19	9.84E-15	8.993342072 ICE2 family ER membrane protein
SJAG_05353	3.710667429	7.58771762	4.177827399	3.409890222	4.33E-06	9.80E-05	10.62867772 ATP-dependent DNA helicase
SJAG_02967	4.138313853	8.801808436	5.335835793	3.465972643	2.25E-08	1.18E-06	11.04998605 hypothetical protein
SJAG_05173	3.303196708	7.226725604	3.660311444	3.566414161	7.30E-06	0.000151772	11.84670678 hypothetical protein
SJAG_05143	5.71378139	11.56219563	7.958952831	3.6032428	4.19E-11	7.25E-09	12.15301865 hypothetical protein
SJAG_00012	5.539356506	9.225290102	5.588526817	3.636763285	4.20E-08	1.95E-06	12.43869549 hypothetical protein
SJAG_06596	4.367710716	7.976444812	4.318643244	3.657801567	1.52E-06	4.09E-05	12.62141335 hypothetical protein
SJAG_00780	7.923204175	10.5848173	6.919632974	3.665184324	5.59E-12	1.45E-09	12.68616691 hypothetical protein

Annexe 4: Late timepoint analysis

SJAG_05354	2.039243288	6.744625138	2.843193938	3.9014312	3.90E-05	0.000613216	14.94334479 hypothetical protein
SJAG_00013	1.514019589	6.706731483	2.582015279	4.124716204	1.35E-06	3.71E-05	17.4446918 hypothetical protein
SJAG_06640	1.456171501	7.435223107	3.195331386	4.239891721	4.73E-07	1.54E-05	18.89446444 hypothetical protein
SJAG_06639	4.372018256	10.29849598	5.767281365	4.531214613	2.13E-10	2.62E-08	23.12232574 hypothetical protein
SJAG_02124	8.720886148	11.86064003	7.320224184	4.540415848	2.77E-08	1.39E-06	23.27026682 cobW
SJAG_00121	3.99677326	7.820224389	2.997673015	4.822551374	1.01E-05	0.000197742	28.29649338 hypothetical protein
SJAG_00240	7.883320447	11.92144262	6.592721636	5.328720986	9.91E-09	5.91E-07	40.18878304 alcohol dehydrogenase Adh4
SJAG_06641	2.76784921	9.274173492	3.857885554	5.416287938	1.95E-08	1.05E-06	42.70366351 hypothetical protein - chp1